Spatio-Temporal Changes in Meteorological Dryness/Wetness Pattern and Hydrological Responses in South China

Dissertation

der Mathematisch-Naturwissenschaftlichen Fakultät

der Eberhard Karls Universität Tübingen

zur Erlangung des Grades eines

Doktors der Naturwissenschaften

(Dr. rer. nat.)

vorgelegt von

Thomas Fischer

aus Berlin

Tübingen

2012

Tag der mündlichen Qualifikation:	14. 01. 2013
Dekan:	Prof. Dr. Wolfgang Rosenstiel
1. Berichterstatter:	Prof. Dr. Thomas Scholten
2. Berichterstatter:	PD Dr. Marco Gemmer

Content

Content 3

Summary 4

Zusammenfassung 7

Acknowledgements 10

1. Introduction 11
   - 1.1 Background 11
   - 1.2 Research Problems 13
   - 1.3 Rationale 15
2. Objectives 16
3. Data and Methodology 17
   - 3.1 Data 17
   - 3.2 Methodology 18
4. Regional Setting 19
5. Overview of the seven Manuscripts 23
   - 5.1 Trends in Annual Temperature, Precipitation, and Dryness/Wetness Pattern 23
   - 5.2 Trends in Monthly Precipitation Extremes 25
   - 5.3 Change-Points in Climate Extremes 27
   - 5.4 Probability Distribution of Precipitation Extremes 29
   - 5.5 Long-term meteorological and hydrological dryness/wetness conditions 32
   - 5.6 Simulated and Projected Climate Extremes 35
   - 5.7 Projected Flood Frequencies and their Uncertainty 37
6. Conclusions 39
7. Outlook 42

References 44

Erklärung 51

List of Manuscripts and Personal Contribution 52

Appendices I – VII 54

Summary

South China is prone to floods and droughts which are often caused by extremes in meteorological dryness and wetness conditions, such as heavy precipitation or dry spells, and their hydrological responses. The monsoon circulation is the driving force behind meteorological extremes and corresponding hydrological challenges in China's river basins. Floods and droughts cause casualties and high agricultural and economic losses, whether directly or indirectly. One of the worst droughts hit Southwest China in the winter of 2009/10 due to a preceding weak South Asian Monsoon. In June 2010, record-breaking floods occurred in the whole of South China due to anomalously intense rainfall as a result of a strong East Asian Summer Monsoon circulation. These events have affected millions of people, caused hundreds of fatalities and triggered harvest losses over tens of thousands of square kilometers of farmland which resulted in direct economic losses of CNY 20bn and CNY 84bn, respectively.

The most important river system in South China is the Zhujiang River Basin which covers rural and mountainous regions in the western part, but also megacities, such as Guangzhou (Canton) and Hong Kong, on the southern coast. The Zhujiang River (Pearl River) covers 80% of the drinking water demand of Hong Kong and hosts an important agricultural basis with approx. 17% of China's rice production. The Zhujiang River is considerably prone to floods and droughts which can have a larger impact on the socio-economic sphere than in other river basins of China. However, scientific information on the susceptibility of regional climate extremes and dryness/wetness pattern are neither available in high resolution nor quality, both in spatial and temporal extent, for the South of China. Data and methodological analyses have so far been inadequately used in existing studies, as most researchers used data of a limited number of stations and with multiple data gaps. Additionally, research areas have been too large in extent to allow sound analyses and interpretations. Only basic trend and frequency tests have been applied so far to investigate the regional climate characteristics. Therefore, an integrated assessment of meteorological dryness/wetness pattern and hydrological responses has not been made available yet. Considering the current challenges in water, food, and economic security, a comprehensive methodological framework, to investigate seasonal and monthly climate extremes and their impacts on the water cycle in the Zhujiang River Basin, is of great importance. There is also scientific need

to tackle the existing deficiencies in data availability, data interpretation, and implementation of the results into planning.

In this context, the objective of the present study is to develop and provide reliable baseline data and evaluation methods for spatio-temporal pattern of the occurrence of extreme weather events for the Zhujiang River Basin. The data interpretation focuses on assessing the vulnerability of communities to climate extremes as a starting point for sustainable development through the improvement of adaptation measures to climate extremes and their hydrological consequences.

In order to achieve the objective, new data are generated with high quality and high spatio-temporal resolution. In this process, the currently highest density of monitoring stations and the longest meteorological and hydrological time-series available in South China have been coupled with the results of global and regional climate models. The relevance of observed, simulated, and projected meteorological and hydrological parameters is tested and statistically or dynamically modeled for the assessment of the vulnerability of communities to climate extremes. Statistical methods, such as standardization, moving averaging, and specific extreme value determination, were developed or modified in order to generate relevant indicators of climate extremes. The time-series were then analyzed on their trends, change-points, frequencies, periodicities, and impacts in dryness / wetness conditions. The causes and interdependencies of the changes are analyzed and interpreted using trend tests (e.g. Mann-Kendall Test and linear regression), particular cumulative summation, modern distribution functions (e.g. Generalized Extreme Value, Generalized Pareto und Wakeby), and combinations of the adapted principal component analysis and the wavelet transform.

Spatio-temporal effects of meteorological dryness/wetness on the river discharge (i.e. droughts and floods) are investigated with regard to reoccurrence and susceptibility. In order to determine the hydrological impacts and responses of extreme weather events, innovative spatio-temporal modeling and interdependency tests, such as new interpolation methods, spatial averaging, and principal component analysis, are applied. These novel approaches in data generation and analytical techniques deliver an accurate methodological framework for the interpretation of spatio-temporal trends, periodicities and frequencies of dryness/wetness conditions. With this approach, significant increases in extreme temperatures can be identified in the entire region. Precipitation extremes, such as dry days and heavy precipitation, have changed only in some parts of the basin. For the first time,

these spatio-temporal differences in precipitation extremes deliver details of the regional variance and the probability to dryer conditions in the western part but to more extreme wet conditions in the northern and coastal areas.

Overall, unexpectedly strong correlations between “meteorological” precipitation extremes and “hydrological” extremes such as high and low peak discharge can be identified for the Zhujiang River Basin. This suggests that the identified changes and frequencies in the meteorological dryness/wetness pattern will have direct hydrological responses. This dependency is proven by the detected cycles of intensive dryness and wetness periods, with 3-, 7- and 11-14-year cycles in both meteorological and hydrological extremes. It can be detected that changes in climate extremes can be attributed to changes in regional atmospheric circulation pattern, predominantly the East Asian Monsoon. The projections of future dryness/wetness pattern on the basis of model calculations and statistical extrapolations show a general trend towards warmer conditions and an increase in regional disparities. The temporal and regional patterns that could be detected deliver a sound basis to identify various regional and local prevention and adaptation measures in South China and to reduce the vulnerability and risks to extreme climate events.

Zusammenfassung

Der Süden Chinas ist anfällig für Überschwemmungen und Dürren, welche häufig durch extreme meteorologische Trockenheit oder Feuchtigkeit und die daraus resultierenden hydrologischen Reaktionen hervorgerufen werden. Die Monsunzirkulation ist die treibende Kraft hinter diesen meteorologischen Extremen und den entsprechenden hydrologischen Auswirkungen in den chinesischen Flussgebieten. Überschwemmungen und Dürren verursachen hohe Opferzahlen und hohe landwirtschaftliche und wirtschaftliche Verluste. Im Winter 2009/10 gab es aufgrund eines vorhergehenden schwachen südasiatischen Monsuns eine der schlimmsten Dürren in Südwestchina. Im darauffolgenden Juni 2010 traten Rekord-Überschwemmungen in ganz Südchina auf, ausgelöst durch anomale Starkniederschläge infolge eines starken ostasiatischen Sommermonsuns. Allein diese beiden Ereignisse zogen mehrere Millionen Menschen in Mitleidenschaft, verursachten Hunderte Tote und hatten Ernteverluste auf Zehntausenden von Quadratkilometern Ackerland zur Folge. Die direkten wirtschaftlichen Schäden beliefen sich auf über 20 Mrd. CNY bzw. 84 Mrd. CNY.

Das wichtigste Fluss-System im Süden Chinas ist das Zhujiang-Einzugsgebiet. Es umfasst ländliche und bergige Regionen in den westlichen Gebieten, aber auch Megacities, wie Guangzhou (Kanton) und Hongkong an der Südküste. Das Zhujiang-Einzugsgebiet deckt 80% des Trinkwasserbedarfs von Hong Kong und stellt mit einer jährlichen Reisproduktion von ca. 17% von ganz China eine bedeutende landwirtschaftliche Basis dar. Der Zhujiang Fluss (Perlenfluss) ist sehr anfällig für Überschwemmungen und Dürren, die jeweils größere Auswirkungen auf die sozio-ökonomische Sphäre haben können als in anderen chinesischen Flussgebieten. Informationen über die Anfälligkeit für regionale Wetter- und Klimaextreme sowie extreme Trockenheit / Feuchtigkeit in Südchina stehen weder in hoher Auflösung noch Qualität, für zeitliche oder räumliche Merkmale meteorologischer und hydrologischer Daten, zur Verfügung. In vorhandenen Studien wurden bislang weder die vorhandenen Daten noch die möglichen Analysemethoden ausreichend angewendet, da die meisten Forscher nur die Messdaten von einigen wenigen Beobachtungsstationen, mit dazu vielen Datenlücken analysieren konnten. Außerdem umfassen diese Studien in der Regel ein zu großes Untersuchungsgebiet um eine aussagekräftige Analyse zu ermöglichen. Darüber hinaus wurden bisher nur einfache Trend-und Frequenz-Tests benutzt, um die regionalen klimatischen Eigenschaften zu bestimmen. Schlussfolgernd bedeutet dies, dass bis heute

keine integrierte Bewertung meteorologischer Extremereignisse mit entsprechenden hydrologischen Reaktionen zur Verfügung steht. Angesichts der aktuellen Herausforderungen im Hinblick auf die Bereitstellung von Wasser und Nahrungsmitteln sowie der Sicherung der wirtschaftlichen Entwicklung Chinas ist ein umfassendes methodisches Rahmenwerk zur Bestimmung der saisonalen und monatlichen Klimaextreme und deren Auswirkungen auf den Wasserkreislauf im Zhujiang-Einzugsgebiet von großer Wichtigkeit. Zusätzlicher Entwicklungsbedarf besteht hinsichtlich der Beseitigung bestehender Mängel in der Verfügbarkeit von klimatischen und hydrologischen Daten, deren Interpretation und die anschließende Umsetzung der Ergebnisse in der Planung.

Vor diesem Hintergrund ist es das Ziel der vorliegenden Arbeit, belastbare Grundlagendaten und Auswertungsmethoden hinsichtlich des räumlich-zeitlichen Musters für das Auftreten von meteorologischen Extremereignissen für das Zhujiang-Einzugsgebiet zu entwickeln und bereitzustellen. Die Dateninterpretation konzentriert sich auf die Bewertung der Anfälligkeit von Gemeinden gegenüber Klimaextremen als Ausgangspunkt für eine nachhaltige Entwicklung durch die Verbesserung von Anpassungsmaßnahmen an Klimaextreme und deren hydrologische Folgen.

Hierzu wurden zunächst Daten von hoher Qualität und mit hoher räumlich-zeitlicher Auflösung generiert. Dabei wurden die bislang höchste Dichte von Beobachtungsstationen und die längsten meteorologischen und hydrologischen Zeitreihen, die für Südchina verfügbar sind, mit globalen und regionalen Klimamodellergebnissen gekoppelt. Beobachtete, simulierte und projizierte meteorologische und hydrologische Parameter wurden hinsichtlich ihrer Relevanz für die Bewertung der Anfälligkeit von Gemeinden gegenüber Klimaextremen getestet und statistisch oder dynamisch modelliert. Um relevante Indikatoren für Klimaextreme zu erzeugen, wurden statistische Methoden, wie z.B. Standardisierung, Gleitende Mittelwertbildung sowie spezifische Extremwertbildung, entwickelt oder modifiziert. Die Datenreihen wurden daraufhin auf ihre Trends, Change-Points, Frequenzen, Periodizitäten und spezifische Auswirkungen auf Trockenheit / Feuchtigkeit hin untersucht. Die Ursachen und Wechselbeziehungen der Veränderungen wurden analysiert und mittels Trend-Tests (z.B. Mann-Kendall Test und Lineare Regression), kumulativer Summierung, moderner Verteilungsfunktionen (z.B. Generalized Extreme Value, Generalized Pareto und Wakeby), sowie mit angepassten Hauptkomponenten-Analysen und Wavelet-Transformationen bemessen und interpretiert.

Räumlich-zeitliche Auswirkungen der meteorologischen Trockenheit bzw. Feuchtigkeit auf den Flussabfluss (d.h. hydrologische Dürren bzw. Überschwemmungen) wurden in Hinblick auf ihre Wiederkehr und diesbezügliche Anfälligkeit hin untersucht. Um die hydrologischen Auswirkungen und Reaktionen von extremen Wetterereignissen zu bestimmen, wurden innovative räumlich-zeitliche Modellierungen und Interdependenz-Tests, räumliche Mittelbildung und Hauptkomponentenanalyse angewendet. Diese neuen Ansätze der Datengenerierung und -analyse liefern ein präzises methodisches Rahmenwerk für die Interpretation der räumlich-zeitlichen Trends, Perioden und Frequenzen von Trockenheit / Feuchtigkeit im Zhujiang-Einzugsgebiet. Die Ergebnisse dieses Rahmenwerkes zeigen eine deutliche Steigerung von extremen Temperaturen in der gesamten Region. Niederschlagsextreme, wie zum Beispiel trockene Tage und Starkniederschläge, haben sich dagegen nur in einigen Teilen des Einzugsgebietes verändert. Diese räumlich-zeitlichen Unterschiede in Niederschlagsextremen liefern erstmalig Details über die sich verändernde regionale Varianz von Trockenheit / Feuchtigkeit. Darüber hinaus können relativ konkrete Aussagen über die Wahrscheinlichkeit hin zu trockeneren Bedingungen im westlichen Teil und zu extremerer Feuchtigkeit im nördlichen und süd-östlichen Teil des Einzugsgebietes getroffen werden.

Insgesamt zeigen die Ergebnisse für das Zhujiang-Einzugsgebiet unerwartet starke Korrelationen zwischen "meteorologischen" Extremniederschlägen und "hydrologischen" Spitzen im Hoch- und Niedrigwasserabfluss. Dies deutet darauf hin, dass jegliche Veränderungen in den Verhaltensmustern von meteorologischer Trockenheit / Feuchtigkeit, die festgestellt werden konnten, direkte hydrologische Auswirkungen zur Folge haben. Diese Abhängigkeit wird durch die erfassten Zyklen intensiver Trockenheits- und Feuchtigkeitsperioden von 3-7 und 11-14 Jahren bestätigt. Es kann aufgezeigt werden, dass diese Veränderungen der Klimaextreme den Änderungen der regionalen atmosphärischen Zirkulation, vor allem des ostasiatischen Monsuns, folgen. Die Projektionen von zukünftigen Trockenheits- und Feuchtigkeitsmustern anhand der Modellrechnungen und statistischen Extrapolationen zeigen einen allgemeinen Trend zu wärmeren Bedingungen und zu einer Intensivierung der regionalen Disparitäten. Das so ermittelte regionale und zeitliche Muster bildete die Grundlage, um verschiedene regionale und lokale Präventions- und Anpassungsmaßnahmen in Südchina zu identifizieren und die Vulnerabilität und Risiken gegenüber klimatologischen Extremereignissen zu verringern.

Acknowledgements

I have been very fortunate to perform this research with the support of many great colleagues and friends.

First and foremost, I wish to thank my principal supervisor Thomas Scholten for his constant support and enthusiasm for my work. I am deeply grateful to Marco Gemmer for his supervision and active participation in my research, both on the application of climate and hydrological data and various methods as well as on professional writing and presentation aspects. His ability to describe complicated processes in simple figures has been very much appreciated. I wish to thank him for his guidance and patience, while introducing me to the world of climate data analysis and the entire working environment and life in Beijing.

Furthermore, I am very thankful for the support given by Jiang Tong and Su Buda by sharing their extensive knowledge and experience in climate and hydrological analyses and model processes and for providing a pleasant work environment. I wish to thank Liu Lüliu and Luo Yong for their substantial support in hydrological modeling and information on climate change issues in China. I also want to thank my colleagues at the Division of Climate Change Impact Assessment of the National Climate Center of the China Meteorological Administration for all the professional and social support given. Many thanks go further to Christoph Menz and Frank Wechsung from the Potsdam Institute for Climate Impact Research for their enduring and patient input to climate modeling.

At last, I want to thank my family and my friends in supporting me with their love and understanding in all my life's decisions.

Thank you all.

Tübingen, October 2012

Thomas Fischer

1. Introduction

1.1 Background

Extreme weather and climate events (summarized as 'climate extremes' in the following) such as rain storms and heat waves are important factors influencing the occurrence of floods and droughts (Easterling et al., 2000; Alexander et al., 2006). These can have severe impacts on ecosystems and socio-economic structures. The recent record-breaking and persistent drought in Yunnan, from autumn 2009 to spring 2010, was directly caused by extreme deficient precipitation of 20% below normal due to a preceding weakened vertical Asian Monsoon circulation. The drought has affected the drinking water supply of more than 7 million people and crop areas of almost 22,000 km^2, causing direct economic losses of more than 20 billion CNY (Lü et al., 2012).

In June of 2010, major floods occurred in South China due to anomalously intense rainfalls caused by a strong East Asian Summer Monsoon, affecting nearly 70 million people, flooding more than 44,000 km^2 of farmland, destroying hundreds of thousands of housings, and totaling in almost 84 billion CNY of direct economic losses. This flood event was caused by preceding torrential rainfall events, resulting in large-scale inundations and numerous devastating landslides. A record-breaking rainfall with above 600 mm precipitation in a six-hour period was observed in Guangdong province (Asia News Network, China Daily, 2010).

These events have extents similar to the devastations reported for the 1998 Yangtze floods and the large droughts of 2003-04 or 1963-64. In recent decades, droughts occurred almost every year in entire China, causing an increase in the proportion of crop losses and threatening the security of drinking water supplies. The annual amount of crops that were lost due to droughts would feed about 85 million people (Wu et al., 2011).

Accordingly, rain storm, flood, and drought events become more important variables in hampering sustainable socio-economic development and securing freshwater resources, especially in the developing countries of Asia (Mertz et al., 2009). Such events do also have adverse consequences on the agricultural production of the crop growing regions. A changing climate will lead to changes in the frequency, intensity, spatial extent, duration, and timing of extreme weather and climate events (Kharin et al., 2007; IPCC, 2012). It is estimated that by 2050, one billion people in Asia will be adversely affected by changes in the hydrological cycle as a growing population and higher standards of living push up the pressure on freshwater resources (Parry et al., 2007).

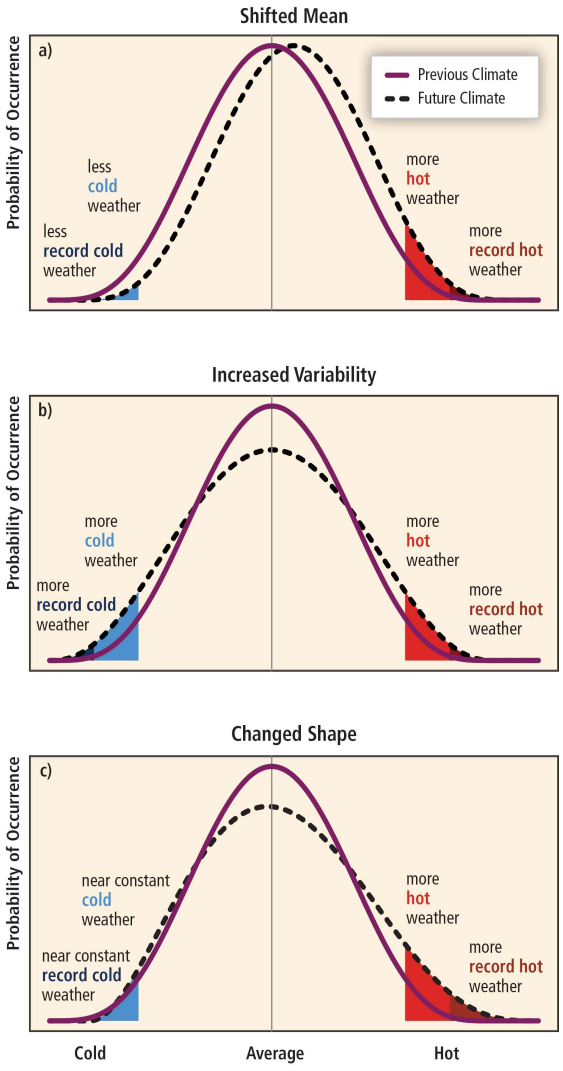

Figure 1 Potential changes in the probability distribution of climate extremes (here: temperature) due to (a) a shift in the mean, (b) an increase in the variability, and (c) a change in the symmetry.
(Source: IPCC, 2012)

Conducting research and applying innovative methodologies to investigate climate extremes will enhance the knowledge on their characteristics, and thus contribute to strengthen the adaptation to and prediction of such extremes. A series of scientific studies has analyzed the characteristics, causes, and impacts of trends and frequencies of climate extremes in East Asia and worldwide (Ding et al., 2008; Solomon et al., 2007; Parry et al., 2007; Klein Tank et al., 2009; Hoskins, 2003; Feng et al., 2007).

Additionally, Barnett et al. (2005) emphasized that the discharge of most large rivers is very sensitive to changes in climate extremes. The changes in climate extremes can be linked to changes in the mean and/or the variability, i.e. changes in the shape of probability distributions of climate parameters (Figure 1), such as temperature, precipitation, and evaporation (Klein Tank et al., 2009; IPCC, 2012).

According to China's first and second National Assessment Reports on Climate Change (MoST, 2006 and 2011), the trends and frequencies of climate extremes have increased in China and will very likely increase in the future. Associated with global warming, the most severe impacts that are projected for East Asia are a decrease in freshwater availability and a significant increase in the variability of river runoff. The recently observed weakening of the East Asian Monsoon (EAM), which plays an important role in regional precipitation patterns and water availability, might lead to decreases in precipitation over southeast

China (Chen et al. 2000). On the contrary, in a global study on precipitation extremes, Easterling et al. (2000) found increasing heavy precipitation pattern over South China for the decades before 2000 (Figure 2).

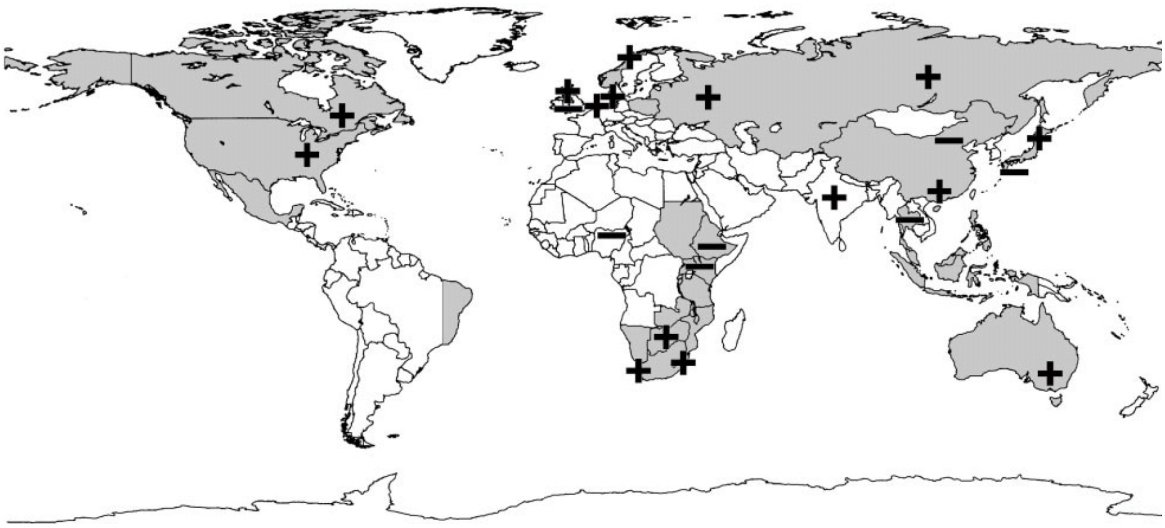

Figure 2 Regions for which the large sets of daily precipitation time series are available for analyses of precipitation extremes. Signs (pluses and minuses) indicate regions where significant changes in heavy precipitation have occurred during the past decades. (Source: Easterling et al., 2000)

1.2 Research Problems

Up to now, not many certain observations and predictions on changes in such extremes are available for the study region (cf. Wang et al., 2012). The high uncertainty in the forecasts is a huge obstacle for regional and local stakeholders in implementing preventive adaptation measures. A related key issue to tackle the increasing climate change is to intensify water resource management and protection, as well as to enhance the ability of early warning of rainstorms, floods and droughts. For this major global issue, more scientific research in the characteristics of extreme events and the associated vulnerability needs to be reinforced (MoST, 2011).

During the past decade, temporal variations in runoff of Chinese rivers, the Yangtze and the Yellow River in particular, have been extensively studied (e.g. Chu et al., 2009; Xu and Milliman, 2009; Xu et al., 2010). Between 1951 and 2000, precipitation has increased in

the south and decreased in the north of China, but most changes of basin-wide precipitation were statistically insignificant. In the Yellow River Basin, the frequency and contribution of moderately heavy rainfall events to total rainfall show a significant decreasing trend in summer (Hu et al., 2012). This might explain the obvious increase in extreme dryness observed in the 1990s (Ma et al., 2004). In the Yangtze River Basin, for example, 7-8 years fluctuations in dryness/wetness conditions have been detected for most parts of the region (Gemmer et al., 2008; Zeng et al., 2012). In addition, a trend towards wetter conditions from 1990 onward is also obvious (Zhao et al., 2012). Changes in precipitation extremes and significant quasi periodicities in the 2–3 and 3–4 year ranges have been observed in the Yangtze River Basin (Becker et al., 2008; Gemmer et al., 2008), and are related to high and low river flows. Gemmer et al. (2008) conclude that flood and drought hazards in the Yangtze River Basin have been aggravated accordingly. The Yangtze runoff shows little changes, while in the north, the Yellow, Liao, and Songhua rivers decreased by 80%, 54% and 14%, respectively (Xu et al., 2010, Liu et al., 2011). The spatial and temporal variability of precipitation and runoff was also analyzed for multiple sub-basins of the Yellow and Yangtze rivers, which show several significant changes. These and further findings (Zhai et al., 1999, 2004; Alexander et al., 2006) imply that extremes in low runoff events (droughts) and extremes in high runoff events (floods) may occur more frequently (Parry et al., 2007). In turn, changes in water resources can also alter local climate conditions and the risk to more intense climate extremes (Hattermann and Kundzewicz, 2010; IPCC, 2012).

Regional changes are, however, diverse and Southeast China for instance experienced an increase in annual temperature and extreme precipitation during the last fifty years (Ding et al. 2005). Parry et al. (2007) highlighted that projected changes in spatial and temporal precipitation pattern for most regions in China are very uncertain. This is emphasized by the low confidence in observed and projected changes in heavy precipitation and dryness pattern for East and South-East Asia (IPCC, 2012). Regarding the temporal scale, changes in seasonal and monthly climate extremes are of higher concern than changes on annual scale (Piao et al., 2010). A closer look into the interdependencies of seasonal and monthly meteorological and hydrological dryness and wetness conditions and the specific uncertainties of projections will help to enhance the understanding of changing spatio-temporal climate patterns.

1.3 Rationale

Observed and projected climate conditions have been intensely analyzed for the Yangtze and Yellow River basins which are the two largest river basins in China. As compared to these two basins, little research has been conducted on the other large river basins in China. It is also difficult to compare and elaborate the findings of existing studies as data sets, station density, time series, climate indices, methodologies, models, and interpretations vary broadly between the existing studies. Hence, the implementation of the available findings into flood/drought adaptation planning such as projects on integrated water resources management or climate change adaptation is rather unfeasible, due to the incoherent use of international or even national standards.

Furthermore, Easterling et al. (2000) emphasize that one of the biggest problems in performing analyses of global climate extremes is a lack of access to high-quality, long-term climate data with the time resolution appropriate for analyzing such extremes. The homogeneity of climate data, especially of extreme events, underlies several factors which can result in high biases. To avoid these deficiencies in data problems, specific indices for climate extremes derived from meteorological parameters, which are responsible for the occurrence of extreme events, must be generated to determine trends, probabilities, and long-term variability in the climate data for an efficient use in various adaptation projects.

In spite of water security issues, i.e. water supply, water demand and water scarcity, the China Ministry of Science and Technology (MoST) has put one focus on climate extremes in South China's monsoon region. As the country's third largest river basin, the Zhujiang River drains the major part of South China. Zhang et al. (2008) concluded that the annual water discharge in the Zhujiang River Basin is mainly influenced by precipitation variability, rather than by the construction of reservoirs and dams.

Considering the current challenges with freshwater resources such as water security, agricultural production such as food security, and economic losses, a comprehensive investigation of seasonal and monthly climate extremes and their impacts on the water cycle in the Zhujiang River Basin is of great importance to tackle the existing deficiencies in data availability and implementation of results.

2. Objectives

Information on temperature trends, precipitation trends, and long-term meteorological and hydrological dryness/wetness conditions, especially in South China's large river basin, is scarce. This is due to the unavailability of data in required spatio-temporal resolution and the lack of scientific research conducted in this area. It is important for regional and local stakeholders to gain more detailed knowledge on the probability distribution, change-points and trends in climate extremes to prevent and adapt to climate induced disasters and socio-economic impacts. For this, the simulation and projection of climate extremes using high resolution regional climate models are required. For feasible adaptation measures, such as a weather-index based flood insurance, the probabilities and uncertainties in projected flood frequency and heavy rainfalls must be made available to regional and local stakeholders. It is also important to interpret the causes of changes in meteorological and hydrological extremes in order to strengthen the scientific basis and increase the preparedness. Based on the need to obtain timely results and solutions for the aforementioned deficiencies,

the objective of the present study is to develop and provide reliable baseline data and evaluation methods for spatio-temporal pattern of the occurrence of extreme weather events for the Zhujiang River Basin.

In order to achieve this objective, a comprehensive methodological framework for the analysis of climate extremes and hydrological responses in South China will be developed by compiling the results of seven peer-reviewed manuscripts. Specific climate risks are determined by generating comprehensive data sets and developing statistical modeling and interpolation methods as described in the subsequent section. Based on this data generating approach, detected regional impacts of climate extremes on the water cycle (droughts and floods) are analyzed with regard to the identified trends and frequencies. The causes of the observed changes in climate extremes are also determined. The significant characteristics and interdependencies of meteorological and hydrological indicators at different spatio-temporal scales can be used for water resources management and climate change adaptation.

3. Data and Methodology

3.1 Data

Quality controlled daily temperature and precipitation data from 192 meteorological stations for 1961-2007 in the Zhujiang River Basin, and daily river discharge data as well as socio-economic and disaster loss data, are provided by the China Meteorological Administration (CMA). This data was successfully checked on homogeneity by the China National Meteorological Information Center. The applied NCEP reanalysis data (western pacific subtropical high, relative humidity, geopotential heights, and u- and v-wind pattern for 1948-2010) are provided on the website of the US National Oceanic and Atmospheric Administration (NOAA). The annual East Asian Summer Monsoon Index data is taken from the website of the Chinese State Key Laboratory of Numerical Modelling for Atmospheric Sciences and Geophysical Fluid Dynamics. The daily data of simulated and projected precipitation and temperature from four general circulation models (GCMs) have been retrieved from the IPCC Data Distribution Centre and from the CMA. The regional climate model (RCM) data is provided by the Potsdam Institute for Climate Impact Research (PIK).

The observed, simulated, and projected meteorological and hydrologic parameters are collected and are tested for their suitability, modified, and statistically modeled to achieve the objective. The parameters, such as temperature, precipitation, wind, and discharge, are analyzed on the basis of various annual and monthly indicators. These indicators are developed according to international standards or following specific methodological necessities in the framework of the study's objective. Among the developed indicators are for example Dry Days, Maximum 5-day Precipitation (RX5), the Standardized Precipitation Index (SPI), and the East Asian Summer Monsoon Index (EASMI), which are investigated on their trends, change-points, frequencies, periodicities, and impacts especially in dryness/wetness pattern.

The highest density of observation stations (192 stations), longest meteorological and hydrologic time series (1961-2007), high resolution GCM/RCM outputs, reanalysis data, and the latest socio-economic and disaster loss data available in South China are used to identify to what extent climate extremes changed and will change, and of how the water cycle is and will be affected.

3.2 Methodology

For investigating the time series and the developed indicators, a variety of state-of-the-art methodologies are applied and further developed. For example, the rank related non-parametric Mann-Kendall test is used to detect significant trends in the time series (Gemmer et al., 2004; Yang et al., 2010), while the linear regression is used to determine the magnitude of the increase or decrease. The CUSUM method (Taylor, 2000; Leung and Wu, 2005) is applied to determine change-points in the time series based on the accumulation of the annual differences. For estimating the significance of change, the confidence levels are identified by a bootstrap technique, where the time series are re-sampled without replacement (Wilks, 2006).

To investigate the probability of occurrence of extreme events, various distribution functions (e.g. Gamma-3, Generalized Extreme Value, Generalized Pareto, and Wakeby) are applied (Palutikof et al., 1999; Hamed and Rao, 1999; Su et al., 2008; Yang et al., 2010). Further, three Goodness-of-Fit tests (Kolmogorov-Smirnov, Anderson-Darling, and Chi^2-Test) are used to detect the most adequate probability distribution which fits best (Corder and Foreman, 2009; Su et al., 2008). In this case, sampling with replacement is used to estimate confidence bounds for the return levels of extreme events in climate extremes and to estimate their natural variability (Davison and Hinkley, 1997, Kay et al., 2009; Kharin et al., 2007).

The Thiessen Polygon method is applied for spatial averaging (Jiang et al., 2007). Each polygon surrounds one station with its corner-points at half the distance between the nearest neighboring stations. To reveal certain spatial interdependencies of climate extremes in the study area, the principal component analysis is used (Bordi et al., 2004). This innovative method employs a multi-dimensional approach of the spatial correlation of all stations or sub-basins to the regional average (Santos et al., 2010; Zhao et al., 2012).

The Fast Fourier power spectrum (Schönwiese, 2006; Wilks, 2006) in combination with the Morlet wavelet analysis (Torrence and Compo, 1998) is used to define significant periodicities. With the power spectrum the strongest cycles in the time-series can be detected, while the wavelet analysis visualizes the increases and decreases in the magnitude. A future continuation of the observed cycles is done by extrapolating the time series based on the strongest cycles (Bordi et al., 2004; Becker et al., 2008). Several GCMs (e.g. ECHAM5, MK3.5, CCSM3, and HIRES), the regional climate model CCLM, and the hydrological model HBV-D are applied to simulate and project future climate extremes and river runoff.

The modern methods are often implemented by using different software packages such as ArcGIS, R, GrADS, Autosignal, and MS Excel. The combination of all techniques and approaches delivers an innovative methodological framework for the interpretation of spatio-temporal trends, frequencies, and characteristics of dryness/wetness conditions.

4. Regional Setting

The Zhujiang River Basin (also known as the Pearl River Basin) is located in South China (Figure 3). The entire basin covers approximately 579,000 km^2 (including the Leizhou Peninsula region), which is slightly larger than France, and embraces the administrative areas of Guangdong Province and Guangxi Autonomous Region almost entirely. It also cuts into the provinces of Yunnan, Guizhou, Hunan, Jangxi, and Fujian (Figure 4). A tropical to sub-tropical climate prevails while the East Asian Monsoon has strong seasonal influences on it (Zhai et al. 2009).

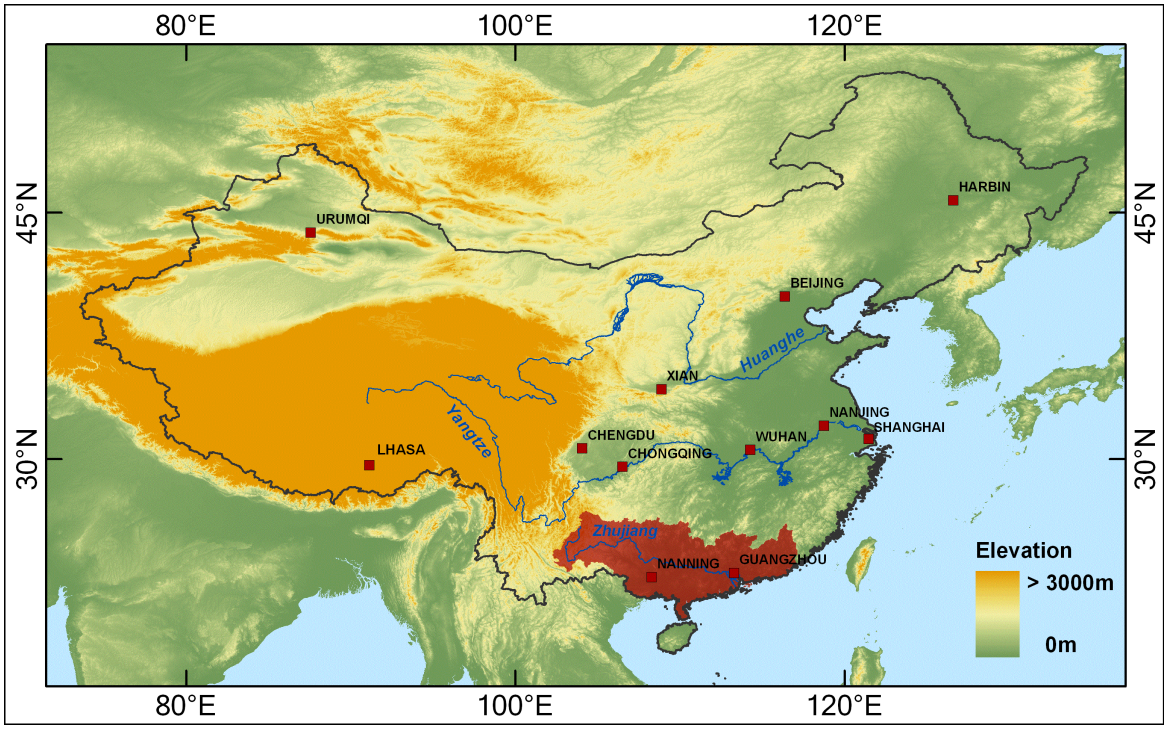

Figure 3 Topography and main rivers/cities of China, plus location of the Zhujiang River Basin (red area)

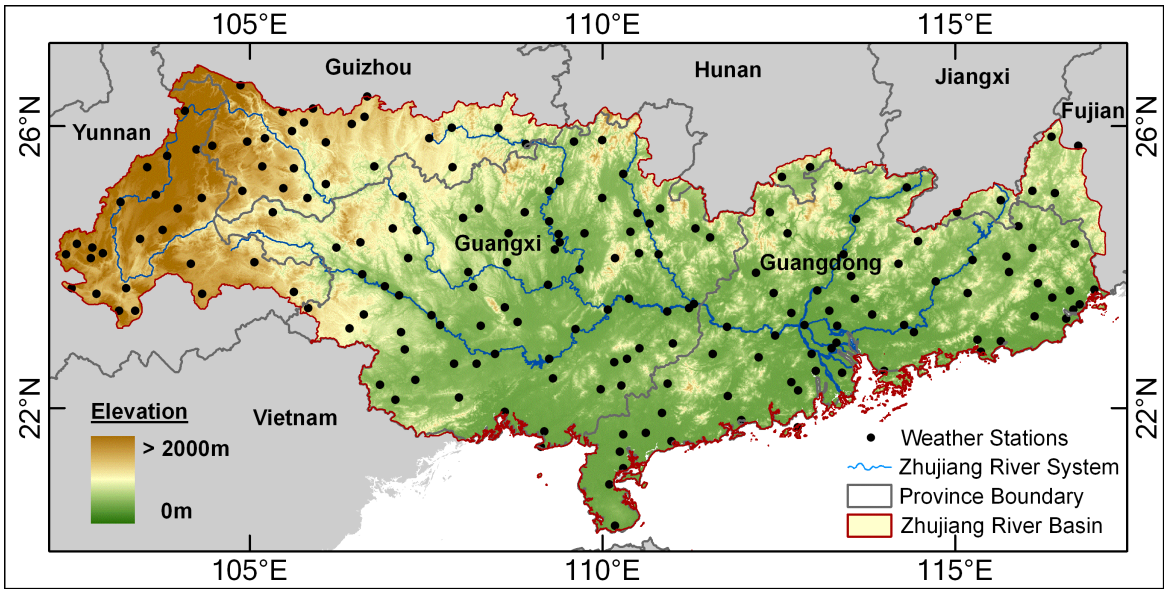

Figure 4 Topography and river system of the Zhujiang River Basin, location of meteorological stations, and province boundaries (and names)

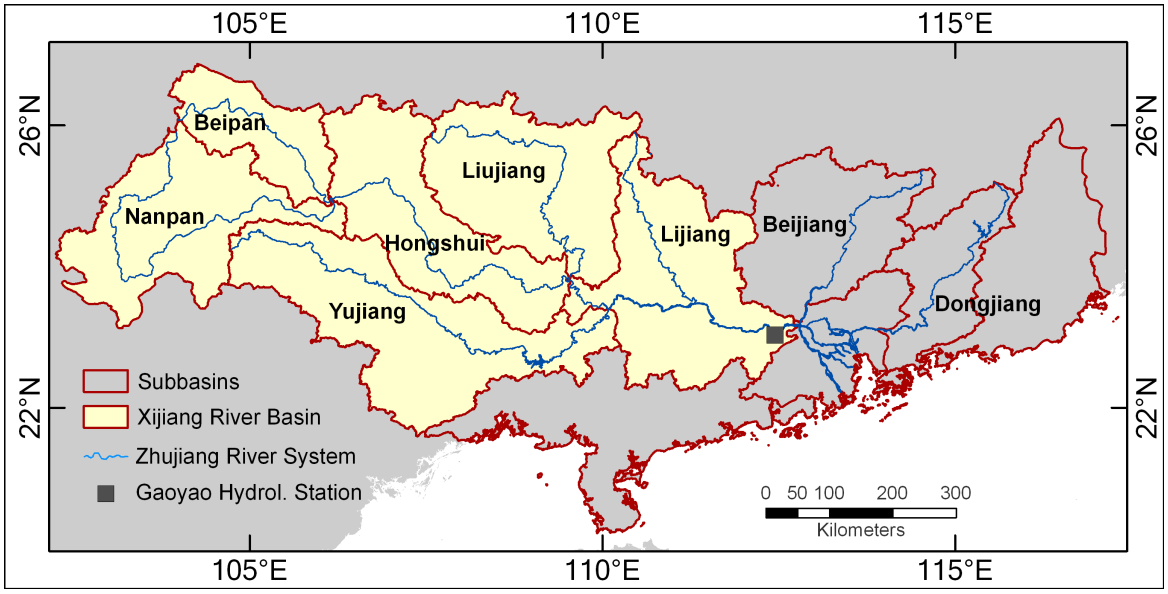

Figure 5 Location of the Xijiang River Basin, the sub-basins (and names) and the hydrological station on the Xijiang River at Gaoyao

The basin is characterized by mountainous areas with peaks above 2500 m in the western part. The northern and north-eastern parts are composed of lower mountain ranges and hills that surround the central and southern (south-eastern) lowland areas. The Zhujiang River consists of three main tributaries, i.e. the Xijiang River, Beijiang River, and Dongjiang River. The largest tributary is the Xijiang River, which accounts for 78% of the total drainage area of the Zhujiang River Basin and is subdivided into six sub-basins, namely Beipan, Nanpan, Yujiang, Hongshui, Liujiang, and Lijiang (Figure 5).

With an average discharge of 7,000m^3/s at Gaoyao hydrological station, the Xijiang drains the entire western and central parts of the basin. Due to the basin's topography (Figure 6), the Xijiang has a south-eastward stream flow direction, while the Beijiang and Dongjiang flow south-westward. At the south-eastern coastal area, the tributaries merge into a large network delta (i.e. Zhujiang River Delta) before they mound into the South China Sea.

The annual temperature in the basin ranges from 13 °C in the elevated western and north-western parts of the basin to 24 °C in the coastal lowlands in the south and south-east. Similarly distributed is the annual average precipitation (1500 mm) with only 800 mm in the west and more than 2000 mm at the coastline. This distribution can be mainly explained by the driving climate factors of the transition from maritime (lowlands) to continental (highlands) of the meteorological stations. A more detailed description of the basins climatic and hydrologic conditions are provided by Yang et al. (2010) and Zhang et al. (2009), while historic and current data related to the basin can be also found on the website of the Pearl River Water Resource Commission (www.pearlwater.gov.cn).

With a population of more than 166 million, the region is currently one of the most economically prosperous areas of China, with very high development rates, and one of China's highest GDP per capita of more than 40,000 CNY per year (National Bureau of Statistics of China: www.stats.gov.cn, 2011). The basin covers remote rural areas but also megacities such as Guangzhou and Shenzhen on the southern coast of South China (Figure 6). The Zhujiang River covers 80% of the drinking water demand of Hong Kong and its basin hosts an important agricultural basis for entire China. Approximately 12% of the country's rice is produced in the basin, which comprises more than 80,000 km^2 of cultivated land.

The population and industrialization have been increasing in recent decades, thus the damage potentials of extreme climate events and other natural disasters have risen (Feng et

al., 2007). Hence, detailed knowledge on and adaptation to potential climate extremes are needed to lower this increasing vulnerability.

Figure 6 Photographs of the Zhujiang River Basin; Rain fed rice terraces near Longsheng, Guangxi (upper left), Lijiang River in the tropical Karst region at Yangshuo, Guangxi (upper right), Xijiang River in agricultural and industrial developed area near Gaoyao, Guangdong (lower left), and Zhujiang River in the city center of Guangzhou, Guangdong at night (lower right), *by T. Fischer, August 2011*.

5. Overview of the seven Manuscripts

The objective of this dissertation thesis is supported by numerous statistical analyses and literature reviews, and interpretations on climate extremes in South China in the last two-and-a-half years. So far, seven manuscripts have been published in or submitted to international journals. In the following sections, each manuscript is summarized using modified abstracts, introductions and main findings of the original papers. They are structured according to the data and methods applied and to the results and conclusions which are essential to the overall objectives.

5.1 Trends in Annual Temperature, Precipitation, and Dryness/Wetness Pattern

(manuscript 1, published in *Quaternary International*, IF[1] 1.768, Appendix I)

Spatial and temporal characteristics of annual temperature and precipitation time series are analyzed in order to identify tendencies in dryness and wetness. Daily temperature and precipitation data from 1961–2007 of 192 weather stations are used. All time series have only minor data gaps and passed the homogeneity check based on the moving t-test (Peterson et al. 1998), the standard normal homogeneity test (Alexandersson 1986), and the departure accumulating method (Buishand 1982). The Mann-Kendall trend test (Gemmer et al., 2004; Yang et al., 2010) and linear regression are applied to nine climate indicators (Klein Tank et al., 2009) which have been generated in order to detect patterns in dryness and wetness conditions. They are further compared with two drought indices, i.e. the Standardized Precipitation Index (SPI; McKee et al., 1993) and the Palmer Drought Severity Index (PDSI; Hayes, 2006).

Significant positive trends are found for mean temperature, number of warm days, longest warm period, dry days, and longest dry period. A significant increase in temperature by more than 0.7 K from 1961 to 2007 is observed in the entire basin and the coastal and far western areas in particular. The temperature changes might be explained the anticipated global warming (Ding et al., 2007). Negative trends are observed for annual cool days, longest cool period, wet days, and longest wet period. The findings are in line with national and international observations (Liu et al., 2009; Trenberth et al., 2007; Zhai et al., 2004), but

[1] Impact Factor for 2010

display the regional disparities in much more detail now, which also underline a stronger increase in temperature at the coastal and western areas than has been published before.

Almost no significant trends in annual mean and extreme precipitation could be found, but a shift to a greater regional imbalance in precipitation patterns within the basin is detected. A major new finding is the more regionalized distribution of annual no rain days and wet/dry periods with a significant trend to more dry days (i.e. fewer rain days) over the entire western part and significant negative trends to shorter wet periods but longer dry periods particularly in the far western corner and the delta region (Figure 7). Rainfall intensity has also increased along the coastline and in the far West of the catchment, which is in line with the findings by Zhang et al. (2009) and can be explained by the increasing number of dry days.

It can be concluded that indicators describing dryness (e.g. annual temperatures and dry days) have increased in magnitude, and dry periods have become longer while wet periods have shortened in time. The spatial distributions of the trends of these indicators show tendencies to stronger regional disparities. The identified spatio-temporal distributions of annual dryness/wetness indicators are partially linked to orographic convection, the transition from maritime to continental climate factors, and to changing wind patterns due to a weakening of the East Asian Summer Monsoon (EASM; Su et al., 2005; Yu et al., 2009; Chou, 2004).

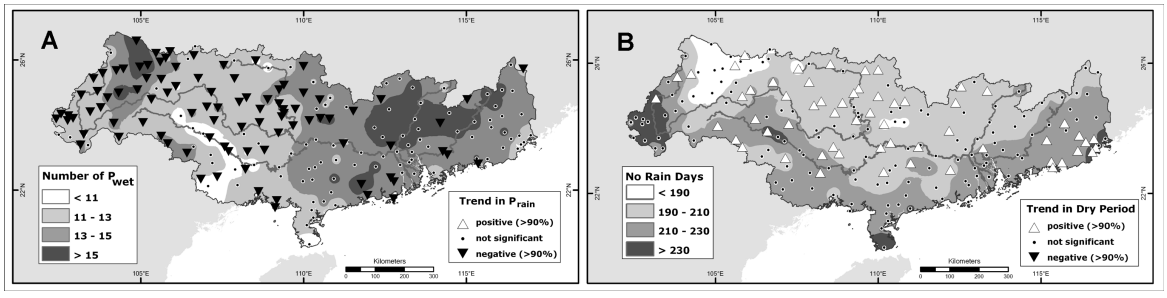

Figure 7 Observed (A) average duration of annual longest wet period (P_{wet}) and trend in annual rain days (P_{rain}), (B) number of annual no rain days and trend in annual longest dry period in the Zhujiang River Basin, 1961-2007.

5.2 Trends in Monthly Precipitation Extremes

(manuscript 2, published in *Journal of Climate*, IF 3.513, Appendix II)

Spatial and temporal characteristics of monthly precipitation trends in the Zhujiang River basin, South China, are analyzed to identify seasonal changes in extremes in more detail. Again the non-parametric Mann-Kendall trend test is applied to daily precipitation data from 192 weather stations for various extreme indicators. Among others, the annual and monthly number of rain days and the annual and monthly amounts in maximum and maximum 5-day precipitation are of special interest. Further, NCEP reanalysis data (http://www.esrl.noaa.gov/psd/; Kalney et al. 1996) are investigated on geopotential heights and wind direction pattern (1948-2010) linked to the East Asian Monsoon.

In line with the findings of manuscript 1, the results show that few stations experienced trends in the precipitation indices on an annual basis. On a monthly basis, significant positive and negative trends above the 90% confidence level appear in all months except December. The trends in the indicators of monthly precipitation, rain intensity, rain days, and monthly maximum precipitation show very similar characteristics. They all experience the most distinct negative trends in October (Figure 8). The findings are somewhat supported on a seasonal basis by Liu et al. (2009) who detected, although not significantly, that autumn precipitation decreased, but spring, summer, and winter precipitation increased. It becomes apparent that if monthly results are merged for seasons (e.g. September, October, and November merged to 'autumn') the information on the significant decrease of precipitation intensity in October would have been lost.

A change of the mean wind direction by around 50° from East-South-East to East-North-East might explain the downward trend in precipitation indicators in October. Dry October months (months with low precipitation indices) can be observed when the mean wind direction is East-North-East (arid) instead of the prevailing mean wind direction East-South-East (moist) which is similar to Wet October months. East-North-East wind directions are typical for the East Asian Winter Monsoon (EAWM). Nearly 90% of the driest October months can be explained by the wind pattern of the EAWM (Figure 9).

In regard to the findings in manuscript 1, the early onset of the EAWM in relation with a weak EASM (Chou, 2004) can be linked to the observed changes in annual and monthly dryness conditions. This identified linkage of large-scale atmospheric circulation with observed regional trends delivers more detailed information on observed changes than

other studies in the same area. This can be attributed to the higher station density and quality of daily data, and the focus on monthly trends in the current study.

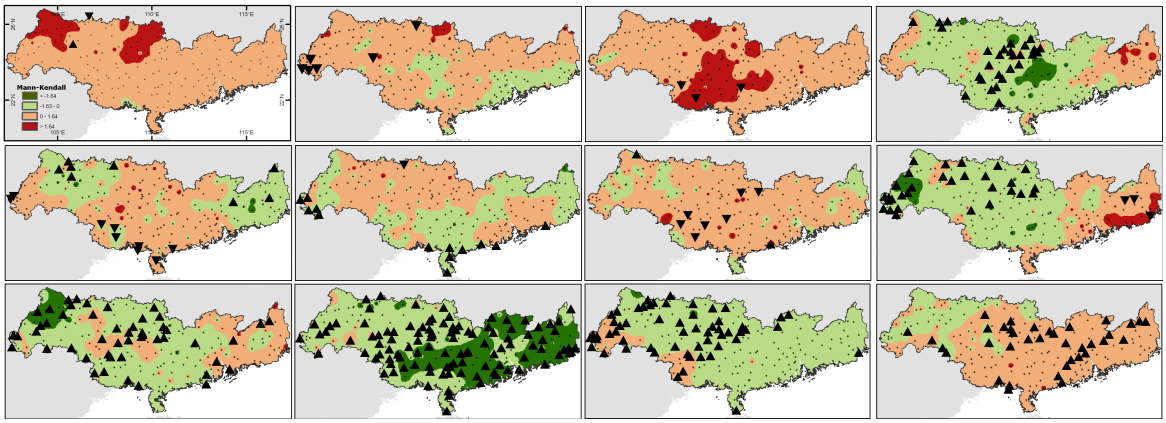

Figure 8 Monthly trends in maximum 5-day precipitation (shadings) and number of dry days (triangles) in the Zhujiang River Basin, 1961-2007.

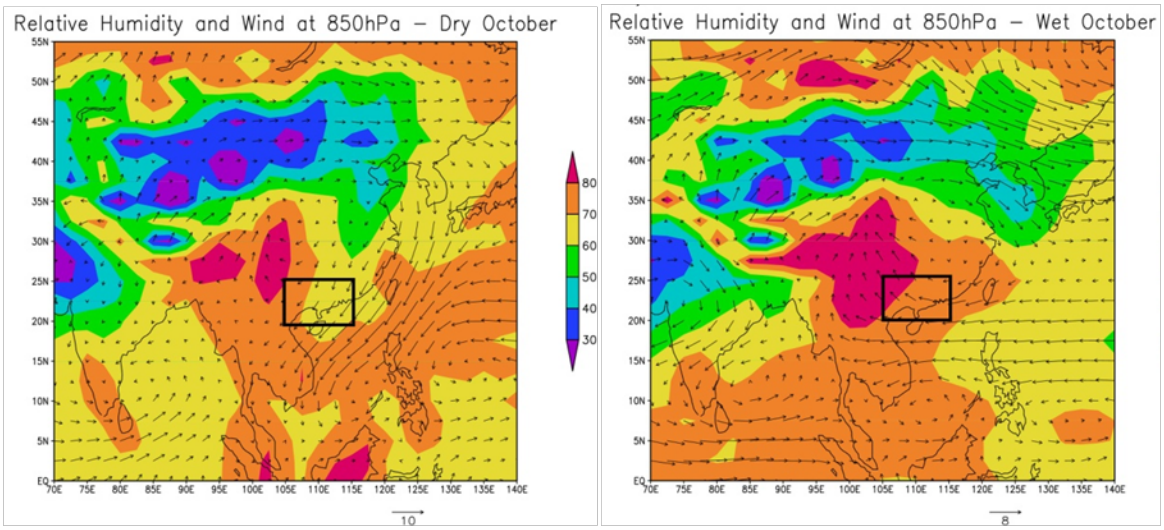

Figure 9 Characteristics of relative humidity (shadings) at 850hPa level and winds (arrows) for average dry October (left panel) and for average wet October (right panel) in the Zhujiang River Basin (black rectangle).

5.3 Change-Points in Climate Extremes

(manuscript 3, published in *Climatic Change*, IF 3.016, Appendix III)

In this manuscript, change-points and corresponding abrupt shifts in time series of annual climate extremes are investigated on their potential connections with atmospheric circulation patterns. Annual mean temperature, maximum temperature, warm days, total precipitation, 5-day maximum precipitation, and dry days (Klein Tank et al., 2009) of 192 meteorological stations for the period 1961–2007 are analyzed using the CUSUM method (Taylor, 2000; Leung and Wu, 2005) and bootstrapping techniques. Similarly, the East Asian Summer Monsoon Index (EASMI; Li and Zeng, 2003; http://www.lasg.ac.cn/staff/ljp/data-monsoon/EAMI1948-present.ascii), the Western Pacific subtropical high Index (WPI; Barnston and Livezey, 1987; http://www.cpc.ncep.noaa.gov/data/) and the NCEP wind directions in October (http://www.esrl.noaa.gov/psd/data/) are also investigated.

Significant change-points (1986/87, 1997/98, 1968/69, and 2003/04) are detected in time series of the indicators at varying numbers of stations. For 1986/87, most stations with a change-point in temperature indicators are located in the eastern and coastal areas of the basin. Stations with this change-point in dry days are located in the western area. Identified change-points signify an abrupt shift to higher/lower amounts in the annual indicators and are mostly caused by spatial changes (movements) of regional climate regimes (Seidel and Lanzante, 2004; Wilks, 2006). The means and trends of the temperature indicators shift upward in the entire basin after 1986/87. The highest magnitudes can be found at the coast and delta. Downward (upward) shifts in total and 5-day maximum precipitation (dry days) are mostly observed in the western and central regions.

Conclusively, the change points result in above-average temperatures, below-average precipitation in winter and spring, and fewer moderate-to-heavy rainfall events in summer. The detected change-points can be explained by changes in the WPI and the EASMI as well as by change-points in wind directions in October (Figure 10). The linkage of the change-points to large-scale atmospheric circulation has not yet been investigated for South China. In years when the WPI and EASMI simultaneously increase and decrease (indices taking reverse directions to negative and positive values), higher annual temperatures and lower annual precipitation amounts occur in the Zhujiang River Basin. In recent decades, the contrast of a slight decrease in summer temperatures over Central Asia and an increase over the North West Pacific caused the weakening of the summer monsoon and the shift of the rain belt over South China, leading to less rain days (Su et al., 2005; Chou, 2004). It not only

underlines and verifies the findings of manuscripts 1 and 2, but changes in the location of the East Asian Jet Stream and shifts in the transition phase from EASM to EAWM can be deduced. Therefore, the results can be used for forecasts of abrupt shifts in climate extremes and rain seasons, to provide valuable data for adaptation measures against climate risks, e.g. for flood control, disaster preparedness, and water resource management.

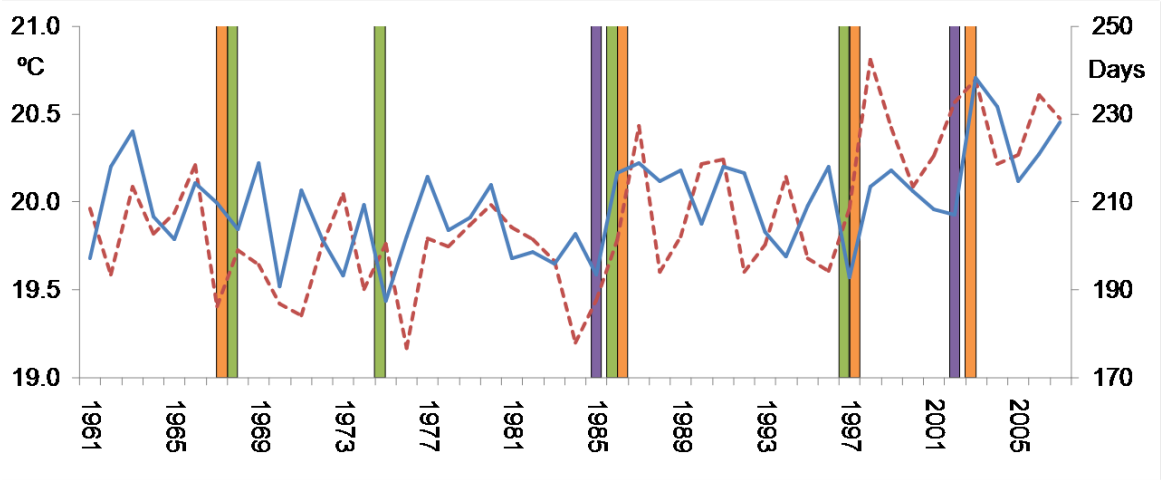

Figure 10 Averaged mean temperature (dashed red line) and dry days (blue line) in the Zhujiang River Basin, change-points of mean temperature and dry days (orange columns), change-points of wind directions in the eastern Zhujiang River Basin in October (purple columns), years of reverse indices for WPI and EASMI (green columns), 1961-2007.

5.4 Probability Distribution of Precipitation Extremes

(manuscript 4, published in *Journal of Hydrometeorology*, IF 2.185, Appendix IV)

Precipitation extremes have caused floods and droughts, which in turn led to economic and agricultural losses and extensive impacts on harvest areas in the Zhujiang River Basin (CMA, 2010; www.pearlwater.gov.cn; www.ers.usda.gov). Increasing trends in economic losses and affected harvest areas can be detected, and a 14-year cycle in affected areas due to droughts can be distinguished (Figure 11). Based on regional experiences in climate change adaptation techniques, the concept of weather-index based insurance is introduced as a new approach in adaptation to climate extremes (Boyd et al., 2011; Parry et al., 2009; The World Bank, 2007; Turvey and Kong, 2010; www.circ.gov.cn). By insuring harvest losses due to certain climate extremes, this approach can decrease the vulnerability of local farmers to climate extremes. After identifying observed changes in climate extremes (see manuscripts above), the analysis of their frequencies is important to improve the management of the associated risks (here: flood risks).

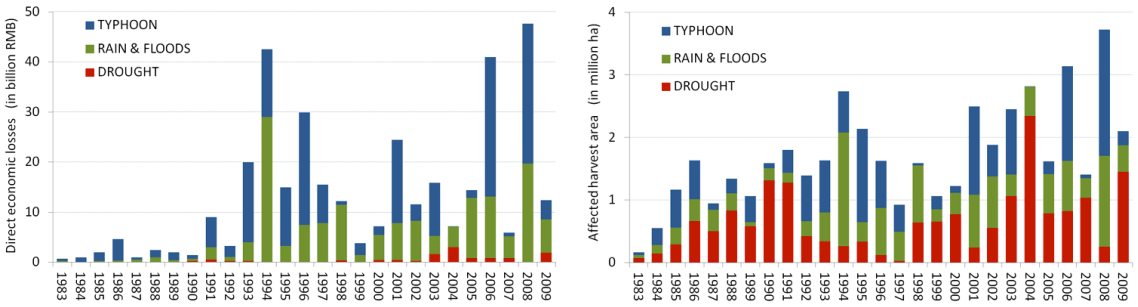

Figure 11 Direct economic losses (in billion RMB; left panel) and Affected harvest area (in million ha; right panel) due to Typhoon, Rain & Floods, and Drought Disaster in Guangdong and Guangxi 1983-2009

The probability of precipitation extremes is necessary to determine return periods of extreme events, and is also a key input in the development of thresholds for weather-index based insurance (Adger et al., 2007; The World Bank, 2007). Therefore, the probability distribution of annual precipitation extremes is analyzed by applying four distribution functions (Gamma-3, Generalized Extreme Value [GEV], Generalized Pareto, and Wakeby) as used and described by Palutikof et al. (1999), Hamed and Rao (1999), Feng et al. (2007), Su et al. (2008), and Yang et al. (2010). Three Goodness-of-Fit tests (Kolmogorov-Smirnov,

Anderson-Darling, and Chi2) are applied to the distribution functions for annual time series (1961–2007) of 192 meteorological stations to identify the most adequate probability distribution which fits best (Corder and Foreman, 2009; Su et al., 2008). To obtain reliable results in the estimation of return levels and hence in the application of all common distribution functions, stationarity in the time series needs to be confirmed beforehand. For this, the methods of linear regression, Mann Kendall test, and Engle's test (Gao et al., 2010; Duchesne, 2006) are applied, to identify stations exhibiting significant trends and conditional heteroscedasticity in residuals. Here, eleven stations out of 192 were excluded from the calculations. For each station-based indicator, 1000 bootstrap members are generated by sampling with replacement (Davison and Hinkley, 1997, Kharin et al., 2007) to estimate confidence bounds for the return levels.

The results show that maximum precipitation and 5-day-maximum precipitation are best described by the Wakeby distribution, which is similar to the findings by Su et al. (2008) for the Yangtze River Basin, which is the only available comparative study for East China so far. However, on basin-scale, the GEV is the most reliable and robust distribution for estimating precipitation indexes for an index-based insurance program in the Zhujiang River Basin. Nonetheless, it is recommended that each station has to be analyzed individually as GEV is not always the best fitting distribution function. Based on the distribution functions, spatio-temporal characteristics of return periods for maximum precipitation and 5-day-maximum precipitation are determined. The return levels of the 25- and 50-year return periods (using GEV) show similar spatial pattern: they are higher in the southeast and lower in the southwest of the basin (Figure 12). This spatial distribution is in line with the annual averages and the findings in manuscripts 1 and 2. They are also to some extent similar to the visualizations by Yang et al. (2010) and Yin et al. (2009), and comparable to the findings of Su et al. (2008) for the Yangtze River Basin. The detected changes in climate extremes are integrated in the actual probability function, but will probably change to even higher thresholds in the future.

Due to increasing economic development and population growth, future climate extremes will probably lead to even higher economic losses. Keeping this in mind, the statistical probability distribution of climate extremes delivers important information for a theoretical weather-index based insurance program and gives further new insights in regional extreme rainfall events and their linkage with economic and agricultural losses in the Zhujiang River Basin.

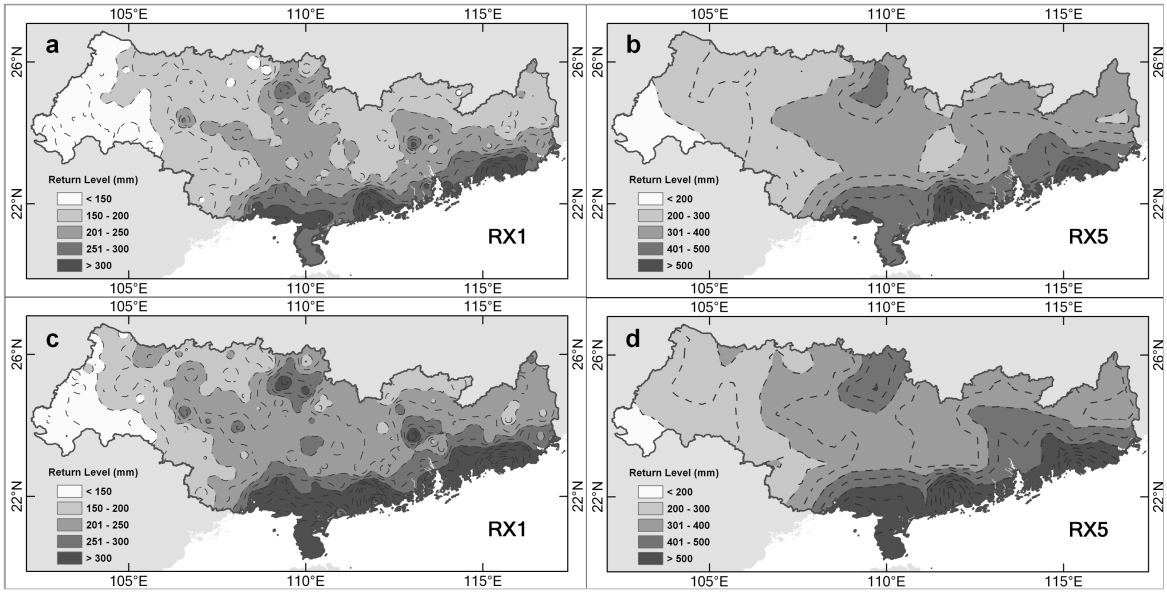

Figure 12 Return levels of the 25-year (a,b) and 50-year (c,d) return period for RX1 (a,c) and RX5 (b,d) in the Zhujiang River Basin, 1961-2007. The dashed lines indicate the 25/50mm interval (RX1/RX5).

5.5 Long-term meteorological and hydrological dryness/wetness conditions

(manuscript 5, accepted in *Hydrology and Earth System Sciences*, IF 2.463, Appendix V)

As assessed in manuscript 4, floods and droughts are frequently causing large economic losses in South China. These conditions vary in space, time, and magnitude. While we focused on short-term precipitation extremes in manuscript 4, we now analyze the long-term meteorological and hydrological dryness and wetness conditions in the Xijiang River Basin. These long-term conditions are of interest, as they do not implicate short-term economic losses but rather long-term indirect losses and/or large-scale drought events (Bordi et al., 2004). Comparing the inter-annual monthly precipitation and monthly discharge (provided by the CMA) in the Xijiang River Basin, a very similar course can be observed. The Thiessen Polygon method (Jiang et al., 2007) is applied to the station-based precipitation data, to generate monthly values for the calculation of the internationally recommended SPI (Bordi et al., 2004; Mishra and Singh, 2010). The SPI is also used to show the temporal characteristics of dryness and wetness pattern in the six sub-basins of the Xijiang River.

An impressive finding is that the SPI-24 correlates high with the standardized discharge index (SDI-24; McKee et al., 1993; Mishra and Singh, 2010) for Gaoyao hydrological station at the mouth of the Xijiang River (Figure 13). Hence, the natural variation in precipitation is responsible for the discharge to a very high degree. This is in line with the findings of Zhang et al. (2008), who concluded that the long-term changes of annual water discharge are mainly controlled by precipitation variation, rather than construction of reservoirs and dams, in the Zhujiang River Basin. Distinct long-term dryness and wetness sequences can be substantiated in the time series for both indices (SPI-24 and SDI-24).

The principal component analysis (Bordi et al., 2004; Santos et al., 2010; Zhao et al., 2012) reveals many spatial interdependencies in dryness and wetness conditions for the sub-basins and explains some spatio-temporal disparities. Moderate dryness conditions have a larger spatial impact than moderate wetness conditions in the sub-basins. The loading pattern of the first principal component shows that the correlation with the entire Xijiang River Basin is highest in the eastern and lowest in the western sub-basins. Further spatial dipole conditions explain the spatio-temporal heterogeneity of dryness and wetness conditions. Accordingly, the precipitation in the eastern sub-basins contributes higher to hydrological wetness conditions than in the western sub-basins, which mainly contribute to dryness patterns.

Using the Fast Fourier power spectrum (Schönwiese, 2006; Wilks, 2006), the spectral analysis for the SPI-24 of the entire Xijiang River Basin and the SDI-24 shows similar peaks for periods of 11-14.7 years, 2.8 years, 3.4-3.7 years, and 6.3-7.3 years. The same periods can be found for the SPI-24 of Xijiang River's six sub-basins with some variability in the magnitude. The Morlet wavelet analysis (Torrence and Compo, 1998) shows that the most significant periods are stable over time since the 1980s.

By using the most significant periodicities the potential course of the reconstructed time series of the SPI-24 and SDI-24 can be statistically extrapolated (Bordi et al., 2004; Becker et al., 2008). These extrapolations do not suggest any spatial or temporal changes in the occurrence of dryness and wetness conditions in the next two decades but display a continuation of the observed cycles at given magnitude (Figure 13). The extrapolation shows a distinct extreme dryness in 2008-09 which is spatially and temporally in line with the observed long-term drought that occurred in Southwest China in 2009-10 (Lü et al., 2012).

Increases in the magnitude of indices describing dryness, and a prolongation of dry periods with an opposing shortening of wet periods was identified in manuscript 1 and 2. These findings can explain the long-term drought sequences which we observed in the SPI-24 and SDI-24 time series during the second half the observed time period. It might also explain why the short-term periods around 3-4 years shifted to slightly longer periods which would then indicate inner-annual changes. Further noticeable are the change-points in precipitation indicators 1985/86 and 2003/04 that have been detected in manuscript 3. Both change-points mark the start of the two most distinct dryness clusters in the SPI-24 and SDI-24 time series.

It can be concluded that long-term hydrological dryness and wetness conditions are directly caused by periodic cycles of meteorological conditions (i.e. precipitation). The applied methodologies prove to be able to identify spatial interdependencies and corresponding regional disparities, and to detect significant periodicities in long-term dryness and wetness conditions in the Xijiang River Basin. The findings display the most accurate interpretation of long-term dryness/wetness conditions due to the highest station density and quality of daily data, and the focus on monthly indices in the current manuscript.

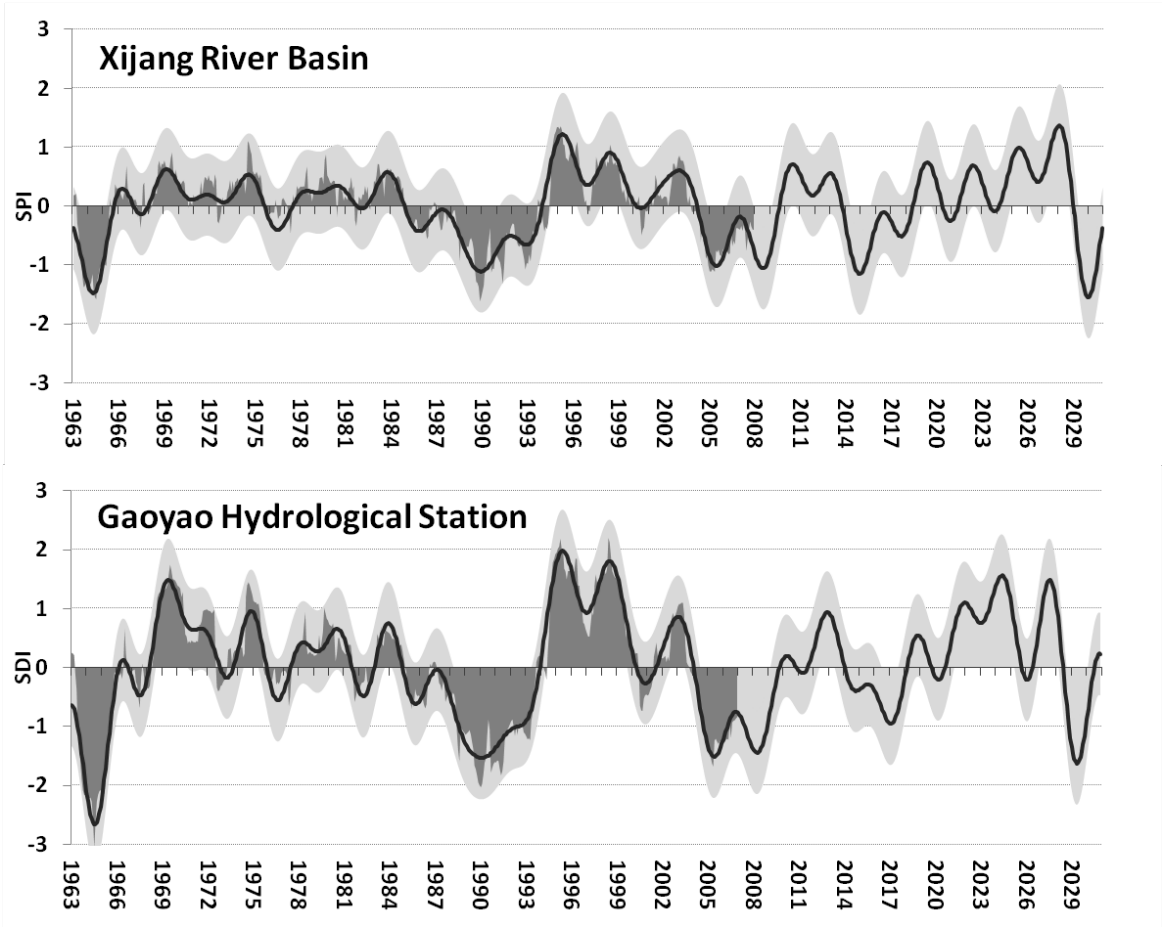

Figure 13 Reconstructed and extrapolated SPI-24 of the Xijiang River Basin (upper panel) and SDI-24 of Gaoyao Hydrological Station (lower panel)

5.6 Simulated and Projected Climate Extremes

(manuscript 6, accepted in *International Journal of Climatology*, IF 2.479, Appendix VI)

Having assessed the observed trends and periodicities in dryness and wetness conditions in the former manuscripts, we now focus on a detailed analysis of simulated and projected climate extremes until 2050. As provided by the Potsdam Institute for Climate Impact Research (PIK), daily output is used from the regional climate model COSMO-CLM (CCLM) as driven by the global circulation model (GCM) ECHAM5 (Steppeler et al., 2003; Böhm et al., 2006; Nikulin et al., 2011; Hollweg et al., 2008; Rockel et al., 2008). The hindcast simulation covers the period from 1961 to 2000 while the projection concentrates on the near future period from 2011 to 2050. Spatio-temporal statistical characteristics are investigated for three temperature and three precipitation indicators (Alexander and Arblaster, 2009; Klein Tank et al., 2009; Su et al., 2008). The six simulated annual and monthly indicators are statistically compared with synoptic observations (Alexander and Arblaster, 2009; Bordi et al., 2004; Corder and Foreman, 2009; Gemmer et al., 2004; Sheskin, 2004; Wilks, 2006). The investigation is based on daily values of 195 grid-points and 192 meteorological stations.

Compared to the observations, slightly higher amounts in temperature indicators and lower amounts in precipitation indicators are simulated. The distribution patterns of the CCLM simulations are visually much more similar with the observations than the ECHAM5 simulations, and CCLM can simulate monthly PRCPTOT and TMEAN more realistic than ECHAM5, which shows high deficiencies in spring. CCLM shows also a better simulation of the seasonal cycle, especially in regard to the precipitation extremes. Due to the reasonable similarities in spatial variation and trends we conclude that CCLM is able to satisfyingly reproduce climate extreme for the simulated period. Therefore, our analyses show that CCLM can be used to project climate extremes in the Zhujiang River Basin for the period from 2011 to 2050.

Based on SRES A1B (IPCC SRES, 2000), the projected changes indicate warmer and wetter conditions in the northern and southern regions, especially in winter and spring (Figure 14). This includes more intense rainfall events, which might potentially increase the risk of flooding in the central parts of the ZRB in these seasons. Warmer and dryer conditions can be expected in the western and eastern regions, especially in summer and fall. These lower precipitation amounts but warmer temperatures will probably increase the evapotranspiration, which potentially leads to a higher risk of drought. The findings of Liu et

al. (2009) are similar to our findings in TMEAN and PRCPTOT, but at less detailed regional and temporal resolution. The findings in GCM projected precipitation extremes by Xu et al. (2011) show opposed trends, i.e. increasing trends in annual consecutive dry days and decreasing trends in annual RX5, for the south china basin (comprising the Zhujiang and the Yangtze River basins). These discrepancies underline the importance of spatial resolution in climate modeling and emphasize the existing high uncertainty in current projections (Chen et al., 2011).

So far, this manuscript is the first projection of future climate extremes in South China with such a high spatial and temporal resolution by a regional climate model and observations available. Regarding the projected climate extremes, adverse consequences in various sectors, such as agriculture, water, and energy should be anticipated.

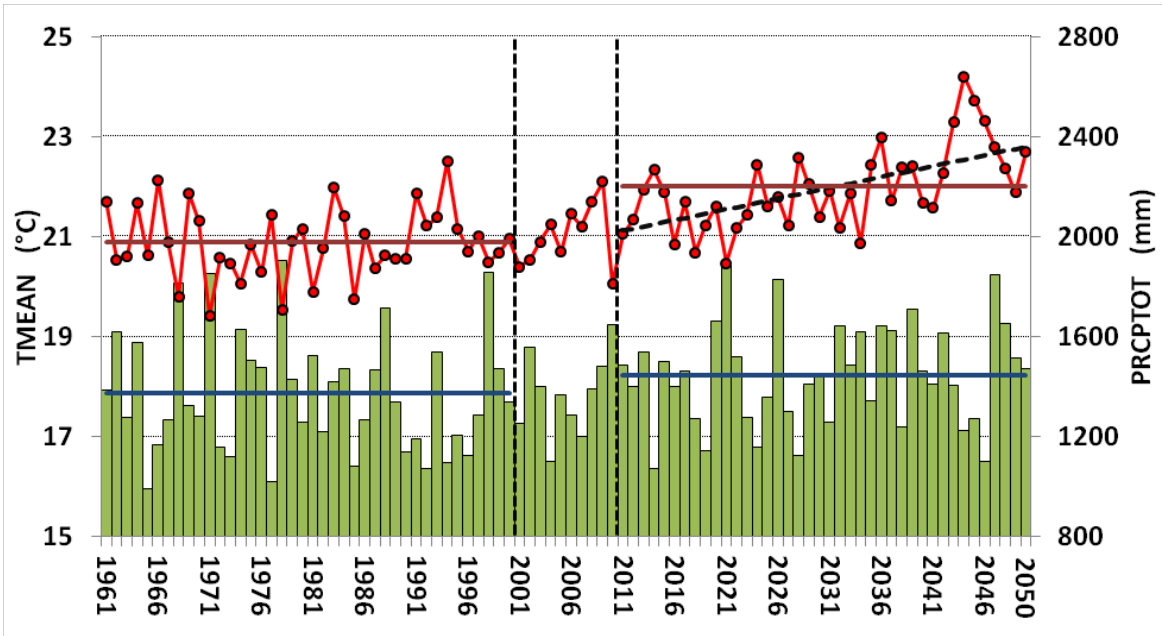

Figure 14 CCLM-simulated (1961-2000) and CCLM-projected (2010-2050) averaged annual mean temperature (red line) and annual total precipitation (green columns), including the means of 1961-2000 and 2011-2050 (dark red / dark blue lines) and the linear trend in mean temperature for 2011-2050 (black dashed line) in the Zhujiang River Basin.

5.7 Projected Flood Frequencies and their Uncertainty

(manuscript 7, accepted in *Quaternary International*, IF 1.768, Appendix VII)

Following the projections of climate extremes in manuscript 6, we now analyze the changes in projected flood frequencies of the Zhujiang River and additionally investigate the uncertainties in the modeling of the hydrological impacts of climate change. We applied the hydrological model HBV-D (Krysanova and Bronstert, 1999) to simulate and project future stream flow based on a multi-model ensemble, which includes the GCM's: ECHAM5, MK3.5, CCSM3, HIRES, and CCLM (http://ipcc-ddc.cru.uea.ac.uk; and as provided by PIK). A monthly re-sampling technique is used to estimate the natural variability (Kay et al., 2009; Jenkins and Lowe, 2003). The magnitude of three uncertainty sources, i.e. emission scenarios, GCM structure, and downscaling techniques, are related to the observed and projected natural variability. The relative change in each uncertainty source and the overall dominance among the three sources are analyzed. As several investigations (Kay et al., 2009; Menzel et al., 2006; Liu et al., 2011) show that uncertainty from hydrological modeling is less important, it is not assessed in this manuscript. Based on the peak over threshold method and the generalized Pareto distribution (Begueria, 2005; Kay et al., 2009; Prudhomme et al., 2003), the changes in flood frequency are presented for five return periods (2, 5, 10, 20, and 50 years) and three future time periods (2020s, 2050s, and 2080s; Figure 15).

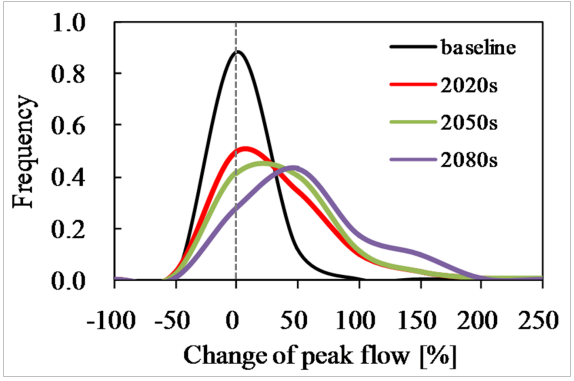

Figure 15 Frequency curves of changes in projected annual maximum 1-day flood peak flows (i.e. flood frequency) for three future periods relative to the baseline period (1961-1990) based on a multi-model ensemble

The results suggest that a steady increase in peak flow will occur in the projected time frame. These increases are subject to various uncertainty sources, which show much stronger variations in comparison to the natural variability of the multi-model ensemble. The range of their relative change and their dominance vary with the lead time and return period (Figure 16). In most of the cases, the dominant uncertainty can primarily be attributed to emission scenarios for all three future time periods. The GCM structure is the second dominant source, especially for the

projected flood frequency in the 2050s. Downscaling techniques represent the lowest uncertainty ranges of the three sources. The uncertainty and projected impact of climate change differs also between the four applied GCMs, as compared to the natural variability CCSM3 and HIRES show higher ranges than MK3.5 and ECHAM5.

The upper bounds (95% percentile) in uncertainty mostly show an increasing tendency with increasing return period, and partially with increasing lead time. Hence, the more extreme the return period (higher flood frequency) the higher is the uncertainty of the model projections. It is therefore essential that climate change impact assessments consider a wide range of climate scenarios derived from different GCMs under multiple emission scenarios and including several downscaling techniques. The uncertainty due to natural variability should also be considered more intensely (Ruosteenoja et al., 2003). The projection of changes in flood frequency of the Zhujiang River and in estimating and quantifying the influence of the uncertainty sources (Wilby and Dawson, 2007; Kay et al., 2009), policy-makers can be better convinced of integrating adaptation to climate extremes into their long-term plans, which can further strengthen the essential water resources management and disaster risk reduction in the Zhujiang River Basin.

In climate modelling, various sources of uncertainties are involved in the detection of climate change impacts amongst natural variability. In estimating and quantifying the influence of such uncertainty sources, policy-makers can be better convinced of integrating climate change into their long-term plans (Kay et al., 2009), which can strengthen e.g. water resources management in the Zhujiang River basin.

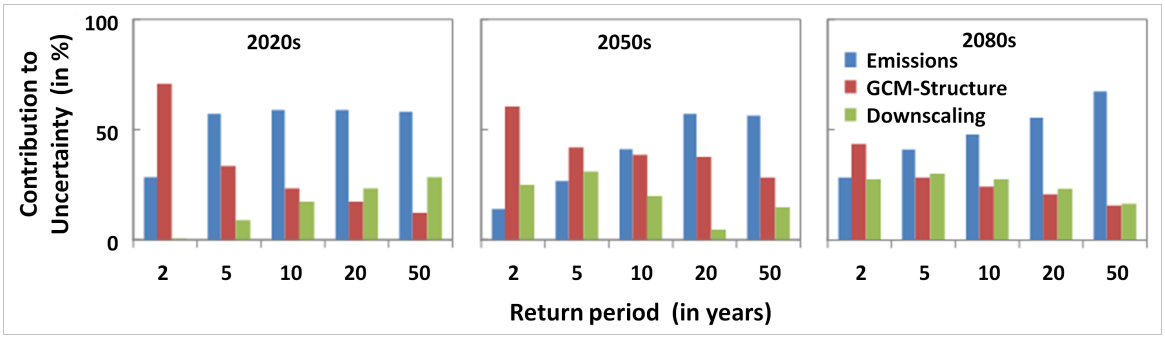

Figure 16 Bar charts of the relative impact range of three uncertainty sources, i.e. emission scenarios (blue), GCM structure (red) and downscaling techniques (green) for five return periods (2, 5, 10, 20 and 50 years) for the future periods of the 2020s (left panel), 2050s (middle panel), and 2080s (right panel)

6. Conclusions

With the methodological approach that was developed, the objectives of the dissertation thesis, comprising the detection of climate extremes and their impacts on dryness/wetness pattern in the Zhujiang River Basin and their past and future changes, has been achieved. Meteorological and hydrological parameters were statistically analyzed based on observations, simulations, and projections. The parameters, such as temperature, precipitation, wind, and river discharge, have been analyzed on the basis of various annual and monthly indicators that have been developed. Among the many indicators were the very important 5-day-maximum precipitation, dry days, and the SPI. These indicators have been analyzed on their trends, change-points, frequencies, periodicities, and impacts, especially regarding dryness and wetness pattern. Further, new data sets have been generated using state-of-the-art global and regional climate models as well as statistical programming. The data and methodological framework have not been made available before and support the interpretation of the causes of detected changes and processes. **It can be concluded that the indicators developed and the novel methodologies applied in the framework of this thesis are valuable tools to analyze spatio-temporal changes in meteorological dryness/wetness pattern and hydrological responses in South China**.

Generally, dryness conditions have increased in magnitude and duration, while wet periods have shortened in time in the Zhujiang River Basin in South China. The spatial distributions of these trends show tendencies to more distinct regional disparities. Few stations in the basin experienced trends in the annual precipitation indices, but on a monthly basis, significant positive and negative trends appear in all months except in December. The trends in monthly precipitation, rain intensity, rain days, and monthly maximum precipitation show very similar characteristics, with the most distinct negative trends in October. The identified spatio-temporal distributions of annual dryness/wetness indicators are partially linked to orographic convection, the transition from maritime to continental climate factors, and to changing wind patterns due to a weakening of the East Asian Summer Monsoon (EASM). The early onset of the East Asian Winter Monsoon (EAWM) in relation with a weak EASM can be linked to the observed changes in annual and monthly dryness conditions. This identified linkage of large-scale atmospheric circulation with observed regional trends delivers more detailed information on observed changes than other studies in the same area. This can be attributed to the higher station density and quality of daily data, and the focus on monthly trends in the current thesis.

The significant change-points (1986/87, 1997/98, 1968/69, and 2003/04) detected in time series of climate extreme indicators at varying numbers of stations, similarly result in temporal steps towards above-average temperatures, slightly below-average precipitation in winter and spring, and fewer moderate-to-heavy rainfall events in summer. The changes are linked to the changing conditions of the East Asian Summer Monsoon and the Western Pacific Subtropical High. The detected change-points can be partially explained by abrupt changes in the indices of the Western Pacific subtropical high (WPI) and the EASM as well as by change-points in wind directions in October. Changes in the location of the East Asian Jet Stream and shifts in the transition phase from EASM to EAWM can be deduced and support the findings in annual and monthly dryness/wetness conditions.

Numerous events within the time series of observed monthly and annual precipitation extremes have caused floods and droughts, which in turn led to economic and agricultural losses and extensive impacts on harvest areas in the Zhujiang River Basin. Increasing trends in economic losses and in affected harvest areas, and a 14-year cycle in affected areas due to droughts can be distinguished in the available loss records. Looking into the probability distribution of flood-supporting extremes, it can be concluded that maximum precipitation and 5-day-maximum precipitation are best described by the Wakeby distribution. However, on basin-scale, the generalized extreme value (GEV) distribution is the most reliable and robust distribution for estimating the probability of precipitation extremes, which is also in accordance with the World Meteorological Organization (WMO). Therefore, the application of GEV is highly recommended for investigations on probability distributions of dryness and wetness conditions in the Zhujiang River Basin.

Strong correlations are detected in annual regional precipitation amounts and river discharge of the Xijiang River as well as for their monthly standardized indexes (SPI and SDI). This is supported by the periodicities in the SPI and SDI of the entire Xijiang River Basin, which show similar peaks for periods of 11-14.7 years, 2.8 years, 3.4-3.7 years, and 6.3-7.3 years. Additionally, it becomes apparent that moderate dryness conditions have a larger spatial impact than moderate wetness conditions in the sub-basins of the Xijiang River Basin. Accordingly, the precipitation in the eastern sub-basins contributes higher to hydrological wetness conditions than in the western sub-basins, which mainly contribute to hydrological dryness patterns. It can be concluded that long-term hydrological dryness and wetness conditions are directly caused by periodic cycles of meteorological conditions (i.e.

regional precipitation pattern). The extrapolated dryness/wetness conditions can be used for potential guidance in the development of adaptation measures in the near future.

The simulation results for regional climate extremes in the Zhujiang River Basin confirm that the regional climate model CCLM is able to satisfyingly reproduce climate extreme in the simulation period. Subsequently, CCLM is used to project climate extremes in for the period from 2011 to 2050. The projected changes in climate extremes indicate warmer and wetter conditions in the northern and southern parts, especially in winter and spring, with more intense rainfall events, which might potentially increase the risk of flooding in the central parts of the ZRB in these seasons. Contrarily, warmer and dryer conditions can be expected in the western and eastern regions, especially in summer and fall. These lower precipitation amounts but warmer temperatures will probably increase the evapotranspiration, which potentially leads to a higher risk of drought.

The results from the hydrological model HBV-D suggest that a steady increase in peak discharge (i.e. flood frequency) of the Xijiang River will occur at least until 2100. The dominant source of uncertainty in this peak discharge projection can primarily be attributed to emission scenarios. The upper bounds (95% percentile) in uncertainty mostly show an increasing tendency with increasing return period, and partially with increasing lead time. Hence, the more extreme the return period (i.e. the shorter the flood frequency) the higher is the uncertainty of the model projections. It is therefore essential that climate change impact assessments consider a wide range of climate scenarios derived from different global climate models under multiple emission scenarios and including several downscaling techniques. The detected changes in climate extremes are integrated in the actual probability function, but will probably change to even higher thresholds in the future.

In this thesis, the highest density of observation stations, longest meteorological and hydrologic time-series, and GCM/RCM outputs available in South China have been generated. They are used to identify spatio-temporal changes in past and future climate extremes and how the water cycle is and will be affected. The innovative methodologies that have been selected, tested, and developed prove to be able to identify spatio-temporal interdependencies and corresponding regional disparities, and to detect significant trends, change-points, and periodicities in short- and long-term dryness and wetness conditions in the Zhujiang River Basin. The approach proves to be excellent to achieve the objectives of the thesis. Such an integrated spatio-temporal analysis has not been available before. Furthermore, the thesis could identify causes of changes in extremes, e.g. changes of

pressure systems in the West North-Pacific. The largest benefit of this thesis is the solid results that can be used by decision makers who are involved in the management of climate risk. The causes of the observed and projected changes have not been identified as such before. They can serve to improve predictions and early warning systems in the Zhujiang River Basin.

7. Outlook

So far, observed changes in climate extremes had an impact on flood and drought events and were partially caused by changes in atmospheric pattern. For the upcoming years, the maximum 1- and 5-day rainfall events are projected to become more intense and might lead to higher surface runoff and flooding, increased soil erosion, and reduced water quality. In contrast, the projected increase in dry days with a larger spatial impact of dryness conditions might lead to water scarcity (i.e. drought), soil degradation, and lowering of the groundwater table. An increase in dry days can also lead to soil desiccation and soil sealing, which in turn increases the potential of flooding. Hence, an increase in dry days and in average maximum 5-day rainfall might be regarded as factors indicating an increasing frequency and magnitude of drought and flood events. All such impacts might directly or indirectly affect the plant growth of the agricultural production with high losses in yield (as detected), which will have adverse consequences on the food security of the entire region. The strong increases in temperature extremes in the entire basin might affect most sectors, e.g. the energy demand or plant growth pattern will change the current economic and agricultural systems. High temperatures in summer will affect the population and economic sectors, as heat-induced health issues and higher cooling demand of public, private, and industrial sectors will appear. Nevertheless, higher temperatures in winter might effectively extend the plant growth period (i.e. longer annual agricultural production) and lessens the heating demand (i.e. less energy consumption). These examples show that the thesis has delivered a sound basis for further sectoral studies, e.g. in agricultural science, forestry science, wetland biology, or energy research.

South China might face an imbalance between the supply and demand of water for supporting the rapid socio-economic development while protecting the natural ecosystems (Cheng and Hu, 2012). The Chinese basins are particularly vulnerable to environmental

factors (Varis et al., 2012), hence, changes in dryness and wetness conditions are expected to further stress freshwater resources and widen the gap between the demand for and supply of water (Cheng and Hu, 2012) in the Zhujiang River Basin. Hard and soft measures to adapt to the adverse consequences, related to the detected changes in dryness/wetness conditions, have to be identified and implemented based on specifically issued policies and regulations. A sustainable water resources management strategy, based on both supply and demand, should be considered at the river basin scale. One good opportunity would be the implementation of an Integrated Water Resources Management (IWRM) which takes into account the socio-economic and environmental concerns in an integrative manner (Varis et al., 2012). This, or a similar approach, should also include mechanisms for climate change adaptation, climate proofing, and disaster risk reduction; incorporating the results presented in this dissertation thesis, to decrease the future vulnerability to climate extremes.

References

Adger, W.N., S. Agrawala, M.M.Q. Mirza, C. Conde, K. O'Brien, J. Pulhin, R. Pulwarty, B. Smit and K. Takahashi, 2007: Assessment of adaptation practices, options, constraints and capacity. Climate Change 2007: Impacts, Adaptation and Vulnerability. Contribution of Working Group II to the Fourth Assessment Report of the Intergovernmental Panel on Climate Change, M.L. Parry, O.F. Canziani, J.P. Palutikof, P.J. van der Linden and C.E. Hanson, Eds., Cambridge University Press, Cambridge, UK, 717-743.

Alexander, L.V. and J.M. Arblaster, 2009: Assessing trends in observed and modelled climate extremes over Australia in relation to future projections. Int. J. Climatology, 29, 417–435.

Alexander, L.V., X. Zhang, T.C. Peterson, J. Caesar, B. Gleason, A.M.G. Klein Tank, M. Haylock, D. Collins, B. Trewin, F. Rahimzadeh, A. Tagipour, P. Ambenje, K. Rupa Kumar, J. Revadekar and G. Griffiths, 2006: Global observed changes in daily climate extremes of temperature and precipitation. J. Geophys. Res., 111, D05109, doi:10.1029/2005JD006290.

Alexandersson, H., 1986: A homogeneity test applied to precipitation data. Journal of Climatology, 6, 661-675.

Asia News Network, China Daily, 2010: 'Finally, South China flood waters begin to recede'. Asiaone news, 28 June 2010 [Online]. Available at http://news.asiaone.com/News/Latest%2BNews/Asia/Story/A1Story20100628-224201.html (Accessed: 29 June 2010).

Barnett, T.P., J. C. Adam, and D.P. Lettenmaier, 2005: Potential impacts of a warming climate on water availability in snow-dominated regions. Nature, 438, 303–309.

Barnston, A. and R. Livezey, 1987: Classification, seasonality and persistence of low-frequency atmospheric circulation patterns. Monthly Weather Review, 115, 1083-1126.

Becker, S., H. Hartmann, M. Coulibaly, Q. Zhang, T. Jiang, 2008: Quasi periodicities of extreme precipitation events in the Yangtze River basin, China. Theor. Appl. Climatol., 94, 139-152.

Begueria, S., 2005: Uncertainties in partial duration series modeling of extremes related to the choice of the threshold value. Journal of Hydrology, 303: 215-230.

Böhm, U., M. Kücken, W. Ahrens, A. Block, D. Hauffe, K. Keuler, B. Rockel, and A. Will, 2006: CLM - the Climate Version of LM: Brief Description and long-term Applications. COSMO Newsletter, 6, 225-235.

Bordi, I., K. Fraedrich, J.M. Jiang, A. Sutera, 2004: Spatio-temporal variability of dry and wet periods in eastern China. Theoretical and Applied Climatology 79, 81-91.

Boyd, Milton, Jeffrey Pai, Zhang Qiao and Wang Ke, 2011: Crop Insurance Principles and Risk Implications for China. Human and Ecological Risk Assessment: An International Journal, Volume 17, Issue 3, 554-565.

Buishand, T.A., 1982: Some methods for testing the homogeneity of rainfall records. Journal of Hydrology, 58, 11-27.

Chen, W.L., Z.H. Jiang, L. Li, and P. Yiou, 2011: Simulation of regional climate change under the IPCC A2 scenario in southeast China. Clim Dyn, 36, 491–507.

Cheng, Hefa and Yuanan Hu, 2012: Improving China's water resources management for better adaptation to climate change. Climatic Change, Volume 112, Number 2, 253-282.

Chou, C., 2004: Establishment of the Low-Level Wind Anomalies over the Western North Pacific during ENSO Development. Journal of Climate, 17, 2195-2212.

Chu, Z.X., Zhai, S.K., Lu, X.X., Liu, J.P., Xu, J.X., Xu, K.H., 2009: A quantitative assessment of human impacts on decrease in sediment flux from major Chinese rivers entering the western Pacific Ocean. Geophys. Res. Lett. 36, L19603. doi:10.1029/2009GL039513.

CMA, 2010: Provincial Disaster Statistics for Guangxi and Guangdong Province 1983-2009. China Meteorological Administration (CMA), Beijing.

Corder, G.W. and D.I. Foreman, 2009: Nonparametric statistics for non-statisticians: a step-by-step approach. John Wiley and Sons, New Jersey, p.264.

Davison, A., and D. Hinkley, 1997: Bootstrap Methods and their Application. Cambridge series in Statistical and Probabilistic Mathematics, Cambridge University Press, Cambridge.

Ding, Y., Z. Wang, and Y. Sun, 2008: Inter-decadal variation of the summer precipitation in East China and its association with decreasing Asian summer monsoon Part I Observed evidences. Int. J. Climatol., 28, 1139–1161.

Duchesne, P., 2006: Testing for multivariate autoregressive conditional heteroskedasticity using wavelets. Journal Computational Statistics & Data Analysis, Volume 51, Issue 4.

Easterling, D. R., J. L. Evans, P. Y. Groisman, T. R. Karl, K. E. Kunkel, and P. Ambenje, 2000: Observed Variability and Trends in Extreme Climate Events: A Brief Review. Bull. Amer. Meteor. Soc., Vol. 81, No. 3, 417-425.

Feng, S., S. Nadarajah, and Q. Hu, 2007: Modeling Annual Extreme Precipitation in China Using the Generalized Extreme Value Distribution. Journal of the Meteorological Society of Japan, 85 (5), 599-613.

Gao, C., M. Gemmer, X. Zeng, L. Bo, B. Su, and Y. Wen, 2010: Projected streamflow in the Huaihe River Basin (2010–2100) using artificial neural network. Stochastic Environmental Research and Risk Assessment, 24 (5), 685-697.

Gemmer, M., Jiang, T., Su, B.D., Kundzewicz, Z.W., 2008: Seasonal precipitation changes in the wet season and their influence on flood/drought hazards in the Yangtze River Basin, China. Quaternary International, 186, 12-21.

Gemmer, M., S. Becker, and T. Jiang, 2004: Observed Monthly Precipitation Trends in China 1951-2002. Theoretical and Applied Climatology, 77, 39-45.

Hamed, K. and A.R. Rao, 1999: Flood Frequency Analysis (New Directions in Civil Engineering). CRC Press, 1 edition, 376 pp.

Hattermann, F.F. and Z.W. Kundzewicz (Eds.), 2010: Water Framework Directive: Model Supported Implementation. A Water Manager's Guide. IWA (International Water Association) Publishing. London, New York, 282 pp.

Hayes, M.J., 2006: Drought Indices. Website of the National Drought Mitigation Center: http://www.drought.unl.edu/whatis/Indices.pdf (accessed 19 March 2010).

Hollweg, H.-D. et al., 2008: Ensemble Simulations over Europe with the Regional Climate Model CLM forced with IPCC AR4 Global Scenarios. Gruppe Modelle & Daten, Technical Report No. 3, Support for Climate- and Earth System Research at the Max Planck Institute for Meteorology, Hamburg, ISSN 1619-2257.

Hoskins, B.J., 2003: Atmospheric processes and observations. Phil. Trans. R. Soc. Lond. A., 361, 1945-1960.

Hu, Y.R., S. Maskey, and S. Uhlenbrook, 2012: Trends in temperature and rainfall extremes in the Yellow River source region, China. Climatic Change, 110, 403–429.

IPCC SRES, 2000: Special Report on Emissions Scenarios: A special report of Working Group III of the Intergovernmental Panel on Climate Change, Nakićenović, N., and Swart, R., ed., Cambridge University Press.

IPCC, 2012: Managing the Risks of Extreme Events and Disasters to Advance Climate Change Adaptation. A Special Report of Working Groups I and II of the Intergovernmental Panel on Climate Change [Field, C.B., V. Barros, T.F. Stocker, D. Qin, D.J. Dokken, K.L. Ebi, M.D. Mastrandrea, K.J. Mach, G.-K. Plattner, S.K. Allen, M. Tignor, and P.M. Midgley (eds.)]. Cambridge University Press, Cambridge, UK, and New York, NY, USA, 582 pp.

Jenkins, G. and J, Lowe, 2003: Handling uncertainties in the UKCIP02 scenarios of climate change. Hadley Centre technical note 44.

Jiang, T., Y.D. Chen, C. Xu, X. Chen, X. Chen, and V.P. Singh, 2007: Comparison of hydrological impacts of climate change simulated by six hydrological models in the Dongjiang Basin, South China. Journal of Hydrology, 336, 316– 333.

Kalnay et al., 1996: The NCEP/NCAR 40-year reanalysis project. Bulletin of the American Meteorological Society, 77, 437-470.

Kay, A., Davies, H., Bell, V., Jones, R., 2009: Comparison of uncertainty sources for climate change impacts: flood frequency in England. Climatic Change, 92, 41–63.

Kharin, V.V., F.W. Zwiers, X. Zhang and G.C. Hegerl, 2007: Changes in temperature and precipitation extremes in the IPCC ensemble of global coupled model simulations. Journal of Climate, 20, 1419-1444, DOI: 10.1175/JCLI4066.1.

Klein Tank, A.M.G., F. Zwiers, and X. Zhang, 2009: Guidelines on - Analysis of extremes in a changing climate in support of informed decisions for adaptation. World Meteorological Organisation (WMO), Climate Data and Monitoring, WCDMP-No. 72, WMO-TD No. 1500, Geneva, Switzerland.

Krysanova, V., Bronstert, A., Müller-Wohlferl, D.I., 1999: Modelling river discharge for large drainage basins: from lumped to distributed approach. Hydrological science Journal, 44, 313-333.

Leung, Y., and M. Wu, 2005: Regime Shift in Summer Rainfall in Southern China. Seventh Joint Meeting of Seasonal Prediction on East Asian Summer Monsoon, Nanjing, China, 11-13 May 2005, Reprint No. 586, Hong Kong Observatory.

Li, J. and Q. Zeng, 2003: A new monsoon index and the geographical distribution of the global monsoons. Advances in Atmospheric Sciences, 20 (2), 299-302.

Liu, L., T. Jiang, and F. Yuan, 2009: Observed (1961-2007) and Projected (2011-2060) Climate Change in the Pearl River Basin. Advances in Climate Change Research, 5 (4), 209-214 (in Chinese).

Liu, L., Z. Liu, X. Ren, T. Fischer and Y. Xu, 2011: Hydrological impacts of climate change in the Yellow River Basin for the 21st century using hydrological model and statistical downscaling model. Quaternary International, Volume 244, Issue 2, 211-220.

Lü J.M., Ju J.H., Ren J.Z. et al., 2012: The influence of the Madden-Julian Oscillation, activity anomalies on Yunnan's extreme drought of 2009–2010. Sci China Earth Sci, 55, 98–112.

Ma, Z.G., L. Dan, and Y.W. Hu, 2004: The extreme dry/wet events in northern China during recent 100 years. Journal of Geographical Sciences, 14 (3), 275-281.

McKee, T.B., N.J. Doeskin, and J. Kleist, 1993: The relationship of drought frequency and duration to time scales. 8th Conference on Applied Climatology. American Meteorological Society, 179–184.

Menzel, L., Thieken, A.H., Schwandt, D., Bürger, G., 2006: Impact of climate change on the regional hydrology – scenario-based modeling studies in the German Rhine catchment. Natual Hazards, 38, 45-61.

Mertz, O., K. Halsnæs, J.E. Olesen, and K. Rasmussen, 2009: Adaptation to Climate Change in Developing Countries. Environmental Management, 43, 743–752.

Mishra, A.K. and V.P. Singh, 2010: A review of drought concepts. Journal of Hydrology, 391, 202–216.

MoST, 2006: National Assessment Report on Climate Change. MoST (Ministry of Science and Technology), CMA (China Meteorological Administration), CAS (Chinese Academy of Science), Science Press, Beijing, 422pp.

MoST, 2011: The Second National Assessment Report on Climate Change. MoST (Ministry of Science and Technology), CMA (China Meteorological Administration), CAS (Chinese Academy of Science), Science Press, Beijing, 710pp.

Nikulin, G. et al., (2011): Precipitation climatology in an ensemble of CORDEX-Africa regional climate simulations. Journal of Climate, submitted.

Palutikof, J.P., B.B. Brabson, D.H. Lister, and S.T. Adcock, 1999: A review of methods to calculate extreme wind speeds. Meteorol. Appl. 6, 119–132.

Parry, M., A. Evans, M. W. Rosegrant, and T. Wheeler, 2009: Climate Change and Hunger - Responding to the Challenge. World Food Programme, International Food Policy Research Institute, New York University Center on International Cooperation, Grantham Institute at Imperial College London, Walker Institute, University of Reading (United Kingdom).

Parry, M.L., O.F. Canziani, J.P. Palutikof, P.J. van der Linden and C.E. Hanson, (Eds.), 2007: Contribution of Working Group II to the Fourth Assessment Report of the Intergovernmental Panel on Climate Change. Cambridge University Press, Cambridge, United Kingdom and New York, NY, USA.

Peterson, T.C., D.R. Easterling, T.R. Karl, et al., 1998: Homogeneity adjustments of in situ atmospheric climate data: a review. International Journal of Climatology, 18, 1493-1517.

Prudhomme, C., Jakob, D., Svensson, C. 2003: Uncertainty and climate change impact on the flood regime of small UK catchments. Journal of Hydrology, 277, 1–23.

Rockel B., A. Will and A. Hense, 2008: The Regional Climate Model COSMO-CLM (CCLM). Meteorologische Zeitschrift, Vol. 17, No. 4, 347-348.

Ruosteenoja, K., Carter, T.R., Jylhä, K., Tuomenvirta, H., 2003: Future climate in world regions: an intercomparison of model-based projections for the new IPCC emissions scenarios. The Finnish Environment 644, Finnish Environment Institute, Helsinki.

Schönwiese, C.-D., 2006: Praktische Statistik für Meteorologen und Geowissenschaftler. 4. Auflage, Gebrüder Bornträger Verlagsbuchhandlung, Berlin, Stuttgart, S.302.

Seidel, D.J. and J.R. Lanzante, 2004: An assessment of three alternatives to linear trends for characterizing global atmospheric temperature changes. Journal of Geophysical Research, 109, D14108, doi:10.1029/2003JD004414.

Sheskin, D.J., 2004: Handbook of parametric and nonparametric statistical procedures. 3rd Edition, Chapman & Hall, CRC Press, Boca Raton, p.1193.

Solomon, S., D. Qin, M. Manning, Z. Chen, M. Marquis, K.B. Averyt, M.Tignor and H.L. Miller (Eds.), 2007: Contribution of Working Group I to the Fourth Assessment Report of the Intergovernmental Panel on Climate Change. Cambridge University Press, Cambridge, United Kingdom and New York, NY, USA.

Steppeler, J., Doms, G., Schättler, U., Bitzer, H.W., Gassmann, A., Damrath, U., and Gregoric, 2003: Meso-gamma scale forecasts using the nonhydrostatic model LM. Meteorol. Atmos.Phys., 82, 75–96.

Su, B., T. Jiang, and W. Jin, 2005: Recent trends in observed temperature and precipitation extremes in the Yangtze River basin, China. Theor. Appl. Climatol. 83 (2006), 139-151.

Su, B., Z. Kundzewicz, and T. Jiang, 2008: Simulation of extreme precipitation over the Yangtze River Basin using Wakeby distribution. Theor. Appl. Climatol., 96 (2009), 209-219.

Taylor, W.A., 2000: Change-Point Analysis: A Powerful New Tool For Detecting Changes. http://www.variation.com/cpa/tech/changepoint.html (accessed 29 August 2010).

The World Bank, 2007: China - Innovations in Agricultural Insurance - Promoting Access to Agricultural Insurance for Small Farmers. The World Bank, Sustainable Development, East Asia & Pacific Region Finance and Private Sector Development, 108 pages.

Torrence, C. and G.P. Compo, 1998. A practical guide to wavelet analysis. Bulletin of the American Meteorological Society, 79, 61-78.

Trenberth, K.E., P.D. Jones, P. Ambenje, R. Bojariu, D. Easterling, A. Klein Tank, D. Parker, F. Rahimzadeh, J.A. Renwick, M. Rusticucci, B. Soden, and P. Zhai, 2007: Observations: Surface and Atmospheric Climate Change. In: Climate Change 2007: The Physical Science Basis. Contribution of Working Group I to the Fourth Assessment Report of the Intergovernmental Panel on Climate Change [Solomon, S., D. Qin, M. Manning, Z. Chen, M. Marquis, K.B. Averyt, M. Tignor and H.L. Miller (eds.)]. Cambridge University Press, Cambridge, United Kingdom and New York, NY, USA.

Turvey, C.G. and Rong Kong, 2010: Weather risk and the viability of weather insurance in China's Gansu, Shaanxi, and Henan provinces. China Agricultural Economic Review, Vol. 2 Issue 1, 5 – 24.

Varis, O., M. Kummu, and A. Salmivaara, 2012: Ten major rivers in monsoon Asia-Pacific: An assessment of vulnerability. Applied Geography, 32, 441-454.

Wang, H.J., J.Q. Sun, H.P. Chen, et al., 2012: Extreme Climate in China: Facts, Simulation and Projection. Meteorologische Zeitschrift, Band 21, Heft 3, 279 – 304.

Wilby, R.L. and Dawson, C.W., 2007: SDSM 4.2 - A decision support tool for the assessment of regional climate change impacts: user manual, UK.

Wilks, D.S., 2006: Statistical Methods in the Atmospheric Sciences. 2nd Ed, International Geophysics Series, Vol. 91, Academic Press, 627 pp.

Wu Z.Y., G.H. Lu, L. Wen, and C.A. Lin, 2011: Reconstructing and analyzing China's fifty-nine year (1951–2009) drought history using hydrological model simulation. Hydrol. Earth Syst. Sci., 15, 2881–2894.

Xu, K., J. D. Milliman, and H. Xu, et al. 2010: Temporal trend of precipitation and runoff in major Chinese Rivers since 1951. Global and Planetary Change, 73, 219–232.

Xu, K.H. and J.D. Milliman, 2009: Seasonal variations of sediment discharge from the Yangtze River before and after impoundment of the Three Gorges Dam. Geomorphology, 104 (3–4), 276–283.

Yang, T., Q. Shao, Z-C. Hao, X. Chen, Z. Zhang, C-Y. Xu, and L. Sun, 2010: Regional frequency analysis and spatio-temporal pattern characterization of rainfall extremes in the Pearl River Basin, China. Journal of Hydrology, 380 (3-4), 386-405.

Yin, Z., Y. Cai, X. Zhao, and X. Chen, 2009: An analysis of the spatial pattern of summer persistent moderate-to-heavy rainfall regime in Guizhou Province of Southwest China and the control factors. Theor Appl Climatol, 97, 205–218.

Yu, S., X. Shi, and X. Lin, 2009: Interannual variation of East Asian summer monsoon and its impacts on general circulation and precipitation. Journal of Geographical Science, 19, 67-80.

Zeng, X.F., Zbigniew, W.K., Zhou, J.Z., Su, B.D., (2012): Discharge projection in the Yangtze River Basin under different emission scenarios based on the Artificial Neural Networks. Quaternary International. doi:10.1016/j.quaint.2011.06.009.

Zhai, P.M., H.B. Zhang, H. Wan, and X.H. Pan, 2004: Trends in Total Precipitation and Frequency of Daily Precipitation Extremes over China. Journal of Climate, Volume 18, 1096-1108.

Zhai, P.M., Sun, A.J., Ren, F.M., Liu, X.L., Gao, B., Zhang, Q., 1999: Changes of climate extremes in China. Climate Change, 42, 203–218.

Zhang, Q., C. Xu, and Z. Zhang, 2009: Trends and abrupt changes of precipitation maxima in the Pearl River basin, China. Atmospheric Science Letters, 10 (2), 132-144.

Zhang, S., X.X. Lu, D.L. Higgitt, C.T.A. Chen, J. Han, H. Sun, 2008: Recent changes of water discharge and sediment load in the Zhujiang (Pearl River) Basin, China. Global and Planetary Change, 60, 365-380.

Zhao, G., X. Mu, G. Hoermann, N. Fohrer, M. Xiong, B.D. Su, X. Li, (2012): Spatial patterns and temporal variability of dryness/wetness in the Yangtze River Basin, China. Quaternary International, doi: 10.1016/j.quaint.2011.10.020.

Erklärung

Hiermit erkläre ich, Thomas Fischer (geb. 20.09.1978), dass ich die beigefügte Dissertation selbstständig verfasst und keine anderen als die angegebenen Hilfsmittel genutzt habe. Alle wörtlich oder inhaltlich übernommenen Stellen habe ich als solche gekennzeichnet.

Ich versichere, dass ich die beigefügte Dissertation nur in diesem und keinem anderen Promotionsverfahren eingereicht habe und, dass diesem Promotionsverfahren keine gescheiterten Promotionsverfahren vorausgegangen sind.

Ich erkläre außerdem, dass mir die Gelegenheit zum vorliegenden Promotionsverfahren nicht kommerziell vermittelt wurde. Ich erkläre insbesondere, dass ich keine Organisation eingeschalten habe, die gegen Entgelt Betreuer für die Anfertigung von Dissertationen sucht oder die für ihn die ihm obliegenden Pflichten hinsichtlich der Prüfungsleistungen ganz oder teilweise erledigt.

_____ _____

Ort, Datum Unterschrift

List of Manuscripts and Personal Contribution

The results of the peer-reviewed or submitted manuscripts form the basis of this cumulative thesis. In the Appendix, each manuscript is presented in its published or submitted form (Appendix I – VII). Here, a list of all manuscripts with their current citation is shown. Additionally, for a quantification of the author's individual participation in the (a) scientific ideas, (b) data generation, (c) analysis and interpretation, and (d) paper writing of each manuscript, the relative contribution is provided accordingly.

Manuscript 1 (Appendix I):
Fischer, T., M. Gemmer, L. Liu and B. Su, 2011: Temperature and precipitation trends and dryness/wetness pattern in the Zhujiang River Basin, South China, 1961-2007. *Quaternary International*, Volume 244, Issue 2, 138-148.

(a) 70% (b) 60% (c) 50% (d) 70%

Manuscript 2 (Appendix II):
Gemmer, M., T. Fischer, T. Jiang, B. Su and L. Liu, 2011: Trends in Precipitation Extremes in the Zhujiang River Basin, South China. *Journal of Climate*, Volume 24, 750–761.

(a) 30% (b) 40% (c) 30% (d) 40%

Manuscript 3 (Appendix III):
Fischer, T., M. Gemmer, L. Liu and T. Jiang, 2012: Change-points in climate extremes in the Zhujiang River Basin, South China, 1961-2007. *Climatic Change*, Volume 110, 783-799.

(a) 80% (b) 70% (c) 70% (d) 80%

Manuscript 4 (Appendix IV):
Fischer, T., B. Su, Y. Luo and T. Scholten, 2012: Probability distribution of precipitation extremes for weather-index based insurance in the Zhujiang River Basin, South China. *Journal of Hydrometeorology*, Volume 13, 1023-1037.

(a) 70% (b) 80% (c) 70% (d) 80%

Manuscript 5 (Appendix V):

Fischer, T., M. Gemmer, B. Su and T. Scholten, (2012): Long-term meteorological and hydrological dryness and wetness conditions in the Zhujiang River Basin, South China. Accepted for publication in *Hydrology and Earth System Sciences*.

(a) 60% (b) 60% (c) 60% (d) 70%

Manuscript 6 (Appendix VI):

Fischer, T., C. Menz, B. Su, and T. Scholten, (2012): Simulated and projected climate extremes in the Zhujiang River Basin, South China, using the regional climate model COSMO-CLM. Accepted for publication in *International Journal of Climatology*.

(a) 70% (b) 80% (c) 70% (d) 70%

Manuscript 7 (Appendix VII):

Liu, L., T. Fischer, T. Jiang and Y. Luo, (2012): Comparison of uncertainties in projected flood frequency of the Zhujiang River, South China. Accepted for publication in *Quaternary International*.

(a) 30% (b) 30% (c) 30% (d) 40%

Appendices I – VII

Appendix I

Fischer, T., M. Gemmer, L. Liu and B. Su, 2011: Temperature and precipitation trends and dryness/wetness pattern in the Zhujiang River Basin, South China, 1961-2007. *Quaternary International*, Volume 244, Issue 2, 138-148.

Quaternary International 244 (2011) 138–148

Contents lists available at ScienceDirect

Quaternary International

journal homepage: www.elsevier.com/locate/quaint

Temperature and precipitation trends and dryness/wetness pattern in the Zhujiang River Basin, South China, 1961–2007

Thomas Fischer*, Marco Gemmer, Liu Lüliu, Su Buda

National Climate Center of the China Meteorological Administration, Beijing 100 081, China

ARTICLE INFO

Article history:
Available online 20 August 2010

ABSTRACT

Spatial and temporal characteristics of temperature and precipitation in the Zhujiang River Basin, South China, are analysed in order to identify tendencies in dryness and wetness. Trend tests are applied to daily temperature and precipitation data from 1961 to 2007 of 192 weather stations. Nine indicators are applied in order to detect cycles of dryness and wetness and are compared with the drought indices Standardized Precipitation Index (SPI) and Palmer Drought Severity Index (PDSI).

Tendencies in temperature and precipitation characteristics can be observed. Significant positive trends (>90% confidence level) can be found for annual temperature, number of warm days, longest warm period, no rain days, and longest dry period. A significant increase in temperature by more than 0.7 K from 1961 to 2007 can be observed in the entire basin and the coastal and far western areas in particular. Negative trends are observed for annual cool days, cool period, wet days, and wet period. Almost no significant trends in annual mean and extreme precipitation are detected. Rain days decreased, and a tendency to longer dry periods and shorter wet periods can be observed.

The magnitude of indices describing dryness has increased in the Zhujiang River Basin, and dry periods have become longer while wet periods have shortened in time. Rainfall intensity has increased along the coastline and in the far west of the catchment. This tendency can be partially explained by the weakening of the East Asian Summer Monsoon. Regarding the high temperature increases, the influences of the urban heat island effect due to urbanization and industrialization, especially along the coast and at the delta, should be considered. The high station density and data quality are very useful for describing detailed changes in wetness and dryness in the Zhujiang River basin.

1. Introduction

Extreme weather events are very likely to cause damage to ecosystems and society. Increasing intensity and/or frequency of such events are of great concern and have been substantiated by various studies on future climate change throughout the world (e.g. Trenberth et al., 2007). An increase in temperature and precipitation extremes will lead to prolonged, more frequent droughts and might also lead to an expansion of drought affected areas (Solomon et al., 2007). For south China, many studies focused on recent and future wet and dry conditions, and extremes of climate and weather events have been observed and predicted (e.g. Ren et al., 2005a,b; Qian and Lin, 2005; Ding et al., 2007; Yang et al., 2010). Changing climatic patterns were observed in southeast China, where an increase in annual precipitation by 60–130 mm during the last fifty years occurred (Ding et al., 2007). In contrast, Qian and Lin (2005) comprehensively analysed regional characteristics of daily precipitation indices at 494 stations in China (1961–2000) and showed that in coastal southeast China, a negative decadal tendency in annual and summer precipitation is apparent.

Bordi et al. (2004) analysed the variability of dry and wet periods from 1951 to 2000 at 160 stations in eastern China. They used the standardized precipitation index (SPI) and the principal component analysis to assess the climatic conditions and the co-variability of the stations. They found that more frequent dry conditions are experienced in the northern part of eastern China, and concluded that long-term fluctuations range from 16 to 4 years.

Zhai et al. (2009a) applied SPI and Palmer's drought severity index (PDSI) to identify the spatial variation of dry and wet conditions in mainland China from 1961 to 2005 and developed an

* Corresponding author. China Meteorological Administration (CMA), National Climate Centre (NCC), 46, Zhongguancun Nandajie, Haidian, Beijing 100 081, China. Tel.: +86 10 5899 9096 (office); fax: +86 10 6217 6804.
E-mail address: thomas.fischer1@cimonline.de (T. Fischer).

1040-6182/$ – see front matter © 2010 Elsevier Ltd and INQUA. All rights reserved.
doi:10.1016/j.quaint.2010.08.010

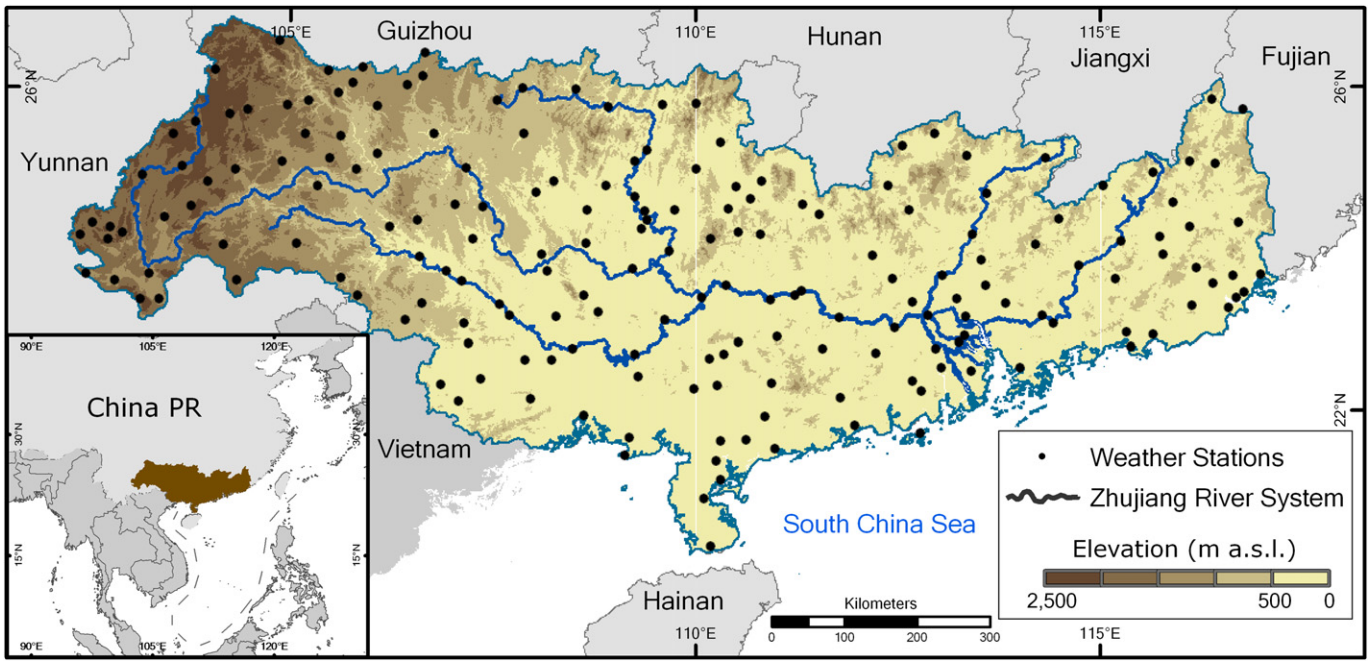

Fig. 1. Topographical sketch map of the Zhujiang River Basin with 192 weather stations.

indication for water resource availability. In their study, 58 stations were analysed for the Zhujiang River Basin (including Hainan), and no significant trends in frequencies of dry/wet days and runoff anomalies in this region were detected.

Zhang et al. (2009a) analysed the SPI for the winter and summer season at 41 stations in the Zhujiang River Basin from 1960 to 2005 and detected few decreasing trends. No statistical significant decreasing trends of severe wet months in summer were found. In contrary, a non-significant increasing trend of wet conditions in winter was detected.

Gemmer et al. (in preparation) observed trends to dryer conditions and stronger precipitation intensities in the Zhujiang River Basin from 1961 to 2007. Increasing annual air temperature (+1.8 °C) 1961–2007 has been detected by Liu et al. (2009) with highest increasing rates in winter and less temperature increase in summer in the Zhujiang River Basin. They also observed an increase of annual precipitation. Zhai et al. (2009b) simulated the SPI with projections of ECHAM5 for 2001–2050. For the Zhujiang River Basin, a trend to more wet conditions in the first half of the 21st century under the SRES-A1B scenario was projected.

These existing studies on climate and wet/dry conditions in the Zhujiang River Basin (and China) deal with different climate variables, number of stations, temporal settings, and time-series. In the face of anticipated climate change, profound information to adapt to changing risks of droughts and floods is very necessary. Therefore, more detailed information on the regional and temporal distribution of dry and wet conditions in the Zhujiang River Basin is needed. This study focuses on the observation of annual temperature and precipitation conditions and their spatio-temporal pattern in the Zhujiang River Basin. The objective of the study is to identify and analyze tendencies in dryness and wetness, making use of the up-to-date highest number of stations and longest high-quality time-series available. The novel approach in combining trend and correlation analysis of various extreme temperature and precipitation indicators and two indices on dryness and wetness gives meaningful information. This is supported by a clear and simple visualization of the results.

2. Data and methodology

2.1. Regional setting

The study is carried out for the Zhujiang River Basin (ZRB) which is located in South China. A comprehensive description of the catchment is provided by Zhai et al. (2009a). The basin covers 579,000 km^2 and has tropical and sub-tropical climates. In summer, the East Asian Summer Monsoon, and in winter, the East Asian Winter Monsoon, influences the region. The basin is covered by mountainous areas in the western part and lowlands in the central and south-eastern parts. Due to this topography, the main stream flow directions of the river system are southeastwards. Zhujiang River discharges into the South China Sea in a large network delta (Zhujiang River Delta). An elevation map including the main river system and the location of 192 weather stations is provided in Fig. 1. Annual temperature in the ZRB ranges from 13 °C in the western and north-western elevated parts of the basin to 24 °C in the coastal lowlands in the south and southeast (Fig. 2). This distribution can be mainly explained by the driving climate factors of the transition from maritime (lowlands) to continental (highlands) of the stations.

2.2. Data

Data sets of 192 weather stations with long-term daily mean temperature and precipitation records from 1st January 1961 to 31st December 2007 in the ZRB are used. The standardized precipitation index (SPI) and the Palmer drought severity index (PDSI) are calculated for data of 51 stations evenly distributed in the ZRB for the period 1st January 1961 to 31st December 2004. Data was provided by the National Meteorological Information Center (NMIC) of the China Meteorological Administration (CMA). The NMIC controlled all data sets for quality (Qian and Lin, 2005) and checked the temperature data for homogeneity using either the standard normal homogeneity test (Alexandersson, 1986), the departure accumulating method (Buishand, 1982), or the moving *t*-test (Peterson et al., 1998). The temperature data records used in

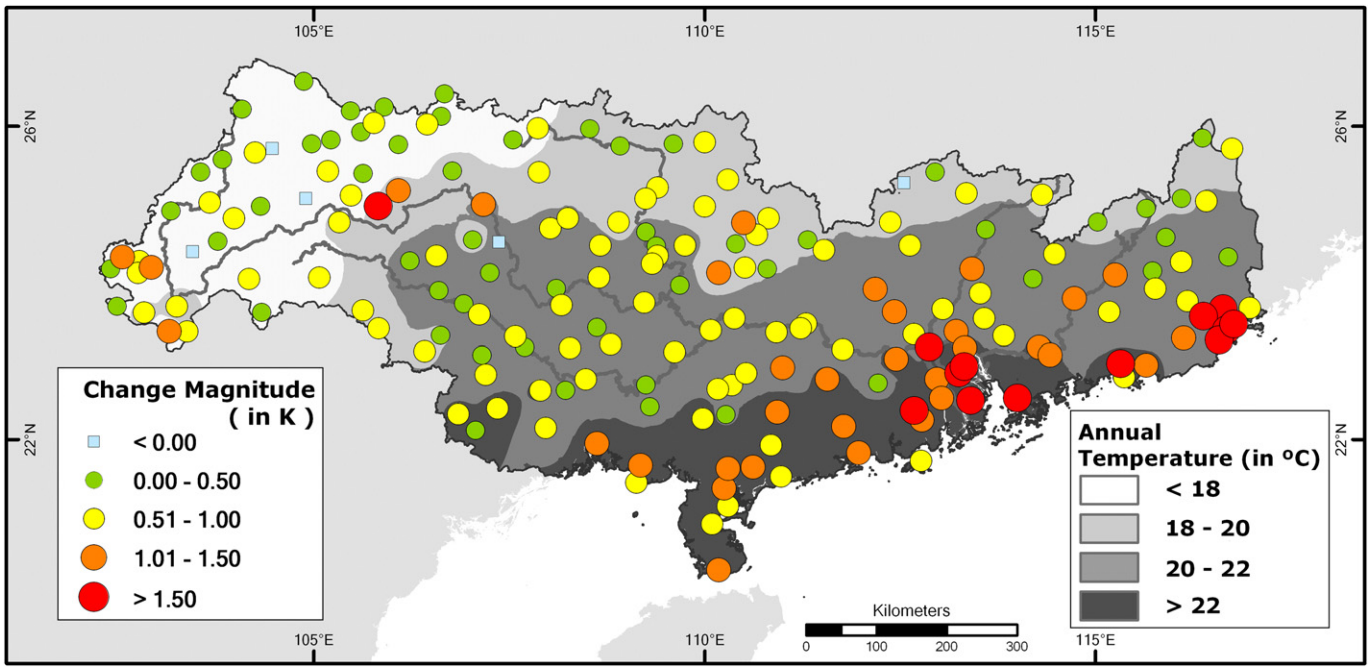

Fig. 2. Annual mean temperature (shading) and temperature change magnitude (symbols) in the Zhujiang River Basin 1961–2007.

this study have been homogeneity-adjusted (Song et al., 2004; Ren et al., 2005a,b), whereas the precipitation data records remain unadjusted. Temperature and precipitation records show less than 0.1% data gaps.

2.3. Methodology

In order to analyse and describe the temporal and spatial distribution of temperature and precipitation changes, 11 indicators were created. Five temperature-based and six precipitation-based indicators reflect intensity, trend, and their possible correspondence in dryness/wetness. In order to determine dryness/wetness, two drought indices (SPI, PDSI) have been calculated and analysed. A list of all indicators created and their definitions can be found in Table 1. Most indicators were defined on fixed terms or thresholds predetermined by CMA or international research standards; similar indicators have been used in various studies (e.g. Beniston and Stephenson, 2004; Schmidli and Frei, 2005; Qian and Lin, 2005; Li et al., 2010). The peaks over threshold indicators (P_{90}, T_{90}, T_{10}) were calculated from daily mean temperature or precipitation records for the time period 1961 to 2007. The approach using percentile values gives insights to the intensity of local changes of climate pattern and thus a better comparability between single stations (Qian and Lin, 2005; Li et al., 2010).

In this paper, frequencies of dry and wet conditions from 1961 to 2004 are examined by calculating and analyzing two drought indices (SPI and PDSI). The Standardized Precipitation Index (SPI) is a meteorological index which was developed by McKee et al. (1993) in order to quantify precipitation deficits/excesses in different climate regimes. In general the SPI is the difference of the (annual/monthly) total precipitation and its mean value, divided by the standard deviation of the time series. Dry and wet events are classified by their severity and calculated for multiple time scales. The standardization is based on an equal probability transformation which depends critically on the assumed statistical distribution (Bothe et al., 2009). Following the studies by McKee et al. (1993), Bordi et al. (2004), and Zhai et al. (2009a), the long-term (1961–2004) precipitation record was fitted to a gamma distribution to obtain the annual conditions of dryness or wetness for the study area. Positive (negative) SPI values indicate higher (lower) than median precipitation (Zhai et al., 2009a). Following McKee et al. (1993), the classification of severity varies between

Table 1
Definition of precipitation and temperature indices.

ID	Name	Definition	Unit
P_{mean}	Mean precipitation	Annual total precipitation	mm
P_{rain}	Rain days/Wet days	Annual number of days with precipitation above or equal to 0.1 mm/d	day
P_{wet}	Wet period	Annual longest rain day (P_{rain}) period	day
$P_{no\ rain}$	No rain days/Dry days	Annual number of days with precipitation below 0.1 mm/d	day
P_{dry}	Dry period	Annual longest no rain day ($P_{no\ rain}$) period	day
P_{90}	Extreme precipitation	Annual number of days above the 90-Percentile of daily precipitation (1961-2007)	day
T_{mean}	Mean temperature	Annual average temperature based on daily mean temperatures	°C
T_{90}	Warm days	Annual number of days above the 90-percentile of daily mean temperatures (1961–2007)	day
T_{warm}	Warm period	Annual longest warm day (T_{90}) period	day
T_{10}	Cool days	Annual number of days below the 10-Percentile of daily mean temperatures (1961-2007)	day
T_{cool}	Cool period	Annual longest cool day (T_{10}) period	day
SPI	Standardized precipitation index		
PDSI	Palmer drought severity index		

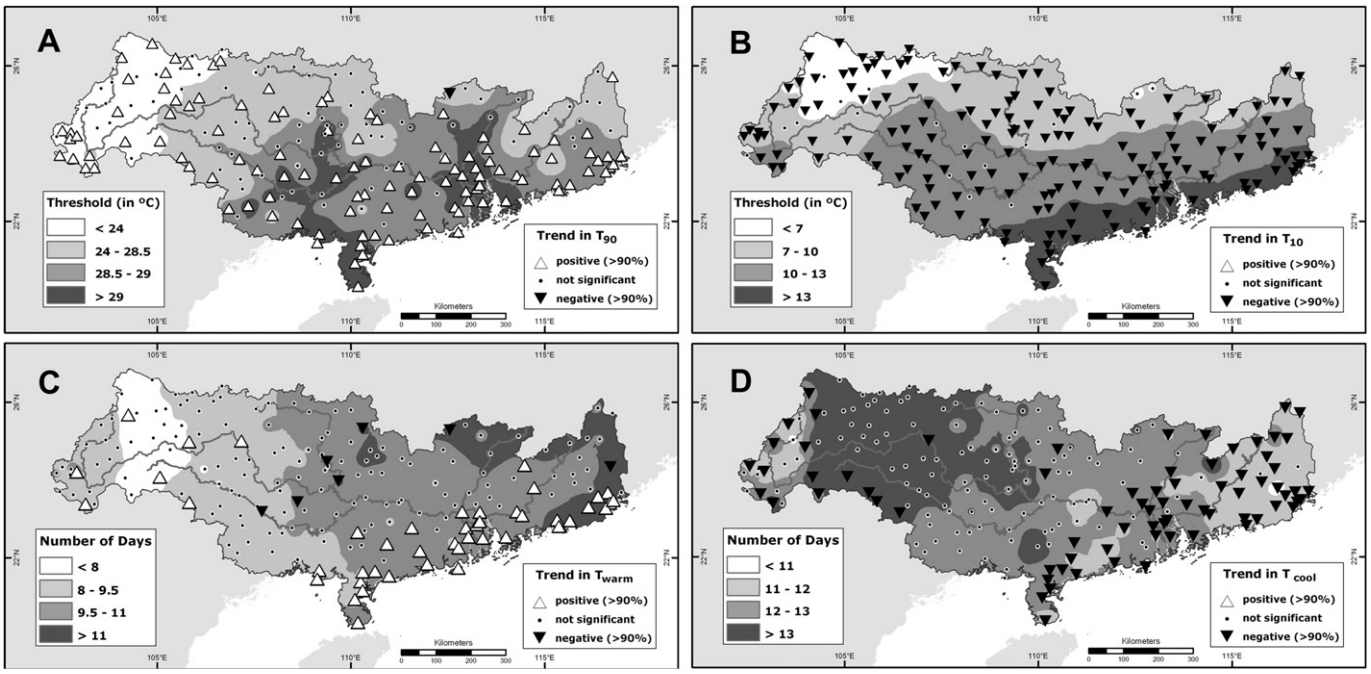

Fig. 3. Observed mean thresholds (shadings) of (A) annual warm days (T_{90}) and (B) annual cool days (T_{10}); observed average days (shadings) of (C) annual longest warm period (T_{warm}) and (D) annual longest cool period (T_{cool}); (A–D) additionally with trends (1961–2007, symbols) at the 90% confidence level in the Zhujiang River Basin.

below −2 (extremely dry) and above 2 (extremely wet). In this analysis, dry and wet years are defined when the annual SPI is below −1 (moderately dry) and above 1 (moderately wet) respectively.

The results of the Palmer Drought Severity Index (PDSI) on annual basis from 1961 to 2004 were analysed to quantify precipitation deficits/excesses and to compare it with the SPI and climate indicators. The PDSI is based on the water balance equation and incorporates precipitation, temperature, and soil moisture data (Hayes, 2006). For this study, annual moisture anomalies between 1961 and 2004 were calculated and converted to severity degrees. Based on Palmer's studies, the classification of severity varies between below −4 (extremely dry) and above 4 (extremely wet) (Hayes, 2006). Similar to the SPI, dry or wet years are defined when the annual PDSI falls below −2 (moderately dry) or exceeds 2 (moderately wet) respectively.

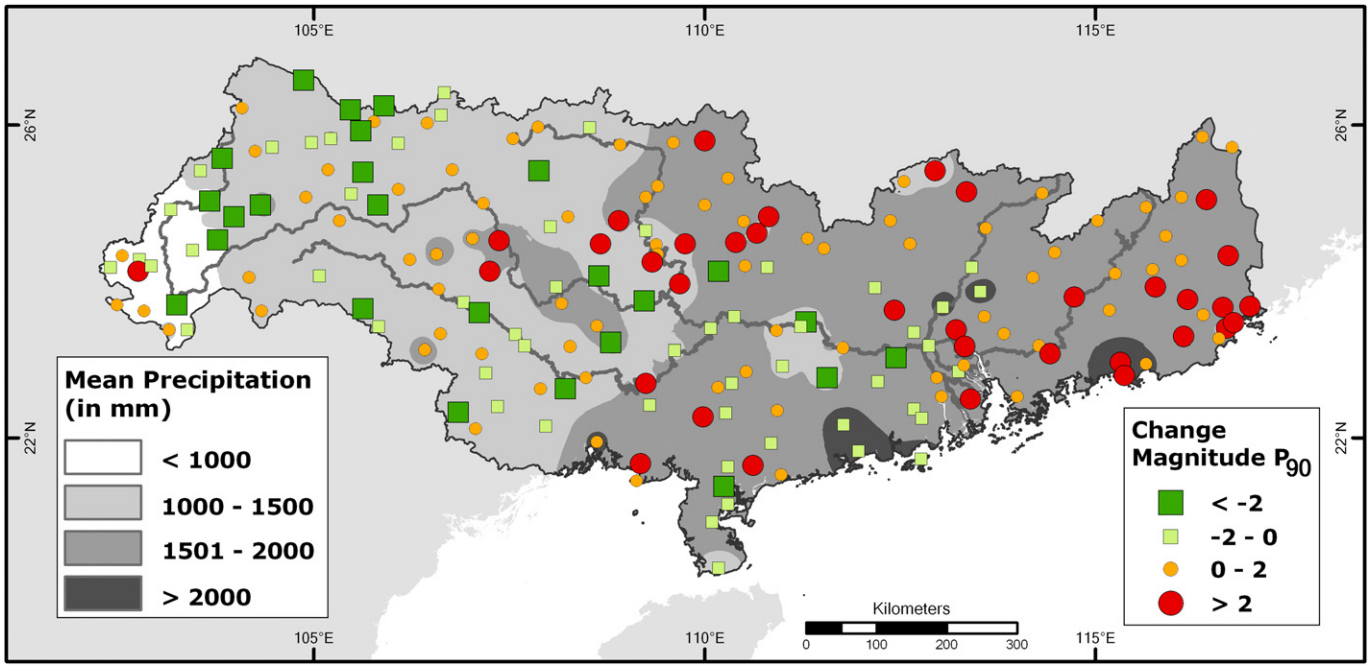

Fig. 4. Annual mean precipitation (shadings) and extreme precipitation (P_{90}) change magnitude (symbols) in the Zhujiang River Basin 1961–2007.

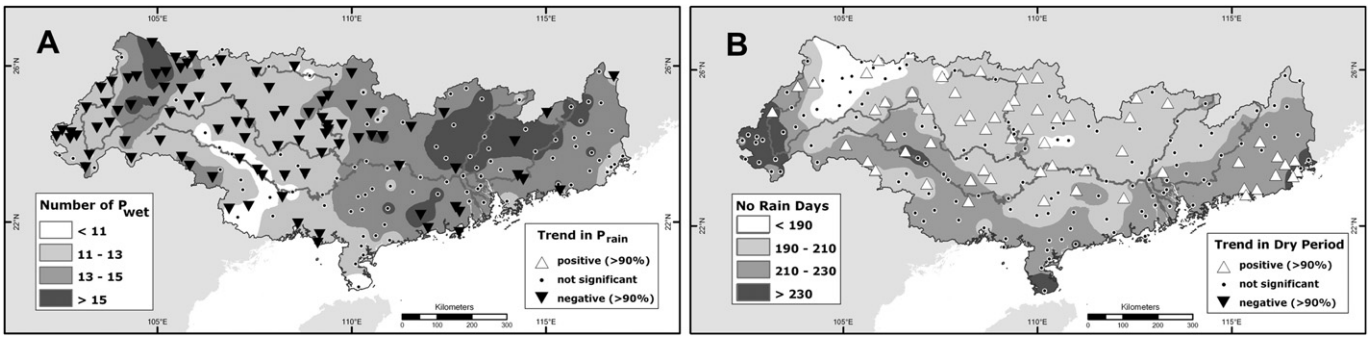

Fig. 5. Observed average number (shading) in (A) annual rain days (P_{rain}) and (B) annual no rain days ($P_{no\ rain}$); both with trends (1961–2007, symbols) of (A) annual longest wet period (P_{rain}) and (B) annual longest dry period (P_{dry}) at the 90% confidence level in the Zhujiang River Basin.

The trends and the absolute changes of the various indicators have been calculated by applying the parametric linear regression and the non-parametric Mann–Kendall test to the data of 192 (51 for SPI and PDSI) weather stations. The regression gradient for the time period 1961–2007 was determined for each station (Kundzewicz and Robson, 2004). Although the linear regression must be handled carefully as it mostly neglects the strong variability of factors in weather and climate data, the gradients reflect the tendencies of certain indicators in absolute terms and can have visual impact.

The Mann–Kendall test is applied on the assumption of independence of the time series. No serial correlation must exist within the time series, as this dependency influences the significance of the Mann-Kendall statistics. Following von Storch (1995), Hamad and Rao (1998), Yue and Wang (2002), and Bayazit and Önöz (2007), the serial correlation, the coefficient of variance, and the dimensionless slope of the linear regression were checked. When a time series shows an autocorrelation coefficient of lag-1 above the 5% significance level (i.e. $1.96/\sqrt{n}$) the pre-whitening method (PW) can be applied as it eliminates the influence of the serial correlation on the significance level of the Mann–Kendall test. The PW is not applicable if the coefficient of variance is small ($CV < 0.40$) or the dimensionless slope is large ($b > 0.005$) (Bayazit and Önöz, 2007). It has also no effect if the time series consists of a large sample size or a high correspondence with the regression gradient (Yue and Wang, 2002).

As some of the station-based time series in this study show a serial correlation, their coefficients of variance and dimensionless slopes were checked. When calculated for the original data series, the Mann–Kendall test statistics correspond very highly with the regression gradient (correlation above 0.95). Based on these results and the aforementioned reasoning of applying a method for eliminating the influence of serial correlation, no pre-whitening or similar method has been applied at these time-series. A comprehensive description on the application and

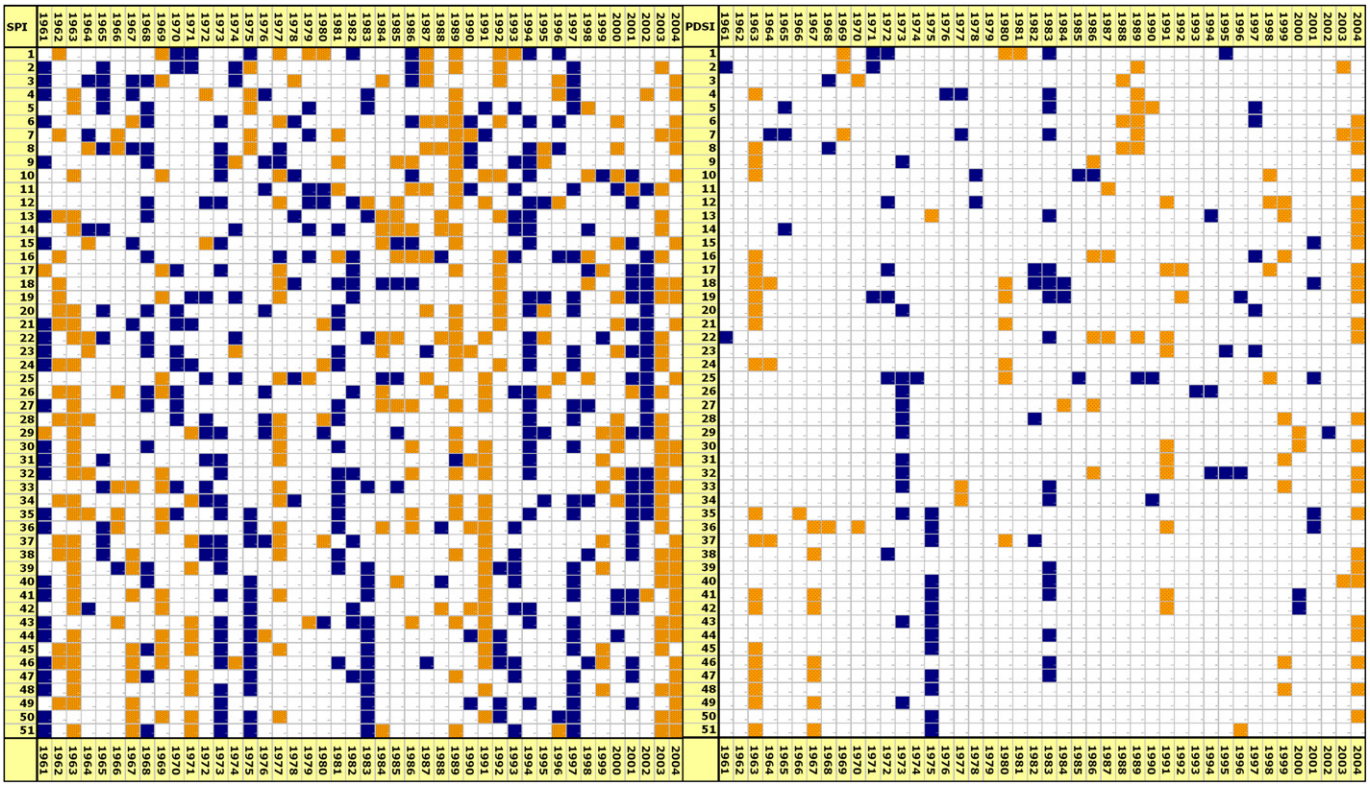

Fig. 6. Spatio-temporal distribution of moderate/severe/extreme dry and wet years according to SPI (left side) and PDSI (right side) for 51 stations (ordered from west to east longitude) in the Zhujiang River Basin 1961–2004.

Table 2
Correlation matrix of station-averaged annual indices in the Zhujiang River Basin 1961–2004.

	SPI	PDSI	P_{90}	Wet days	Wet period	Dry days	Dry period	Warm days	Warm period	Cool days
SPI	1									
PDSI	0.84	1								
P_{90}	0.91	0.78	1							
Wet days	0.81	0.82	0.67	1						
Wet period	0.48	0.46	0.42	0.54	1					
Dry days	−0.81	−0.82	−0.68	−1.00	−0.54	1				
Dry period	−0.43	−0.40	−0.32	−0.50	−0.23	0.51	1			
Warm days	−0.50	−0.45	−0.45	−0.56	−0.50	0.55	0.16	1		
Warm period	−0.21	−0.06	−0.20	−0.24	−0.16	0.23	0.11	0.69	1	
Cool days	−0.19	0.07	−0.20	0.17	−0.08	−0.15	−0.13	−0.13	−0.15	1

definition of the Mann–Kendall test is further provided by Yang et al. (2010), Liu et al. (2008), Zhang et al. (2009b) and Gemmer et al. (2004). The significance of positive or negative trends for the temperature- and precipitation-based indicators was expressed by using the 90% confidence level as threshold. Trends above this threshold only were considered as significant and used for the analyses.

The standard Pearson's product-moment coefficient was also used to identify the correlation and multiple correlation of the basin-averaged annual indicators. The results give insights to the dependency of the indicators to each other and relations to the power of impact can be drawn.

The indicators and trends were spatially interpolated using the Inverse Distance Weighting (IDW) method in the Geographical Information System ArcGIS. A raster image is created whose cell values are calculated using the weighted averages of 12 neighbouring stations. The weighting is based on the local influence of distant points (stations) which decrease with distance (Gemmer et al., 2004). As 192 (51) station values were used, the power parameter of each station was set to 2 to receive a reasonable and smooth visualization.

3. Results

3.1. Observed temperature trends and extremes

3.1.1. Annual and monthly temperature

Following the results of the Mann–Kendall test applied to the daily mean temperature time-series, significant positive trends of annual mean temperature can be observed for 157 of 192 stations. The highest number of stations without significant trends is located in the north-western part of the basin. Looking at the changes in absolute terms (change magnitude), which are based on the results of the linear regression analysis, stations with an increase above 1 K are mostly located along the coastline and in the far western tip of the basin. Around ten stations exceed 1.5 K in mean temperature rise for the 47 years time-series (1961–2007) and can be found in the delta region and the Far East of the basin (Fig. 2).

On monthly basis, significant positive trends can be found at many stations for all months. In four months (May, July, August, September), few significant negative trends (between 3 and 6 stations each) appear.

In summary, annual and monthly mean temperatures have increased in the entire basin whereas the temperatures increased less in summer than in winter.

3.1.2. Warm and cool days

Records for the annual warm days (T_{90}) in the ZRB are found in the summer half (April to September) of each year only. The station-based thresholds for T_{90} range from 19.5 °C in the west to above 29 °C in the south and central parts as well as in the Zhujiang River Delta (Fig. 3A). All over the study area, for 112 of 192 stations (58%) significant positive trends in the annual number of warm days are observed. Most stations without significant trends can be found along the northern border; also one single station is found with a significant negative trend.

The stations' mean magnitude of change of T_{90} shows an increase by more than 14 warm days. Stations with the highest gradient (above a 30 days increase) can predominantly be found along the coastline and in the far West of the basin, with an accumulation of stations in the delta region and the most eastern part of the basin.

Cool days (T_{10}) in the ZRB, in contrast, appear in the winter half (October to March). The spatial distribution of the thresholds for cool days (T_{10}) shows a North (low) to South (high) disparity with a strong decrease in the north-western part. For 174 of 192 stations, significant negative trends of T_{10} can be observed (Fig. 3B). No significant positive trend can been found. Based on the results of the linear regression, the average decrease of T_{10} from 1961 to 2007 is directly opposed to the increase of T_{90} values. Around 45 cool days per year were observed in 1961. These were reduced to less than 30 days in 2007. The spatial distribution of the absolute changes (change magnitude) follows the same pattern as that for T_{90}; some high values are also measurable in the west-central area.

Following these calculations, a significant increase of warm days (T_{90}) and an even more significant decrease of cool days (T_{10}) can be expressed.

3.1.3. Warm and cool periods

The basin-wide annual average of T_{warm} (annual longest period of warm days [T_{90}]) is 10 days. At station level, a west to east increase (from 7 to 13 days) can be observed (Fig. 3C). An exception is the far western part of the ZRB (West of 104°E longitude) which shows a rise to higher numbers towards the west. It can be perceived that the periods of warm days (T_{90}) are shorter in the west and longer in the east of the ZRB.

Based on results of the Mann–Kendall trend test, a significant positive trend of T_{warm} can be found at 45 stations which are mainly located along the coastline and scattered in the western part of the basin. In the central-north area, 6 of 7 stations with significant negative trends can be found (Fig. 3C). In total, the ZRB experiences an average increase in T_{warm} by 2 days. Stations showing an extreme increase of more than 10 days from 1961 to 2007 can be located in the delta region and along the eastern coastline of the basin. Most of the stations with declining magnitudes (less than 5 days decline) can be located in the west-central part of the basin.

For the cool period (T_{cool}) the basin-wide annual average is around 13 days. With a similar distribution as that detected for T_{warm}, a NW to SE decrease (from 17 to 10 days) can be observed. As

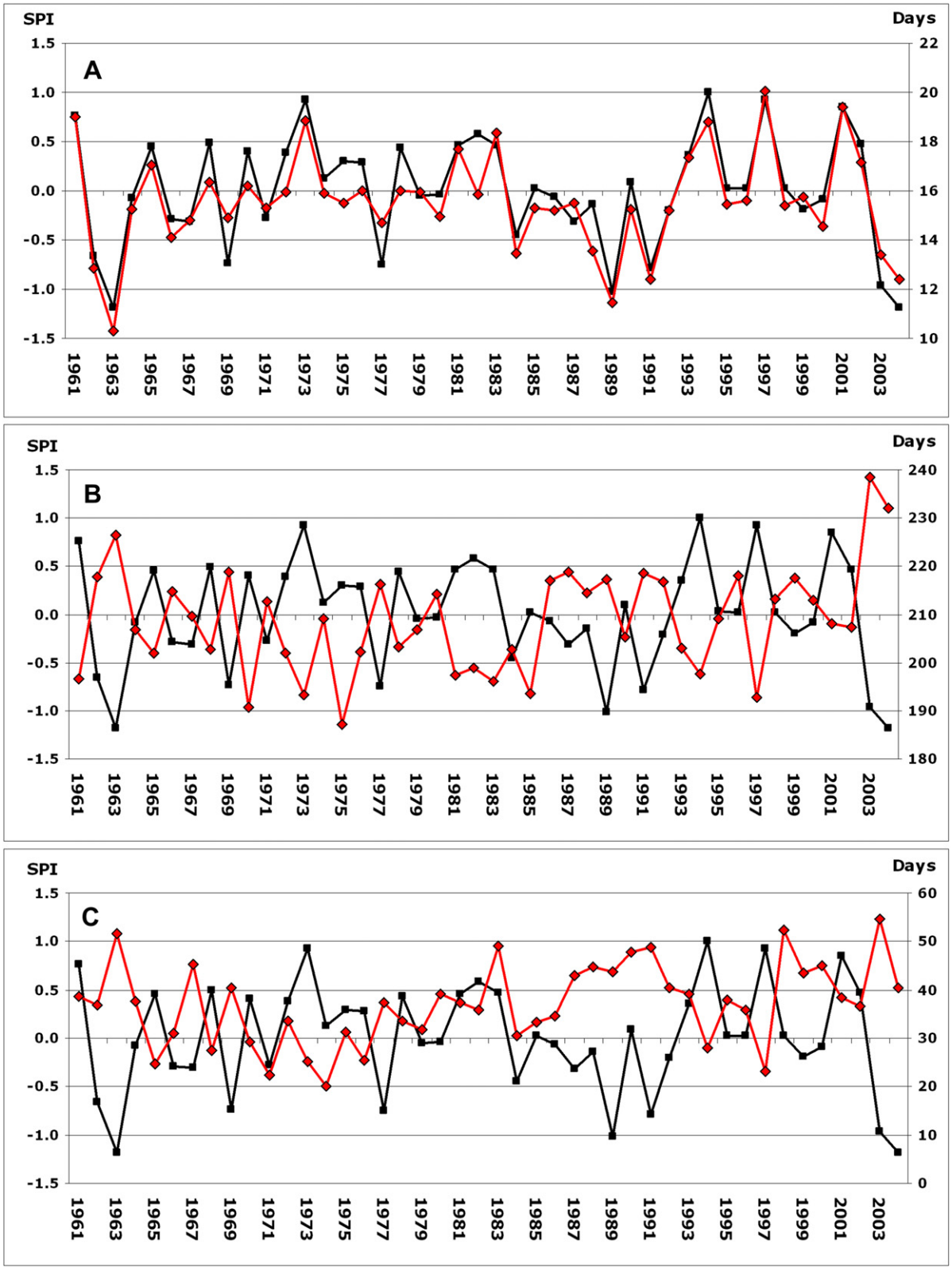

Fig. 7. Comparison of basin-wide annual SPI (black line) with (A) station-averaged annual extreme precipitation (P_{90}), (B) station-averaged annual no rain days ($P_{no\ rain}$), and (C) station-averaged annual warm days (T_{90}) for the Zhujiang River Basin.

can be seen in Fig. 3D, the far western part (west of 104°E) shows a strong gradient which has its low in the west. Therefore, the longest cool periods are observed in the north-western part and the shortest cool periods in the east and far west of the study area.

Based on the results of the Mann–Kendall trend test, 74 stations experienced a significant negative trend in T_{cool}. These are mainly located along the coastline and scattered in the western part of the basin. For the entire basins, a cool period in 2007 lasted 10 days in

Table 3
Multiple-correlation of station-averaged annual indices in the Zhujiang River Basin 1961–2004.

Y	X1	X2	Multiple R
SPI	Dry days	Warm days	0.82
PDSI	Dry days	Warm days	0.82
SPI	Dry days	P_{90}	0.95
PDSI	Dry days	P_{90}	0.87
SPI	Warm days	P_{90}	0.92
PDSI	Warm days	P_{90}	0.79
SPI	Warm days	Cool days	0.56
DSI	Warm days	Cool days	0.45

average, which is 6 days (37%) less than the average of 1961. No significant positive trend or magnitude in annual T_{cool} can be observed.

Comparing the spatial trends of the indicators T_{warm} and T_{cool}, it is clear that warm periods are prolonged in the same areas where cool periods shortened in time.

3.2. Observed precipitation trends and extremes

3.2.1. Annual, monthly, daily, and extreme precipitation

On average from 1961 to 2007, the annual total precipitation was above 2000 mm along the south-eastern coastline and below 1000 mm in the mountainous western parts of the ZRB (Fig. 4). Only 7 stations show significant negative trends, located in the west of the ZRB. One single station with a significant positive trend is located in the eastern corner of the basin. The absolute change (change magnitude) detected by the linear regression reveals a distinct west-east disparity. Several stations in the north-western part (more than 15) and central part (around 18) show declining precipitation by more than 100 mm in the analysed 47 years. Stations with increased annual total precipitation (above 100 mm rise in 2007 compared to 1961) are found in the entire eastern part, the northeast and some south-coastal areas.

Main precipitation is concentrated during summer. The winter season is comparatively dry, with around 50 mm of rain per month; compared to around 200 mm in summer months.

For extreme precipitation days (P_{90}) the threshold gradually increases from as low as 16 mm/day in the northwest to more than 45 mm/day in the southeast. The spatial disparity of the average number of P_{90} is converse; many days of extreme precipitation (up to 21) occur in the north-western part and the lowest number (below 15) can be detected along the coast and apparently in the far west corner. Significant trends can be found at few stations only. 7 (3) stations with significant positive (negative) trends are located in the western and eastern corners as well as in the centre (northwest and southwest). The area of positive trends (up to 5 days) and negative trends (up to 4 days) follows the same pattern as mentioned before; stations with high (low) numbers in P_{90} have negative (positive) change magnitudes (Fig. 4).

Extreme precipitation events increased significantly at stations with high values and decreased at those with low values. This explains an aggravation of the spatial divergence in both annual extreme precipitation and annual total precipitation. More details on monthly precipitation extremes in the ZRB are provided by Gemmer et al. (in preparation).

3.2.2. Rain and no rain days

For each of the 192 stations in the ZRB the number of annual rain days (P_{rain}) varies strongly. Stations with the highest number of rain days (up to 210 days/year) occur in the north-western highlands and northern central-east lowlands of the Zhujiang basin. The lowest number of rain days (around 110 days/y) can be found at stations along the coastline and in the far western corner of the basin. To some extent, a disparity from south to north (inland) can be identified. This is not in line with the annual precipitation which shows the highest amounts (above 2000 mm/y) along the coastline and the lowest amounts (below 1000 mm/y) in the far west (see above). In general, more rain days are found in the summer months and less in the winter months at each station.

The results of the trend test for the number of annual P_{rain} show no positive trends. In contrary, significant negative trends are apparent at 94 stations. Most of these stations are located in the western half of the basin (Fig. 5A). Based on the results of the linear regression, at stations with significant trends the number of annual rain days decreased by more than 20 days during the period 1961–2007. From the spatial distribution of changes in annual precipitation, an interrelation with the distribution of annual rain days can be detected. On average, the western parts experience less rain days and less rainfall throughout the course of the time-series as opposed to higher precipitation in the eastern half.

The temporal and spatial distribution of the annual number of days with no rain ($P_{no\ rain}$) are in contrary to the patterns detected for P_{rain}. The number ranges from 150 to 250 for the stations. Stations that observed many no rain days (above 220) can be found along the coastline and in the far western corner of the basin (Fig. 5B).

3.2.3. Wet and dry periods

The indicators of the annual longest rain day period (P_{wet}) and no rain day period (P_{dry}) accentuate the most distinct duration of wet/dry conditions. For most stations, a high variability is found. Most wet periods occurred during the summer months and all dry periods during the winter months. According to the basin-wide means, an annual wet period in average lasts 13 days, whereas the annual dry period lasts around 27 days. The spatial distribution of both indicators (P_{wet} and P_{dry}) shows strong similarities to the distribution of P_{rain} and $P_{no\ rain}$. As can be seen in Fig. 5A, the far western part (west of 104°E) and the central-western part (106°E–108°E) show very low (high) numbers for P_{wet} (P_{dry}).

Trend directions for P_{wet} are divergent and significant positive trends can be found at 7 stations only. These stations experience a prolongation of annual longest wet periods and are mainly located in the central part of the basin. In the western and eastern areas, 28 stations with significant negative trends can be found. A shortening of wet periods is observed. The basin experiences an average decrease in T_{wet} by 1 day. Stations showing distinct decreases by more than 5 days (1961–2007) can be located in the far western corner and near the delta of the basin.

For P_{dry}, significant positive trends can be found at 59 stations. These stations are mostly located in the central-northern part (Fig. 5B). It is worth mentioning that all stations with significant increases (more than 10 days in magnitude) are located in the far south-eastern corner. For the entire basin, an average prolongation of the dry period by 5 days can be detected for the time-series.

The main finding regarding longest wet and dry periods is the tendency to longer dry periods and shorter wet periods, which might imply that more severe dry events and more intensive rainfall events have occurred.

3.3. Drought indices

The annual SPI and annual PDSI for 51 stations from 1961 to 2004 are calculated in order to explain the impacts of drought on the ZRB. Fig. 6 shows the temporal and spatial distribution of moderate dry and wet years. The stations are numbered from west to east based on their location (°E). Results for the SPI show much more moderate events than the PDSI. No obvious trend can be

found for the majority of stations. For the SPI, station 34 only shows significant positive trends, and significant negative trends can be found at stations 2 and 30.

At five stations (2, 3, 5, 7, and 13) significant negative trends of the PDSI can be found. For both parameters, negative trends indicate a tendency to a higher number of dry years; positive trends indicate a tendency towards wet conditions at the respective station. Following the location of the stations, it can be assumed that a slight tendency to more dry years is experienced for the western part of the basin.

The temporal variations and frequencies of droughts and wet conditions in the basin were analysed by Zhai et al. (2009a) who studied all main watersheds of China. For the ZRB, the frequency of dry years between 1961 and 2005 was 15.7% (6.7%) according to the results of the SPI (PDSI) calculated by the authors; the frequency of wet years was 16.4% (4.6%), respectively (Zhai et al., 2009a). The observed frequencies of the SPI and PDSI show a relatively even distribution of dry/wet years in time. This is also consistent with the analysis of Bordi et al. (2004). However, the spatial distribution of dry years shows distinct regional pattern. A subjective analysis of this spatial distribution (Fig. 6) shows a high inconsistency of the western stations compared to a relative uniformity of the stations in the east.

Several distinct dry and wet years can be detected when comparing the SPI with the PDSI. For the western part of the ZRB, following dry (wet) years are noticeable: 1963, 1987, 1989, and 2004 (1961, 1968, 1973, and 1994/7). In the eastern part of the ZRB, dry years (1963, 1967, 1971, 1977, 1991, and 2003/4) and wet years (1961, 1973/5, 1981/3, and 1994/7) are much more dominant than in the West. The main peak years for the entire basin can be summarized as 1963, 1989/91, and 2003/04 for dry years and 1961, 1973, and 1994/97 for wet years.

3.4. Correlation of indicators

In the following, potential correlations between the variables used above are analysed. Pearson's product–moment coefficient was used to identify the correlation of the basin-averaged annual indicators (Table 2). In Fig. 7 the annual SPI and an annual indicator (P_{90}, $P_{no\ rain}$ and T_{90}) are plotted in an adjusted scale. Using this visualization, the significant correlations of the SPI and interesting indicators are more comprehensible.

The SPI is calculated with precipitation data only, and implies that wet years are most often accompanied by extreme precipitation events. In contrast, dry years experience almost no extreme precipitation events. Therefore, the correlation of the SPI and P_{90} is 0.91 what is significantly high (Fig. 7A). Significant correlations of SPI/PDSI and dry days (wet days) ranging 0.81 (0.82) respectively can be explained for similar reasons (Fig. 7B). The multiple-correlation of SPI/PDSI with both dry days and P_{90} resulted in a very strong correlation of 0.95/0.87 (Table 3) which demonstrates impressively the high correspondence of extreme precipitation and dry days to dryness/wetness patterns. Of interest are the correlation results of warm days and dry days (0.55), wet days (−0.56), and SPI (−0.50) (Fig. 7C). Correlations above 0.5 (or below −0.5) indicate a moderate to strong affinity.

The multiple-correlation of warm days and dry days with the SPI (0.82) is even slightly higher than dry days and SPI alone (−0.81). All indicated periods (wet/dry/warm/cool period) show fewer correlations with SPI/PDSI than the indicators mentioned above. Both warm and cool periods correlate slightly negatively with the SPI and P_{90}. From the multiple-correlation of T_{cool}, T_{warm}, and SPI (PDSI), a relatively moderate affinity of 0.56 (0.45) can be found. It is more likely that dry (wet) years occur when high (low) numbers for both longest warm and cool periods have occurred.

A high number of warm days occur more frequently during dry years and years with above average dry days, vice-versa. This finding is more significant when focusing on the peak years of drought and wetness.

4. Conclusions and discussion

The methodologies applied deliver some new insights to tendencies of dryness/wetness pattern in the ZRB, South China, therefore achieving the objective of the paper. The results will be followed up by the authors, and more stations will be used for calculating the SPI (PDSI) in order to achieve regionally more focused results. The data at hands for this study, however, were sufficient to achieve the objectives.

The detected significant positive trend of observed annual mean temperature, rather in winter than in summer, in the ZRB from 1961 to 2007 is in line with international and national observations as well as projections (Ren et al., 2005a,b; Zhai et al., 2005; Trenberth et al., 2007; Liu et al., 2009). The increasing (decreasing) number of warm (cool) days by 14 (15) days underlines the observed warming condition. The significant increases (decreases) in the duration of the longest warm (cool) period by more than 21% (37%) show a strong shift to warmer, more extreme, climates. It is interesting to find that areas where warm periods prolong automatically experience shorter cool periods (in winter).

Main causes of these surface temperature changes and warm/cool periods might be explained by the anticipated global warming (Ding et al., 2007). The temperature increase has been observed basin-wide, and not only at urban agglomerations, including the densely populated Zhujiang River Delta, and therefore potential influences of the urban heat island effect (UHIE) can be neglected at this point. Nevertheless, simulation results demonstrate that rapid urbanization can substantially alter regional climate conditions in the Zhujiang River Delta (Lin et al., 2009), including monthly mean temperature and precipitation. This is based on a change detection analysis of 18 Landsat scenes from the 1970s to 2000 by Lin et al. (2009). Chen et al. (2005) observed the UHIE in Hubei province for 1961–2000. They analysed the warming rates of urban and rural areas and calculated the related contribution of the UHIE. For urban agglomerations a contribution rate of sixty percent during the forty years was estimated. Similar but lower findings were made by Zhou and Ren (2005) for North China, where they estimated a UHIE contribution rate of up to 37.9%. All these results indicate an essential influence of UHIE to temperature increases, especially in urban agglomerations. Following this, the UHIE in the ZRB might have a certain impact on the climate conditions especially when focusing on the urban areas along the coastline with their significant warming trends and should not be neglected but considered when analyzing the temperature increase in urban regions.

Almost no significant trends have been found for annual total and extreme precipitation events, but regional tendencies can be pointed out. The observed tendency of significant increase (decrease) of extreme precipitation at stations with high (low) thresholds (west–east disparity) is noteworthy, as it describes a shift to a greater regional imbalance in precipitation patterns within the basin. A major finding is the more regionalized distribution of rain/no rain days and wet/dry periods with a significant trend to fewer rain days over the entire western part and significant negative trends of wet periods particularly in the far western corner and the delta region. Some similar findings with lower resolution can be compiled from Qian and Lin (2005) for south China.

The significant increase of the number of dry periods in the south-eastern corner complete the picture of regional imbalance with rising extremes in both temperature and precipitation. The corresponding indices (T_{warm}, T_{cool}, P_{dry}, and P_{wet}) were defined by

the single longest period per year only. Two consecutive periods might be only one day suspended from each other, but might add up to a longer period when added if not suspended, or occurring at the year break, and are therefore not utilized in the index. Results looking into consecutive periods will be produced by the authors in future.

The observed increase of precipitation intensity can be explained by a decreasing number of rain days while stable amounts of total precipitation on monthly and annual basis. This finding is in line with the observations made by Gemmer et al. (in preparation), Zhang et al. (2009b), and Qian and Lin (2005). The coastal and eastern areas as well as the far western part of the ZRB have experienced longer dry periods and shorter wet periods.

The analysis of the SPI (PDSI) does not show significant trends, except for very few of the 51 stations, and generally no changes in dry or wet conditions can be detected, what is in line with the findings of Zhai et al. (2009a) and Zhang et al. (2009a). The time-consuming calculation and analysis of SPI and PDSI at all 192 available weather stations could eventually deliver significant, more regionally focused results, and will be conducted by the authors in the next steps.

Most parts of the ZRB, considering temperature and precipitation, are influenced by the East Asian Summer Monsoon and the East Asian Winter Monsoon. The spatial distribution of annual rain and no rain days might be strongly caused by orographic convection, the transition from maritime to continental climate factors, and by the weakening of the East Asian Summer Monsoon (Wang and Ding, 1997; Su et al., 2005; Yu et al., 2009). According to Su et al. (2005), the summer temperature over Central Asia decreased slightly in recent decades whereas the temperature over the North West Pacific has become warmer. This contrast caused the weakening of the summer monsoon and the shift of the rain belt over Southern China, leading to less rain days (Chou, 2004; Su et al., 2005). The shift of the transition phase between the end of the EASM and the onset of the EAWM could be another aspect in the decrease in rain days, but this has not been studied in detail (Gemmer et al., in preparation). The detected expansion of drought periods in the ZRB is more negative than any impacts that wetness (i.e. with regards to flood events) might have.

Acknowledgments

This study was supported by the National Basic Research Program of China (973 Program) (No. 2010CB428401), the Special Fund of Climate Change of the China Meteorological Administration (CCSF-09-16) and by the National Natural Science Foundation of China (40910177). The positions of Marco Gemmer and Thomas Fischer at the National Climate Center are supported by the German Development Cooperation through the Center for International Migration and Development (www.cimonline.de).

References

Alexandersson, H., 1986. A homogeneity test applied to precipitation data. Journal of Climatology 6, 661–675.
Bayazit, M., Önöz, B., 2007. To prewhiten or not to prewhiten in trend analysis? Hydrological Sciences Journal 52, 611–624.
Buishand, T.A., 1982. Some methods for testing the homogeneity of rainfall records. Journal of Hydrology 58, 11–27.
Beniston, M., Stephenson, D.B., 2004. Extreme climatic events and their evolution under changing climatic conditions. Global and Planetary Change 44, 1–9.
Bordi, I., Fraedrich, K., Jiang, J.-M., Sutera, A., 2004. Spatio-temporal variability of dry and wet periods in eastern China. Theoretical and Applied Climatology 79, 81–91.
Bothe, O., Fraedrich, K., Zhu, X., 2009. The large-scale circulations and summer drought and wetness on the Tibetan plateau. International Journal of Climatology. doi:10.1002/joc.1946.
Chen, Z., Wang, H., Ren, G., Xiang, H., Xue, L., 2005. Change of urban heat island intensity and its effect on regional temperature series: a case study in Hubei Province. Chinese Journal on Climatic and Environmental Research 10, 771–779 (In Chinese).
Chou, C., 2004. Establishment of the low-level wind anomalies over the western North Pacific during ENSO development. Journal of Climate 17, 2195–2212.
Ding, Y., Ren, G., Shi, G., Gong, P., Zheng, X., Zhai, P., Zhang, D., Zhao, Z., Wang, S., Wang, H., Luo, Y., Chen, D., Gao, X., Dai, X., 2007. China's national assessment report on climate change (I): climate change in China and the future trend. Advances in Climate Change Research 3, 1–5.
Gemmer, M., Becker, S., Jiang, T., 2004. Observed monthly precipitation trends in china 1951–2002. Theoretical and Applied Climatology 77, 39–45.
Gemmer, M., Fischer, T., Jiang, T., Su, B., Liu, L., 2010. Trends of precipitation extremes in the Zhujiang River Basin, South China. Journal of Climatology, in preparation.
Hamad, K.H., Rao, A.R., 1998. A modified Mann–Kendall trend test for autocorrelated data. Journal of Hydrology 204, 182–196.
Hayes, M.J., 2006. Drought indices. Website of the National Drought Mitigation Center. Available from: http://www.drought.unl.edu/whatis/Indices.pdf (accessed 19.03.10).
Kundzewicz, Z.W., Robson, A.J., 2004. Change detection in hydrological records – a review of the methodology. Journal of Hydrological Sciences 49 (1).
Li, Z., Zheng, F., Liu, W., Flanagan, D, 2010. Spatial distribution and temporal trends of extreme temperature and precipitation events on the Loess Plateau of China during 1961–2007. Quaternary International 226 (1–2), 92–100.
Lin, W., Zhang, L., Du, D., Yang, L., Lin, H., Zhang, Y., Li, J., 2009. Quantification of land use/land cover changes in Pearl River Delta and its impact on regional climate in summer using numerical modeling. Regional Environmental Change 9, 75–82.
Liu, Q., Yang, Z., Cui, B., 2008. Spatial and temporal variability of annual precipitation during 1961–2006 in Yellow River Basin, China. Journal of Hydrology 361, 330–338.
Liu, L., Jiang, T., Yuan, F., 2009. Observed (1961-2007) and projected (2011–2060) climate change in the Pearl River Basin. Advances in Climate Change Research 5 (4), 209–214 (In Chinese).
McKee, T.B., Doeskin, N.J., Kleist, J., 1993. The relationship of drought frequency and duration to time scales. 8th Conference on Applied Climatology. American Meteorological Society, 179–184.
Peterson, T.C., Easterling, D.R., Karl, T.R., 1998. Homogeneity adjustments of in situ atmospheric climate data: a review. International Journal of Climatology 18, 1493–1517.
Qian, W., Lin, X., 2005. Regional trends in recent temperature indices in China. Meteorology and Atmospheric Physics 90, 193–207.
Ren, G., Xu, M., Chu, Z., Guo, J., Li, Q., Liu, X., Wang, Y., 2005a. Recent progresses in studies of regional temperature changes in China. Chinese Journal on Climatic and Environmental Research 10 (4), 702–716 (In Chinese).
Ren, G., Xu, M., Chu, Z., Guo, J., Li, Q., Liu, X., Wang, Y., 2005b. Changes of surface air temperature in China during 1951–2004. Chinese Journal on Climatic and Environmental Research 10 (4), 717–727 (In Chinese).
Schmidli, J., Frei, C., 2005. Trends of heavy precipitation and wet and dry spells in Switzerland during the 20th century. International Journal of Climatology 25, 753–771.
Song, F., Hu, Q., Qian, W., 2004. Quality control of daily meteorological data in China, 1951–2000: a new dataset. International Journal of Climatology 24, 853–870.
Solomon, S., Qin, D., Manning, M., Chen, Z., Marquis, M., Averyt, K.B., Tignor, M., Miller, H.L., 2007. Contribution of Working Group I to the Fourth Assessment Report of the Intergovernmental Panel on Climate Change. Cambridge University Press, Cambridge, United Kingdom and New York, NY, USA.
Su, B., Jiang, T., Jin, W., 2005. Recent trends in observed temperature and precipitation extremes in the Yangtze River basin, China. Theoretical and Applied Climatology 83, 139–151.
Trenberth, K.E., Jones, P.D., Ambenje, P., Bojariu, R., Easterling, D., Klein Tank, A., Parker, D., Rahimzadeh, F., Renwick, J.A., Rusticucci, M., Soden, B., Zhai, P., 2007. Observations: surface and atmospheric climate change. In: Solomon, S., Qin, D., Manning, M., Chen, Z., Marquis, M., Averyt, K.B., Tignor, M., Miller, H.L. (Eds.), Climate Change 2007: The Physical Science Basis. Contribution of Working Group I to the Fourth Assessment Report of the Intergovernmental Panel on Climate Change. Cambridge University Press, Cambridge, United Kingdom and New York, NY, USA.
von Storch, H., 1995. Misuses of statistical analysis in climate research. In: von Storch, H., Navarra, A. (Eds.), Analysis of Climate Variability Applications of Statistical Techniques. Springer, New York.
Wang, Q., Ding, Y., 1997. Climatological characteristics of evolution of East Asian winter monsoon. Quarterly Journal of Applied Meteorology 8 (2), 186–196.
Yang, T., Shao, Q., Z-Hao, C., Chen, X., Zhang, Z., Xu, C.-Y., Sun, L., 2010. Regional frequency analysis and spatio-temporal pattern characterization of rainfall extremes in the Pearl River Basin, China. Journal of Hydrology 380 (3–4), 386–405.
Yu, S., Shi, X., Lin, X., 2009. Interannual variation of East Asian summer monsoon and its impacts on general circulation and precipitation. Journal of Geographical Science 19, 67–80.
Yue, S., Wang, C.Y., 2002. The applicability of pre-whitening to eliminate the influence of serial correlation on the Mann–Kendall test. Water Resources Research 38 (6), 4–17.
Zhai, P., Zhang, X., Wan, H., Pan, X., 2005. Trends in total precipitation and frequency of daily precipitation extremes over China. Journal of Climate 18, 1096–1108.

Zhai, J., Su, B., Krysanova, V., Vetter, T., Gao, C., Jiang, T., 2009a. Spatial variation and trends in pdsi and spi indices and their relation to streamflow in 10 large regions of China. Journal of Climate. doi:10.1175/2009JCLI2968.1.

Zhai, J., Liu, B., Hartmann, H., Su, B., Jiang, T., Fraedrich, K., 2009b. Dryness/wetness variations in China during the first 50 years of the 21st century. Hydrological Earth Systems Science Discussions 6, 1385–1409.

Zhang, Q., Xu, C., Becker, S., Zhang, Z.X., Chen, Y.D., Coulibaly, M., 2009a. Observed changes of drought/wetness episodes in the Pearl River basin, China, using the standardized precipitation index and aridity index. Theoretical and Applied Climatology 98, 89–99.

Zhang, Q., Xu, C., Zhang, Z., 2009b. Trends and abrupt changes of precipitation maxima in the Pearl River basin, China. Atmospheric Science Letters 10 (2), 132–144.

Zhou, Y., Ren, G., 2005. Identifying and correcting urban bias for regional surface air temperature series of north china over period of 1961–2000. Chinese Journal on Climatic and Environmental Research 10 (4), 743–753 (In Chinese).

Appendix II

Gemmer, M., T. Fischer, T. Jiang, B. Su and L. Liu, 2011: Trends in Precipitation Extremes in the Zhujiang River Basin, South China. *Journal of Climate*, Volume 24, 750–761.

Trends in Precipitation Extremes in the Zhujiang River Basin, South China

MARCO GEMMER AND THOMAS FISCHER

National Climate Center of the China Meteorological Administration, Beijing, China

TONG JIANG

National Climate Center of the China Meteorological Administration, Beijing, and Nanjing University of Information Science and Technology, Nanjing, China

BUDA SU AND LÜ LIU LIU

National Climate Center of the China Meteorological Administration, Beijing, China

(Manuscript received 9 March 2010, in final form 19 September 2010)

ABSTRACT

Spatial and temporal characteristics of precipitation trends in the Zhujiang River basin, South China, are analyzed. Nonparametric trend tests are applied to daily precipitation data from 192 weather stations between 1961 and 2007 for the following indices: annual, monthly, and daily precipitation; annual and monthly number of rain days and precipitation intensity; annual and monthly maximum precipitation; 5-day maximum precipitation, number of rainstorms with >50 mm day^{-1}, and peaks over thresholds (90th, 95th, and 99th percentile).

The results show that few stations experienced trends in the precipitation indices on an annual basis. On a monthly basis, significant positive and negative trends above the 90% confidence level appear in all months except December. Trends in the indices of monthly precipitation, rain intensity, rain days, and monthly maximum precipitation show very similar characteristics. They experience the most distinct negative (positive) trends in October (January). A change of the mean wind direction by 50° from east-southeast to east-northeast explains the downward trend in precipitation in October. Dry October months (months with low precipitation indices) can be observed when the mean wind direction is east-northeast (arid) instead of the prevailing mean wind direction, east-southeast (moist). The former is typical for the East Asian winter monsoon (EAWM). Nearly 90% of the driest October months can be explained by wind directions typical for the EAWM. The upward trend in precipitation indices in January cannot be explained by changes in large-scale circulation. The analysis of the precipitation indices delivers more detailed information on observed changes than other studies in the same area. This can be attributed to the higher station density, the quality of daily data, and the focus on monthly trends in the current study.

1. Introduction

According to China's National Assessment Report on Climate Change (Ding et al. 2007), changes in annual precipitation have been observed in China for the last century. In the last decades, an increase in national average precipitation was detected, with increasing spring precipitation but slightly decreasing autumn precipitation. The Fourth Intergovernmental Panel on Climate Change (IPCC) Assessment Report (Trenberth et al. 2007) is in line with China's National Assessment Report on Climate Change and indicates that the frequency of heavy precipitation events will very likely increase in China. Regional changes are, however, diverse—southeast China, for instance, experienced an increase in annual precipitation by around 60 to 130 mm during the last 50 years (Ding et al. 2007). The East Asian monsoon plays an important role in regional precipitation patterns. A strong (weak) winter monsoon with northerly winds leads to decreased (increased) winter precipitation over south China (Chen et al. 2000; Zhou and Wu 2010).

It is therefore important to understand regional changes in precipitation patterns and the causes of these changes. Several studies have analyzed precipitation records for

Corresponding author address: Dr. Marco Gemmer, National Climate Center, 46, Zhongguancun Nandajie, Haidian 100081, Beijing, China.
E-mail: marco@gemmeronline.de

DOI: 10.1175/2010JCLI3717.1

the whole of China. Feng et al. (2007) have analyzed annual maximum precipitation time series (1-, 2-, 5-, and 10-day) for 651 stations in China from 1951 to 2000 and detected negative trends in extreme events in north China. Significant positive trends were observed at stations in the Yangtze River basin and northwestern China, where extreme events with a 50-yr return period in the 1950s became more frequent 25-yr events in the 1990s. More results for China using longer time series and analyzing linear trends in rain days with different intensities are provided by Fu et al. (2008). Liu et al. (2005) used 272 stations in China and examined change rates for eight regions and different seasons from 1960 to 2000 and found a nonsignificant increase of precipitation in southeast coastal China.

Qian and Lin (2005) comprehensively analyzed regional characteristics of daily precipitation indices at 494 stations in China (1961 to 2000) and showed interdecadal differences. In coastal southeast China, a negative decadal tendency in annual and summer precipitation was detected. Likewise, Wang and Zhou (2005) used linear regressions to analyze trends in annual and seasonal mean precipitation in China during 1961–2001. The results show decreasing extreme events in summer and a higher decreasing trend in autumn. Yang and Lau (2004) focused on spring and summer precipitation and noted positive trends in spring precipitation for a gridded dataset covering 1951–98, while Yao et al. (2008) focused on the time series 1978–2002 and concluded that for summer precipitation, the amount of total precipitation and light–moderate precipitation exhibited positive trends over southeast China.

Zhai et al. (1999) detected no significant trends in annual precipitation but a significant increase in above-normal mean intensity of precipitation in east China from 1951 to 1995. Zhai et al. (2005) applied trend techniques to a time series covering 1951–2000 and delivered the currently most comprehensive analysis of annual and extreme precipitation in China. Annual total, spring, and extreme precipitation significantly increased along the southeastern coastline of China, and winter precipitation increased in the south.

More and more studies on precipitation changes focus on a river-basin scale in order to identify results for hydrologically homogeneous areas as compared to administrative boundaries. Significant increasing trends in extreme precipitation have been observed for the Zhujiang River basin, also known as the Pearl River basin, in the last decades (Luo et al. 2008; Yang et al. 2010). These studies have mostly analyzed time series of annual and seasonal precipitation in the Zhujiang River basin to define precipitation extremes and their spatial pattern (Zhang et al. 2009a–c). Only few of these studies examined the temporal and spatial variations in monthly precipitation events.

Yang et al. (2010) analyzed the regional frequency of annual precipitation extremes based on consecutive 1-, 3-, 5-, and 7-day averages for 42 stations in the Zhujiang River basin from 1960 to 2005. It was identified that major precipitation events in regions of low elevation in the lower (southeastern) part of the basin occur mainly in May, June, July, and August, whereas the main precipitation periods for the mountainous region upstream are June, July, and August.

Liu et al. (2009) observed variations of seasonal precipitation in the Zhujiang River basin at 64 stations (1961–2007) and showed a decrease in autumn precipitation but increases in spring, summer, winter, and annual precipitation. An enhancement of interannual variability of annual and winter precipitation and a weakening of autumn precipitation is projected using the general circulation model (GCM) ECHAM5-Max Planck Institute Ocean Model (MPI-OM; Roeckner et al. 2003).

Based on data from 63 stations for the period 1959–2003, Luo et al. (2008) observed a downward trend in precipitation over the Beijiang River basin (northeastern tributary of Zhujiang) in the early flood period (April–June), especially in May, and an upward trend in July and in the dry season (October–March). The common precipitation belt over the Beijiang River, which is caused by frontal precipitation when the front of warm air masses from the south meets cold air masses from the north, has shifted northward in recent years. This has caused positive precipitation trends in the north and negative trends in the south of the catchment.

Zhang et al. (2009b) calculated a decreasing precipitation concentration index (CI) for the southwestern and northeastern parts as well as for the West River and East River basin of the Zhujiang River basin using precipitation data from 42 stations from 1960 to 2005. The study also described a significant increasing precipitation CI after 1990 in the West River basin, in the lower North River basin, and in the upper Beipan River basin.

Based on daily precipitation data for 47 stations from 1951 to 2005, Zhang et al. (2009a) did not detect significant trends in annual, summer, or winter precipitation. However, the trends in precipitation intensity, variability of precipitation, and high-intensity rainfall events increased. Zhang et al. (2009c) identified trends toward dryness in the rainy season (April–September) and an increase of wet conditions in the dry season (December–February).

Previous studies on the Zhujiang River basin have detected seasonal changes in precipitation, but most research focused on summer precipitation. Little has been

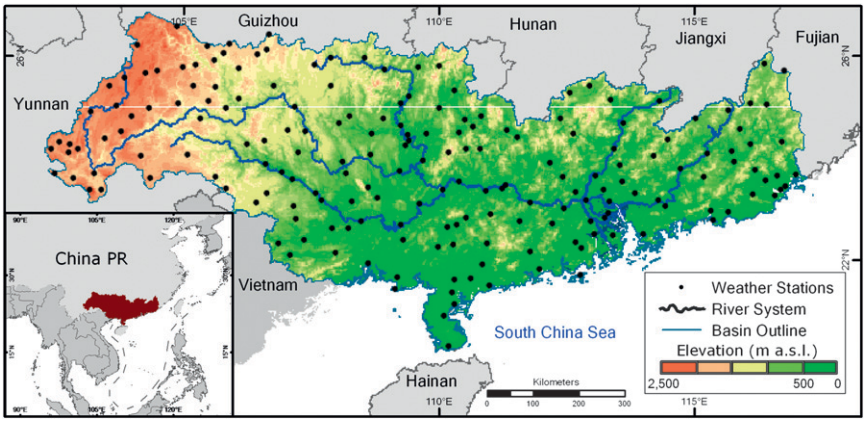

FIG. 1. Topographical map of the Zhujiang River basin showing the 192 weather stations.

written about the characteristics and causes of precipitation extremes—for example, changes in precipitation intensity on a daily basis and their statistical trends. The station density used in existing studies for the whole of China is sufficient to describe large-scale changes, but insufficient on a regional scale. In addition, the causes of precipitation trends are not entirely understood. The objective of this paper is to analyze trends in and causes of precipitation extremes in the Zhujiang River basin at the highest possible spatiotemporal resolution allowed by available data.

2. Data and methodology

a. Study area

The Zhujiang (Pearl River) basin is located in South China and falls within the provinces of Guangdong, Guangxi, Guizhou, and Yunnan. The Zhujiang River basin is one of China's largest river basins (Zhai et al. 2010) and drains an area of 579 000 km^2 (including the Leizhou Peninsula region). It has a tropical and subtropical climate. The annual mean temperature varies from 14°C in the west to 22°C in the east, and the annual average precipitation is 800 mm in the west and more than 2000 mm at the coastline (average for the basin: 1500 mm). The months from June to August are influenced by the East Asian summer monsoon. The basin is characterized by mountainous areas with peaks above 2500 m in the western part. The northern and northeastern parts are composed of lower mountain ranges and hills that surround the central and southern (southeastern) lowland areas. Following these elevation steps, the flow directions of the rivers are mainly from west and north toward the coast of the South China Sea in the southeast of the basin. The river system forms a large network delta before it enters into the sea. A comprehensive overview on the hydrological setting of the basin is given by Zhang et al. (2009b). Figure 1 provides a topographical sketch map of the Zhujiang River basin with the location of 192 weather stations and the main river system.

b. Data

Daily precipitation data covering the Zhujiang River basin were provided by the National Climate Center (NCC) of the China Meteorological Administration (CMA). For the basin, 253 stations passed the internal homogeneity check of the China National Meteorological Center (CNMC), including the moving t test (Peterson et al. 1998), standard normal homogeneity test (Alexandersson 1986), and departure accumulating method (Buishand 1982). Stations that were installed after 1961 and those with data gaps were excluded. As a result, 192 weather stations with precipitation records for 47 years (1 January 1961 to 31 December 2007) were selected. Data gaps account for less than 0.01% (less than 100 daily records out of over 3 000 000), and were reconstructed by the median precipitation from at least three neighboring stations. In most of these cases, 0-mm precipitation was interpolated as the neighboring stations did not record precipitation. In four cases, daily precipitation of less than 2 mm was interpolated.

National Centers for Environmental Prediction (NCEP) reanalysis data (geopotential height, and u- and v-wind pattern for 1948–2010) provided by the National Oceanic and Atmospheric Administration/Oceanic and Atmospheric Research/Earth System Research Laboratory (NOAA/OAR/ESRL) Physical Sciences Division (PSD) were examined to understand the causes of observed precipitation trends (Kalnay et al. 1996).

Based on the CMA classification, a rain day is considered if at least 0.1 mm day^{-1} can be measured. Rainstorms are classified by minimum 50 mm day^{-1}. An overview of the indices is given in Table 1.

TABLE 1. Definition of precipitation indices.

Name	Definition	Unit
Mean precipitation	Annual or monthly avg precipitation	mm
Annual max precipitation	Highest one-day precipitation in one year	mm
Monthly max precipitation	Highest one-day precipitation in one month	mm
Annual 5-day max precipitation	The highest precipitation that was measured during five consecutive days in one year	mm
Monthly 5-day max precipitation	The highest precipitation that was measured during five consecutive days in one month	mm
Rain days	Annual or monthly number of days >0.1 mm day^{-1}	day
Precipitation intensity	Precipitation amount per rain day	mm day^{-1}
Rainstorm days	Annual number of days >50 mm day^{-1}	day
Peak over threshold 90%	Annual number of precipitation days above the 90th percentile, 1961–2007	day
Peak over threshold 95%	Annual number of precipitation days above the 95th percentile, 1961–2007	day
Peak over threshold 99%	Annual number of precipitation days above the 99th percentile, 1961–2007	day

c. *Methodology*

The Mann–Kendall trend test was applied to detect trends at all 192 stations (1961–2007) for annual, monthly, and daily precipitation sums; annual and monthly number of rain days and rain intensity; annual and monthly maximum precipitation; 5-day maximum precipitation, and number of rainstorms (>50 mm day^{-1}). Trends for the indicator peak over threshold were calculated for the 90th, 95th, and 99th percentile, representing the annual number of days above the 90th, 95th, and 99th percentile for each station (1961–2007). The thresholds were calculated with daily data based on the time series 1961–2007.

The 90% confidence level was taken as the threshold to classify the significance of positive and negative trends for all indices. Trends below 90% confidence level were not considered. A comprehensive description and reference list of the Mann–Kendall trend test is provided by Gemmer et al. (2004) and Gao et al. (2010).

The inverse distance weighting (IDW) method is used to interpolate results for each station and to project the results two-dimensionally in the Arc geographical information system (ArcGIS). This interpolation method has been used and described by Gemmer et al. (2004). The interpolation results were compared with interpolations carried out by the kriging method (Goovaerts 2000; Yang et al. 2010), and little discrepancy was found. The Kriging method produced less generalized areas and followed the steps in the digital elevation model in more detail. For the sake of the readability of the illustrations in the necessary size for this journal, maps are produced by applying the IDW method. Interpolation was carried out for the following figures: 1) Fig. 2 shows the long-term annual precipitation for the Zhujiang River basin (1961–2007) using data interpolated from the 192 stations; 2) the shading in Fig. 4 shows the trend in January precipitation, the area being interpolated from the results of 192 stations; and 3) the shading in Fig. 5 shows the trend in October precipitation, the area being interpolated from the results of 192 stations.

To distinguish between dry and wet years (Fig. 8), the annual values of five precipitation indices are standardized by subtracting the indicator's arithmetic mean

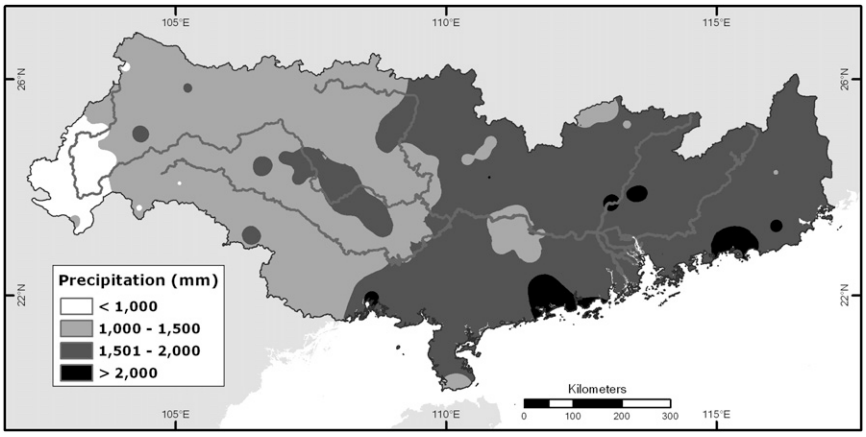

FIG. 2. Annual mean precipitation in the Zhujiang River basin, 1961–2007.

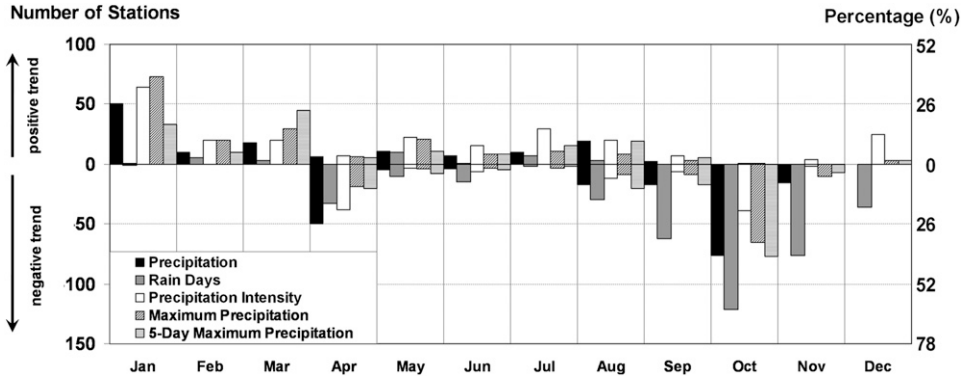

FIG. 3. Observed monthly precipitation trends 1961–2007 at the 90% confidence level in the Zhujiang River basin for five indices.

from the annual value and dividing it by the indicator's standard deviation. For each year, the arithmetic mean of the five annual values is calculated. When the arithmetic mean of the five annual standardized values is negative (positive), we determine a dry (wet) year. The degree dryness and wetness is higher when the values are higher.

3. Results

a. Annual and monthly precipitation trends

Annual precipitation (multiannual mean from 1961 to 2007) in the Zhujiang River basin shows an increase from west to south, from less than 1000 mm to more than 2000 mm at the coastline in the east (Fig. 2). The annual average precipitation in the basin is 1500 mm. The Mann–Kendall trend test was applied to the annual precipitation of the 192 stations in the Zhujiang River basin. Hardly any significant trends in annual precipitation during 1961–2007 can be detected. Only eight out of 192 stations (4%) show significant trends above the 90% confidence level. Seven of these stations are located in the mountainous west of the Zhujiang River basin and show negative trends. The other station is located in the east and shows a positive trend (not displayed).

The monthly precipitation (multiannual mean over 1961–2007) in the Zhujiang River basin shows a distinct seasonality. Sixty-one percent of the annual precipitation falls from May to August. With an average of 266 mm (29 mm), June (December) is the month with the highest (lowest) precipitation. The Mann–Kendall trend test was applied to the monthly precipitation time series of the 192 stations. December is the only month that shows no significant trend at any station at a 90% confidence level (Fig. 3). Monthly precipitation in January and October shows the largest trends in precipitation indices. Precipitation in January shows significant upward trends at 50 stations (26%) and October precipitation shows significant downward trends at 76 stations (40%). Precipitation in April has significantly decreased at 50 stations (26%). However, the increasing and

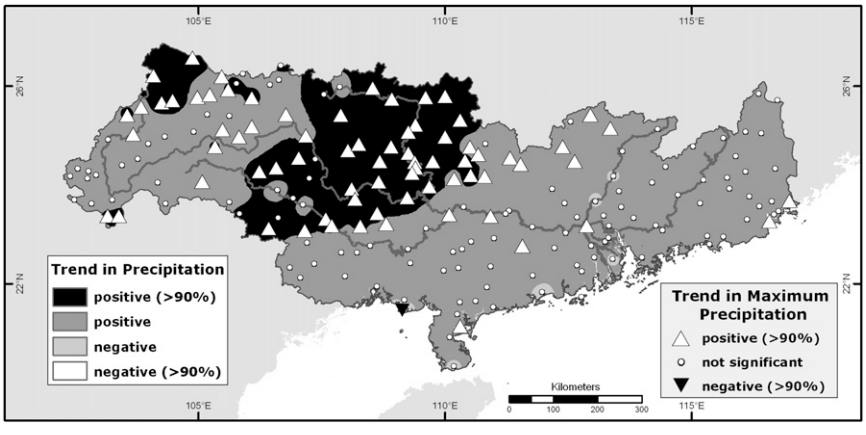

FIG. 4. January precipitation trends (area, left legend) and maximum precipitation trends (symbols, right legend) in the Zhujiang River basin, 1961–2007.

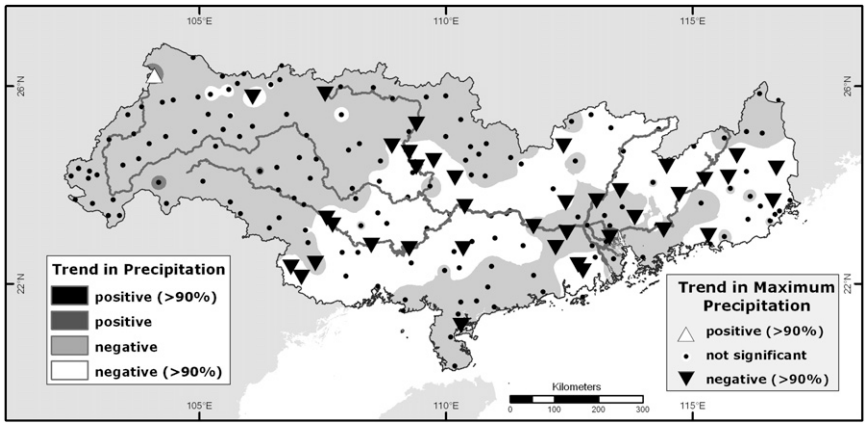

FIG. 5. As in Fig. 4, but for October.

decreasing trends of the four other precipitation indices (Fig. 3) are less dominant in April than in January or October.

Positive precipitation trends in January are concentrated in a belt from the tributaries in the west of the basin to the northern boundary. This spatial distribution is similar to the area that experienced trends in maximum precipitation in January (Fig. 4). The negative precipitation trends for October can be found in a belt stretching from the middle reaches of the Zhujiang in the center of the basin to the boundary in the east along the coastline. This area is similar to the region for which trends in monthly maximum precipitation in October can be detected (Fig. 5).

Significant negative trends in monthly precipitation can only be detected from April to June and from August to November. Positive trends occurred from January to September only. Both positive (19 stations or 10%) and negative precipitation trends (17 stations or 9%) can be detected in August.

b. *Trends in annual extremes*

Annual maximum precipitation (the highest rainfall per day at one station per year) can be detected in areas that are similar to the spatial distribution of annual mean precipitation (Fig. 2). Annual maximum precipitation is below 80 mm in the west of the catchment, between 120 and 160 mm along the coastline, and more than 160 mm in spots along the coast. The Mann–Kendall test detects trends in annual maximum precipitation at a 90% confidence level, but this precipitation index decreased at 6 stations (3%) and increased at 12 stations (6%) only. The results are not displayed as no large-scale trend can be found for annual maximum precipitation.

The annual 5-day maximum precipitation (long-term annual average) is less than 140 mm in the western part and more than 260 mm in the south and southeast coast of the research area. The Mann–Kendall test shows negative trends at a 90% confidence level at 5 stations (3%) and positive trends at 8 stations (4%) only and is not displayed.

The number of annual rain days shows a significant downward trend at a 90% confidence level at 94 stations (49%). These trends were mainly experienced in the west of the Zhujiang River basin. The trend test shows no clear signal for the annual number of rainstorms days (>50 mm day^{-1}). Positive trends can be detected at 12 stations (6%) and negative trends occurred at 2 stations (1%) only.

The results for the Mann–Kendall test on the peak over threshold at 90th, 95th, and 99th percentile detects trends at few stations only. For the 90th percentile, seven positive (4%) and three (2%) negative trends were detected. Eleven positive (6%) and two (1%) negative trends occurred for the 95th percentile. Fourteen positive (7%) and four (2%) negative trends are detected for the 99th percentile.

c. *Trends in monthly extremes*

The results of the Mann–Kendall trend test for indices on a monthly basis are more diverse and concise than those for annual data. Figure 3 displays the results of the trend test for five indices on a monthly basis, indicating the number of stations and percentage of stations that have experienced significant trends. The results for trends in monthly precipitation have been discussed in the previous subsection. For the five indices, significant trends in either a negative or positive direction appear in certain months. The only exception is August, where monthly precipitation and monthly 5-day maximum precipitation show a balanced number of positive and negative trends.

The number of monthly rain days in October experienced the most dominant trend of all indices. Rain days are significantly decreasing in October at 121 stations (63%), followed in the ranking by November (76 stations or 35%) and September (62 stations or 32%). No increasing trend for rain days can be found at any station in these three months. A decreasing trend in rain days occurred exclusively in the months between April and December. In general, hardly any positive trends in the number of monthly rain days can be found in the Zhujiang River basin. Only May shows a slight increase in rain days at 10 stations (5%).

Precipitation intensity shows a scattered appearance over the months. The highest increase in precipitation intensity can be observed in January (64 stations or 33%), followed by July (29 stations or 15%) and December (25 stations or 13%). No station experienced a decreasing trend in precipitation intensity in these months. Negative trends in precipitation intensity mainly occurred in October (39 stations or 20%) and April (38 stations). The magnitude of these decreasing trends is much lower compared to the 64 stations (33%) with increasing trends in precipitation intensity in January.

Maximum precipitation experienced the highest increase in January (73 stations or 38%) and the most severe decrease in October (65 stations or 34%).

Monthly 5-day maximum precipitation experienced a significant increase in March (45 stations or 23%) and January (33 stations or 17%). October experienced a negative trend in 5-day maximum precipitation amounts over the period from 1961 to 2007. This decreasing trend was detected at 77 stations (40%).

Figures 4 and 5 illustrate trends in monthly precipitation and maximum precipitation in January and October, respectively. January and October represent the most dominant increase and decrease in the precipitation indices. The figures show that the northwest of the Zhujiang River basin experienced higher precipitation and increased maximum precipitation in January. A band stretching along the middle and lower reaches of the Zhujiang River experienced a decrease in precipitation and lower maximum precipitation in October. It is noteworthy that the trends in the indices, whether positive or negative, occurred in the same regions and stations for a given month. With the exception of one station for one index, no significant negative trends can be detected for any of the indices between January and March. With the exception of six stations, the months October and November experienced negative trends for the indices and no positive trends.

Considering all five indices, January (October) experienced the most pronounced increasing (decreasing) trend in precipitation and the analyzed precipitation extremes.

4. Interpretation: Relation to large-scale circulation

Yang et al. (2010) described an approach to link flood seasons in the Zhujiang River basin with large-scale circulation and identified monthly mean moisture transports from the southwest Pacific Ocean and Indian Ocean as being the driver of wet and dry seasons.

In another example from the Yangtze River catchment, reasons for positive precipitation trends in July were found in variations in the meridional wind pattern at the 850-hPa level, which account for an increased transport of warm moist air to the Yangtze River catchment during the summer months (Becker et al. 2006). Hartmann et al. (2009) found phases and anti-phases in high precipitation at some stations in the Yangtze River catchment that are linked with SST in the Bay of Bengal. The detected directions of 850-hPa winds on a seasonal basis are in line with the seasonal water vapor flux in the Zhujiang River basin described by Zhang et al. (2009c).

We have therefore investigated geopotential heights and winds at 850 hPa for January and October for the entire time series covering the period 1961–2007 in order to explain reasons for the observed monthly (extreme) precipitation trends in the Zhujiang River basin. Interesting conclusions can be drawn. Figure 6 summarizes the findings and displays geopotential heights and winds at 850 hPa. The mean geopotential heights and winds for the time series (upper panel) are shown for January (Fig. 6a) and October (Fig. 6b).

a. January precipitation

When investigating the observed data, the positive precipitation trends in January cannot be explained by a shift in precipitation from December or February to January, as neither December nor February shows negative trends. In an attempt to explain the changes in January and October, focus is placed on the East Asian winter monsoon (EAWM).

According to the mean geopotential height at 850-hPa level, and as can be seen from Fig. 6a, January precipitation in the Zhujiang River basin is influenced by an interaction between three high pressure areas. Here, the most distinct area is over west China; others are a large area over southeast China crossing Taiwan toward the west Pacific, and one over India. Prevailing winds in the Zhujiang River basin circulate over southeast China, the west Pacific, and the South China Sea, and the wind direction is south–southwest.

Figure 6c shows a composite of the monthly circulation pattern for years with high January precipitation (1969, 1983, 1992, 1997, and 2003). This circulation pattern is similar in each of the years with ''wet'' January.

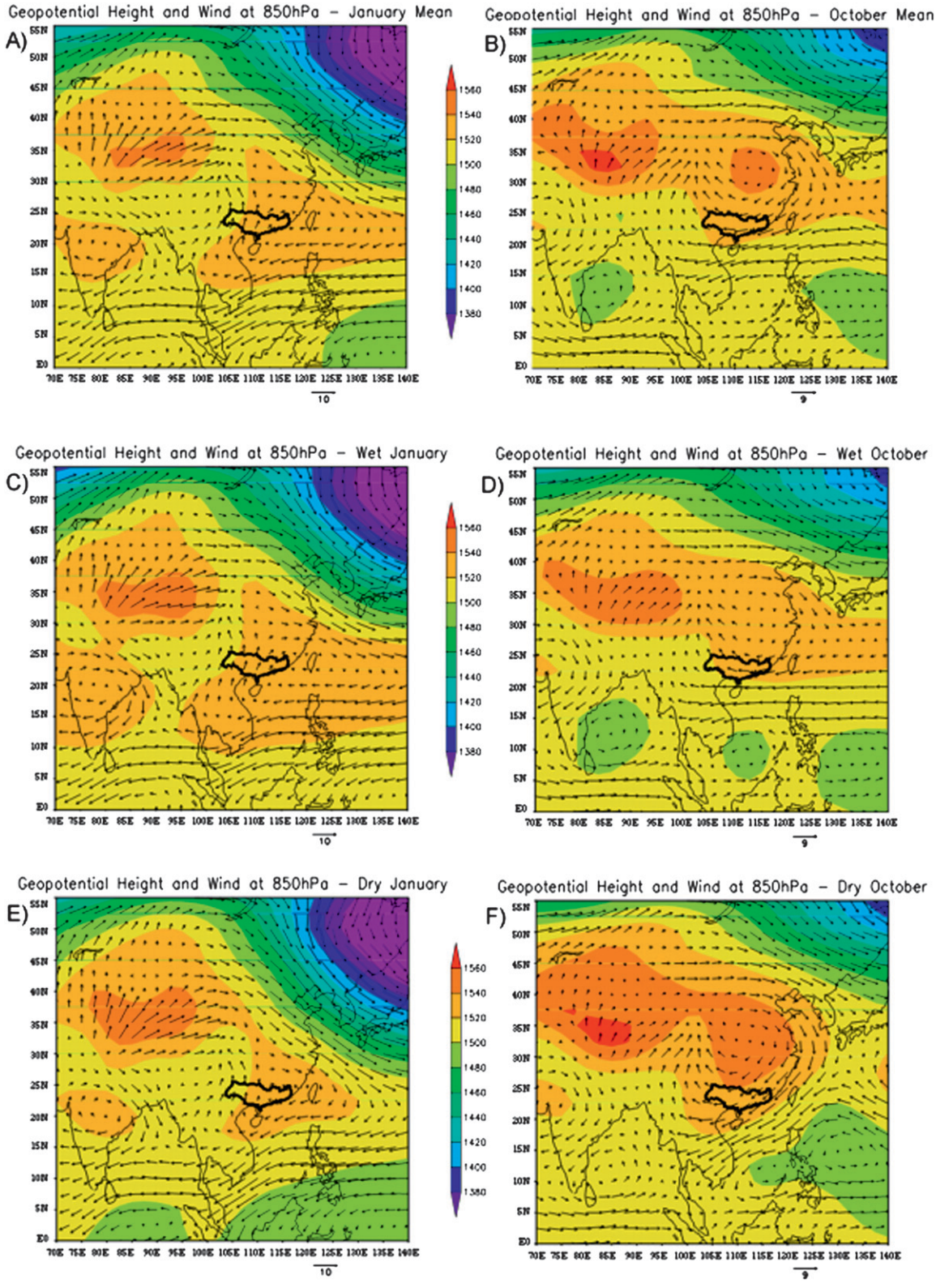

FIG. 6. Characteristics of 850-hPa geopotential height and winds: (a) mean of all Januarys 1961–2007, (b) mean of all Octobers 1961–2007, (c) composite of Januarys with high precipitation, (d) composite of Octobers with high precipitation, (e) composite of Januarys with low precipitation, and (f) composite of Octobers with low precipitation (the Zhujiang River basin is outlined in black; winds at 850 hPa are theoretical for the Qinghai–Tibet Plateau or any higher mountain range).

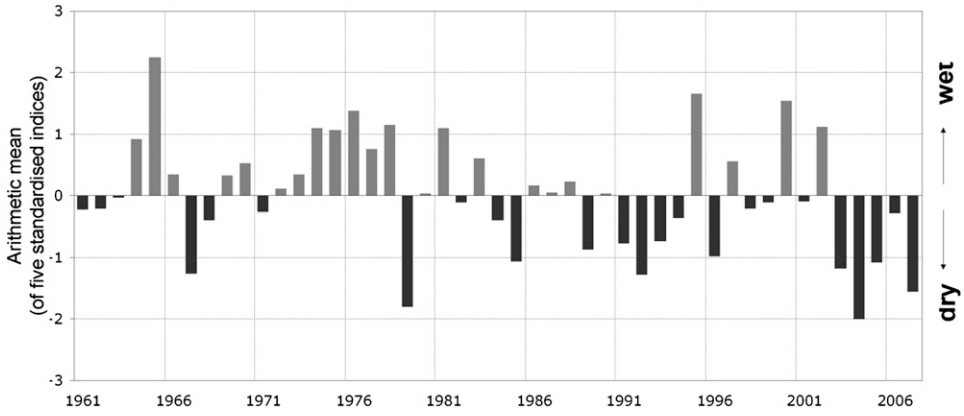

FIG. 7. Arithmetic mean of five standardized precipitation indices (monthly precipitation, 5-day max precipitation, precipitation intensity, rain days, maximum precipitation) for October from 1961 to 2007 in the Zhujiang River basin.

The circulation is influenced by a distinct high over west China and a band of high pressure that covers the entire east and southeast Asian continent. Circulation is similar to the multiannual mean (Fig. 6a), but the circulation over the Zhujiang River basin is less strong. A composite of the large-scale system for the years 1963, 1976, 1986, 1994, and 2006 with low January precipitation (dry January) is shown in Fig. 6e. It is quite similar to the mean; however, the high over India is less distinct. At the same time, the western extension of the anticyclone over southeast China hardly covers the coastal area. The speed of the winds entering the Zhujiang River basin is below average.

When examining the monthly time series of winds at 850 hPa since 1961, it can be concluded that average and high precipitation in January occurs when a high pressure field north of the Himalayas forms, the intensity and size of which is stronger than that of the high over India. Reasons for positive precipitation trends in January, however, cannot entirely be explained by changes in large-scale circulation. The atmospheric conditions are, to a certain extent, stable in January with no distinct changes in the mean wind directions. The positive trends might be related to local climatic conditions in the topographically diverse basin of the Zhujiang River; they might also be driven by the different wind speed that can be observed for years with precipitation means above and below January.

b. October precipitation

The average large-scale circulation in October is shown in Fig. 6b. In the multiannual mean in October, two anticyclones form over west and east China, respectively. Strong easterly winds are supported by a low pressure system over the Philippines and are blocked from entering the Zhujiang River basin. In October, the long-term wind direction in the basin is easterly and the winds have crossed the East China Sea. Strong winds from the east transport water vapor to the basin if the high over east China has not developed. The system is further supported by the belt of lower pressure south of China.

In Fig. 6d, the circulation in October has been composited for five years with high October precipitation (1965, 1976, 1995, 2000, and 2002). Winds from the east-southeast transport water vapor to the Zhujiang River basin. Precipitation, number of rain days, and other precipitation indices in October are higher in the basin if the high over west China is small in size.

Figure 6f shows a composite of the large-scale circulation in October for the years 1967, 1979, 1992, 2004, and 2007, which show the most significant negative precipitation indices (see Fig. 7). It represents the October circulation during dry conditions. Low October precipitation indices are detected if a high pressure system forms over east China and if this is bordered by a trough to the east. The mean wind direction is north-northeast. The water vapor is potentially lower as it is transported directly from north China and the Bohai Sea.

The negative trend in precipitation indices in October is influenced by a large-scale high over west China and a deep pressure system in the western North Pacific that forms a trough, changing the mean wind direction in the Zhujiang River basin from east to northeast or east-northeast. This is the so-called East Asian Trough, which is typical for the EAWM (Wang et al. 2009). Wang and Ding (1997) described the onset of the EAWM as being in October. The EAWM is delivering dry, cold air from northeast China to the Zhujiang River basin.

Figure 7 shows the annual arithmetic mean (see section 2) of five standardized precipitation indices (monthly precipitation, 5-day maximum precipitation, precipitation intensity, rain days, and maximum precipitation) in the

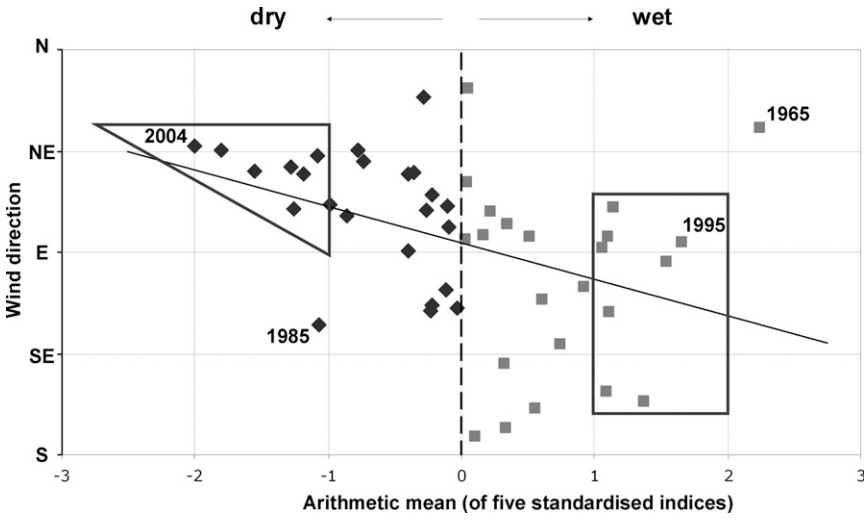

FIG. 8. Arithmetic mean of five standardized precipitation indices (monthly precipitation, 5-day maximum precipitation, precipitation intensity, rain days, maximum precipitation) in the Zhujiang River basin for October 1961–2007, mean wind direction in the eastern part of the Zhujiang River basin October 1961–2007, linear trend (line), and highlighted severe dry (triangle) and wet (square) Octobers.

Zhujiang River basin in October from 1961 to 2007. As can be seen, some years show pronounced negative means and indicate dry October months (2007, 2005, 2004, 2003, 1992, 1979, 1985, and 1967). Figure 8 shows the arithmetic mean of the same five standardized precipitation indices for October during 1961 to 2007 and the according mean wind direction in the eastern part of the Zhujiang River basin for each index (e.g., wind direction in dry and wet October months). The linear trend of the wind direction 1961–2007 is also displayed. It becomes clear that years with extremely negative means of standardized precipitation indices (dry October months) occurred when the large-scale winds at 850 hPa entered the Zhujiang River basin from the northeast. With the exception of 1985, the nine October months with a mean of -1 or below (i.e., the nine most severe dry October months, indicated by the triangle in Fig. 8) can be explained by general circulation typical for the EAWM (89%). Wet October months can be observed in years when the mean wind direction is east or southeast (indicated by the square in the right part of Fig. 8) with the exception of 1965. The dry (wet) October in the exceptional year 1985 (1965) might be explained by local circumstances—for example, occurrence of a tropical cyclone or heat wave instead of by large-scale wind patterns. The linear trend displayed in Fig. 8 illustrates that the more wind comes from northeast (southeast) in October, the drier (wetter) the weather conditions are. The observed trends toward lower precipitation in October might be related to an early onset of the EAWM, but is definitely caused by the change of the mean wind directions. Over the time series 1961–2007, the mean wind direction in the Zhujiang River basin has experienced a change by 50° from east-southeast to east-northeast (Fig. 9). Checking the occurrence of El Niño and La Niña years leads to the assumption that low precipitation and its indices in October are associated with northerly winds in the transition phase between two El Niño events. This is consistent with the findings of Zhou et al. (2007), who found many strong EAWM in the years before the developing year of an El Niño or during the decaying La Niña years.

5. Discussion and conclusions

The paper has made use of some basic methods to analyze data on precipitation trends in the Zhujiang River basin that have not been made available in the current form elsewhere. The approach is very helpful to

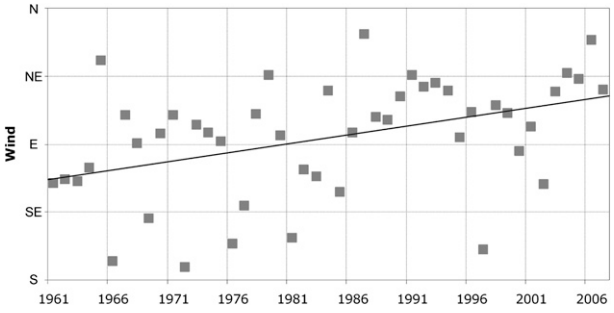

FIG. 9. Mean wind direction in the eastern part of the Zhujiang River basin for October 1961–2007 and its linear trend.

detect positive and negative trends in precipitation and indices related to precipitation extremes on a monthly and daily basis. Few stations show significant trends above a 90% confidence level for annual indices. The only index that shows a somewhat negative direction is the number of annual rain days. This is consistent with the findings of Zhang et al. (2009a). Annual maximum precipitation shows trends at 18 of 192 stations. This is the highest number of detected trends on an annual basis and indicates that less than 9% of all stations in the Zhujiang River basin show significant trends in annual extreme precipitation events (maximum precipitation, rainstorm days, intensive rain days, extremely intensive rain days for 90/95/99 percentile rain events). No spatial pattern can be detected for the stations with significant trends. Zhang et al. (2009a) also report that no trends can be detected for annual precipitation in the Zhujiang River basin. We can therefore conclude that no distinct regions in the Zhujiang River basin have experienced trends for annual indices.

Our results for the monthly precipitation trends as well as for the monthly indices of rain days, intensity, maximum precipitation, and 5-day maximum precipitation are somewhat in line with the seasonal findings by Zhang et al. (2009a), who estimate increasing trends in total precipitation, precipitation intensity, and rain days in winter [(December–February (DJF)]. Our findings are also supported on a seasonal basis by Liu et al. (2009), who detected that autumn precipitation decreased, but spring, summer, and winter precipitation increased during the period covered by the same time series.

Each of the previous studies delivered findings that are correct for the time series of data and the number of stations used. Comparing this paper's results on monthly and daily basis with previous studies on seasonal basis shows that much more interpretation is possible on monthly basis. If monthly results were merged for seasons (e.g., September, October, and November merged to ''autumn''), the information on the significant decrease of precipitation intensity in October would have been lost. Additionally, monthly changes of wind direction that could explain trends in October precipitation could not be assessed.

In this study, 192 stations that passed a homogeneity and quality check have been used, compared to other studies that used less than one quarter of these stations without official checks. This, in combination with the use of the maximum possible number and quality of stations, delivers new information on the quality and quantity of observed trends.

The observed positive precipitation trends in January cannot be explained by changes in large-scale wind directions. Reasons might be found in local climatic conditions or in the generally low monthly precipitation. Generally, the wind speed is different in years with observed high, mean, and low precipitation in January, which might be a factor causing positive trends. This will be examined in future studies.

The change of the mean wind direction in years with below-average precipitation and rain days in October is an interesting finding that has not been described before. Chou (2004) described a weak anomalous cyclone over the Philippine Sea and the South China Sea in the developing summer of an El Niño event. October, marking the transition period between the East Asian summer monsoon (EASM) and the EAWM, has not received much attention in climate studies yet, but it appears to be sensitive with regards to areal precipitation. The negative trends in the precipitation indices in October are consistent with the trend in the mean wind direction at 850 hPa. Therefore, low precipitation records in October can be explained by pressure systems typical for the EAWM and winds from northeast and east-northeast in the eastern part of the Zhujiang River.

In forthcoming research, the authors will further examine the return periods of extreme events on a monthly basis for below- (above-) average October (January) precipitation and indices and investigate links with the statistical onset of the EAWM.

Acknowledgments. This study was supported by the National Basic Research Program of China (973 Program) 2010CB428401 and the Non-Profit Industry Fund of the Ministry of Water Resources (200701005). The positions of Marco Gemmer and Thomas Fischer at the National Climate Center are supported by German Development Cooperation through the Center for International Migration and Development (http://www.cimonline.de). Cordial thanks are extended to the editor Dr. Nathan Gillett and the anonymous reviewers for their professional comments and suggestions, which greatly improved the quality of this manuscript, and to Dr. Andreas Wilkes of the World Agroforestry Center (ICRAF) China Programme, who helped improve the English of this manuscript.

REFERENCES

Alexandersson, H., 1986: A homogeneity test applied to precipitation data. *J. Climatol.,* **6,** 661–675.

Becker, S., M. Gemmer, and T. Jiang, 2006: Spatiotemporal analysis of precipitation trends in the Yangtze River catchment. *Stochastic Environ. Res. Risk Assess.,* **20,** 435–444, doi:10.1007/s00477-006-0036-7.

Buishand, T. A., 1982: Some methods for testing the homogeneity of rainfall records. *J. Hydrol.,* **58,** 11–27.

Chen, W., H.-F. Graf, and R. Huang, 2000: The interannual variability of East Asian Winter Monsoon and its relation to summer monsoon. *Adv. Atmos. Sci.,* **17,** 48–60.

Chou, C., 2004: Establishment of the low-level wind anomalies over the western North Pacific during ENSO development. *J. Climate,* **17,** 2195–2212.

Ding, Y., and Coauthors, 2007: China's National Assessment Report on Climate Change (I): Climate change in China and the future trend. *Adv. Climate Change Res.,* **3** (Suppl.), 1–5.

Feng, S., S. Nadarajah, and Q. Hu, 2007: Modeling annual extreme precipitation in China using the generalized extreme value distribution. *J. Meteor. Soc. Japan,* **85,** 599–613.

Fu, J., W. Qian, X. Lin, and D. Chen, 2008: Trends in graded precipitation in China from 1961 to 2000. *Adv. Atmos. Sci.,* **25,** 267–278.

Gao, C., M. Gemmer, X. Zeng, B. Liu, B. Su, and Y. Wen, 2010: Projected streamflow in the Huaihe River basin (2010–2100) using artificial neural network. *Stochastic Environ. Res. Risk Assess.,* **24,** 685–697.

Gemmer, M., S. Becker, and T. Jiang, 2004: Observed monthly precipitation trends in China 1951–2002. *Theor. Appl. Climatol.,* **77,** 39–45.

Goovaerts, P., 2000: Geostatistical approaches for incorporating elevation into the spatial interpolation of rainfall. *J. Hydrol.,* **228,** 113–129.

Hartmann, H., L. King, T. Jiang, and S. Becker, 2009: Quasi-cycles in Chinese precipitation time series and in their potential influencing factors. *Quat. Int.,* **208,** 28–37.

Kalnay, E., and Coauthors, 1996: The NCEP/NCAR 40-Year Reanalysis Project. *Bull. Amer. Meteor. Soc.,* **77,** 437–471.

Liu, B., M. Xu, M. Henderson, and Y. Qi, 2005: Observed trends of precipitation amount, frequency, and intensity in China, 1960–2000. *J. Geophys. Res.,* **110,** D08103, doi:10.1029/2004JD004864.

Liu, L., T. Jiang, and F. Yuan, 2009: Observed (1961–2007) and projected (2011–2060) climate change in the Pearl River basin (in Chinese). *Adv. Climate Change Res.,* **5,** 209–214.

Luo, Y., S. Liu, S. Fu, J. Liu, G. Wang, and G. Zhou, 2008: Trends of precipitation in Beijiang River basin, Guangdong Province, China. *Hydrol. Processes,* **22,** 2377–2386.

Peterson, T. C., and Coauthors, 1998: Homogeneity adjustments of in situ atmospheric climate data: A review. *Int. J. Climatol.,* **18,** 1493–1517.

Qian, W., and X. Lin, 2005: Regional trends in recent precipitation indices in China. *Meteor. Atmos. Phys.,* **90,** 193–207.

Roeckner, E., and Coauthors, 2003: The atmospheric general circulation model ECHAM5. Part I: Model description. Max-Planck-Institute for Meteorology Rep. 349, 127 pp.

Trenberth, K. E., and Coauthors, 2007: Observations: Surface and atmospheric climate change. *Climate Change 2007: The Physical Science Basis,* S. Solomon et al., Eds., Cambridge University Press, 235–336.

Wang, L., R. Huang, L. Gu, W. Chen, and L. Kang, 2009: Interdecadal variations of the East Asian winter monsoon and their association with quasi-stationary planetary wave activity. *J. Climate,* **22,** 4860–4872.

Wang, Q., and Y. Ding, 1997: Climatological characteristics of evolution of East Asian Winter Monsoon. *Quart. J. Appl. Meteor.,* **8,** 186–196.

Wang, Y., and L. Zhou, 2005: Observed trends in extreme precipitation events in China during 1961–2001 and the associated changes in large-scale circulation. *Geophys. Res. Lett.,* **32,** L09707, doi:10.1029/2005GL022574.

Yang, F., and K.-M. Lau, 2004: Trend and variability of China precipitation in spring and summer: Linkage to sea surface temperatures. *Int. J. Climatol.,* **24,** 1625–1644.

Yang, T., Q. Shao, Z.-C. Hao, X. Chen, Z. Zhang, C.-Y. Xu, and L. Sun, 2010: Regional frequency analysis and spatio-temporal pattern characterization of rainfall extremes in the Pearl River basin, China. *J. Hydrol.,* **380,** 386–405.

Yao, C., S. Yang, W. Qian, Z. Lin, and M. Wen, 2008: Regional summer precipitation events in Asia and their changes in the past decades. *J. Geophys. Res.,* **113,** D17107, doi:10.1029/2007JD009603.

Zhai, J., B. Su, V. Krysanova, T. Vetter, C. Gao, and T. Jiang, 2010: Spatial variation and trends in PDSI and SPI indices and their relation to streamflow in 10 large regions of China. *J. Climate,* **23,** 649–663.

Zhai, P., A. Sun, F. Ren, X. Liu, B. Gao, and Q. Zhang, 1999: Changes of climate extremes in China. *Climatic Change,* **42,** 203–218.

——, X. Zhang, H. Wan, and X. Pan, 2005: Trends in total precipitation and frequency of daily precipitation extremes over China. *J. Climate,* **18,** 1096–1108.

Zhang, Q., C.-Y. Xu, S. Becker, Z. X. Zhang, Y. D. Chen, and M. Coulibaly, 2009a: Trends and abrupt changes of precipitation maxima in the Pearl River basin, China. *Atmos. Sci. Lett.,* **10,** 132–144.

——, ——, M. Gemmer, Y. D. Chen, and C. Liu, 2009b: Changing properties of precipitation concentration in the Pearl River basin, China. *Stochastic Environ. Res. Risk Assess.,* **23,** 377–385.

——, ——, and Z. Zhang, 2009c: Observed changes of drought/wetness episodes in the Pearl River basin, China, using the standardized precipitation index and aridity index. *Theor. Appl. Climatol.,* **98,** 89–99.

Zhou, L.-T., and R. Wu, 2010: Respective impacts of the East Asian winter monsoon and ENSO on winter rainfall in China. *J. Geophys. Res.,* **115,** D02107, doi:10.1029/2009JD012502.

Zhou, W., X. Wang, T. J. Zhou, C. Li, and J. C. L. Chan, 2007: Interdecadal variability of the relationship between the East Asian winter monsoon and ENSO. *Meteor. Atmos. Phys.,* **98,** 283–293.

Appendix III

Fischer, T., M. Gemmer, L. Liu and T. Jiang, 2012: Change-points in climate extremes in the Zhujiang River Basin, South China, 1961-2007. *Climatic Change*, Volume 110, 783-799.

Climatic Change (2012) 110:783–799
DOI 10.1007/s10584-011-0123-8

Change-points in climate extremes in the Zhujiang River Basin, South China, 1961–2007

Thomas Fischer · Marco Gemmer · Lüliu Liu · Buda Su

Received: 21 October 2010 / Accepted: 18 May 2011 / Published online: 8 June 2011

Abstract In this paper, change-points in time series of annual extremes in temperature and precipitation in the Zhujiang River Basin are analyzed with the CUSUM test. The data cover the period 1961–2007 for 192 meteorological stations. Annual indicators are analyzed: mean temperature, maximum temperature, warm days, total precipitation, 5-day maximum precipitation, and dry days. Significant change-points (1986/87, 1997/98, 1968/69, and 2003/04) are detected in the time series of most of the indicators. The change-point in 1986/87 is investigated in more detail. Most stations with this change-point in temperature indicators are located in the eastern and coastal areas of the basin. Stations with this change-point in dry days are located in the western area. The means and trends of the temperature indicators increase in the entire basin after 1986/87. The highest magnitudes can be found at the coast and delta. Decreasing (increasing) tendencies in total and 5-day maximum precipitation (dry days) are mostly observed in the western and central regions. The detected change-points can be explained by changes in the indices of the Western Pacific subtropical high and the East Asian summer monsoon as well as by change-points in wind directions. In years when the indices simultaneously increase and decrease (indices taking reverse directions to negative and positive) higher annual temperatures and lower annual precipitation occur in the Zhujiang River Basin. The high station density and data quality are very useful for spatially assessing

T. Fischer (✉) · M. Gemmer · L. Liu · B. Su
National Climate Center, China Meteorological Administration,
46, Zhongguancun Nandajie, Haidian, Beijing, 100 081, People's Republic of China
e-mail: thomas.fischer1@cimonline.de, tom.fischer8@gmx.de

T. Fischer
Xinjiang Institute of Ecology and Geography, Chinese Academy of Sciences,
Urumqi, People's Republic of China

B. Su
Nanjing University of Information Science and Technology,
Nanjing, People's Republic of China

change-points of climatic extreme events. The relation of the change points to large-scale oscillation can provide valuable data for planning adaptation measures against climate risks, e.g. for flood control, disaster preparedness, and water resource management.

1 Introduction

In China, an increasing population lives in areas vulnerable to extreme events such as floods, rain storms, and droughts. These extreme weather events are very likely to cause damages to ecosystems and hence affect the socio-economic sphere. The fast growing population and industrialization in major river basins in China in recent decades have increased the damage potentials that extreme climate events and other natural disasters have (Feng et al. 2007). Weather extremes are common in China due to the huge Asian landmass influencing the large-scale circulation and China's various climate regimes (Zhai et al. 2005). Flood, rain storm, and drought events become more important variables in hampering sustainable development. The intensity and frequency of these extremes are of main concern and have been substantiated by multiple studies on climate change in China and in the world (Ding et al. 2007; Trenberth et al. 2007; Klein Tank et al. 2009; Hoskins 2003).

The East Asian Summer Monsoon (EASM) and the Western Pacific subtropical high (WP) have been identified as strong influencing climate factors in the South China region (Ding et al. 2008; Yin et al. 2009; Yu et al. 2009). Morrill et al. (2003) and Qian et al. (2007) identified that variations in components of the climatic system have the potential for triggering rapid and major shifts in the Asian monsoon precipitation.

A fundamental approach to understand the behavior of extreme events is the detection of trends and change-points in time-series (Hoskins 2003; Seidel and Lanzante 2004). For South China, many studies already dealt with trends in temperature and precipitation extremes, which often found higher frequency and increasing intensity. Increasing annual temperature and precipitation in the Zhujiang River Basin of South China for the period of 1961–2007 have been detected by Liu et al. (2009). They observed the highest temperature increases in the winter season. For the annual extreme high temperatures in China, an insignificant rise was detected by Ren et al. (2005a). According to Ding et al. (2007), southeast China experienced an increase in annual precipitation by around 60 to 130 mm during the last fifty years. Qian and Lin (2005) found different results when analyzing regional characteristics of daily precipitation indices for 494 stations in China (1961–2000) and depict a negative decadal tendency in annual and summer precipitation in coastal southeast China. Gemmer et al. (2011) observed increasing tendencies to dryer conditions and stronger precipitation intensities using 192 quality-controlled precipitation datasets for the Zhujiang River Basin from 1961–2007. Analyzing the SPI, no significant trends in frequencies of dry/wet days and runoff anomalies have been detected by Zhai et al. (2009) in this region. This was also elaborated by Fischer et al. (2010) who observed significant negative trends in dry days on the basis of 192 quality-controlled time-series. All of these studies applied the Mann–Kendall test and/or the linear regression to identify trends in climate indicators.

An important question is whether climate trends occurred gradually or rapidly. Qian et al. (2007) already linked climate change-points and regime shifts in China to

the interaction of mid- and low latitude atmospheric circulations by. Zhang et al. (2009a) applied a Bayesian change-point analysis to annual, summer, and winter precipitation and intensity, using data of 47 meteorological stations in the Zhujiang River Basin. The authors concluded that the abrupt changes in the precipitation totals occurred in the late 1970s, 1980s and early 1990s and these of the precipitation intensity occurred in 1972–1975. The precipitation intensity generally increased after the change-point. Leung and Wu (2005) used the cumulative summation (CUSUM) method to identify regime shifts in summer rainfall in South China during the period 1952–2003. They discovered one shift from wet to dry conditions between the mid-1970s and another shift from dry to wet in the early 1990s. A northward shift of the Meiyu (summer monsoon rainfall) belt of East China in 1999 has been observed by Si et al. (2009) using the Empirical Orthogonal Function analysis. Implying trends to dryer conditions in South China, they associated this shift to changes in the atmospheric circulation over East Asia.

Most variations in climate and atmospheric circulation are certainly natural, while some components could be associated with increased concentrations of greenhouse gases or other anthropogenic effects (Miller et al. 1994). The studies of shifts in climate regimes and of various natural climate variations are of paramount importance (Hoskins 2003; Seidel and Lanzante 2004). Detection of abrupt changes in climate systems (change-point detection) has been rarely applied to temperature and precipitation indicators in the Zhujiang River Basin, South China, a densely populated area which has already been subject to the negative impacts of weather extremes. The changing temporal patterns, i.e. change-points and trends, are variables essential for adaptation measures in flood control, disaster preparedness, and water resource management. Time-series of observed climate data for assessing and estimating climate variables are therefore relevant for the implementation of necessary adaptation measures (Adger et al. 2007; Klein Tank et al. 2009).

The objectives of this study are therefore, (1) to detect abrupt changes in climate indicators in the Zhujiang River Basin, (2) to analyze the trends and spatial extent, and (3) to investigate their relation with characteristics of atmospheric circulation patterns. This approach will give insights to the spatio-temporal behaviour of extreme climate events and their underlying causes which, for example, is required for planning of climate change adaptation measures in South China.

2 Data and methodology

2.1 Regional setting

The Zhujiang River Basin (also known as the Pearl River Basin) is located in South China. The basin covers approximately 579,000 km^2 and embraces the administrative areas of Guangdong Province and Guangxi Autonomous Region almost entirely. It also cuts into the provinces of Yunnan, Guizhou, Hunan, Jangxi, and Fujian. A tropical to sub-tropical climate prevails while the East Asian Monsoon has strong influences on it. The basin has mountainous areas in the western part but got mainly low lands in the central and south-eastern parts. The Zhujiang River consists of three main tributaries, i.e. the Xijiang River, Beijiang River, and Dongjiang River. The Xijiang River is the largest and drains the entire western and central parts of

the basin, while the other two catchments are found in the east. All three have a south-east (-west) ward stream flow direction due to the basin's topography. At the south-eastern coastal area, the tributaries merge into a large network delta (i.e. Zhujiang River Delta) before they mound into the South China Sea. A more detailed description of the basins climatic and hydrologic conditions are provided by Yang et al. (2010) and Zhang et al. (2009b), while historic and current data related to the basin can also be found on the website of the Pearl River Water Resource Commission (www.pearlwater.gov.cn). An elevation map including the location of the 192 weather stations used in this study and the course of the main river system is provided in Fig. 1.

Fig. 1 Overview map of the Zhujiang River Basin in South China, indicating elevation (*shading*), administrative boundaries (*grey lines*) incl. names, and the location of the meteorological stations (*black dots*)

2.2 Data

Daily temperature and precipitation records of 192 meteorological stations in the Zhujiang River Basin for the period 1961–2007 are used. The data set was provided by the National Meteorological Information Center (NMIC) of the China Meteorological Administration (CMA). The data sets were controlled on their quality by the NMIC (Qian and Lin 2005). The NMIC checked the data on homogeneity using the departure accumulating method (Buishand 1982). Due to the results, the temperature data records used in this study have been homogeneity-adjusted (Song et al. 2004; Ren et al. 2005a, b). The precipitation data records remain unadjusted. Less than 0.1 percent of data gaps appear in the daily temperature and precipitation records.

The East Asian Summer Monsoon index (EASMI) is based on the intensity of the normalized seasonality of the wind field at 850 hPa (10–40° N, 110–140° E) for June to August (Li and Zeng 2003). The annual EASMI data is available on the website of the Chinese State Key Laboratory of Numerical Modelling for Atmospheric Sciences and Geophysical Fluid Dynamics (http://www.lasg.ac.cn/staff/ljp/data-monsoon/EAMI1948-present.ascii).

The WP index (WPI) specifies the low-frequency variability of a north-south dipole of the western North Pacific. It signifies the zonal and meridional variation of the location and intensity of the East Asian jet stream entrance region, i.e. the northward shift of the Western Pacific subtropical high (Barnston and Livezey 1987). The WPI data (monthly/annual) is provided by the U.S. National Centers for Environmental Prediction (NCEP) on their website (http://www.cpc.ncep.noaa.gov/data/).

Vector data of monthly u-/v-winds (gridded for 22.5–25° N and 112.5–115° E) within the eastern part of the Zhujiang River Basin are also derived from NCEP website (http://www.esrl.noaa.gov/psd/data/).

2.3 Methodology

2.3.1 Indicators

Based on daily temperature and precipitation data (1961–2007), six climate indicators are created for the detection of change-points in temperature and precipitation extremes (Table 1). Temperature indicators are the annual mean temperature (T_{mean}), the annual maximum temperature (T_{max}), and the annual number of warm days (T_{90}). The precipitation indicators consist of the annual total precipitation (P_{total}), the annual 5-day maximum precipitation (P_{5day}), and the annual number of dry days (P_{dry}). The climate indicators were defined on fixed terms predetermined by the China Meteorological Administration or international standards (Li et al. 2010; Qian and Lin 2005; Su et al. 2008; Klein Tank et al. 2009). The peak over threshold indicator (i.e. T_{90}) is based on the time period 1961–2007. This approach on percentile values provides a good comparability of single stations (Li et al. 2010).

2.3.2 Change-point detection

A change-point analysis is applied to six climate indicators (1961–2007) for 192 meteorological stations. A combination of cumulative sum charts and bootstrapping is applied to detect abrupt changes within the time-series (Taylor 2000; Leung and

Table 1 List of six temperature and precipitation indicators used for analysis in the Zhujiang River Basin (1961–2007)

ID	Name	Definition	Unit
T_{mean}	Mean temperature	Annual average value of daily mean temperature	°C
T_{max}	Maximum temperature	Annual maximum value of daily mean temperature	°C
T_{90}	Warm days	Annual number of days above the 90-percentile of mean temperature	days
P_{total}	Total precipitation	Annual total precipitation	mm
P_{5day}	5-day maximum precipitation	Annual maximum consecutive 5-day precipitation	mm
P_{dry}	Dry days	Annual number of days with precipitation below 0.1 mm	days

Wu 2005). The difference between the annual values and the arithmetic mean (μ) of the time-series are calculated and cumulated as follows:

$$S_i = S_i - 1 + (x_i - \mu) \qquad (\text{with } i = 1, \ldots, \text{ n and } S_0 = 0) \tag{1}$$

where S_i is the cumulative sum, μ is the arithmetic mean of the time-series, x is the variable.

The cumulative sums (S_i) are plotted and interpreted. CUSUM delivers information on segments with notable slopes and abrupt turns in direction, which give an indication of a shift in the average. The confidence level is determined by performing a bootstrap analysis. As an estimator of the magnitude of change (S_{diff}) we define the difference of the maximum cumulative sum:

$$S_{diff} = \max S_i - \min S_i \qquad (\text{with } i = 0, \ldots, \text{ n}) \tag{2}$$

In this study 1,000 bootstrap samples (S_i^0) of n samples (here: 47) for each station and climate indicator are generated. For each bootstrap sample the CUSUM is performed and its respective magnitude of change ($S_{i\,diff}^0$) is calculated following Eq. 2. The confidence level is determined by the difference of bootstrap samples with $S_{i\,diff}^0 < S_{diff}$ and the total number of bootstrap samples (here: 1,000). We consider change-points if the significance is marked by a confidence level of minimum 95%, i.e. at least 950 out of 1,000 bootstrap samples have a magnitude of change ($S_{i\,diff}^0$) below the magnitude of change (S_{diff}) of the original data.

The CUSUM estimator (Taylor 2000) detects whether a change occurred. The point furthest from zero (S_m) in the CUSUM chart is the last point (m) in time (here: year) before the change:

$$S_m = \max |S_i| \qquad (\text{with } i = 0, \ldots, \text{n}) \tag{3}$$

The best occurrence of the detected change is between m and $m + 1$. After detecting a significant change-point, the original data is divided into two segments, one before and one after the change-point. The whole of the change-point detection procedure is repeated with each segment and sub-segment until no significant change reoccurs. The same procedure was applied for the time-series of wind direction in the eastern part of the Zhujiang River Basin in October. In this study, up to four change-points are detected for single time-series. For each year and climate indicator, the

basin-wide number of change-points is determined as the sum of stations which show a change-point in the respective year and indicator time-series (Taylor 2000; Leung and Wu 2005). The results are combined to several 2-year-periods, which comprise the highest numbers in change-points encountered.

2.3.3 The z-score and shift of indicator classes

In order to spatially visualize the absolute changes of the indicators, the flat steps method (Seidel and Lanzante 2004) was used. Here, the arithmetic means (μ_1 and μ_2) of the periods before and after the most significant change-point were calculated for each station. The standard score (z) is calculated (Wilks 2006) in order to compare the station-based indicator values. It indicates by how many standard deviations the arithmetic mean of the period after the change-point (μ_2) is above or below the arithmetic mean of the period before the change-point (μ_1). The z-score reflects the tendency in changing temporal patterns of the indicators in standardized terms. The z-score is a dimensionless quantity derived by subtracting the time-series mean from an individual raw score and then dividing the difference by the time-series standard deviation:

$$z = (x - \mu)/\sigma \tag{4}$$

where μ is the arithmetic mean of the time-series (i.e. μ_1), x is the variable (i.e. μ_2), and σ is the standard deviation of the time-series (i.e. standard deviation of μ_1). A z-score of 1.0 for example depicts a shift by one standard deviation of the time-series after the change-point as compared to the time-series before the change-point. The further the z-score is away from zero, the larger is the actual shift of the two time-series' means.

Varying indicator classes (three to six) are used to illustrate the spatial shift of the arithmetic mean of the period after the change-point (μ_2) to the arithmetic mean of the period before the change-point (μ_1). The z-scores, indicators classes and the shifts were spatially interpolated using the Inverse Distance Weighting (IDW) method (Gemmer et al. 2004).

3 Results

3.1 Change-point detection

Each time-series for each indicator (192 stations) was analyzed for significant change-points. In numerous time-series, change-points were not detected, while in some others more than one change-point occurred. The number of stations where no change-points were detected varies greatly for each indicator. As can be seen in Table 2, in T_{mean}, only 9% of the stations but up to 88 (87)% in P_{total} (P_{5day}) did not experience any abrupt changes. Correspondingly, much more stations with change-points are found for temperature indicators than for precipitation indicators.

Some distinct 2-year-periods show relatively high number of stations with significant change-points. For T_{mean}, three significant change-points were detected in the years 1986/87, 1997/98, and 1968/69 which occurred at 42%, 71%, and 11% of all stations in the Zhujiang River Basin (Table 2). Change-points in T_{max} and T_{90} were detected for a lower percentage of stations. The highest percentage of stations (11%

Table 2 Number of stations (#), and percentage of total stations (%), with detected change-point (CUSUM) at the most significant 2-year-periods for temperature and precipitation indicators (192 stations in the Zhujiang River Basin 1961–2007)

Change-point	T_{mean}		T_{max}		T_{90}		P_{total}		P_{5day}		P_{dry}	
	#	%	#	%	#	%	#	%	#	%	#	%
1967–1968	22	11	6	3	9	5	2	1	1	1	0	0
1986–1987	81	42	21	11	52	27	2	1	1	1	64	33
1997–1998	137	71	14	7	47	24	0	0	2	1	12	6
2003–2004	4	2	18	9	13	7	0	0	1	1	15	8
No CP	18	9	71	37	48	25	168	88	167	87	87	45

and 27% respectively) had a significant change-point in 1986/87, followed by 1997/98 (7% and 24% respectively). Especially in T_{90}, change-points were also estimated for the late 1970s, early 1980's and early 1990's at 13% to 17% of all stations. For P_{total} and $P_{5day,}$ few stations (highest of 7% in 1984/85 and 1992/93) showed change-points throughout the time-series (not displayed). In P_{dry}, more than 33% of all stations experienced a significant change-point in 1986/87. With less stations (6% and 8%) and similar to the temperature indicators, change-points are also detected for 1997/98 and 2003/04. The most significant results of the CUSUM change-point analysis for

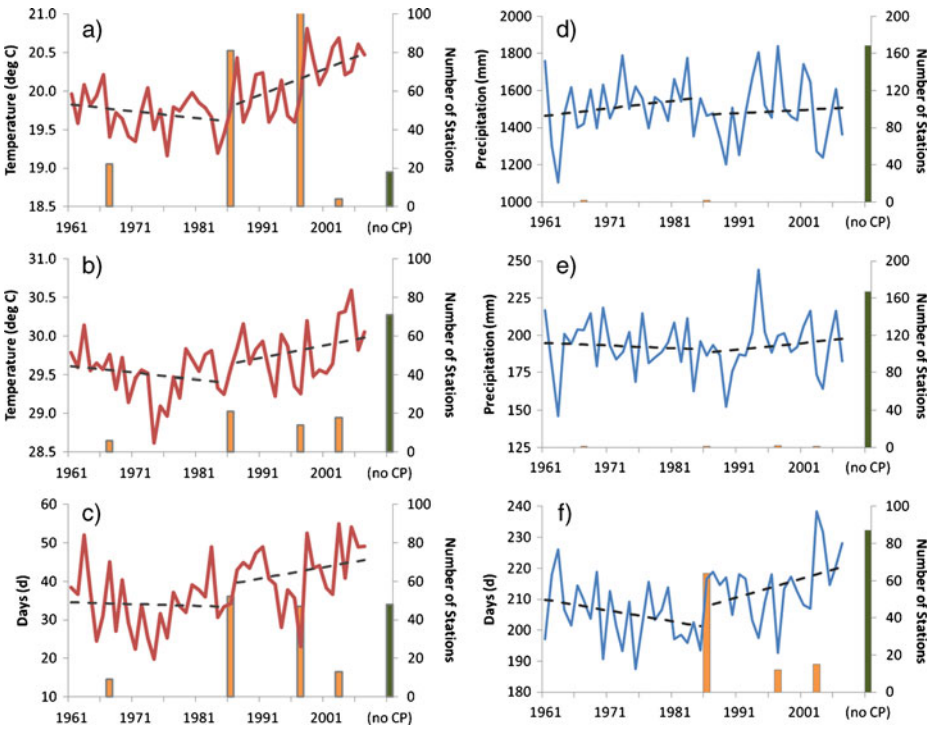

Fig. 2 Basin-averaged time-series (1961–2007) of **a** T_{mean}, **b** T_{max}, **c** T_{90}, **d** P_{total}, **e** P_{5day}, and **f** P_{dry} (*red or blue line*, *left axis*), number of stations with most significant or no change-points (*yellow or green column*, *right axis*), and trends (*dashed lines*) for the periods of 1961–1986 and 1987–2007

Table 3 Annual means, z-score, and trends (unit per year) of six temperature and precipitation indicators in the time-periods before (1961-1986) and after (1987-2007) the detected most significant change-point (1986/87), averaged of 192 stations in the Zhujiang River Basin

Indicators	T_{mean}	T_{max}	T_{90}	P_{total}	P_{5day}	P_{dry}
Annual mean 1961–1986 (μ_1)	19.7°C	29.5°C	33.9d	1517 mm	192.5 mm	205.3d
Annual mean 1987–2007 (μ_2)	20.2°C	29.8°C	42.6d	1489 mm	193.1 mm	214.4d
z-score (μ_2 to μ_1)	1.4	0.5	0.9	−0.1	0.0	0.7
Linear trend 1961–1986 (unit/a)	−0.01	−0.01	−0.05	4.12	−0.17	−0.36
Linear trend 1987–2007 (unit/a)	0.03	0.02	0.30	1.71	0.45	0.61

the six indicators (1961–2007) at 192 stations are listed in Table 2 and illustrated in Fig. 2, where the change-points are visualized in the background of the respective basin-averaged indicator' time-series.

According to the findings, the years with the majority of significant change-points for the entire Zhujiang River Basin are 1986/87 and 1997/98. The change-point in 1986/87 is often valid for the highest number of stations and found for most of the indicators (T_{mean}, T_{max}, T_{90}, and P_{dry}). Therefore, this change-point (1986/87) is chosen for the spatial analysis of the mean shift of each indicator.

Hence, two time-periods (1961–1986 and 1987–2007) are statistically described. Their arithmetic means, average z-score, and linear trends for the entire Zhujiang River Basin can be derived from Table 3. Illustrated in standardized terms by the z-score, an increase in the mean of T_{mean} (by 0.5°C), T_{max} (by 0.3°C), T_{90} (by 8.7d), and P_{dry} (by 9.1d) can be observed while a stable mean in P_{5day} and a slight decrease in the mean of P_{total} (by 28 mm) can be detected for the entire basin. The corresponding linear trends in 1961–1986 are decreasing at all indicators except for P_{total}, while in 1987–2007 all trends show an increasing tendency (Table 3). Most significant are the trends in T_{mean} and P_{dry} (Fig. 2a, f), while no significance is found for P_{total} and P_{5day} (Fig. 2d, e).

3.2 Temporal change (z-score)

The z-score reflects the standardized spatial shift of the mean before and after the change-point (1986/87). Estimated for each station and indicator, the interpolated z-scores are displayed in Fig. 3. The stations with significant change-points in 1986/87 are highlighted (black dots), and it can be seen that most of them are located in the areas of high z-scores (here: strong increases). Concerning the change-point of less significant years (e.g. 1997/98), it is assumed that the shift (trend) in all indicators has the same direction as of 1961–1986 or 1987–2007, and is expressed as part of the corresponding mean (e.g. 1987–2007).

A high number of stations experienced change-points in 1986/87 and show positive station-based z-scores for T_{mean} (Fig. 3a). Most areas, except the mountainous parts in the north-west, have z-scores above 1.0, which implies a strong increase to higher mean temperatures (by 0.3°C to 1.2°C) for the period after the change-point (1987–2007). The z-scores of T_{max} and T_{90} reflect similar features. Most stations show positive z-scores (except T_{max} in the central area), while even higher z-scores (above 1.0) are detected in the south-east (along the coast and delta) (Fig. 3b, c). These indicate a strong increase to higher maximum temperatures (by 0.5°C to 1.3°C) and more warm days (by 8d to 35d) near the coast and delta.

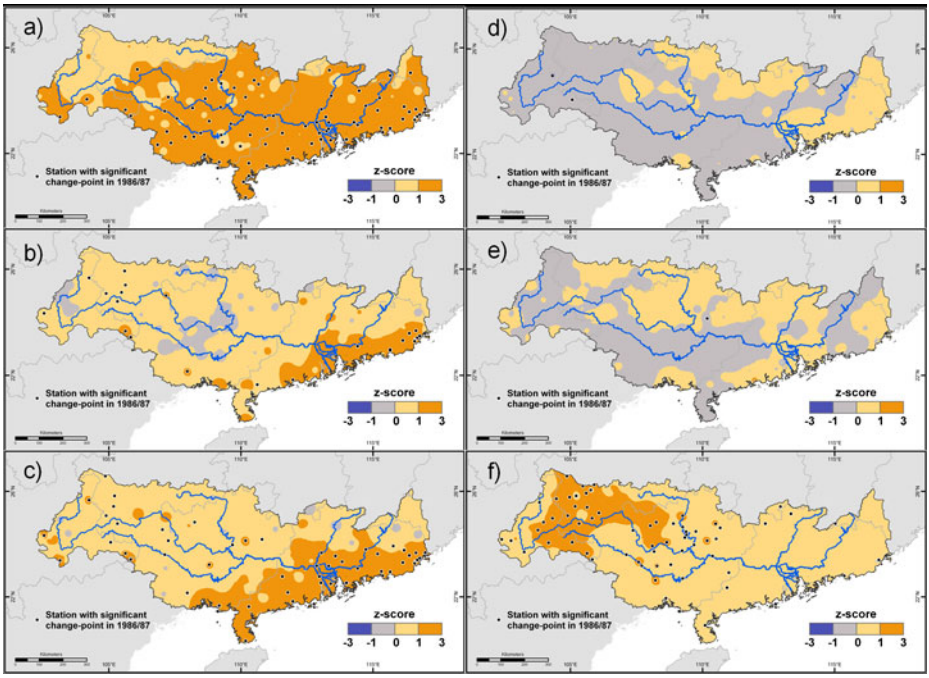

Fig. 3 Spatial distribution of the *z*-score (standardized mean for 1987–2007 in relation to the mean and standard deviation of 1961–1986) of **a** T_{mean}, **b** T_{max}, **c** T_{90}, **d** P_{total} **e** P_{5day}, and **f** P_{dry} (*shadings*); and stations with significant change-point in 1986/87 (points) in the Zhujiang River Basin

Total precipitation and 5-day-maximum precipitation have a similar distribution of *z*-scores. *Z*-scores in most of the western and south-central areas of the basin are slightly negative, while most of the north-central and eastern parts have slightly positive scores (Fig. 3d, e). Only slight changes occurred as almost no change-points exist for these indicators. The entire basin experiences slightly positive *z*-scores in P_{dry}, while in the western part high *z*-scores (above 1.0) are observed (Fig. 3f). This area experiences an increase by 10 to 22 more dry days in the period 1987–2007 compared to 1961–1986.

3.3 Spatial shift

Figure 4 shows the spatial shifts for each indicator's mean of 1987–2007 against the mean 1961–1986. In the low lying central and eastern parts of the basin, an obvious northward shift of T_{mean} classes can be observed (Fig. 4a). The border of the T_{mean} class >22°C extensively progressed northward and along the coast from the Leizhou Peninsula. In the western mountainous areas, a slight shift in T_{mean} can be detected towards higher altitudes. For maximum temperature indicators, an expansion from the centre to all geographical directions can be observed. A south-eastward shift to >31°C in T_{max} can be identified in most parts of the coast and delta, though before (1961–1986) only the central areas experienced high maximum temperatures (Fig. 4b). With a more west- and southward direction, warm days show a more

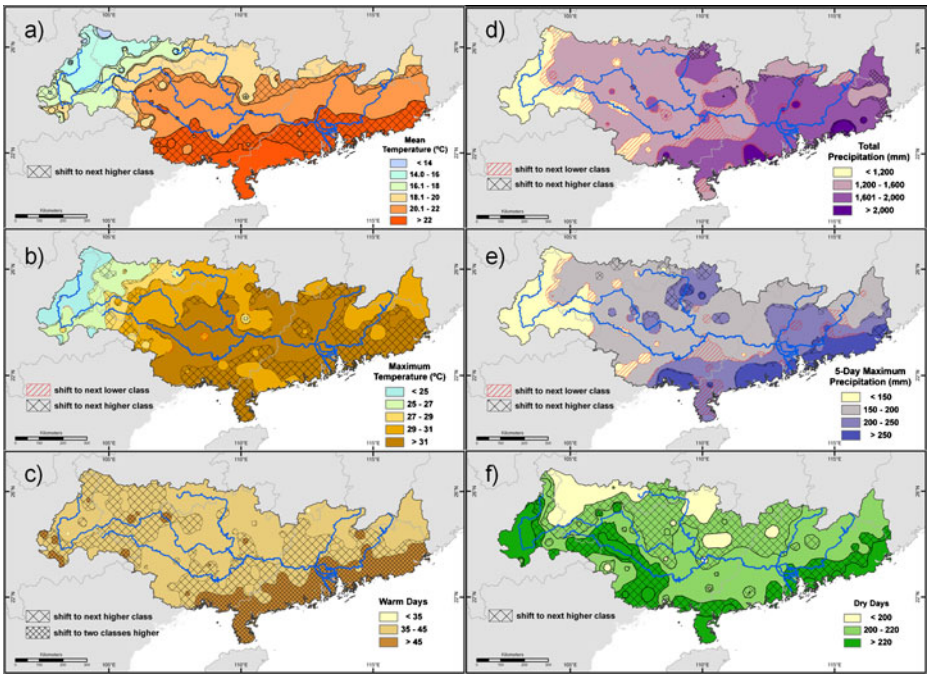

Fig. 4 Averaged annual mean of 1987–2007 (*shadings*) and corresponding regime shift of indicator classes against the time-period 1961–1986 (*texture*) of **a** T_{mean}, **b** T_{max}, **c** T_{90}, **d** P_{total} **e** P_{5day}, and **f** P_{dry} interpolated for 192 station-based time-series in the Zhujiang River Basin (1961–2007)

south-east coverage. Figure 4c shows that stations along the coast and few stations in the west experienced shifts by two classes (from <30d to >45d), which emphasizes a strong change in T_{90}.

Few small progressing (more in the north-east) and retreating (more in the south-west) shifts are detected for P_{total} and P_{5day} (Fig. 4d, e). In contrary, P_{dry} classes shift northward and in the western region relatively extensively upwards (to higher altitudes). In 1987–2007, the class containing >220 dry days can be found along the southern border of the watershed (from west to east). Before, only few areas (in the far west and east, and Leizhou Peninsula) experienced extensive dry days (Fig. 4f). Similarly, a shift from the class <200d to the class 200–220d is observed in the north-central areas.

4 Interpretation: analysis of circulation pattern

4.1 Change-points in wind directions

Temperature and precipitation in the Zhujiang River Basin are strongly influenced by the East Asian Monsoon System. This is expressed by changes in wind directions (Li and Zeng 2003; Feng et al. 2007; Gemmer et al. 2011). The question is whether the detected change-points of the climate indicators can be explained by changes

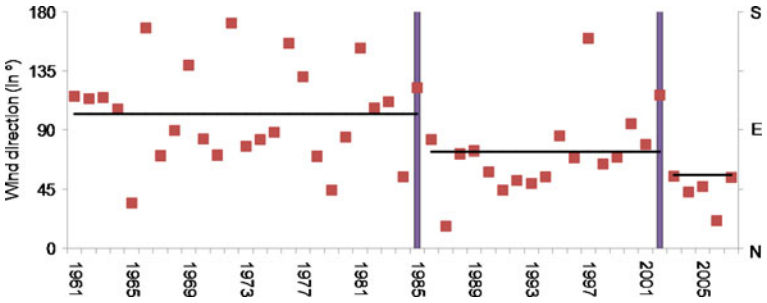

Fig. 5 Average wind directions in October (*red squares*) in the eastern Zhujiang River Basin, years with significant change-points (*purple columns*), and mean wind directions of the periods separated by change-points (*black lines*)

in the atmospheric circulation. Therefore, a change-point analysis is carried out for time-series of wind directions in October for the eastern part of the Zhujiang River Basin. Wind directions in October were chosen because the EASM ends in average in October. Recent findings by Gemmer et al. (2011) also emphasize October as being a key month concerning temporal precipitation changes and trends (especially in dry days). Therefore, October is the turning point from EASM to the East Asian Winter Monsoon and marks the season when the WP starts influencing South China.

The analysis shows that at least two significant change-points can be detected in the wind directions in October: 1985/86 and 2002/03 (Fig. 5). The shifts of the wind direction are around 30° each from an ESE-direction (1961–1985) to an E-direction (1986–2002) and then to an ENE-direction (2003–2007). A high variation (between S- and NE-directions) is evident in the period before the 1985/86 change-point. Noteworthy is the extreme outlier in 1997 which shows a SSE-direction.

4.2 Reverse characteristics of EASMI and WPI

The wind pattern in October is strongly influenced by the EASM and WP. Therefore, it is analyzed whether the EASMI and WPI influence the detected change-points of the climate indicators. Change-points cannot be detected in the time-series' of the EASMI and WPI. However, the EASMI and WPI show special characteristics that

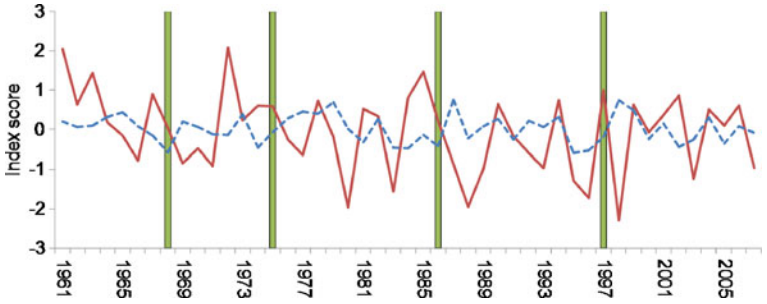

Fig. 6 EASMI (*red line*) and WPI (*dashed blue line*), years of simultaneous increase in WPI and decrease in EASMI (*green columns*)

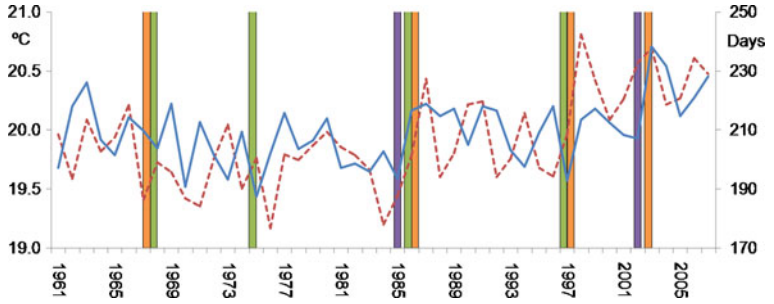

Fig. 7 Averaged mean temperature (T_{mean}, *dashed red line*) and dry days (P_{dry}, *blue line*) in the Zhujiang River Basin (1961–2007), change-points of T_{mean} and P_{dry} (*orange columns*), change-points of wind directions in October (*purple columns*) in the eastern Zhujiang River Basin (1961–2007), years of reverse indices for WPI and EASMI (*green columns*)

are concurrent to the change points in the climate indicators. Four years (1968/69, 1975/76, 1986/87, and 1997/98) show a negative WPI and positive EASMI which are succeeded by a year with positive WPI and negative EASMI, i.e. the indices take reverse directions (Fig. 6).

These years match the change-points of the analyzed temperature and precipitation indicators in the Zhujiang River Basin, except for 1975 (Fig. 7). The change-points of the wind directions in the eastern Zhujiang River Basin in October are one year prior to the estimated change-points of T_{max} and P_{dry}.

5 Discussion

5.1 Discussion on circulation pattern

Strong negative values of the EASMI are brought into relation with high summer precipitation amounts in the Yangtze River Basin (Li and Zeng 2003), but with low summer precipitation amounts in South China (i.e. Zhujiang River Basin). For recent decades, Ding et al. (2008) noticed a regime transition of summer precipitation from a positive-negative-positive north-south pattern to a dipole north–south pattern with two abrupt change-points (1978 and 1992). This transition and a simultaneous weakening of the EASM are leading to less moisture transport and convergence. This is pre-dominantly caused by a weakening of the tropical easterly jet (Ding et al. 2008). Yin et al. (2009) identified a similar positive-negative pattern (high–low pressure at 500 hPa) north and south of 40°N latitude of east China during the EASM, and related it to fewer moderate-to-heavy rainfall events in Guizhou province in June to August. If the pattern is reversed, more persistent moderate-to-heavy rainfall events are experienced. These modes of circulation are associated by Yin et al. (2009) with the northward intrusion of the WP. Yu et al. (2009) identified a zonal dipole oscillation (referred to as APD) at 500 hPa in the East Asia–West Pacific region and stated that anomalies in APD (low/high values) cause high/low summer precipitation over the southern Yangtze River Basin (bordering the northern Zhujiang River Basin).

During winter and spring, a north–south dipole of circulation anomalies over the western North Pacific exists, with one centre located over the Kamchatka Peninsula and another broad centre of opposite sign (i.e. WP) covering portions of southern East Asia and the western subtropical North Pacific. Strong positive or negative phases of this pattern (WPI) reflect pronounced zonal and meridional variations in the location and intensity of the entrance region of the East Asian jet steam. The positive phase of the WP pattern is associated with above-average temperatures over the lower latitudes of the western North Pacific and with below-average precipitation across the central North Pacific (Barnston and Livezey 1987).

According to Su et al. (2005), the summer temperature over Central Asia decreased slightly in recent decades whereas the temperature over the North West Pacific has become warmer. This contrast caused the weakening of the summer monsoon and the shift of the rain belt over South China, leading to less rain days (Su et al. 2005; Chou 2004). Considering the change-points found in the wind directions in October and based on findings by Gemmer et al. (2011), the shift of the transition phase between the end of the EASM and the onset of the East Asian winter monsoon could be another link to explain change-points in precipitation indicators.

5.2 Discussion on change-point detection and trends

The change-point analysis for the indicators reveals that the highest number of stations show significant change-points in 1986/87. Change-points in the years 1967/68 (T_{mean}, T_{max}, T_{90}), 1997/98 and 2003/04 (T_{max} and P_{dry}) are less significant but noteworthy.

For T_{mean}, most stations with change-points in 1986/87 are located in the eastern and coastal areas of the Zhujiang River Basin. For annual dry days, such stations are located in the western areas. This difference in distribution is also found in the intensity of the z-scores. Increases in temperature indicators are found in the entire basin, with the highest scores at the coast and delta, which can also be found in the different shifts of classes of indicators towards the north and the coast. Decreasing (increasing) tendencies in total and 5-day maximum precipitation (dry days) are mostly experienced in the western and central parts of the basin, with a significant northward shift to more dry days.

For different regions of China, change-points in time-series of annual temperature and precipitation in 1986/87 were, for example, detected in the upper Yellow River Basin (Zhao et al. 2007), in the Tarim River Basin (Chen et al. 2006), and in Inner Mongolia (You et al. 2010). These studies support the findings of the most significant change-point in 1986/87.

As almost no change-points in total precipitation were estimated, the findings of Zhang et al. (2009a) cannot entirely be supported, as they detected abrupt changes in precipitation totals of 47 stations which occurred in the late 1970s, 1980s and early 1990s. Using the CUSUM method, Leung and Wu (2005) observed shifts in summer rainfall at nine stations in South China (1952–2003) from wet to dry conditions between the mid-1970s and from dry to wet in the early 1990s. In our study, a change-point in total precipitation can only be detected at seven percent of the stations for the early 1990s and the mid 1980s. The shift in summer rainfall in 1999, estimated by Si et al. (2009), can therefore not be proven for the Zhujiang River Basin. In comparison with Zhang et al. (2009a), Si et al. (2009), and Leung and Wu (2005),

the dissimilar results might be explained by the use of different methods or different time-scales and time-periods.

The detected basin-averaged increase and spatial distribution in T_{mean} (by 0.5°C) and T_{90} (by 8.7d) is in line with the findings of Ren et al. (2005b), Fischer et al. (2010), and Qian and Lin (2005). They highlight an increase in annual mean temperature by around 0.4°C for South China (1951–2004), or a mean basin-wide increase by 0.7°C (1961–2007). Qian and Lin (2005) estimated an increase by 4.8d in warm days in South China for 1961–2000, while Fischer et al. (2010) found a basin-wide average increase by 14 warm days for 1961–2007. Using daily precipitation data of 47 stations (1951–2005), Zhang et al. (2009a) did not detect significant trends in annual precipitation. Similar findings were made by Gemmer et al. (2011), who found very few negative trends in annual and maximum precipitation at 192 stations (1961–2007), significant trends in dry days. Both studies support our findings in precipitation indicators, especially the increase in dry days (by 9.1d).

Observed change-points for T_{mean}, T_{max}, T_{90}, and P_{dry} can be explained by two atmosphere–ocean indices related to the study region (EASMI and WPI) and wind directions in October (Li and Zeng 2003; Barnston and Livezey 1987; Gemmer et al. 2011). The years of the simultaneous increase/decrease in WPI/EASMI match the estimated change-points (1986/87, 1997/98, and 1968/69) in the Zhujiang River Basin, except for 1975. The two change-points in wind directions in October both occur one year prior the change-points in T_{max} and P_{dry} (1986/87 and 2003/04). These staggered occurrences might be explained by time-lagged climatic teleconnections, which will be investigated in further research.

6 Conclusions

In the Zhujiang River Basin, climate change-points (1986/87, 1997/98, 2003/04, and 1967/68) can be linked to changes in the indices of the EASM and WP. These change points result in above-average temperature, below-average precipitation in winter and spring, and fewer moderate-to-heavy rainfall events in summer in the Zhujiang River Basin.

The abrupt shift to higher annual temperatures and less annual precipitation events detected can partly be explained by simultaneous increase/decrease of the WPI and EASMI.

It will be possible to plan adaptation measures against climate risks, e.g. for flood control, disaster preparedness, and water resource management, when using information of change points. Although climate-proofing of infrastructure, e.g. inland dykes, reservoirs, should take into account climate trends and projected changes, change points are not foreseen as a standard procedure. The results of this study show that climate change points may lead to abrupt changes of external conditions in the disaster management system. More focus should therefore be put on the assessment on the linkage between large-scale oscillation and change points in climate indices which can serve early warning systems. The information can feed into existing disaster preparedness models that are used at national meteorological observations in South China and Southeast Asia.

Acknowledgements This study was supported by the National Basic Research Program of China (973 Program; No. 2010CB428401), the Special Fund of Climate Change of the China Meteorological

Administration (CCSF2011-11), by the National Natural Science Foundation of China (40910177, 41001021) and in support of the SuMaRiO Project funded by the Bundesministerium für Bildung und Forschung (BMBF) of Germany. The positions of Thomas Fischer and Marco Gemmer at the National Climate Center are supported by the German Development Cooperation through the Center for international Migration and Development (www.cimonline.de).

References

Adger WN, Agrawala S, Mirza MMQ, Conde C, O'Brien K, Pulhin J, Pulwarty R, Smit B, Takahashi K (2007) Assessment of adaptation practices, options, constraints and capacity. In: Parry ML, Canziani OF, Palutikof JP, van der Linden PJ, Hanson CE (eds) Climate change 2007: impacts, adaptation and vulnerability. Contribution of working group II to the fourth assessment report of the Intergovernmental Panel on Climate Change. Cambridge University Press, Cambridge, pp 717–743

Barnston A, Livezey R (1987) Classification, seasonality and persistence of low-frequency atmospheric circulation patterns. Mon Weather Rev 115:1083–1126.

Buishand TA (1982) Some methods for testing the homogeneity of rainfall records. J Hydrol 58: 11–27

Chen Y, Takeuchi K, Xu C, Chen Y, Xu Z (2006) Regional climate change and its effects on river runoff in the Tarim Basin, China. Hydrolog Process 20(10):2207–2216

Chou C (2004) Establishment of the low-level wind anomalies over the Western North Pacific during ENSO development. J Clim 17:2195–2212

Ding Y, Ren G, Shi G, Gong P, Zheng X, Zhai P, Zhang D, Zhao Z, Wang S, Wang H, Luo Y, Chen D, Gao X, Dai X (2007) China's National Assessment Report on Climate Change (I): climate change in China and the future trend. Adv Clim Change Res 3(Suppl.):1–5

Ding Y, Wang Z, Sun Y (2008) Inter-decadal variation of the summer precipitation in East China and its association with decreasing Asian summer monsoon Part I Observed evidences. Int J Climatol 28:1139–1161

Feng S, Nadarajah S, Hu Q (2007) Modeling annual extreme precipitation in china using the generalized extreme value distribution. J Meteorol Soc Jpn 85(5):599–613

Fischer T, Gemmer M, Liu L, Su B (2010) Temperature and precipitation trends and dryness/wetness pattern in the Zhujiang River Basin, South China, 1961–2007. Quaternary Int 2010:1–11. doi:10.1016/j.quaint.2010.08.010

Gemmer M, Becker S, Jiang T (2004) Observed monthly precipitation trends in China 1951–2002. Theor Appl Climatol 77:39–45

Gemmer M, Fischer T, Jiang T, Su B, Liu L (2011) Trends of precipitation extremes in the Zhujiang River basin, South China. J Clim 24(3):750–761

Hoskins BJ (2003) Atmospheric processes and observations. Phil Trans R Soc Lond A 361:1945–1960

Klein Tank AMG, Zwiers F, Zhang X (2009) Guidelines on—analysis of extremes in a changing climate in support of informed decisions for adaptation. World Meteorological Organisation (WMO), Climate Data and Monitoring, WCDMP-No. 72, WMO-TD No. 1500, Geneva, Switzerland

Leung Y, Wu M (2005) Regime shift in summer rainfall in Southern China. In: Seventh joint meeting of seasonal prediction on East Asian summer monsoon, Nanjing, China, 11–13 May 2005. Reprint no. 586, Hong Kong Observatory

Li J, Zeng Q (2003) A new monsoon index and the geographical distribution of the global monsoons. Adv Atmos Sci 20(2):299–302

Li Z, Zheng F, Liu W, Flanagan D (2010) Spatial distribution and temporal trends of extreme temperature and precipitation events on the Loess Plateau of China during 1961–2007. Quaternary Int 226:92–100

Liu L, Jiang T, Yuan F (2009) Observed (1961–2007) and Projected (2011–2060) Climate Change in the Pearl River Basin. Adv Clim Change Res 5(4):209–214 (in Chinese)

Miller AJ, Cayan DR, Barnett TP, Graham NE, Oberhuber JM (1994) The 1976–77 climate shift of the Pacific Ocean. Oceanography 7(1):21–26

Morrill C, Overpeck JT, Cole JE (2003) A synthesis of abrupt changes in the Asian summer monsoon since the last deglaciation. Holocene 13(4):465–476

Qian W, Lin X (2005) Regional trends in recent temperature indices in China. Meteorol Atmos Phys 90:193–207

Qian W, Lin X, Zhu Y, Xu Y, Fu J (2007) Climatic regime shift and decadal anomalous events in China. Clim Change 84:167–189
Ren G, Chu Z, Zhou Y, Xu M, Wang Y, Tan G, Zhai P, Shao X et al (2005a) Recent progresses in studies of regional temperature changes in China. Chin J Clim Environ Res 10(4):702–716 (in Chinese)
Ren G, Xu M, Chu Z, Guo J, Li Q, Liu X, Wang Y (2005b) Changes of surface air temperature in China during 1951–2004. Chin J Clim Environ Res 10(4):717–727 (in Chinese)
Seidel DJ, Lanzante JR (2004) An assessment of three alternatives to linear trends for characterizing global atmospheric temperature changes. J Geophys Res 109:D14108. doi:10.1029/2003JD004414
Si D, Ding Y, Liu Y (2009) Decadal northward shift of the Meiyu belt and the possible cause. Chin Sci Bull 54:4742–4748
Song F, Hu Q, Qian W (2004) Quality control of daily meteorological data in China, 1951–2000: a new dataset. Int J Climatol 24:853–870
Su B, Jiang T, Jin W (2005) Recent trends in observed temperature and precipitation extremes in the Yangtze River basin, China. Theor Appl Climatol 83(2006):139–151
Su B, Kundzewicz Z, Jiang T (2008) Simulation of extreme precipitation over the Yangtze River Basin using Wakeby distribution. Theor Appl Climatol 96(2009):209–219
Taylor WA (2000) Change-point analysis: a powerful new tool for detecting changes. Available at: http://www.variation.com/cpa/tech/changepoint.html
Trenberth KE, Jones PD, Ambenje P, Bojariu R, Easterling D, Klein Tank A, Parker D, Rahimzadeh F, Renwick JA, Rusticucci M, Soden B, Zhai P (2007) Observations: surface and atmospheric climate change. In: Solomon S, Qin D, Manning M, Chen Z, Marquis M, Averyt KB, Tignor M, Miller HL (eds) Climate change 2007: the physical science basis. Contribution of working group I to the fourth assessment report of the Intergovernmental Panel on Climate Change. Cambridge University Press, Cambridge
Wilks DS (2006) Statistical methods in the atmospheric sciences, 2nd edn., International Geophysics Series, Vol. 91, Academic Press, p 627
Yang T, Shao Q, Hao Z-C, Chen X, Zhang Z, Xu C-Y, Sun L (2010) Regional frequency analysis and spatio-temporal pattern characterization of rainfall extremes in the Pearl River Basin, China. J Hydrol 380(3–4):386–405
Yin Z, Cai Y, Zhao X, Chen X (2009) An analysis of the spatial pattern of summer persistent moderate-to-heavy rainfall regime in Guizhou Province of Southwest China and the control factors. Theor Appl Climatol 97:205–218
You L, Dai X, Qiu H (2010) Analysis on annual mean temperature abrupt change of Inner Mongolia during 1961—2006. Meteorol J Inner Mongolia 2010-02. doi:CNKI:SUN:NMQX.0.2010-02-003
Yu S, Shi X, Lin X (2009) Interannual variation of East Asian summer monsoon and its impacts on general circulation and precipitation. J Geophys Res 19:67–80
Zhai P, Zhang X, Wan H, Pan X (2005) Trends in total precipitation and frequency of daily precipitation extremes over China. J Clim 18:1096–1108
Zhai J, Su B, Krysanova V, Vetter T, Gao C, Jiang T (2009) Spatial variation and trends in PDSI and SPI indices and their relation to streamflow in 10 large regions of China. J Clim 23:649. doi:10.1175/2009JCLI2968.1
Zhang Q, Xu C, Becker S, Zhang ZX, Chen YD, Coulibaly M (2009a) Trends and abrupt changes of precipitation maxima in the Pearl River basin, China. Atmos Sci Lett 10(2):132–144
Zhang Q, Xu C, Zhang Z (2009b) Observed changes of drought/wetness episodes in the Pearl River basin, China, using the standardized precipitation index and aridity index. Theor Appl Climatol 98:89–99
Zhao F, Xu Z, Huang J (2007) Long-term trend and abrupt change for major climate variables in the upper Yellow River Basin. Acta Meteorol Sin 21:204–214

Appendix IV

Fischer, T., B. Su, Y. Luo and T. Scholten, 2012: Probability distribution of precipitation extremes for weather-index based insurance in the Zhujiang River Basin, South China. *Journal of Hydrometeorology*, Volume 13, 1023-1037.

Probability Distribution of Precipitation Extremes for Weather Index–Based Insurance in the Zhujiang River Basin, South China

THOMAS FISCHER

National Climate Center, China Meteorological Administration, Beijing, China, and Department of Geosciences, University of Tübingen, Tübingen, Germany

BUDA SU AND YONG LUO

National Climate Center, China Meteorological Administration, Beijing, China

THOMAS SCHOLTEN

Department of Geosciences, University of Tübingen, Tübingen, Germany

(Manuscript received 29 March 2011, in final form 15 December 2011)

ABSTRACT

In a changing climate, understanding the frequency of weather extremes is crucial to improving the management of the associated risks. The concept of weather index–based insurance is introduced as a new approach in weather risk adaptation. It can decrease the vulnerability to precipitation extremes that cause floods and economic losses in the Zhujiang River basin. The probability of precipitation extremes is a key input and the probability distribution of annual precipitation extremes is analyzed with four distribution functions [gamma 3, generalized extreme value (GEV), generalized Pareto, and Wakeby]. Three goodness-of-fit tests (Kolmogorov–Smirnov, Anderson–Darling, and Chi Squared) are applied to the distribution functions for annual time series (1961–2007) of 192 meteorological stations. The results show that maximum precipitation and 5-day-maximum precipitation are best described by the Wakeby distribution. On a basin scale, the GEV is the most reliable and robust distribution for estimating precipitation indexes for an index-based insurance program in the Zhujiang River basin. However, each station has to be analyzed individually as GEV is not always the best-fitting distribution function. Based on the distribution functions, spatiotemporal characteristics of return periods for maximum precipitation and 5-day-maximum precipitation are determined. The return levels of the 25- and 50-yr return periods show similar spatial pattern: they are higher in the southeast and lower in the southwest of the basin. This spatial distribution is in line with the annual averages. The statistical distribution of precipitation indexes delivers important information for a theoretical weather index–based insurance program.

1. Introduction

a. Weather extremes in south China

In China, extreme weather events regularly cause damages to ecosystems and affect the socioeconomic sphere (e.g., the agricultural production). The population that is living in areas vulnerable to weather extremes such as floods, rain storms, and droughts is increasing. Weather extremes are common in China because of the monsoon systems over East Asia and China's various climate regimes (Zhai et al. 2005). The potential for economic damages from extreme climate events and other natural disasters increased in recent decades because of the fast-growing population and industrialization in major river basins in China (Feng et al. 2007). The intensity and frequency of these extremes have been analyzed in several studies on climate change in China and at the global scale (Ding et al. 2007; Trenberth et al. 2007; Klein Tank et al. 2009). For the climate and weather extremes in south China, the East Asian summer monsoon (EASM) and the western Pacific subtropical high (WP) have been identified as strong influencing factors (Ding et al. 2007; Fischer et al. 2011, 2012; Gemmer et al. 2011; Yin et al. 2009).

Corresponding author address: Thomas Fischer, China Meteorological Administration (CMA), National Climate Centre (NCC) 46, Zhongguancun Nandajie, Haidian, Beijing 100 081, China.
E-mail: tom.fischer8@gmx.de

DOI: 10.1175/JHM-D-11-041.1

b. *Impacts of precipitation extremes and weather insurance concept*

Heavy rainfall has led to catastrophic flooding in southern China and caused decreasing annual grain production and direct economic losses observable in economic data from the China Meteorological Administration (CMA), the Pearl River Water Resources Commission (PRWRC), and the Economic Research Service (ERS) from the United States Department of Agriculture. Thus, these flood and heavy rainfall events have adverse effects on farmers' livelihoods. According to the World Food Programme (WFP), weather-indexed crop insurance programs can help farmers to cope with disaster losses and help governments predict the onset of natural hazards to take appropriate measures to cushion their impacts and to reduce vulnerability (Hazell et al. 2010; Parry et al. 2009). Crop insurance has been one of the most successful risk management and longest-running stabilization programs for farmers in many parts of the world (Boyd et al. 2011). Recently, the China Insurance Regulatory Commission (CIRC) is encouraging insurers to apply new methods to extend agricultural insurance cover to improve food security and decrease the vulnerability to weather-related losses in the country (www.circ.gov.cn). Based on several case studies, Skees (2007) concludes that properly designed and targeted index-based weather insurance products can facilitate the development of robust rural financial markets. In weather-indexed crop insurance, a contract is written against a prespecified index that establishes a relationship between weather phenomena (e.g., heavy rainfall) and crop failure (i.e., losses in agricultural production). Based on another study by Turvey and Kong (2010), farmers in China would have an interest in purchasing weather insurance, with a strong interest in precipitation insurance.

Statistically, weather index insurance covers the extreme tail of the probability distribution of weather events for a specified region (Belete et al. 2007). The determination of the index depends on the probabilities associated with the given risk. This typically depends on long datasets of acceptable quality, which enable the estimation of the likelihood of an extreme event, the level of vulnerability and exposure, and the economic losses incurred (Jiang et al. 2010). Commonly, the probability distribution of the indexed parameter is calculated on observed data. The probability distribution of the extreme tails is often expressed in return levels of reconstructed and observed climate variables (i.e., precipitation extremes) at specific return periods. An accurate estimation of return levels at given return periods are relevant for the determination of indices for weather index–based crop insurance and other adaptation measures (Adger et al. 2007; Belete et al. 2007; Klein Tank et al. 2009; Semmler and Jacob 2004; Lehner et al. 2006).

These statistical distributions are often used to model time series and to define the frequency of annual extremes. The r-yr return level is the quantile that has a probability $1/r$ of being exceeded in a particular year. In general, the distributions of hydrological time series are assessed to distinguish the extent of an r-yr return level of a 100-yr flood event, for instance (Petrow and Merz 2009). Less often, studies focus on the distribution of meteorological time series of maximum precipitation and rain storm events, as these extreme precipitation indicators are the main climate elements where flood risks are concerned (e.g., Feng et al. 2007; Groisman et al. 1999; Klein Tank et al. 2009; Nadarajah and Choi 2007; Su et al. 2009; Vovoras and Tsokos 2009; Yang et al. 2010; Zhai et al. 1999).

Insurance providers require preliminary research on the accurate estimation of potential weather indexes for crop insurance products in south China. In addition, it is important to identify which distribution function fits best for the determination of the extreme tails of these precipitation extremes.

c. *Distribution functions and state of research in south China*

In China, the most commonly applied distribution function for precipitation extremes in the last decades was the three-parameter gamma distribution (GA3; similar to the Pearson type-3 distribution) for comparing extreme floods (Groisman et al. 1999; Wang et al. 2008). For example, Wang et al. (2008) applied the gamma distribution and the Kolmogorov–Smirnov (KS) test to detect changes in extreme precipitation and extreme streamflow in southern China. The gamma distribution is also used as the standard distribution in the calculation of the standardized precipitation index (SPI; Zhai et al. 2010; Fischer et al. 2011) and for precipitation intensity estimation in the Intergovernmental Panel on Climate Change (IPCC) Fourth Assessment Report (AR4; Solomon et al. 2007).

Recently, the World Meteorological Organization (WMO) recommended the use of the generalized extreme value (GEV) for block maxima and the generalized Pareto (GPA) distribution for peak-over-threshold events (Klein Tank et al. 2009). Several studies applied these distributions with diverse results (e.g., Solomon et al. 2007, etc.). For 651 stations in China, time series of annual maximum precipitation (1, 2, 5, and 10 day) from 1951 to 2000 have been analyzed by Feng et al. (2007). Applying the GEV distribution, they concluded that 50-yr events in these regions in the 1950s became more

frequent and developed to 25-yr events in the 1990s. They detected negative trends in extreme events in north China but significant positive trends in the Yangtze River basin and northwestern China. For eastern China, Jiang et al. (2009) analyzed extreme precipitation from daily records and concluded that the GPA distribution is superior to other extreme value distributions such as GEV. For the Zhujiang River basin (ZRB) in south China, Yang et al. (2010) analyzed annual consecutive 1-, 3-, 5-, and 7-day precipitation for 42 stations from 1960 to 2005 and determined the best fitting of six different distributions for six predefined regions. In that study, GEV is among the best-fitting distributions for the estimation of return periods of 1, 10, 50, and 100 years. They also showed the spatial distribution of the different calculated return periods.

Relatively recent studies investigated and applied the five-parameter Wakeby (WAK) distribution for the estimation of return periods of extreme precipitation indicators (Park et al. 2001; Öztekin 2007; Su et al. 2009). To obtain reliable quantile estimates with the WAK distribution, Park et al. (2001) investigated the use of L moments for the estimation of the five parameters. Similar research was undertaken by Öztekin (2007), who concluded that based on results by the Anderson–Darling (AD) test the WAK distribution fits best for station data in the eastern United States. Su et al. (2009), who calculated the maximum precipitation and the Munger index to estimate observed and projected extreme precipitation events in the Yangtze River basin, selected the best-fitting distribution for flood/drought frequencies by comparing the GEV, general logistic (GLO), GPA, and WAK distributions. Here, the WAK distribution proved the best fit based on the Kolmogorov–Smirnov test. The 50-yr return periods were estimated for simulated (1951–2000) and projected (2001–50) time series.

Most of the aforementioned studies analyze the spatial pattern of extreme events at certain return periods, while some also investigate the best-fitting distributions. The results indicate the probability of extreme events and can be used in the planning of adaptation measures.

d. Objectives

For the preliminary research of the theoretical development of a weather index–based insurance program in south China, reported annual economic losses caused by flood events are associated with annual extreme precipitation indicators and annual grain production. An accurate estimation of return levels at given return periods is required to determine the theoretical thresholds. An investigation on four commonly used distribution functions for precipitation extremes will be carried out on the hypothesis that GEV is the overall best-fitting distribution for 192 stations in the Zhujiang River. Different goodness-of-fit tests will be applied to obtain insights on the reliability and robustness of each distribution function, as this has not been done yet. Based on the results, a spatial analysis of the frequency of annual precipitation extremes in the ZRB is presented and set into context with the theoretical development of a weather index–based crop insurance program.

2. Data and methodology

a. Regional setting

Located in south China, the Zhujiang River basin (also known as the Pearl River basin) stretches almost entirely over the administrative areas of Guangdong Province and Guangxi Autonomous Region. With an area of approximately 579 000 km^2, it is ranked as the third largest within China. The East Asian summer and winter monsoons have strong influences on the seasonal climate regimes, which are categorized as tropical to subtropical climates. In the western part of the basin the topography shows mountainous areas, while the central and southeastern parts are mainly hilly low lands. The Zhujiang River is a construct of three main rivers (i.e., the Beijiang River, Dongjiang River, and Xijiang River). The streamflow has a southeast- to southwestward direction because of the basin's topography. All three main rivers, including tributaries, merge into a large network delta (i.e., Zhujiang River Delta) at the southeastern coast. A map with the location of the 192 weather stations used in this investigation and the main river system is provided in Fig. 1.

b. Data

Daily precipitation records of 192 meteorological stations (Fig. 1) in the ZRB for the period 1961–2007 are used. Earlier instrumental records are unavailable. The dataset was provided by the National Meteorological Information Center (NMIC) of the CMA. The datasets were controlled on their quality by the NMIC (Qian and Lin 2005). The NMIC checked the data on homogeneity using the departure accumulating method (Buishand 1982). The precipitation data records remain unadjusted, while less than 0.01% of data gaps appear in the daily precipitation records. The same dataset was used and investigated by Gemmer et al. (2011) and Fischer et al. (2011, 2012). Multiple findings (including figures and tables) on precipitation extremes, wetness and dryness pattern, and change points in the ZRB can be retained from these articles.

Historical and recent data on major flood events in the ZRB (i.e., economic losses and affected area and population) are taken from the website of the PRWRC

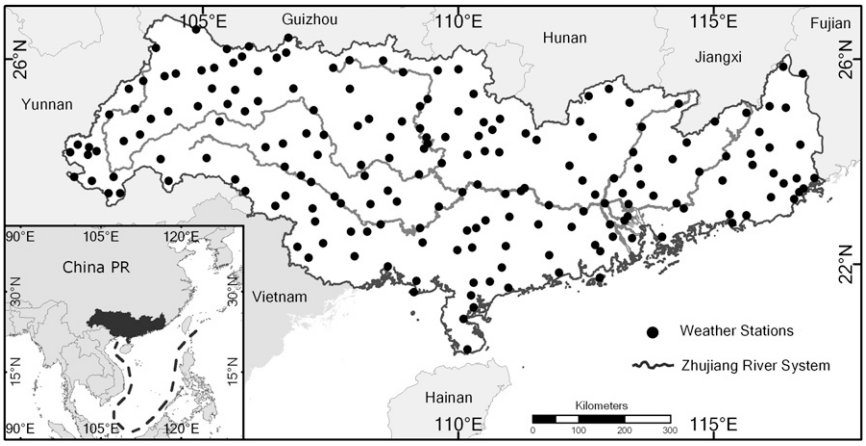

FIG. 1. Overview map of the Zhujiang River basin in south China, indicating location of meteorological stations (black dots) and the river system (gray curved line).

(www.pearlwater.gov.cn), while the annual overall economic losses from all natural hazards of Guangxi Autonomous Region are taken from the Provincial Disaster Statistics for Guangxi Autonomous Region 1950–2000 as provided by the CMA. The estimated annual grain production from 1963–2007 for the provinces of Guangdong and Guangxi is extracted from the ERS website (www.ers.usda.gov).

c. *Methodology*

1) INDICATORS

Based on observed daily precipitation data (1961–2007), two indicators are created in order to analyze and describe annual 1- and 5-day maximum precipitation extremes, which represent flood indexes' weather index–based insurance. The precipitation indicators consist of the annual maximum 1-day precipitation (RX1) and annual maximum consecutive 5-day precipitation (RX5). The indicators were defined on fixed terms predetermined by CMA and international standards (Li et al. 2010; Qian and Lin 2005; Su et al. 2009; Klein Tank et al. 2009).

For reliable results in estimated return levels, and hence in the application of all common distribution functions, a main assumption is that the time series are stationary. Significant trends, cycles, and autocorrelation (heteroscedasticity) indicate nonstationarity. Hence, the methods of linear regression, Mann–Kendall test, and Engle's test (on autocorrelation) are applied to the RX1 and RX5 of each station to identify stations exhibiting significant trends and autoregressive conditional heteroskedasticity (ARCH) effects in residuals at the 0.05 significance level (Gemmer et al. 2004; Gao et al. 2010; Duchesne 2006). Based on the two trend tests on the extreme indicators RX1 (RX5), significant trends are found at 8 (9) and 4 (3) out of 192 stations. Autocorrelation at lag 1 was detected at 4 and 7 stations. At these stations, the residual indicator time series are not independently distributed. The stations with significant trend and/or autocorrelation show no obvious spatial patterns in their location. Hence, the influence of large-scale covariates is rather unlikely. Conclusively, 181 time series are assumed to be stationary, while 11 time series show significant trends or autocorrelation, and are therefore excluded from the distribution analysis.

2) DISTRIBUTION FUNCTIONS

To identify the best-fitting distribution function for extreme precipitation at 181 stations in the ZRB, a comparative frequency analysis is applied to the precipitation indicators (RX1 and RX5). Following the examples by Feng et al. (2007), Su et al. (2009), and Yang et al. (2010), only the four most commonly used three- and five-parameter distributions are considered. Here, the GA3, GEV, and GPA distributions and the WAK distribution are used. In reference to the GEV and GPA distributions, a good overview of the advantages and disadvantages of the peak-over-threshold and block maxima approaches is given by Palutikof et al. (1999). The indicator values of the total available time period from 1961 to 2007 (47 years) are chosen for estimating the distributions, because results for longer return periods (e.g., of 25 years) are more accurate than from values of a shorter time period. The definition of the cumulative distribution functions of GA3, GEV, and GPA (Klein Tank et al. 2009; Hamed and Rao 1999; Su et al. 2009) are presented in Table 1. Here, x is an individual raw score, γ is a location parameter similar to the time series' mean, β and k are continuous shape

TABLE 1. Respective cumulative and probability distribution functions of GA3, GEV, GPA, and WAK.

Distribution	Cumulative distribution function (GA3, GEV, GPD) probability distribution function (WAK)	Domains
GA3	$F(x) = \frac{\Gamma_{(x-\gamma)/\beta}(\alpha)}{\Gamma(\alpha)} \quad \Gamma(\alpha) = \int_0^\infty t^{\alpha-1}e^{-t}\,dt$	$\gamma \le x < +\infty;\ \alpha > 0;\ \beta > 0$
GEV	$F(x) = \begin{cases} \exp[-(1+kz)^{-1/k}] & k \neq 0 \\ \exp[-\exp(-z)] & k = 0 \end{cases}$	$1 + kz > 0$ for $k \neq 0$
GPA	$F(x) = \begin{cases} 1 - \left[1 + K\left(\frac{X-\mu}{\sigma}\right)\right]^{-1/k} & k \neq 0 \\ 1 - \exp\left[-\left(\frac{X-\mu}{\sigma}\right)\right] & k = 0 \end{cases}$	$-\infty < x < \infty$ for $k = 0$ $\mu \le x < \mu - \sigma/k$ for $k < 0$ $\mu \le x < \infty$ for $k \ge 0$
WAK	$x(F) = \xi + \frac{\alpha}{\beta}[1 - (1-F)^{\beta}] - \frac{\gamma}{\sigma}[1 - (1-F)^{-\sigma}]$	$\xi \le x < \infty$ if $\sigma \ge 0$ and $\gamma > 0$ $\xi \le x < \xi + \alpha/\beta + \gamma/\sigma$ if $\sigma < 0$ or $\gamma = 0$

parameters, and z is the time series' mean (μ) subtracted from an individual raw score (X) and divided by the time series' standard deviation (σ). While for the probability distribution function of WAK (Table 1), β, γ, and σ are shape parameters, and ξ and α are location parameters (Hamed and Rao 1999; Su et al. 2009).

Several methods can be used for the estimation of distribution function parameters. The most common are the maximum likelihood method, the method of moments, the probability weighted moments method, and the L-moments method. According to Hamed and Rao (1999), the maximum likelihood method is the most efficient since it provides the smallest sampling variance of the estimated quantiles. The L-moments method has advantages when dealing with small and moderate samples (Hosking and Wallis 1997). The use of different parameter estimation methods may result in different quantile estimates as each parameter estimation method has its own strengths and limitations. In this paper, the maximum likelihood method (with one thousand iterations) and the L-moments approach are applied.

3) UNCERTAINTY QUANTIFICATION

We apply the bootstrapping method to more reliably assess the associated variability of the parameter estimation. For each station-based indicator, 1000 bootstrap members are generated by sampling with replacement (Davison and Hinkley 1997; Kharin et al. 2007). The 10% and 90% confidence bounds for each distribution function are generated for the return levels of the 25- and 50-yr return periods (Kao and Ganguly 2011). To quantify the uncertainty in parameter estimation of each distribution function due to sample errors in annual precipitation extremes, we compare the percentage differences of the confidence bounds to the estimated return level of the original sample. A higher percentage displays a higher (i.e., more uncertain) variability of the return level estimators of the used candidate distribution. Further procedures, equations, and estimations of parameter uncertainty can be derived from Hamed and Rao (1999), Su et al. (2009), Yang et al. (2010), and Hosking and Wallis (1997).

4) GOODNESS OF FIT

As a second step, the adequacy for each probability distribution (i.e., goodness of fit) is assessed. Three goodness-of-fit tests (KS, AD, and χ^2 tests) are applied in order to determine the distribution with the best fit—that is, the most adequate probability distribution (Corder and Foreman 2009; Su et al. 2009).

(i) Kolmogorov–Smirnov test

The KS test derives the distance between the empirical cumulative distribution function (ECDF) of the observed time series and the cumulative distribution function (CDF) of the candidate distribution (Corder and Foreman 2009; Su et al. 2009; Schönwiese 2006). The KS test statistic (D_n) for a given candidate cumulative distribution function [$F(x)$] is the largest vertical difference between $F(x)$ and $F_n(x)$. The equation for the KS test statistic (D_n) and the ECDF are defined in Table 2. Here, $\sup_x$ is the least upper bound of the set of distances and $I_{Xi \le x}$ is an indicator function, which is 1 if $X_i \le x$ or 0 if otherwise. If D is greater than the critical value (here 0.198) at the 0.05 significance level, the hypothesis on the distributional form is rejected.

(ii) Anderson–Darling test

The AD test is similarly to the KS test used to compare an ECDF to the CDF of a candidate distribution. The AD statistic (A^2) measures how well the data follow a particular distribution. For a given dataset and distribution, the better the distribution fits the data, the smaller this statistic will be. The calculation is weighted more heavily in the tails of the distribution than the KS test (Corder and Foreman 2009; D'Agostino and Stephens 1986). For the

TABLE 2. Functions of goodness-of-fit tests (KS, AD, and χ^2).

Goodness-of-fit test	Functions for test statistics
KS test	$D_n = \sup_x \lvert F_n(x) - F(x)\rvert \quad F_n(x) = \frac{1}{n}\sum_{i=1}^{n} I_{X_i \le x}$
AD test	$A^2 = -n - \frac{1}{n}\sum_{i=1}^{n}(2i-1)\{\ln F(X_i) + \ln[1 - F(X_{n-i+1})]\}$
χ^2 test	$\chi^2 = \sum_{i=1}^{k}\frac{(O_i - E_i)^2}{E_i} \quad E_i = F(x_2) - F(x_1)$

equation described in Table 2, if A^2 is greater than the critical value (here 2.502) at the 0.05 significance level, the hypothesis on the distributional form is rejected. The critical value is approximated depending on the sample size only and not on the distribution.

(iii) χ^2 test

The χ^2 test (normally used for independence determination) is used here to determine if the empirical data can be fitted well to the candidate distribution. In general, this test is applied to binned data with a certain degree of freedom (Corder and Foreman 2009; Schönwiese 2006). The calculation of the χ^2 statistic is shown in Table 2, where O_i is the observed frequency for bin i, and E_i is the expected frequency for bin i with F as the CDF of the candidate distribution, while x_1, x_2 are the limits for bin i. Here, the values of the test statistics have a degree of freedom of 3, 4, or 5. Hence, the critical values at the 0.05 significance level are 7.81, 9.49, or 11.07, respectively.

5) RETURN LEVELS

As stated by Klein Tank et al. (2009), information on multidecadal time scales are particularly relevant for adaptation planning and typical thresholds of weather indexes for insurance products (Adger et al. 2007; Belete et al. 2007), because nearly all infrastructure design relies on assessment of probabilities of extremes with return periods of 20 years or more. To further allow comparisons with relevant findings in recent literature (Feng et al. 2007; Su et al. 2009; Yang et al. 2010), the return levels in this study are calculated for the 25- and 50-yr return periods (quantiles 0.96 and 0.98, respectively) for each indicator and meteorological station. Based on the test results, the best-fitting distribution function for each station is determined according to the highest scores and robustness of the three goodness-of-fit tests. Additionally, the averaged percentage differences of the 10% and 90% confidence bounds to the estimated 25- and 50-yr return levels are calculated for each distribution function and presented as a basin average.

The return levels of the 25- and 50-yr return period of both indicators are spatially interpolated using the inverse distance weighting (IDW) method. This method is chosen because of its common use in previous articles on the ZRB (Gemmer et al. 2011; Fischer et al. 2011, 2012) and other relevant literature (e.g., Su et al. 2009). Although IDW usually performs with less accuracy than the kriging method (Shi et al. 2007; Chen et al. 2011), it does not assign values outside the range of the given points as is done within kriging, and hence a potential secondary overestimation of the return levels can be avoided, while local differences are more accentuated (Anderson 2011). With IDW, the weighted averages of 12 neighboring stations are used to calculate a raster image that presents the spatial distribution of the estimated indicators. The weighting is based on the local influence of distant points (stations), which decreases with distance (Gemmer et al. 2004).

3. Results

a. Indicators

The spatial distribution of RX1 and RX5 arithmetically averaged for the period 1961–2007 is displayed in Fig. 2. A very similar and obvious west-to-southeast disparity in the amounts of RX1 and RX5 can be found. The lowest average amounts in extreme precipitation (RX1 amounts are below 80 mm and RX5 amounts are below 120 mm) fall in the western parts, while the highest values (RX1 amounts are above 160 mm and RX5 amounts are above 240 mm) (RX1 > 160 mm;

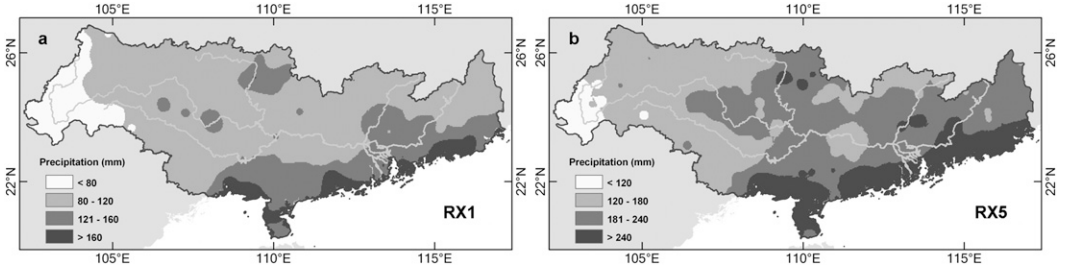

FIG. 2. Average annual (a) 1- and (b) 5-day-maximum precipitation (RX1 and RX5) in the ZRB, 1961–2007.

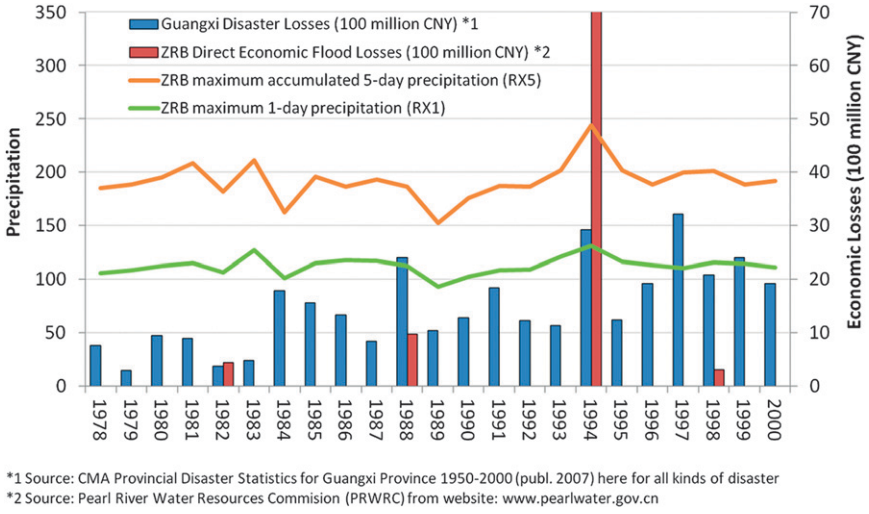

FIG. 3. Extreme precipitation [RX1 (green line) and RX5 (orange line)], economic flood losses in the ZRB (red column), and overall disaster losses in Guangxi Province (blue columns).

RX5 > 240 mm) are recorded along the southeastern coast of the basin.

b. *Association of indicators with flood events and economic data*

The two basin-averaged annual indicators, the annual economic losses due to floods for the ZRB, and the overall disaster losses of Guangxi are presented in Fig. 3. Only four major flood events with reported economic losses are documented for the ZRB from 1978 to 2000, with the highest losses (above ¥7 billion, where ¥ is the symbol for Chinese yuan) in 1994. It can be seen that the highest amount of the heavy rainfall indicators in 1994 coincides with higher than usual overall economic losses in Guangxi Province. Taking the relatively steady trend in grain production of Guangdong and Guangxi into account (Fig. 4), some obvious corresponding low peak events in 1988, 1994, and 2002 can be distinguished, and decreases by more than 0.5 ton ha^{-1} are apparent. The loss event in 1994 can be found in RX1 and RX5 (Fig. 5), while the loss event in 1988 is not well represented in RX1 and RX5. In Fig. 5, the RX5 values of 1994 are visualized for all stations. The affected regions can be quite obviously distinguished for the northern and southern parts of the basin. The highest rainfall amounts in 1994 were detected in these areas, where similar high losses might be assumed.

c. *Distribution functions*

As a first step of the comparative frequency analysis, the parameters for the candidate distribution (GA3, GEV, GPA, and WAK) are estimated for each time series and two indicators at 181 stations. For each station and indicator, the four distribution functions are calculated and integrated into a database. Based on this, the probability density curves, the cumulative probability, and the probability difference (*P–P* plot) can be statistically interpreted and visualized for every single station and indicator. The averaged percentage differences of the 10% and 90% confidence bounds to the 25- and 50-yr return levels for each candidate distribution as basin averages are presented in Table 3. It can be seen that GEV and GPA show smaller differences than GA3 and WAK. This indicates that the parameter estimation with GEV and GPA is slightly less affected in the case of sample errors in annual precipitation extremes.

As an example, the estimated parameters of the four candidate distributions at Xuwen station are shown in Table 4. The distribution functions are drawn according to their parameters (Fig. 6). In Fig. 6a the empirical probability density in comparison to all four candidate

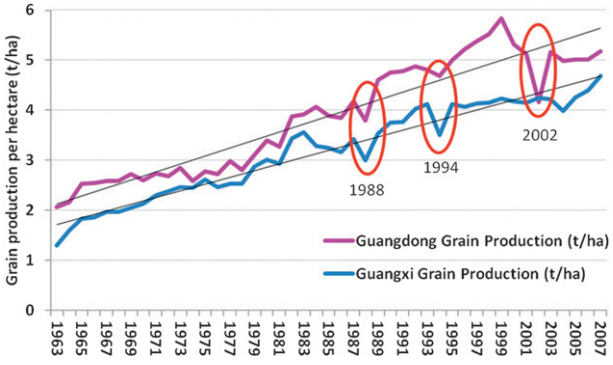

FIG. 4. Agricultural grain production (t/ha) of Guangdong and Guangxi Provinces of China, 1963–2007.

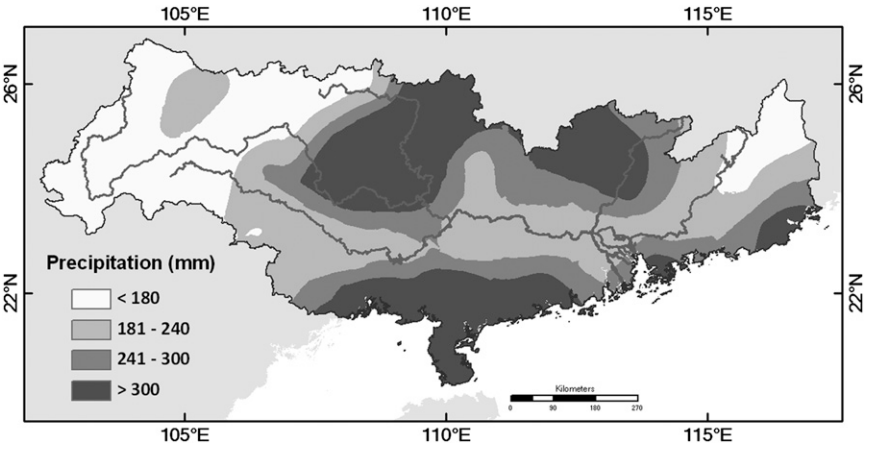

FIG. 5. Maximum consecutive 5-day precipitation (RX5) in 1994 in the ZRB.

distributions is shown. The probability density of RX5 is shown as columns with a left-sided distribution. The highest probability density is above 0.10 (at around 190 and 250 mm), where at the right tail end the two most extreme events in the 47 years of record can be distinguished. The estimated probability curves of GA3 and GEV (red and blue curves) show a right-sided bell curve with relatively similar shape, scale, and location. Compared to GA3 and GEV the curve of WAK (purple curve) shows a narrower shape, a higher scale, and a more right-shifted location, while the GPA (green curve) probability curve simply slopes downward from the left ($P > 0.09$ at 120 mm) to the right.

In Fig. 6b, the S-shaped GA3, GEV, and WAK curves are relatively close to the (stepwise) empirical cumulative probability curve. The GPA curve is simpler in its shape but also follows the empirical curve quite closely. To determine the actual difference of the candidate probability distribution to the empirical probability distribution, the *P–P* plot (Fig. 6c) allows an easy interpretation. The closer the candidate's probability is to the diagonal line (0.0–1.1), the better it fits to the empirical probability. In Fig. 6c, the GPA line shows the highest distance from the diagonal line, while the other three show a very similar behavior and are closer to the empirical probability.

d. Goodness of fit

In the present study, goodness-of-fit tests (KS, AD, and χ^2) are applied to all four candidate distributions of the two indicators at 181 stations. The statistics are calculated, proven on significance at the 0.05 significance level, and can be ranked based on a direct comparison of all four candidate distributions (the lowest value ranks first). Exemplarily, in Table 5, the test statistics for the four candidate distributions and for each goodness-of-fit test, as well as the corresponding return levels and the averaged percentage differences to the 10% and 90% confidence bounds, are presented for RX5 at Xuwen station.

In Table 6, the number of stations for which the calculation of the test statistics was successful (i.e., availability) are summarized. Some statistics are not available as some parameters of the candidate distribution could not be estimated or the hypotheses of the tests were rejected. The number of significant stations ($\alpha = 0.05$) are also presented in Table 6. Table 7 includes the number of

TABLE 3. Averaged percentage differences of the 10% and 90% confidence bounds to the 25- and 50-yr return levels for each of the four candidate distribution functions (GA3, GEV, GPA, and WAK) for two extreme precipitation indicators (RX1 and RX5) at 181 stations in the ZRB, 1961–2007.

	RX1		RX5	
Distribution	25 year	50 year	25 year	50 year
GA3	±13.3%	±17.2%	±13.9%	±17.4%
GEV	±11.5%	±15.3%	±12.6%	±16.3%
GPA	±12.4%	±15.5%	±12.7%	±16.1%
WAK	±13.2%	±18.1%	±14.4%	±18.3%

TABLE 4. Estimated parameters of four candidate distribution functions (GA3, GEV, GPA, and WAK) for annual maximum consecutive 5-day precipitation (RX5) at Xuwen station, 1961–2007.

Distribution	Parameters
GA3	$\alpha = 3.3359$; $\beta = 46.977$; $\gamma = 77.337$
GEV	$k = 0.0127$; $\sigma = 66.77$; $\mu = 194.66$
GPA	$k = -0.3952$; $\sigma = 156.52$; $\mu = 121.87$
WAK	$\alpha = 394.98$; $\beta = 5.492$; $\gamma = 79.256$
	$\sigma = -0.0156$; $\xi = 95.175$

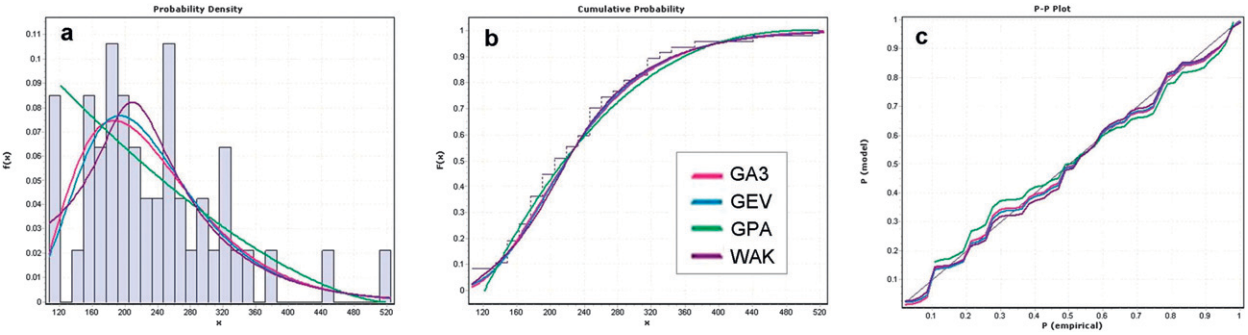

FIG. 6. (a) Probability density, (b) cumulative probability, and (c) *P–P* plot of annual 5-day-maximum precipitation (RX5) and four candidate distributions (GA3, GEV, GPA, and WAK) at Xuwen station, 1961–2007. In (a) and (b) the *x* axis shows the precipitation (mm) and the *y* axis the probability [$f(x)$]; in (c) the *x* axis represents the empirical probability [f(RX5)] and the *y* axis the candidate probabilities [$f(x)$].

stations where the candidate distribution is ranked first in a direct comparison of all four candidate distributions. To validate the reliability and robustness of the candidate distributions from a different perspective, the numbers of stations at which the statistics are below a certain threshold ($D < 0.09$, $A^2 < 0.50$, and $\chi^2 < 4.00$) are also shown in Table 7.

1) KOLMOGOROV–SMIRNOV TEST RESULTS

As can be seen in Table 6, the results of the KS test of the observed time series show that the calculation of the distributions' test statistics (D) was successful for most of the stations and all available statistics are significant at the 0.05 confidence level (here 0.198 with $n = 47$). For RX1 (RX5), only at 5 (4) stations are the WAK statistics not available.

In Table 7, the KS test statistics for each candidate CDF and for each station are ranked according to their point-oriented highest distance to the empirical CDF. The candidate distribution with the shortest distance is ranked first (rank 1). WAK was ranked first at 118 (126) of 181 rankings, followed by GEV with 43 (31) of 181. The number of stations [RX1 (RX5)] below the threshold of $D < 0.09$ (taken from Su et al. 2009) are highest for WAK [174 (168)], followed by GEV [168 (153)] and GA3 [127 (128)].

2) ANDERSON–DARLING TEST RESULTS

The calculation of the AD test statistics (A^2) for RX1 (RX5) was successful at most of the stations, but not all statistics are significant at the 0.05 confidence level (here 2.502 with $n = 47$). At 5 (4) stations the WAK statistics are not available. All statistics are significant for GEV. No significance was found at 7 (4) stations for GA3, at 49 (51) stations for WAK, and at 175 (177) stations for GPA (Table 6). The significant candidate distributions are ranked according to their lowest distance to the weighted squared empirical distribution statistic (Table 7). WAK was ranked first at 92 (89) of 181 rankings, followed by GEV with 61 (68) of 181 stations. The number of stations below the chosen threshold of $A^2 < 0.50$ are highest for GEV [171 (167)], followed by GA3 [141 (148)] and WAK [124 (114)], and very low for GPA [6 (4)].

3) χ^2 TEST RESULTS

The availability of χ^2 test statistics shows higher differences between the candidate distributions than those of KS and AD test statistics (cf. Table 6). The availability is given for GEV at all stations (181), for GA3 at

TABLE 5. Goodness-of-fit test results (KS, AD, and χ^2) for four candidate distribution functions (GA3, GEV, GPA, and WAK), and estimated return levels for 25 and 50 years [F(0.96) and F(0.98)], including the averaged difference to the 10% and 90% confidence bounds (percentage difference in brackets) of RX5 at Xuwen station, 1961–2007.

Distribution	KS (D)	AD (A^2)	χ^2	25-yr return level	50-yr return level
GA3	0.048	0.22	7.31	411 ± 51.4 (12.5%)	456 ± 65.0 (14.3%)
GEV	0.043	0.17	0.30	413 ± 50.9 (12.3%)	462 ± 70.5 (15.3%)
GPA	0.075	14.82*	n/a	407 ± 54.4 (13.4%)	434 ± 70.5 (16.2%)
WAK	0.053	0.16	0.28	416 ± 55.6 (13.4%)	468 ± 76.6 (16.4%)

* Not significant; n/a = not available.

TABLE 6. Availability and significance of stations according to the goodness-of-fit test results (KS, AD, and χ^2) for four candidate distribution functions (GA3, GEV, GPA, and WAK) of two extreme precipitation indicators (RX1 and RX5) at 181 stations in the ZRB, 1961–2007.

		KS		AD		χ^2	
Indicator	Distribution	Availability	Significance	Availability	Significance	Availability	Significance
RX1	GA3	181	181	181	174	174	169
	GEV	181	181	181	181	181	178
	GPA	181	181	181	6	6	6
	WAK	176	176	176	127	135	134
RX5	GA3	181	181	181	177	177	173
	GEV	181	181	181	181	181	180
	GPA	181	181	181	4	4	3
	WAK	177	177	177	116	123	120

174 (177), for WAK at 135 (123), and for GPA at 6 (4) stations. Not all available statistics are significant at the 0.05 confidence level (here 7.81, 9.49, or 11.07 depending on the degree of freedom). In Table 7, the significant candidate distributions are ranked based on their distance to the binned empirical probability distribution. For RX1, GEV and WAK ranked first for similar number of stations (>70), while for RX5 a relatively even distribution of first ranks between GA3, GEV, and WAK can be found. GPA ranks first two (one) times only. For RX1 (RX5), the number of stations below the chosen threshold of $\chi^2 < 4.00$ are highest for GEV [135 (132)], followed by GA3 [114 (125)], and WAK [102 (99)], and very low for GPA [5 (3)].

4) COMBINED TEST RESULTS

Following the goodness-of-fit tests' results, the adequacy of each candidate probability distribution can be determined. The overall outcome shows similar results for RX1 and RX5 (Table 6 and Table 7). Comparing the three tests, only GEV achieves successful calculation of test statistics (availability) for all stations. Availability of GA3 statistics is relatively high, while for WAK and GPA fewer results are found for χ^2. The significant test statistics show similar responses. For RX1 (RX5), all test statistics for GEV are significant, except for 3 (1) times when χ^2 was applied. GA3 shows also a high number of significant results in significance testing. In the AD testing, WAK shows a high variation with nonsignificance at one-third of available statistics, while GPA is nonsignificant at almost all statistics (Table 6).

Within the four candidate distributions, the five-parameter WAK ranks proportionately highest for both indicators at 181 possible stations. Comparing the three-parameter distribution functions, GEV ranks first more often than GA3 and GPA. Analyzing the test statistics below a certain threshold ($D < 0.09$, $A^2 < 0.50$, and $\chi^2 < 4.00$), the results reveal that the statistics of WAK and GEV show most often relatively low values, followed by GA3, while the statistics of GPA show generally the highest values (Table 7). Low values of available statistics indicate a good reliability and robustness of the candidate distribution.

TABLE 7. First rank and number of stations under a certain threshold according to the goodness-of-fit test results (KS, AD, and χ^2) for four candidate distribution functions (GA3, GEV, GPA, and WAK) of two extreme precipitation indicators (RX1 and RX5) at 181 stations in the ZRB, 1961–2007.

		KS		AD		Chi^2	
Indicator	Distribution	Rank 1*	$D < 0.09$	Rank 1*	$A^2 < 0.50$	Rank 1*	$\chi^2 < 4.00$
RX1	GA3	10	127	23	141	40	114
	GEV	43	168	61	171	71	135
	GPA	10	128	5	6	2	5
	WAK	118	174	92	124	68	102
RX5	GA3	10	128	21	148	58	125
	GEV	31	153	68	167	59	132
	GPA	14	104	3	4	1	3
	WAK	126	168	89	114	63	99

* Number of times the candidate distribution function was ranked first out of the available candidate distribution functions.

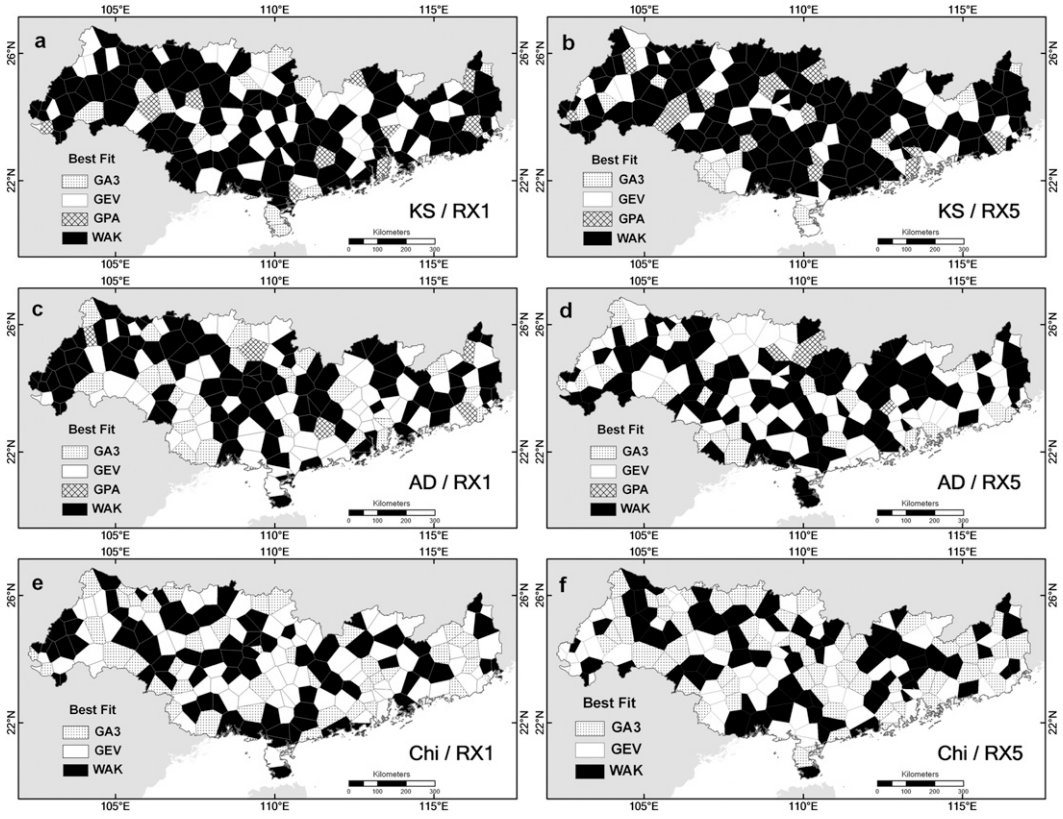

FIG. 7. Spatial distribution of (a),(c),(e) first-ranking candidate distributions (GA3, GEV, GPA, and WAK) of RX1 and (b),(d),(f) RX5 for (a),(b) the KS, (c),(d) AD, and (e),(f) χ^2 tests (1961–2007).

5) SPATIAL DISTRIBUTION OF TEST RESULTS

To spatially analyze the test results, the first-ranking candidate distributions were visualized for each goodness-of-fit test on the station area level for RX1 and RX5 (Fig. 7). No spatial pattern or relationship of the first-ranking candidate distributions can be recognized for RX1 or RX5. The results illustrated in Fig. 7 indicate that the geographic location of stations does not play an important role in the estimation and calculation of reliable distribution functions.

e. Return levels

1) CALCULATED RESULTS

For both indicators, all four candidate distribution functions are used to estimate return levels of 25- and 50-yr return periods in the ZRB (1961–2007). Taking

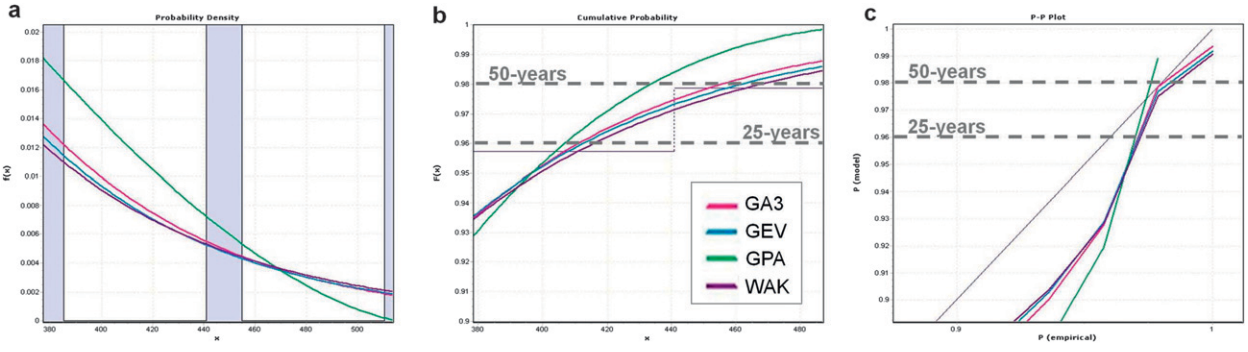

FIG. 8. As in Fig. 6, but for the right (upper) tail section with precipitation above 380 mm or from $f(x) > 0.90$. The (a) blue columns and (b),(c) the light-gray lines signify the empirical distribution. In (b) and (c) the dashed dark-gray lines indicate the 25- and 50-yr return periods [$f(x) = 0.96/f(x) = 0.98$].

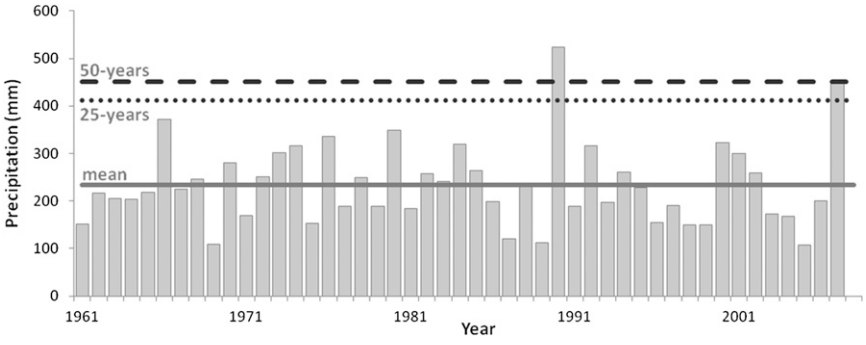

FIG. 9. RX5 (columns) at Xuwen station, 1961–2007. The dotted (dashed) line indicates the 25 (50)-yr return level at 412 mm (455 mm) as arithmetic averages of all four candidate distributions (GA3, GEV, GPA, and WAK), while the full gray line signifies the arithmetic mean 5-day-maximum precipitation.

all results of both indicators at 181 stations into account, the return levels range from GPA (lowest return level) to GA3, GEV, and finally WAK (highest return levels).

Figure 8 shows the right (upper) tail section of the aforementioned curves/lines for RX5 at Xuwen station. Similar curves can be detected for GA3, GEV, and WAK, and a different path for GPA. As can be seen in Table 4, the test statistics of GA3, GEV, and WAK have similarly low values (except GA3 with χ^2), while values of GPA are higher (KS), not significant (AD), or even not available (χ^2). The return levels are estimated higher for WAK and GEV. Hence, considering the ranking results, the return levels of GEV and WAK should be assumed as fitting best for RX5 at Xuwen station. The return levels of GA3 and especially GPA involve an underestimation of the 25- and 50-yr return periods.

A station-based calculation and visualization of the temporal distribution of extreme precipitation amounts, including the return level thresholds, can be used to easily identify the years when, for example, 25- and 50-yr events occurred. This is shown in Fig. 9 for RX5 at Xuwen station, where the 50-yr return level was reached once (in 1990) and 25-yr return level was crossed twice (in 1990 and 2007). These one- and two-time occurrences can be logically explained by the sample size of 47 years (1961–2007). Based on such temporal findings, further analyses (e.g., on local extreme events) can be realized.

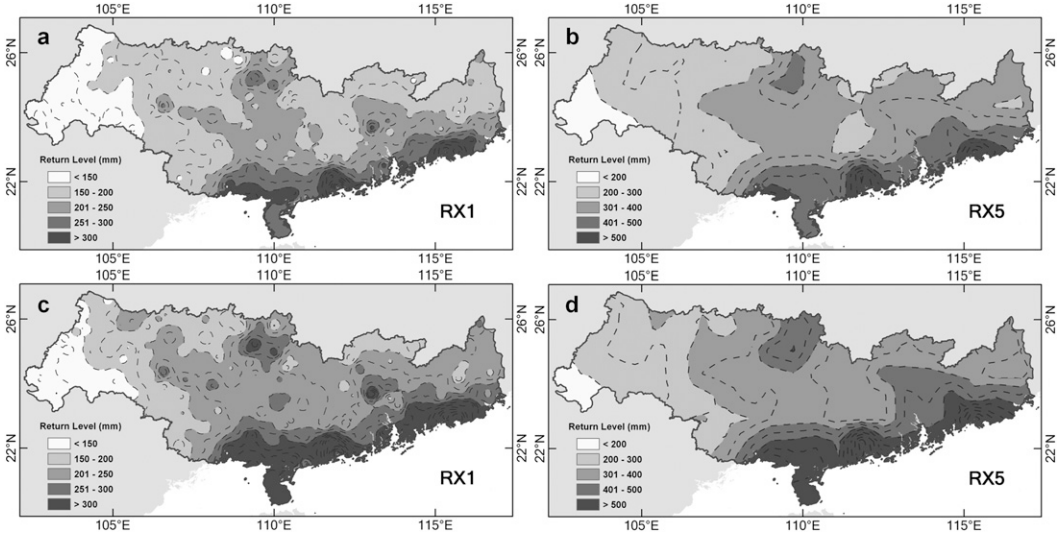

FIG. 10. Return levels of the (a),(b) 25- and (c),(d) 50-yr return periods for (a),(c) RX1 and (b),(d) RX5 in the ZRB, 1961–2007. The dashed lines indicate the 25-/50-mm interval (RX1/RX5).

2) SPATIAL DISTRIBUTION OF RETURN LEVELS

Mapping the spatial distribution of return levels provides a simple (supra) regional overview for decision makers concerned with weather extremes and risks. The return levels in this paper were calculated with each candidate distribution function and interpolated and mapped for both extreme indicators in the ZRB (not shown). Comparing the maps, no distinct spatial anomalies are apparent because of the large range in return levels for the entire basin and relatively small differences between the results of each candidate distribution. Hence, we only visualize the return levels of RX1 and RX5 for the 25- and 50-yr return period based on GEV (Fig. 10), as the GEV distribution function can be considered to fit best the time series of both indicators because of the good availability and high robustness of its test statistics.

For both indicators, the spatial distribution of the return levels of the 25- and 50-yr return periods show similar characteristics (Fig. 10) and are also very akin to the averaged annual amounts (cf. Figure 2). In general, the 25- and 50-yr return levels for RX1 and RX5 increase from west to southeast. For RX5, the 25 (50)-yr return levels range from less than 200 mm to more than 500 mm (Figs. 10b,d). The highest 25 (50)-yr return levels with a maximum of 796 mm (942 mm) are reached along the southeast coast and in a small area in the central north. The lowest return levels with a minimum of 137 mm (143 mm) are found in the western mountainous region. The basin-averaged 25 (50)-yr return levels are for RX1 200 mm (228 mm) and for RX5 329 mm (379 mm), respectively.

4. Discussion and conclusions

a. Distribution functions

The WMO recommends the use of GEV in the analysis of climate extremes (Klein Tank et al. 2009). In this study, four commonly used distribution functions were used in order to investigate whether the WMO's recommendation can be underlined for a humid area in south China. Different goodness-of-fit tests were used for analyzing the reliability and robustness of each distribution function. GEV was successfully used (successful parameter estimation or proven test assumption) with all three tests for all stations but one. GA3 was available with all three tests at most of the time series, while GPA and WAK showed especially low availability with χ^2. Most test statistics were significant for GEV and GA3, while WAK and GPA showed fewer significant test statistics with AD. In direct comparison, WAK ranked first with each test followed by GEV and GA3.

It is noted that the test results (in significance and ranking) of each goodness-of-fit test often differ within each time series. As every test depicts different criteria, this means more weighting should be put on the test results depending on the focus of further analysis. In the case of climate extremes, the tails of the distributions are of main concern (for extreme return periods); hence, in this study, the AD test is weighted higher than KS and χ^2 as it focuses more on the tail ends of a distribution. Based on the results of the KS, AD, and χ^2 tests, we determine that the GEV distribution fits best for both extreme precipitation indicators at 181 meteorological stations in the ZRB.

In the case of single-station analysis, WAK does often fit better but is less often available than GEV and shows a higher uncertainty in parameter estimation. The results of this investigation agree upon the hypothesis that GEV is the overall best-fitting distribution for climate extremes as recommended by the WMO. GEV shows a high availability and high significance for most test statistics regionwide and a relatively low uncertainty in parameter estimation due to sample errors in annual precipitation extremes. It should be noted that the applied statistical distributions can reasonably fit the observed time series of extreme precipitation data, but differences in the estimated quantiles may be apparent, since estimation of higher extreme quantiles is based on the upper tail of the probability distribution. For the development of a theoretical weather index–based insurance, it depends on the regional scale of the area to cover, of which one of the best-fitting distributions is recommended. If it only covers a small area of few stations, the best-fit distribution of those stations should be considered. The use of GEV should be considered for larger areas.

Our findings are in line with those of Yang et al. (2010), who concluded that GLO, GEV, Generalized Normal (GNO), and Pearson Type III (PE3) distribution fit best to estimate return periods for indicated precipitation events at 42 stations in the ZRB based on the *Z*-distance goodness-of-fit test. The determination of the best-fitting distribution was not the focus in their paper, hence a more detailed approach including three tests and with much higher resolution (192 stations instead of 42 stations) is presented in our study. Su et al. (2009) concluded that the Wakeby distribution is the best-fitting distribution for precipitation maxima in the Yangtze River basin (north of the study region), which is partially in line with the current study. These results would have similarly favored WAK as the best-fitting distribution in our study. As our study focused more on the identification of the best-fitting distribution, the differences might be the result of the application of different goodness-of-fit tests, station densities, and even different time series data

sources. Thus, the use of a variety of goodness-of-fit tests allows a more precise analysis with distinct findings, which has been done in the current study.

b. Frequencies

Based on the results, a spatial analysis on the frequency of annual precipitation extremes in the ZRB is presented. The GEV was used to identify return levels of both precipitation extremes for different return periods. Data on different return periods are displayed separately. This paper delivers practical maps on the return levels at given time periods. Distinct patterns in the spatial distribution of return levels for the 25- and 50-yr return periods of each indicator were detected. A west to southeast disparity (low to high levels) for both 1- and 5-day-maximum precipitation is apparent. The highest return levels for both indicators can be found in the southeast of the basin (e.g., delta region) and in the central northern part. Low return levels for 1- and 5-day-maximum precipitation are estimated for the western and southwestern area.

The spatial distribution of the 50-yr return level of 1- and 5-day-maximum precipitation (RX1 and RX5) shows similar disparity to the distributions of the 100-yr return levels of annual maximum 1-day and 5-day rainfall (AM1R and AM5R) by Yang et al. (2010), with highest levels located at the southeast coast and the central–northern region. The spatial distribution of RX1 in the northwestern part is also relatively similar to the findings in summer rainfall of Guizhou Province by Yin et al. (2009) and the precipitation maxima of the Yangtze River basin by Su et al. (2009).

c. Final conclusions

Conclusively, the results of calculating and estimating the best-fitting distribution function (i.e., GEV) as well as the estimated return levels for the Zhujiang River basin can be adopted in the planning of weather index–based crop insurance or rainstorm control measures and for the production of practical maps that correspond to typical return periods in other sectoral planning (e.g., the 50-yr return period in flood management). The research in return periods of extreme precipitation might give assistance to the potential development of a weather index–based crop insurance. In future studies, projected changes of return levels should also be addressed to give estimates on future frequencies of precipitation extremes and flood/drought events.

Acknowledgments. This study was supported by the National Basic Research Program of China (973 Program, 2010CB428401), the Special Fund of Climate Change of the China Meteorological Administration (Fund CCSF-09-16), and by the National Natural Science Foundation of China (Fund 40910177). Many thanks go to Dr. Marco Gemmer, who continuously provided comments and suggestions to this study, and to the anonymous reviewers. The positions of Thomas Fischer and Marco Gemmer at the National Climate Center are supported by the German Development Cooperation through the Center for international Migration and Development (www.cimonline.de).

REFERENCES

Adger, W. N., and Coauthors, 2007: Assessment of adaptation practices, options, constraints and capacity. *Climate Change 2007: Impacts, Adaptation and Vulnerability,* M. L. Parry et al., Eds., Cambridge University Press, 717–743.

Anderson, S., cited 2011: An evaluation of spatial interpolation methods on air temperature in Phoenix, AZ. [Available online at http://www.cobblestoneconcepts.com/ucgis2summer/anderson/anderson.htm.]

Belete, N., and Coauthors, 2007: China: Innovations in agricultural insurance—Promoting access to agricultural insurance for small farmers. Sustainable Development, East Asia & Pacific Region, Finance and Private Sector Development, The World Bank Rep., 108 pp.

Boyd, M., J. Pai, Z. Qiao, and W. Ke, 2011: Crop insurance principles and risk implications for China. *Hum. Ecol. Risk Assess.,* **17,** 554–565.

Buishand, T. A., 1982: Some methods for testing the homogeneity of rainfall records. *J. Hydrol.,* **58,** 11–27.

Chen, G. X., G. P. Wu, L. Chen, L. Y. He, and C. Jiang, 2011: Surface modelling of annual precipitation in the DongJiang River basin, China. *Proc. 19th Int. Conf. on Geoinformatics,* Shanghai, China, IEEE, 412–415.

Corder, G. W., and D. I. Foreman, 2009: *Nonparametric Statistics for Non-Statisticians: A Step-by-Step Approach*. John Wiley and Sons, 264 pp.

D'Agostino, R. B., and M. A. Stephens, 1986: *Goodness-of-Fit Techniques*. Statistics: A Series of Textbooks and Monographs, Vol. 68, Marcel Dekker, 576 pp.

Davison, A. C., and D. V. Hinkley, 1997: *Bootstrap Methods and Their Application*. Cambridge Series in Statistical and Probabilistic Mathematics, Cambridge University Press, 592 pp.

Ding, Y., and Coauthors, 2007: China's National Assessment Report on Climate Change (I): Climate change in China and the future trend. *Adv. Climate Change Res.,* **3** (Suppl.), 1–5.

Duchesne, P., 2006: Testing for multivariate autoregressive conditional heteroskedasticity using wavelets. *J. Comput. Stat. Data Anal.,* **51,** 2142–2163.

Feng, S., S. Nadarajah, and Q. Hu, 2007: Modeling annual extreme precipitation in China using the generalized extreme value distribution. *J. Meteor. Soc. Japan,* **85,** 599–613.

Fischer, T., M. Gemmer, L. Liu, and B. Su, 2011: Temperature and precipitation trends and dryness/wetness pattern in the Zhujiang River Basin, South China, 1961–2007. *Quat. Int.,* **244,** 138–148.

——, ——, ——, and T. Jiang, 2012: Change-points in climate extremes in the Zhujiang River Basin, South China, 1961–2007. *Climatic Change,* **110,** 783–799.

Gao, C., M. Gemmer, X. Zeng, L. Bo, B. Su, and Y. Wen, 2010: Projected streamflow in the Huaihe River Basin (2010–2100) using artificial neural network. *Stochastic Environ. Res. Risk Assess.,* **24,** 685–697.

Gemmer, M., S. Becker, and T. Jiang, 2004: Observed monthly precipitation trends in China 1951–2002. *Theor. Appl. Climatol.,* **77,** 39–45.

——, T. Fischer, T. Jiang, B. Su, and L. Liu, 2011: Trends of precipitation extremes in the Zhujiang River basin, South China. *J. Climate,* **24,** 750–761.

Groisman, P.Ya., and Coauthors, 1999: Changes in the probability of heavy precipitation: Important indicators of climatic change. *Climatic Change,* **42,** 243–283.

Hamed, K., and A. R. Rao, 1999: *Flood Frequency Analysis*. New Directions in Civil Engineering, CRC Press, 376 pp.

Hazell, P., J. Anderson, N. Balzer, A. Hastrup Clemmensen, U. Hess, and F. Rispoli, 2010: The potential for scale and sustainability in weather index insurance for agriculture and rural livelihoods. International Fund for Agricultural Development (IFAD) and World Food Programme (WFP) Publ., 153 pp.

Hosking, J. R. M., and J. R. Wallis, 1997: *Regional Frequency Analysis: An Approach Based on L-Moments*. Cambridge University Press, 242 pp.

Jiang, T., L. Vaucel, M. Gemmer, T. Fischer, B. Su, L. Cao, and X. Li, 2010: Weather index-based insurance in China: The challenges of dealing with data. *Extended Abstracts, Sixth Int. Microinsurance Conf.,* Manila, Philippines, Microinsurance Network and Munich Re Foundation, 8 pp.

Jiang, Z., Y. Ding, L. F. Zhu, L. Zhang, and L. H. Zhu, 2009: Extreme precipitation experimentation over eastern China based on Generalized Pareto Distribution (in Chinese). *Plateau Meteor.,* **28,** 573–580.

Kao, S.-C., and A. R. Ganguly, 2011: Intensity, duration, and frequency of precipitation extremes under 21st-century warming scenarios. *J. Geophys. Res.,* **116,** D16119, doi:10.1029/2010JD015529.

Kharin, V. V., F. W. Zwiers, X. Zhang, and G. C. Hegerl, 2007: Temperature and precipitation extremes in the IPCC ensemble of global coupled model simulations. *J. Climate,* **20,** 1419–1444.

Klein Tank, A. M. G., F. Zwiers, and X. Zhang, 2009: Guidelines on analysis of extremes in a changing climate in support of informed decisions for adaptation. World Meteorological Organization Tech. Doc. WMO-TD 1500, WCDMP-No. 72, 52 pp.

Lehner, B., P. Döll, J. Alcamo, T. Henrichs, and F. Kaspar, 2006: Estimating the impact of global change on flood and drought risks in Europe: A continental, integrated analysis. *Climatic Change,* **75,** 273–299.

Li, Z., F. Zheng, W. Liu, and D. Flanagan, 2010: Spatial distribution and temporal trends of extreme temperature and precipitation events on the Loess Plateau of China during 1961–2007. *Quat. Int.,* **226,** 92–100.

Nadarajah, S., and D. Choi, 2007: Maximum daily rainfall in South Korea. *J. Earth Syst. Sci.,* **116,** 311–320.

Öztekin, T., 2007: Wakeby distribution for representing annual extreme and partial duration rainfall series. *Meteor. Appl.,* **14,** 381–387.

Palutikof, J. P., B. B. Brabson, D. H. Lister, and S. T. Adcock, 1999: A review of methods to calculate extreme wind speeds. *Meteor. Appl.,* **6,** 119–132.

Park, J., H. Jung, R. Kim, and J. Oh, 2001: Modelling summer extreme rainfall over the Korean Peninsula using wakeby distribution. *Int. J. Climatol.,* **21,** 1371–1384.

Parry, M., A. Evans, M. W. Rosegrant, and T. Wheeler, 2009: Climate change and hunger: Responding to the challenge. World Food Programme Publ, 104 pp.

Petrow, T., and B. Merz, 2009: Trends in flood magnitude, frequency and seasonality in Germany in the period 1951–2002. *J. Hydrol.,* **371,** 129–141.

Qian, W., and X. Lin, 2005: Regional trends in recent temperature indices in China. *Meteor. Atmos. Phys.,* **90,** 193–207.

Schönwiese, C.-D., 2006: *Praktische Statistik für Meteorologen und Geowissenschaftler*. 4th ed. Bornträger, 302 pp.

Semmler, T., and D. T. Jacob, 2004: Modeling extreme precipitation events—A climate change simulation for Europe. *Global Planet. Change,* **44,** 119–127.

Shi, Y. F., L. Li, and L. L. Zhang, 2007: Application and comparing of IDW and Kriging interpolation in spatial rainfall information. *Geoinformatics 2007: Geospatial Information Science,* J. Chen and Y. Pu, Eds., International Society for Optical Engineering (SPIE Proceedings, Vol. 6753), 67531I, doi:10.1117/12.761859.

Skees, J. R., 2007: Challenges for use of index-based weather insurance in lower income countries. University of Kentucky Agricultural Experiment Station Number 07-04-091, 24 pp.

Solomon, S., D. Qin, M. Manning, M. Marquis, K. Averyt, M. M. B. Tignor, H. L. Miller Jr., and Z. Chen, Eds., 2007: *Climate Change 2007: The Physical Science Basis*. Cambridge University Press, 996 pp.

Su, B., Z. Kundzewicz, and T. Jiang, 2009: Simulation of extreme precipitation over the Yangtze River Basin using Wakeby distribution. *Theor. Appl. Climatol.,* **96,** 209–219.

Trenberth, K. E., and Coauthors, 2007: Observations: Surface and atmospheric climate change. *Climate Change 2007: The Physical Science Basis,* S. Solomon et al., Eds., Cambridge University Press, 235–336.

Turvey, C. G., and R. Kong, 2010: Weather risk and the viability of weather insurance in China's Gansu, Shaanxi, and Henan provinces. *China Agric. Econ. Rev.,* **2,** 5–24.

Vovoras, D., and C. P. Tsokos, 2009: Statistical analysis and modeling of precipitation data. *Nonlinear Anal.,* **71,** 1169–1177.

Wang, W., X. Chen, P. Shi, and P. van Gelder, 2008: Detecting changes in extreme precipitation and extreme streamflow in the Dongjiang River Basin in southern China. *Hydrol. Earth Syst. Sci.,* **12,** 207–221.

Yang, T., Q. Shao, Z.-C. Hao, X. Chen, Z. Zhang, C.-Y. Xu, and L. Sun, 2010: Regional frequency analysis and spatio-temporal pattern characterization of rainfall extremes in the Pearl River Basin, China. *J. Hydrol.,* **380** (3–4), 386–405.

Yin, Z., Y. Cai, X. Zhao, and X. Chen, 2009: An analysis of the spatial pattern of summer persistent moderate-to-heavy rainfall regime in Guizhou Province of Southwest China and the control factors. *Theor. Appl. Climatol.,* **97,** 205–218.

Zhai, J., B. Su, V. Krysanova, T. Vetter, C. Gao, and T. Jiang, 2010: Spatial variation and trends in PDSI and SPI indices and their relation to streamflow in 10 large regions of China. *J. Climate,* **23,** 649–663.

Zhai, P., A. Sun, F. Ren, X. Liu, B. Gao, and Q. Zhang, 1999: Changes of climate extremes in China. *Climatic Change,* **42,** 203–218.

——, X. Zhang, H. Wan, and X. Pan, 2005: Trends in total precipitation and frequency of daily precipitation extremes over China. *J. Climate,* **18,** 1096–1108.

Appendix V

Fischer, T., M. Gemmer, B. Su and T. Scholten, (2012): Long-term meteorological and hydrological dryness and wetness conditions in the Zhujiang River Basin, South China. Accepted for publication in *Hydrology and Earth System Sciences*.

Long-term meteorological and hydrological dryness and wetness conditions in the Zhujiang River Basin, South China

T. Fischer[1,2], M. Gemmer[1,2], B. Su[1,3], and T. Scholten[2]

[1] {National Climate Center of the China Meteorological Administration, Beijing, China}
[2] {Department of Geosciences, University of Tübingen, Germany}
[3] {Nanjing University of Information, Science and Technology, China}

Correspondence to: T. Fischer (tom.fischer8@gmx.de) and B. Su (subd@cma.gov.cn)

Abstract

Floods and droughts are frequently causing large economic losses in China. These conditions vary in space, time, and magnitude. In this study, long-term meteorological and hydrological dryness and wetness conditions are analyzed for the Xijiang River Basin which is the largest tributary of the Zhujiang (Pearl) River. A very similar inter-annual course of precipitation and discharge can be observed. The standardized precipitation index (SPI) is used to show dryness and wetness pattern in the six sub-basins of the Xijiang River. The SPI-24 correlates high with the standardized discharge index (SDI-24) for Gaoyao hydrological station at the mouth of Xijiang River. Distinct long-term dryness and wetness sequences are found in the time series for the SPI-24 and SDI-24. The principal component analysis reveals many spatial interdependencies in dryness and wetness conditions for the sub-basins and explains some spatio-temporal disparities. Moderate dryness conditions have a larger spatial impact than moderate wetness conditions in the sub-basins. The loading pattern of the first principal component shows that the correlation with the entire Xijiang River Basin is highest in the eastern and lowest in the western sub-basins. Further spatial dipole

conditions explain the spatio-temporal heterogeneity of dryness and wetness conditions. Accordingly, the precipitation in the eastern sub-basins contributes more to the hydrological wetness conditions than in the western sub-basins, which mainly contribute to dryness patterns.

The spectral analysis for the SPI-24 (entire Xijiang River Basin) and SDI-24 shows similar peaks for periods of 11-14.7 years, 2.8 years, 3.4-3.7 years, and 6.3-7.3 years. The same periods can be found for the SPI-24 of Xijiang River's six sub-basins with some variability in the magnitude. The wavelet analysis shows that the most significant periods are stable over time since the 1980s. The extrapolations of the reconstructed time series do not suggest any spatial or temporal changes in the occurrence of dryness and wetness conditions in the next two decades but a continuation of the observed cycles at given magnitude. It can be concluded that long-term hydrological dryness and wetness conditions are directly caused by periodic cycles of meteorological conditions (i.e. precipitation). The applied methodologies prove to be able to identify spatial interdependencies and corresponding regional disparities, and to detect significant periodicities in long-term dryness and wetness conditions in the Xijiang River Basin.

Keywords: dryness; wetness; precipitation; discharge; Xijiang; South China

1. Introduction

Spatio-temporal changes in dryness and wetness patterns have been observed for large areas in China for the past 50-60 years since the meteorological observation network has been extended. China is influenced by complex atmospheric circulation regimes that result in diverse precipitation patterns which cause more frequent meteorological weather risks such as extreme droughts or serious floods than in other parts of the world (Bordi et al., 2004). Decadal sequences of flood and drought years are historically documented for China, including the Huanghe (Yellow) River, the Yangtze River, and the Zhujiang (Pearl) River. A significant share of the global economic losses due to floods in the last decades has been recorded in China. According to the Munich Reinsurance (Berz and Kron 2004), the floods on the Yangtze and Songhua Rivers in 1998 and the 1996 floods on the Yangtze, Huanghe and Huaihe rivers caused material damages of 30.7 billion USD and 24 billion USD,

respectively (nominal 1998 and 1996 price level). Droughts in the north, northeast, and southwest of China in 2009 have caused about 18 billion USD direct economic losses.

Regional climate characteristics and the spatio-temporal variation of dryness and wetness in China have been described nationally (Zhai et al., 2010a,b), regionally (Bordi et al., 2004; Zhai and Qi, 2009), and on basin scales (Zhang et al., 2005; Gemmer et al., 2008; Fischer et al., 2011 and 2012). The highest number of articles on observations of precipitation and river discharge in China are available for the Yangtze and the Yellow River, describing how precipitation patterns and surface hydrology have changed. For example, Zhai et al. (2010b) show changes to more dry conditions and their impacts on the stream flow in the western regions of the yellow and Yangtze Rivers in the past 50 years, while Liu et al. (2011) describe a projected increase in spring/summer precipitation and corresponding stream flow of the Yellow River for the 21st century. In the past few years, more literature on these topics has been made available for the Zhujiang River.

The Zhujiang River Basin is located in subtropical, southern China. This third largest river basin in China is home to more than 160 million people. The population and industrialization have been increasing in recent decades, thus the damage potentials of extreme climate events and other natural disasters have risen (Feng et al., 2007; Fischer et al., 2011 and 2012; Gemmer et al., 2011). Precipitation and discharge in the Zhujiang River Basin with its tributaries is an important field of study in order to understand their interaction and consequences.

As many other large rivers in China, the Zhujiang River is characterized by dams. The total storage capacity of reservoirs in the basin had reached 65 km3 by 2005, which is 23% of the annual water discharge of the Zhujiang River (Dai et al., 2008). Annual water discharges are mainly influenced by precipitation variability, while the construction of reservoirs/dams in the Zhujiang River Basin had little influence on water discharge (Zhang et al., 2008). As precipitation variability has the highest impact on water discharge, recent findings on precipitation trends, climate extremes, and change points (Fischer et al., 2011 and 2012) suggest that the hydrology in the Zhujiang River Basin has also changed. Xu et al. (2010) indicated that annual discharge of the Zhujiang River correlates well with basin-averaged precipitation. However, Gemmer et al. (2011) have observed increasing tendencies to dryer conditions and stronger precipitation intensities for the Zhujiang River Basin from 1961 to 2007. Fischer et al. (2011) have observed increased numbers of dry days and Zhang et al. (2009) confirmed a tendency to drier conditions in the West of the basin. Another

study suggests that the Zhujiang River has the largest human footprint of the 10 largest river basins in South and East Asia (Varis et al., 2011). The assessment of observations in climatological and hydrological time series has delivered some results already showing spatio-temporal changes of stream flow in the past 50 years, mostly on annual scale. The characteristics and frequencies of long-term droughts and wetness conditions in the Zhujiang River Basin have yet to be explained.

Most of the studies mentioned above employed standard methods for assessing spatio-temporal changes in annual, seasonal, monthly precipitation and discharge, and their trends, e.g. the standardized precipitation index or aridity index, and nonparametric trend tests. In this manuscript, we place a broader view of long-term dryness and wetness period fluctuations (1961-2030) in the Xijiang River Basin of the Zhujiang River Basin using the standardized precipitation index which is recommended by the World Meteorological Organization (WMO) to characterize meteorological droughts (Klein Tank et al., 2009). The standardized discharge index is employed to characterize hydrological dryness and wetness conditions in order to analyze how long-term precipitation patterns have impacted the discharge of the river and to evaluate the characteristics of long-term climatological and hydrological dryness and wetness conditions.

2. Regional Settings, Data, and Methods

2.1 Regional Settings

The Zhujiang River Basin in subtropical South China (Fig. 1) covers an area of approximately 450,000 km2 with a population of more than 160 million. The region is currently one of the most economically prosperous areas of China, with very high development rates, and one of China's highest GDP per capita of more than 40,000 CNY per year (National Bureau of Statistics of China: www.stats.gov.cn). Since the 1950's, approximately 9000 dams with a reservoir storage capacity of 65 km3 have been constructed (Dai et al., 2008; Waterpub, 2012). In 2008, the Longtan hydropower station, China's third-largest with an estimated capacity of 4.9 GW, started operation in the upper reaches of the Hongshui River (China Daily, 2008).

The largest tributary of the Zhujiang River is the Xijiang (West) River, which accounts for 78% of the total drainage area of the Zhujiang River Basin. At Gaoyao hydrological

station the daily average discharge of the Xijiang River is observed. To examine an even higher level of spatial differentiation, the Xijiang River Basin is subdivided into its six sub-basins (Beipan, Nanpan, Yujiang, Hongshui, Liujiang, and Lijiang, see Fig. 1). Due to the availability of discharge data at Gaoyao and the high importance in total drainage, the Xijiang River Basin and its six sub-basins are examined on their long-term climatological and hydrological dryness and wetness conditions.

2.2 Data

Daily precipitation data of 118 weather stations in the Xijiang River Basin (Fig. 1) for the period 1961-2007 and daily average discharge data of the hydrological station at Gaoyao on the Xijiang River for the period 1961-2006 are used. The data sets were provided by the National Meteorological Information Center (NMIC) of the China Meteorological Administration (CMA). The data sets were controlled on their quality by the NMIC (Qian and Lin, 2005). The NMIC checked the data on homogeneity using the departure accumulation method (Buishand, 1982). Less than 0.1 percent of data gaps appear in the daily precipitation records.

2.3 Methods

2.3.1 Standardized Precipitation and Discharge Indices (SPI & SDI)

Weighted area averages in precipitation are calculated for six sub-basins (Fig. 1) of the Xijiang River Basin using the Thiessen polygon method provided within the ArcGIS software package. This method is a common approach for modelling the spatial distribution of rainfall based on station observations (Jiang et al., 2007). Here, for each sub-basin, the areal percentage of each Thiessen polygon within its boundary is used to determine the weight of each station's total precipitation and standardized precipitation index (SPI). This is used to calculate the weighted area average annual precipitation and monthly SPI for the according sub-basin. Following this, the areal percentages of the six sub-basins of the Xijiang tributary are used to calculate the weighted area average annual precipitation and monthly SPI for the entire Xijiang River Basin.

The SPI is calculated using the statistical software R, to quantify dryness and wetness periods (McKee et al., 1993). It is a meteorological index using monthly precipitation data (Mishra and Singh, 2010). Comprehensive descriptions on the SPI and its application in China are available e.g. from Bordi et al. (2004), Zhang et al. (2009), Zhai et al. (2010a,b), and Zhao et al. (2011). In our analyses, we consider the categories of the SPI / SDI values according to Lloyd-Hughes and Saunders (2002), who defined the values at -1.00 to -1.49 as moderate drought (-1.50 to -1.99 as severe drought, and -2 or less as extreme drought), and the values at 1.00 to 1.49 as moderately wet (1.50 to 1.99 as severely wet, and 2 or more as extremely wet). In this study, the SPI is calculated with weighted area averaged monthly precipitation data at a 24-months scale (SPI-24), which is suitable for the determination of meteorological and hydrological long-term dryness and wetness conditions (Bordi et al., 2004).

The standardized discharge index (SDI) is performed in an analogous manner to the SPI. It contains monthly discharge data instead of precipitation data and expresses hydrological excess or deficit availability of water. McKee et al. (1993) suggested the application of the SPI procedure to other water variables, such as observed discharge data. Hence, the method can be derived from McKee et al. (1993), Nalbantis and Tsakiris (2009), and Mishra and Singh (2010), although the respective terminology and input data vary in each of the manuscripts. To our best knowledge, the SDI has not been applied in the Zhujiang River Basin yet. In this study, the SDI is calculated with averaged monthly discharge data at a 24-months scale (SDI-24).

2.3.2 Principal Components Analysis

The principal component analysis (PCA) is broadly used for identifying patterns in climate data and to highlight their similarities and differences (Santos et al., 2010). We use the PCA to sum up the spatial patterns of co-variability of dryness and wetness according to the SPI-24 series at different stations. A set of linearly independent spatial patterns (loadings) are generated, which describe the correlations with the specific principal components (PC). The PCA is introduced by Bordi et al. (2004, 2007) and Zhao et al. (2011), and calculated by using the statistical software R.

2.3.3 Power Spectrum and Continuous Wavelet Analysis

The fast Fourier transform is used to generate the power spectrum of the signal in the monthly time series (Schönwiese, 2006; Wilks, 2006). The significant periodicities embedded in the time series can be determined based on the amplitude of the corresponding signal. Similarly, a continuous wavelet transform is used to break up the signal into shifted and scaled versions of the original wavelet by decomposing a time series into a time-frequency space (Torrence and Compo, 1998). In this study, we apply the Morlet wavelet, which is the most commonly used continuous wavelet transform to visualize the amplitudes in the time-frequency space. All calculations are done by using related packages of the statistical software R. The results can be used to detect periodicities and their changes in time (i.e. time-frequency relationships) in climatological datasets. Gao et al. (2010) used the continuous wavelet transform likewise in order to assess the fluctuation of monthly observed and projected average stream flows (return periods of extremes) in the Huaihe River basin in China. Becker et al. (2008) determined quasi periodicities of extreme precipitation events in the Yangtze River basin by employing the continuous wavelet analysis.

2.3.4 Extrapolation

The SPI-24 and SDI-24 time series are extrapolated between 2007 and 2030 in order to determine the periodicity of dryness and wetness conditions. We apply the fast Fourier transform again, but this time only to the significant periodicities indentified in the power spectrum. The estimation of future monthly values follows an optimization and extrapolation process for the observed time series as developed by Bordi et al. (2004). We use the parameterized software autosignal. The predicted values are generated based on the assumption that the significant periods are stable in time, i.e. the periodicity is similar for the following two decades (Becker et al., 2008). In order to characterize the reliability of this assumption, the results of the wavelet analyses are investigated on the stability of the significant periods.

3. Results

3.1 Relationship between Precipitation and Discharge

Figure 2 shows the time series of area averaged annual precipitation in the Xijiang River Basin and the mean annual discharge at Gaoyao hydrological station from 1961 to 2006. The annual average precipitation is about 1,350mm and the inter-annual variability is 10% according to the coefficient of variation. Two distinct minima in annual precipitation (below 1,100mm) can be observed for 1963 and 1989. A maximum in precipitation (above 1,700mm) occurred in 1994.

The average discharge between 1961 and 2006 is 7,000m3/s (Fig. 2). The inter-annual variability is 19%. Two minima in discharge (below 5,000m3/s) appeared simultaneously with the precipitation minima (1963, 1989). Two maxima (above 10,000m3/s) can be observed in 1968 and 1994. A strong correlation (0.88) is found for the monthly area averaged precipitation and monthly discharge at Gaoyao station from 1961 to 2006.

Figure 3 shows the average monthly precipitation in the Xijiang River Basin and the average monthly discharge at Gaoyao hydrological station for the period 1961-2006. The monthly precipitation maximum occurs in June with nearly 250mm. The highest monthly average discharge can be measured in July with nearly 16,000m3/s. The distinct seasonality is also expressed in this figure with a distinct dry period from November to March, with monthly precipitation of less than 50mm and monthly discharge minima of less than 4,000m3/s. The highest inner-annual variability of monthly precipitation can be observed in December with 69%, while the highest monthly variability of discharge is in March (64%). The high percentages are mainly due to the low average values of these months.

For illustration purposes, the monthly precipitation and discharge values of 1963 and 1994 are shown Figure 4. In comparison with the long-term average, much less (more) precipitation and discharge was observed in 1963 (1994), especially in the summer months from May to August. Precipitation and discharge amounted for 50%-80% less in 1963 and 30%-60% more in 1994.

This section underlines the strong correlation between the monthly area averaged precipitation and monthly discharge. Based on the monsoon climate in the research area, the inneranual variability of precipitation and discharge appears natural, the latter following the course of the former. It is of high interest whether the interannual variability of precipitation and discharge are short term or lead to long-term dryness and wetness

conditions, both in hydrological and meteorological terms. The magnitude and periodicity of dryness and wetness and their interrelation are analyzed in the following.

3.2 Relationship between SPI-24 and SDI-24

Figure 5 shows the area averaged SPI-24 weighted for the Xijiang River Basin and the SDI-24 for Gaoyao Hydrological Station. The SPI-24 (Fig. 5 upper panel) reveals that wet conditions (SPI values > 1) prevailed for about 20 years after a drought (SPI values < -1) ended in 1965. Uninterrupted dryness conditions at different magnitudes characterized the period 1985-1995. The wetness conditions after 1995 are again nearly uninterrupted for 10 years. After 2004, a sequence of dryness conditions prevailed in the basin. The most distinct peaks in wetness conditions occurred around 1974 and 1995. Peaks in dryness conditions occurred around 1964, 1990, and 2005.

The SDI-24 (Fig. 5 lower panel) is very similar to the corresponding SPI-24 and takes the same chronological positive and negative course. The peaks and durations of climatological dryness and wetness conditions in the SPI-24 can simultaneously be found in the SDI-24. The highest peak for climatological drought around 1964 for instance is also the most severe hydrological drought. The coefficient for the correlation between the average SPI-24 for the weighted sub-basins and the corresponding SDI-24 is 0.94.

The identified peak years in SPI-24/SDI-24 are chronologically similar to the maxima and minima in the annual total precipitation and annual average discharge (cf. Fig. 2). The SPI-24/SDI-24 reveals long-term dryness and wetness conditions for the Xijiang River Basin. The strong similarities imply a very high influence of natural precipitation pattern on the discharge, which can be spatially determined and explained by investigating the SPI-24 of the six sub-basins.

The SPI-24 for the six sub-basins is illustrated in Figure 6. Sequences of wetness and dryness vary in the sub-basins. In general, the sub-basins take the same course as the averaged SPI-24 for the entire basin (Fig. 5). However, the wetness conditions after 1965 are more distinct 1) in magnitude for the Beipan sub-basin (Northwest) and 2) in duration for the Nanpan sub-basin. Beipan shows a more distinct magnitude in the drought of the early 1990s whereas it was longer in e.g. the Liujiang sub-basin (Southeast).

Focusing on moderate wetness conditions (SPI > 1) and dryness conditions (SPI < -1), one can see that the droughts around 1965, 1990 and 2005 were simultaneously measured

in all six sub-basins. The less distinct drought around 1986 was measured in 50% of the sub-basins. Most of the moderate wetness conditions were simultaneously recorded in 2-3 of the sub-basins only (e.g. 1983, 2003). The wetness around 1975 occurred in 5 of the sub-basins, but moderate wetness conditions were never recorded in all of the six sub-basins at the same time. Figure 6 underlines the distinct spatial variability of dryness and wetness sequences which can well describe the averaged SDI-24 and show that moderate dryness conditions have a larger spatial impact than moderate (and higher) wetness conditions.

The correlation coefficient between the SPI-24 for each sub-basin and the SDI-24 varies between 0.65 (Beipan) and Hongshui and Yujiang (each 0.82). This suggests that each sub-basin has a considerable impact on the SDI-24 at Gaoyao hydrological station, but some sub-basins contribute higher to the discharge.

Conclusively, changes in the SDI-24 can be profoundly explained by the average SPI-24 weighted for the sub-basins. We have identified distinct long-term dryness and wetness conditions in the Xijiang River Basin. To determine the temporal characteristics of dryness and wetness and their changes, we analyze their frequencies in the following.

3.3 Peak dry and wet periods

Frequencies of peak (moderate) dry and wet conditions (SPI < -1 and SPI > 1) can be explained in different ways. Here, the duration and magnitude of dryness and wetness are of highest concern. The duration of wet and dry conditions is regarded as being scattered if the values fall below a given threshold (Mishra and Singh, 2010). Four distinct moderate drought events and four slightly less distinct wetness periods are found for the entire time period from 1963 to 2006 (Fig. 5). Distinct drought events occurred during 1963-65, 1988-90, 1990-92, and 2004-06. In summer 1990, a relatively wet period of few months separates the two distinct drought events. The moderate wetness events (1968-70, 1974/75, 1994-96, and 1997/98) show a higher disparity between the sub-basins i.e. most events occur only in half of the sub-basins (Fig. 6).

Table 1 shows the duration (in months) and the magnitude (as sum of SPI-24 or SDI-24) of hydrological and meteorological dryness and wetness according to the SPI-24 and SDI-24 for conditions below -1 (moderate dryness) and above +1 (moderate wetness) only. Most of the meteorological dryness conditions occurred in the sub-basins, the entire Xijiang River Basin, and Gaoyao at the same time periods while the wet periods are less developed.

However, as can be seen, the 1963-65 dryness in the SDI-24 for instance had the same duration as the 1988-90 dryness, but was higher in magnitude. The 2004-06 drought ranks third both in duration and magnitude. The SPI-24 corresponds likewise. The longest and highest wetness conditions in the SDI-24 occurred in the 1990s. 1994-96 shows the longest and highest wetness conditions in both the SDI-24 and SPI-24.

Regarding each sub-basin's role in contributing to the intensity of the hydrological dry or wet conditions at Gaoyao, for each examined dryness or wetness event different sub-basins contributed varyingly strong (Table 1). For example, the drought event in 1963-65 occurred longer and stronger in the eastern sub-basins; hence those were supporting the long duration and high magnitude discharge at Gaoyao with a higher proportion. Contrarily to that, the long drought event at Gaoyao in 2004-2006 was very strongly affected by the more than two-year drought in Beipan. It can be also seen that all of the sub-basins contributed to dryness conditions to a higher or lower extent, while proportionately the (north-) eastern sub-basins contribute stronger to the wetness conditions at Gaoyao.

The SPI-24 values of the sub-basins of Xijiang River have each a certain share of the dryness and wetness conditions at Gaoyao hydrological station. This finding will be further investigated and specified with the principal components analysis (PCA) in the following.

3.4 Principal Component Analysis of SPI-24

PC scores are investigated in order to illustrate the spatio-temporal variability of dryness and wetness conditions in the Xijiang River Basin that have been described above. The PC scores of the SPI-24 are displayed in Figure 7. The first three loadings explain 92% of the variance. PC-1 (Fig. 7a) explains 67% and shows multi-year fluctuations. PC-2 shows a higher frequency of negative values and describes 14% of the variance (Fig. 7b) whereas PC-3 falls below 11% with balanced positive and negative values (Fig. 7c). As expected, the magnitude of all PC scores is highest in PC-1 given the high percentage. PC-3 shows a higher tendency to dryness in magnitude and duration as compared to PC-2.

The loading patterns (linearly independent spatial pattern) of PC-1, PC-2, and PC-3 in each of the sub-basins are displayed in Figure 8. In Figure 8a, the correlation between the sub-basins' PC-1 loading and the averaged PC-1 loading is highest in Liujiang sub-basin. Nevertheless, the loading of PC-1 is spatially homogeneous in the Xijiang River Basin. The loading of PC-2 (Fig. 8b) is negative for three sub-basins in the East and positive in the West.

PC-3 (Fig. 8c) also reflects a dipole pattern but from South to North. These dipole conditions explain the opposing course of the sub-basins' SPI-24 in some few years (especially in the mid-1980's) and the difference in magnitude in others.

The PCA's loading patterns describe a generally good spatial homogeneity of the appearance of dryness and wetness conditions in the Xijiang River Basin. Spatially heterogeneous appearance of dryness and wetness in some years can be explained by the loading patterns. In the following, we investigate the periodicity of the peak dryness and wetness conditions that have been detected spatially and temporally.

3.5 Periodicities of SPI-24 and SDI-24

The results of the spectral analysis (Fig. 9) show similar peaks in the SPI-24 and the SDI-24. The highest peaks (power magnitude) for the SPI-24 and SDI-24 are located between 0.006 and 0.008 representing significant frequencies (at 90% confidence level) at 11-14.7 year periods. Lower peaks are found at frequencies of 2.8 years, 3.4-3.7 years, and 6.3-7.3 years. The magnitude of the peaks varies slightly between the SPI-24 and SDI-24. This underlines that the dryness and wetness conditions are subject to distinct periodic reoccurrence and that the cycles in the SPI-24 dominate cycles in the SDI-24.

The results of the spectral analysis for the six sub-basins of Xijiang River are shown in Figure 10. All sub-basins show the most significant (at 90% confidence level) peaks located at 11 and 14.7 year periods. In the Beipan and Nanpan sub-basins, the 11 year peak is much stronger. The 14.7 year period is the strongest in the other four sub-basins. Other peaks are similar to those for the SPI-24 and SDI-24. However, Yujiang sub-basin is the only watershed with a distinct peak at 3.7 years which is nearly as high as that for the 11-14.7 year period. Lower peaks are found at frequencies of 2.8 years, 3.4-3.7 years, and 6.3-7.3 years for all sub-basins. These periods highlight consistency with the periods in the SPI-24 of the entire Xijiang River Basin and the SDI-24 of Gaoyao hydrological station with some variation in magnitude.

Figure 11 shows the results of the wavelet analyses of the SPI-24 (entire Xijiang River Basin) and the SDI-24. As can be seen, the significant periodicity in the SPI-24 and SDI-24 with 11-14.7 year frequency is stable over time since the 1980s and has the highest significance in the 1980s and 1990s. The peak in the SPI-24 of 3.4-3.7 year frequency shifts

slightly over time after the 1980s. It loses some significance in the late 1990s and shifts to a slightly lower frequency.

As the PCA suggests spatial disparities in dryness and wetness conditions, we analyze the wavelet pattern of the SPI-24 over the sub-basins (Fig. 12). The 11-14.7 year frequency is apparent for all sub-basins and is stable over time and in intensity except for Yujiang. The latter is apparently dominated by the frequency of 3.7 years. The sub-basins Beipan and Hongshui for instance are dominated by the 11-14.7 year frequency over the entire time series whereas the frequency has slightly longer periods in the Hongshui sub-basin. The frequency of 3.4-3.7 years is also most persistent in the Hongshui sub-basin. The sub-basins located in the south and east (Yujiang and Lijiang) lack significant periodicities in the first decade of their time series. The periodicity around 3.7 years in Beipan and Nanpan eases in the 1960s, whereas it first starts in Lijiang and Liujiang after 1980s.

In the following, we extrapolate the significant peaks in periodicity of the spectral analysis assuming that the observed periods that cause dryness and wetness conditions will prevail in the future.

3.6 Extrapolation of SPI-24 and SDI-24

Figure 13 shows the SPI-24 and SDI-24 extrapolated until 2030. The extrapolation of the SPI-24 (entire Xijiang River Basin) is dominated by the significant short-term periodicity of 2.8 and 3.4-3.7 years, respectively, that can be seen in the reconstructed frequency (black line from 1963 to 2006). The beginning of the extrapolation (from 2007 until 2014) shows a change from slight wetness to moderate dryness conditions. After 2014, the extrapolation points out an increase in SPI-24 values which peak in moderate wetness conditions in 2028 which are then followed by moderate dryness conditions. Likewise, the reconstructed frequency and the extrapolation of the SDI-24 with the observed periodicities show a similar course as the SPI-24.

The reconstructed frequency for each of the six sub-basins (Fig. 14) shows the periodicity that has been detected in the power spectrum. The extrapolation is based on the continuation of the selected periodicities. Distinct spatial disparities in the extrapolation (and reconstruction) of the SPI-24 can be seen. The period 2007-2008 is highlighted by a shift from dry to normal conditions except for Beipan which shows an aggravation of the dryness conditions towards an extreme drought starting in 2008. Based on the periodicity of

each sub-basin, the course of the SPI-24 shows different magnitudes and durations in the extrapolations. A 3.7 year periodicity is most apparent in Yujiang and Hongshui sub-basins. The extrapolation clearly relies on these periods for the two sub-basins whereas the extrapolation for the other sub-basins is controlled by longer periods.

4. Discussion and Conclusions

The main interest of this study was to evaluate how long-term precipitation patterns have impacted the discharge of Xijiang River. Therefore, the characteristics of long-term climatological and hydrological dryness and wetness conditions were analyzed. It can be concluded that the discharge of Xijiang River based on its SDI-24 directly relies on the area weighted SPI-24 of the Xijiang River Basin. Hence, the natural variation in precipitation is responsible for the discharge to a very high degree. This is in line with the findings of Zhang et al. (2008), who concluded that the long-term changes of annual water discharge are mainly controlled by precipitation variation, while the construction of reservoirs/dams has made little influence on water discharge in the Zhujiang River Basin. We can also conclude that each sub-basin has a considerable strong impact on the SDI-24 at Gaoyao hydrological station, while some sub-basins contribute higher to the discharge (correlation up to 85%) than others. With the calculation of the spatial interdependencies of the sub-basins using the PCA, it was possible to determine that all sub-basins contribute to hydrological dryness conditions, while mainly the north-eastern sub-basins can be made responsible for wetness conditions. The western sub-basins have rather little influence in hydrological wetness conditions of Xijiang River. We can also conclude that meteorological dryness conditions are larger in spatial extent (i.e. covering all sub-basins) than wetness conditions.

We found that distinct cycles of dryness and wetness occurred chronologically over periods of several years. The precipitation in the Xijiang River Basin and the discharge of Xijiang River are dominated by significant periods of 11-14.7 years and significant cycles of shorter periodicity (2.8 years, 3.4-3.7 years, and 6.3-7.3 years). The controlling force of the long-term hydrological status at Xijiang River is therefore an 11-14.7 year oscillation in the precipitation. Additionally, spatial disparities can be observed in the sub-basins which are an interesting feature but can be explained by regional disparities in annual and monthly precipitation patterns with annual values decreasing from the East to the West of the river basin (Gemmer et al., 2011).

An increase in dry days has been detected by Gemmer et al. (2011) for the same precipitation time series. Furthermore, increases in the magnitude of indices describing dryness, and a prolongation of dry periods with an opposing shortening of wet periods were identified by Fischer et al. (2011). These findings can explain the long-term drought sequences which we observed in the SPI-24 and SDI-24 time series during the second half the observed time period. It might also explain why the short-term periods, around 3-4 years, shifted to slightly longer periods which would then indicate inner-annual changes. Further noticeable are the change points in precipitation indices in 1985/86 and 2003/04 that have been detected by Fischer et al. (2012). Both change points mark the start of the two most distinct dryness clusters in the SPI-24 and SDI-24 time series. To some extent, Gemmer et al. (2011) and Fischer et al. (2011 and 2012) link the observed changes to the weakening of the East Asian Summer Monsoon (EASM).

Compared to earlier studies, our approach of analyzing long-term changes and periodicities disaggregates extreme events and allows a broader view on meteorological and hydrological statuses. With the standardization of long-term precipitation cycles, they can be compared with the hydrology. With the understanding of the periods and reoccurring dryness and wetness conditions, it is important to consider the identified periods in any water-related planning.

The extrapolation of the significant periodicities identified in the power spectrum is a statistical prediction obtained through the fast Fourier transform and not based on modelling results from global or regional climate models. It is assumed that the significant periods will pertain in the near future with their extrapolation suggesting certain spatial and/or temporal changes in the occurrence of dryness and wetness conditions in the next two decades, but no obvious tendencies to significantly higher or lower magnitudes. This prediction of no significant trends in regional precipitation pattern in the first three decades of the 21st century can be supported by the findings of Sun and Ding (2010). By using a multi-model ensemble of global circulation models, they projected an increase in summer precipitation for the whole of South China merely starting around the 2040's. Similarly, Fischer et al. (submitted) projected climate extremes in the Zhujiang River Basin, using the regional climate model CCLM, and did not identify any significant trends in precipitation extremes for the period 2011-2050. Furthermore, Zeng et al. (2012) applied the outputs from the global circulation model ECHAM5 to an artificial neural network to project future river discharge of the Yangtze River, but did not identify any obvious trends.

Based on these findings, we can draw the hypothesis that it is more important to investigate periodic events rather than trends or extremes. This hypothesis is fully supported by the statistical approach applied as compared to a physical or dynamical approach based on global or regional climate models. Although we are unable to reliably predict the stability of the periodicities using few statistical spectral-analysis methods (Ghil et al., 2011), we can place more confidence on our short-term extrapolations, as these rely on the observed significant periodicities, than on near-future projections of global or regional climate models (cf. Becker et al., 2008).

In future, nonetheless, a physical based approach can be used to further test this hypothesis at a smaller regional scale, where regional disparities will have to be considered. A recent example can be drawn for the Beipan sub-basin. The extrapolation showed distinct extreme dryness conditions in 2008-09 which are spatially and temporally in line with the observed long-term drought that occurred in Southwest China in 2009-10 (Lü et al., 2012). Here, an anomalous weakening of the vertical Asian monsoon circulation in South Asia has been found responsible for this drought event. The extrapolation for Beipan takes a different course than the other sub-basins, which the newly available statistics prove to be correct. It has yet to be confirmed whether the magnitude of the peaks are precise.

The PCA has shown regional disparities in the SPI-24 of the sub-basins. The area averaged SPI-24 for the Xijiang River Basin agrees well with the SDI-24 and each sub-basin might have different long-term dryness and wetness conditions. At a regional level, any significant changes in the sub-basins will have effect on the discharge and long-term dryness/wetness conditions of Xijiang River. This factor might have been underestimated in previous studies (e.g. Zhang et al., 2008). The method using the weighted SPI-24 for instance shows that Beipan has a distinct impact on Xijiang's hydrology, especially during dryness conditions such as in 2008-09. Therefore, our methodology proves to be able to detect significant periodicities and to display regional disparities in long-term dryness and wetness conditions.

Our initial investigations on the origin of the long-term dryness and wetness occurrences and the corresponding periodicities did not show any inter-connections with large-scale atmospheric circulation indices (e.g. El Niño–Southern Oscillation [ENSO], Madden-Julian-Oscillation [MJO]). Such physical explanations for the observed periodicities are needed to gain more confidences on the future stability of the cycles, and hence, of the reliability of our extrapolation results (Ghil et al., 2011). Studies by Bordi et al. (2004),

Fischer et al. (2012), Gemmer et al. (2011), Lü et al. (2012), and Zhang et al. (2008) suggest that several large-scale atmospheric circulations are responsible for certain changes in the strength of the East Asian Monsoon, which further leads to changing periodicities, change points, and trends in precipitation pattern. Nonetheless, the extrapolation of the significant periodicities in the next decades provides valuable information on the potential occurrence and magnitude of dryness and wetness conditions for such as flood risk forecast and drought preparedness.

This study highlights the close relationship of spatio-temporal meteorological dryness and wetness conditions with hydrological responses. Considering that natural factors are responsible for the variation in precipitation, very little influence of human activities can be found in the monthly characteristics of hydrological processes. Water resource management planning and future research on the projection or prediction of hydrological long-term dryness and wetness conditions in the Zhujiang River Basin should particularly take periodicities in regional precipitation patterns into consideration.

Acknowledgements

This study was supported by the National Basic Research Program of China (973 Program) (No. 2012CB955903) and National Natural Science Foundation of China (40910177). The positions of Thomas Fischer and Marco Gemmer are supported by the Center for International Migration and Development (www.cimonline.de).

References

Becker, S., H. Hartmann, M. Coulibaly, Q. Zhang, T. Jiang, 2008. Quasi periodicities of extreme precipitation events in the Yangtze River basin, China. Theor. Appl. Climatol., 94, 139-152.

Berz, G., W. Kron, 2004. Überschwemmunskatastrophen und Klimaänderung: Trends und Handlungsoptions aus (Rück-) Versicherungssicht, p. 264-269. In J. L. Lozan, H. Graßl, P. Hupfer, L. Menzel, and C.-D. Schönwiese [eds.], Warnsignal Klima: Genug Wasser für alle? Wissenschaftliche Auswertungen, Hamburg, Germany.

Bordi, I., K. Fraedrich, J.M. Jiang, A. Sutera, 2004. Spatio-temporal variability of dry and wet periods in eastern China. Theoretical and Applied Climatology 79, 81-91.

Bordi, I., K. Fraedrich, M. Petitta, A. Sutera, 2007. Extreme value analysis of wet and dry periods in Sicily. Theor. Appl. Climatol., 87, 61-71.

Buishand, T.A., 1982. Some methods for testing the homogeneity of rainfall records. Journal of Hydrology, 58, 11-27.

China Daily, 2008: 'China's 3rd-largest hydropower station to be fully operating this year'. China Daily, 2 September 2008 [Online], Available at http://www.chinadaily.com.cn/china/2008-09/02/content_6991918 (Accessed: 19 January 2012).

Dai, S.B., S.L. Yang, A.M. Cai, 2008. Impacts of dams on the sediment flux of the Pearl River, southern China. Catena, 76, 36-43.

Feng, S., S. Nadarajah, Q. Hu, 2007. Modeling Annual Extreme Precipitation in China Using the Generalized Extreme Value Distribution. Journal of the Meteorological Society of Japan, 85, 599-613.

Fischer, T., C. Menz, B. Su, and T. Scholten, (submitted): Simulated and projected climate extremes in the Zhujiang River Basin, South China, using the regional climate model COSMO-CLM. Submitted to International Journal of Climatology (Jan. 2012).

Fischer, T., M. Gemmer, L. Liu and B. Su, 2011: Precipitation Trends and dryness/wetness pattern in the Zhujiang River Basin, South China, 1961-2007. Quaternary International, Volume 244, Issue 2, 138-148.

Fischer, T., M. Gemmer, L. Liu and T. Jiang, (2012): Change-points in climate extremes in the Zhujiang River Basin, South China, 1961-2007. Climatic Change, Volume 110, Issue 3, 783-799.

Gao, C., M. Gemmer, X. Zeng, B. Liu, B. Su, Y. Wen, 2010. Projected Streamflow in the Huaihe River Basin (2010-2100) using Artificial Neural Networks (ANN). Stochastic Environmental Research and Risk Assessment, 24, 685-697.

Gemmer, M., T. Fischer, T. Jiang, B. Su, L. Liu, 2011. Trends of Precipitation Extremes in the Zhujiang River Basin, South China. Journal of Climate, 24, 750-761.

Gemmer, M., T. Jiang, B.D. Su, and Z.W. Kundzewicz, 2008. Seasonal precipitation changes in the wet season and their influence on flood/drought hazards in the Yangtze River Basin, China. Quaternary International 186, 12-21.

Ghil, M., P. Yiou, S. Hallegatte, et al., 2011: Extreme events: dynamics, statistics and prediction. Nonlin Processes Geophys, 18, 295-350.

Jiang, T., Y.D. Chen, C. Xu, X. Chen, X. Chen, and V.P. Singh, 2007. Comparison of hydrological impacts of climate change simulated by six hydrological models in the Dongjiang Basin, South China. Journal of Hydrology, 336, 316– 333.

Klein Tank, A.M.G., F. Zwiers, and X. Zhang, 2009: Guidelines on - Analysis of extremes in a changing climate in support of informed decisions for adaptation. World Meteorological Organisation (WMO), Climate Data and Monitoring, WCDMP-No. 72, WMO-TD No. 1500, Geneva, Switzerland.

Liu L.L., Liu Z.F., Ren X.Y., Fischer, T., Xu Y. 2011. Hydrological impacts of climate change in the Yellow River Basin for the 21st century using hydrological model and statistical downscaling model. Quaternary International 244: 211-220.

Lloyd-Hughes, B. and M.A. Saunders, 2002: A drought climatology for Europe. Int. J. Climatol., 22, 1571–1592.

Lü J.M., Ju J.H., Ren J.Z. et al., 2012. The influence of the Madden-Julian Oscillation, activity anomalies on Yunnan's extreme drought of 2009–2010. Sci China Earth Sci, 55, 98–112.

McKee, T.B., N.J. Doesken, J. Kleist, 1993. The relationship of drought frequency and duration to time scales. Preprints Eighth Conf on Applied Climatology, Anaheim, CA. Am. Meteor. Soc., Boston. pp 179–184.

Mishra, A.K. and V.P. Singh, 2010. A review of drought concepts. Journal of Hydrology, 391, 202–216.

Nalbantis, I., and G. Tsakiris, 2009. Assessment of hydrological drought revisited. Water Resources Management, 23(5), 881-897.

Qian, W., X. Lin, 2005: Regional trends in recent temperature indices in China. Meteorol. Atmos. Phys., 90, 193-207.

Santos, J.F., M.M. Portela, and I. Pulido-Calvo, 2011: Regional Frequency Analysis of Droughts in Portugal. Water Resources Management, DOI 10.1007/s11269-011-9869-z

Schönwiese, C.-D., 2006: Praktische Statistik für Meteorologen und Geowissenschaftler. 4. Auflage, Gebrüder Bornträger Verlagsbuchhandlung, Berlin, Stuttgart, S.302.

Sun, Y. and Y.H. Ding, 2010: A projection of future changes in summer precipitation and monsoon in East Asia. Sci China Earth Sci, 53, 284-300.

Torrence, C. and G.P. Compo, 1998. A practical guide to wavelet analysis. Bulletin of the American Meteorological Society, 79, 61-78.

Varis, O., M. Kummu, and A. Salmivaara: 2012: Ten major rivers in monsoon Asia-Pacific: An assessment of vulnerability. Applied Geography, 32, 441-454.

Waterpub, 2012: 'Zhujiang River'. China Water Conservancy and Hydropower Press, Available at http://www.waterpub.com.cn/JHDB/DetailRiver.asp?ID=5 (Accessed: 19 January 2012).

Wilks, D.S., 2006: Statistical Methods in the Atmospheric Sciences. Second Edition, Elsevier Inc., USA, p.649.

Xu, K.H., J.D. Milliman, and H. Xu, 2010: Temporal trend of precipitation and runoff in major Chinese Rivers since 1951. Global and Planetary Change, 73, 219–232.

Zeng X., Z.W. Kundzewicz, J. Zhou, and B. Su, (2012): Discharge projection in the Yangtze River basin under different emission scenarios based on the artificial neural network. Quaternary International, doi:10.1016/j.quaint.2011.06.009

Zhai, J.Q., B. Liu, H. Hartmann, B.D. Su, T. Jiang, K. Fraedrich, 2010a. Dryness/wetness variations in ten large river basins of China during the first 50 years of the 21st century. Quaternary International, 226, 101-111.

Zhai, J.Q., B.D. Su, V. Krysanova, T. Vetter, C. Gao, C.T. Jiang, 2010b. Spatial variation and trends in PSDI and SPI indices and their relation to streamflow in 10 large regions of China. Journal of Climate, 23, 649-663.

Zhai, L.X., F.Qi, 2009. Spatial and temporal pattern of precipitation and drought in Gansu Province, Northwest China. Natural Hazards, 49, 1-24.

Zhang, Q., C.-Y. Xu, Z. Zhang, 2009. Observed changes of drought/wetness episodes in the Pearl River basin, China, using the standardized precipitation index and aridity index. Theoretical and Appied Climatology, 98, 89-99.

Zhang, Q., T. Jiang, M. Gemmer, S. Becker, 2005. Precipitation, temperature and runoff analysis from 1950 to 2002 in the Yangtze basin, China. Hydrol. Sci., 50, 65-80.

Zhang, S., X.X. Lu, D.L. Higgitt, C.T.A. Chen, J. Han, H. Sun, 2008. Recent changes of water discharge and sediment load in the Zhujiang (Pearl River) Basin, China. Global and Planetary Change, 60, 365-380.

Zhao, G., X. Mu, G. Hoermann, N. Fohrer, M. Xiong, B.D. Su, X. Li, (2011). Spatial patterns and temporal variability of dryness/wetness in the Yangtze River Basin, China. Quaternary International, xxx, 1-9, DOI: 10.1016/j.quaint.2011.10.020.

Tables

Table 1: Duration and magnitude of peak periods of moderate drought (SPI<-1) and moderate wetness (SPI>1) in the six sub-basins of the Xijiang River Basin, the entire basin (Xijiang), and at Gaoyao hydrological station (SDI<-1, SDI>1), 1963-2006

Figures

Fig. 1: Location of the six sub-basins in the Xijiang River Basin of the Zhujiang River Basin

Fig. 2: Annual Precipitation (grey bars) in the Xijiang River Basin and Annual Discharge (black line) at Gaoyao Hydrological Station 1961-2006

Fig. 3: Average Monthly Precipitation (grey bars) in the Xijiang River Basin and Average Monthly Discharge (black line) at Gaoyao Hydrological Station 1961-2006

Fig. 4: Average Monthly Precipitation (grey bars) in the Xijiang River Basin and Average Monthly Discharge (black line) at Gaoyao Hydrological Station in 1963 (left) and 1994 (right)

Fig. 5: SPI-24 of the Xijiang River Basin (upper panel) and the SDI-24 of Gaoyao Hydrological Station (lower panel)

Fig. 6: SPI-24 of the six sub-basins in the Xijiang River Basin

Fig. 7: PC scores of the SPI-24 in the Xijiang River Basin

Fig. 8: Loading pattern of PC-1 (a), PC-2 (b), and PC-3 (c) in the six sub-basins of the Xijiang River Basin

Fig. 9: Spectral analysis of the SPI-24 (left panel) and SDI-24 (right panel)

Fig. 10: Spectral analysis of the SPI-24 of the six sub-basins in the Xijiang River Basin

Fig. 11: Wavelet analysis of the SPI-24 (left panel) and the SDI-24 (right panel)

Fig. 12: Wavelet analysis of the SPI-24 of the six sub-basins in the Xijiang River Basin

Fig. 13: Observed (dark gray shadings) and reconstructed time series (black line; confidence interval = light gray shading) plus extrapolation (starting in 2007) of the SPI-24 (upper panel) and SDI-24 (lower panel) 1963-2030

Fig. 14: Observed (dark gray shadings) and reconstructed time series (black line; confidence interval = light gray shading) plus extrapolation (starting in 2007) of the SPI-24 of the six sub-basins in the Xijiang River Basin 1963-2030

Table 1: Duration and magnitude of peak periods of moderate drought (SPI<-1) and moderate wetness (SPI>1) in the six sub-basins of the Xijiang River Basin, the entire basin (Xijiang), and at Gaoyao hydrological station (SDI<-1, SDI>1), 1963-2006

Event	Period	**Duration** (months)							
		Nanpan	Beipan	Hongshui	Liujiang	Yujiang	Lijiang	Xijiang	Gaoyao
moderate drought (<-1)	1963-65	14	9	16	20	20	19	18	25
	1988-90	17	14	11	8	16	3	10	25
	1990-92	8	11	3	4	5	22	7	20
	2004-06	2	27	6	3	6	8	6	22
	event sum	41	61	36	35	47	52	41	92
moderate wetness (>1)	1968-70	0	13	12	7	0	0	0	21
	1974/75	3	0	2	2	8	12	2	11
	1994-96	0	0	13	20	5	21	12	26
	1997/98	0	0	2	3	2	15	1	23
	event sum	3	13	29	32	15	48	15	81
Event	Period	**Magnitude** (sum of monthly SPI values)							
		Nanpan	Beipan	Hongshui	Liujiang	Yujiang	Lijiang	Xijiang	Gaoyao
moderate drought (<-1)	1963-65	-21.4	-11.3	-23.1	-25.1	-26.8	-24.7	-23.0	-51.0
	1988-90	-23.0	-25.8	-15.7	-9.5	-21.1	-3.4	-13.1	-35.7
	1990-92	-8.5	-20.1	-3.2	-4.6	-6.0	-30.5	-7.8	-29.3
	2004-06	-3.4	-33.4	-6.4	-3.1	-6.3	-10.2	-6.5	-29.5
	event sum	-56.3	-90.6	-48.5	-42.4	-60.2	-68.8	-50.4	-145.5
moderate wetness (>1)	1968-70	0.0	16.0	13.5	7.7	0.0	0.0	0.0	29.1
	1974/75	3.3	0.0	2.3	2.1	9.2	14.0	2.2	13.5
	1994-96	0.0	0.0	20.0	35.2	5.3	28.0	14.4	43.8
	1997/98	0.0	0.0	2.1	3.4	2.2	18.0	1.0	35.7
	event sum	3.3	16.0	37.9	48.5	16.7	60.0	17.6	122.1

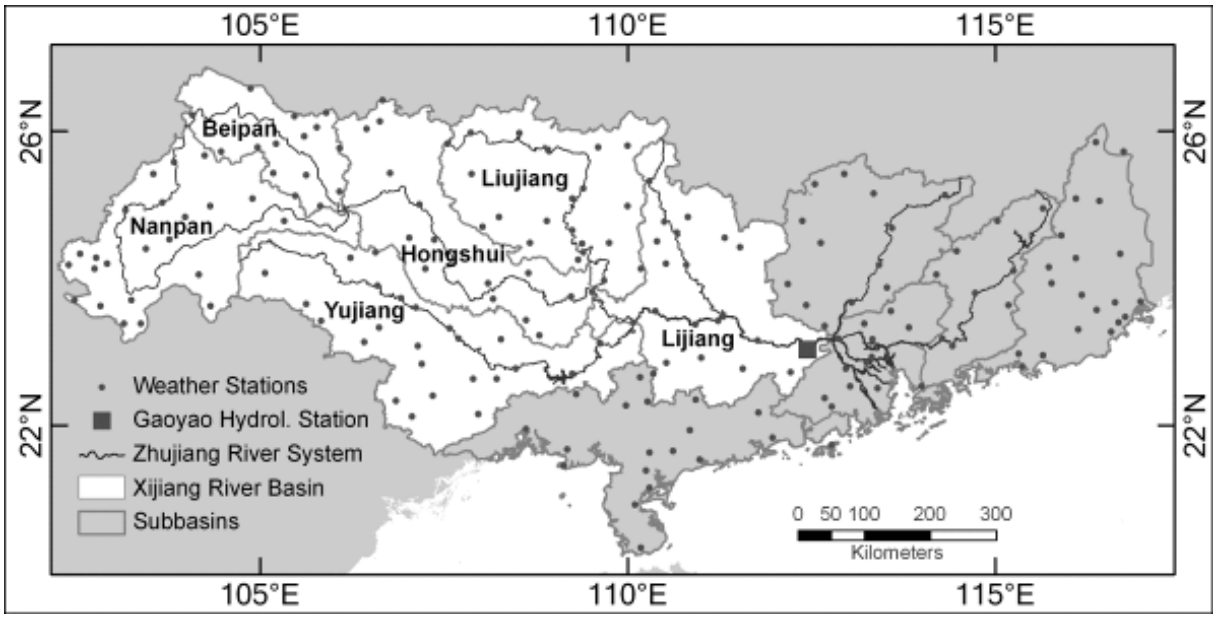

Fig. 1: Location of the six sub-basins in the Xijiang River Basin of the Zhujiang River Basin

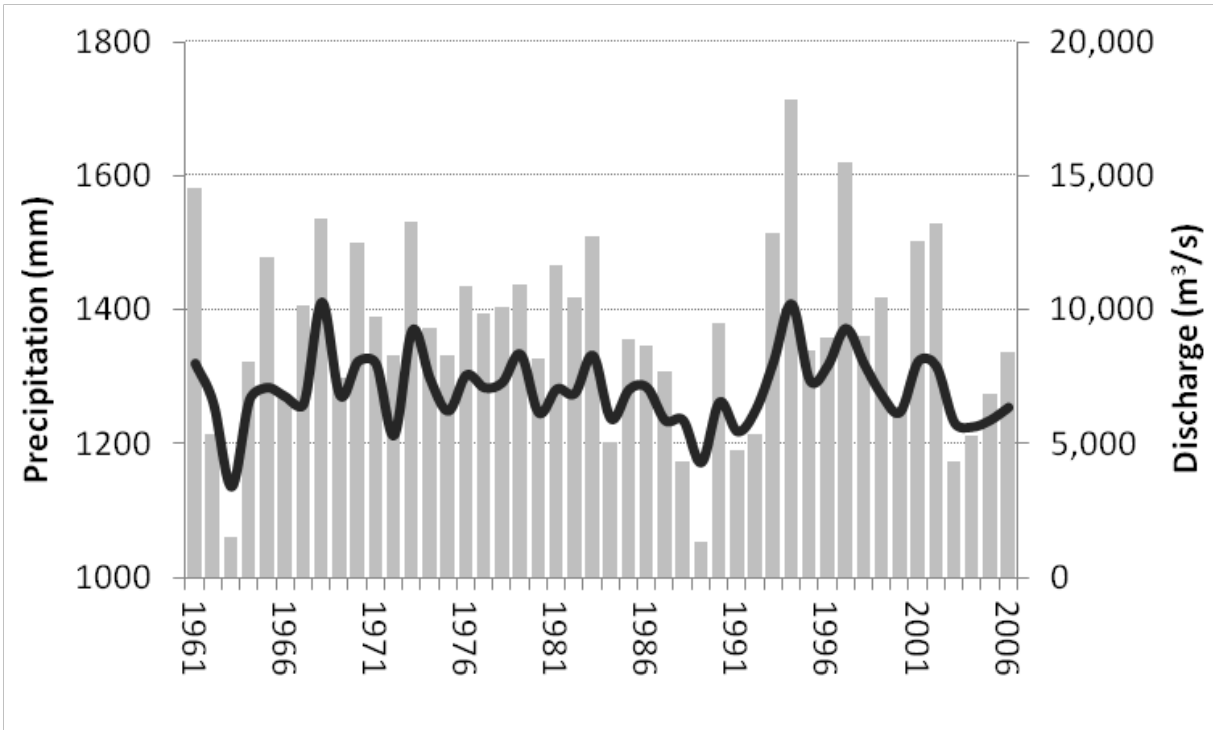

Fig. 2: Annual Precipitation (grey bars) in the Xijiang River Basin and Annual Discharge (black line) at Gaoyao Hydrological Station 1961-2006

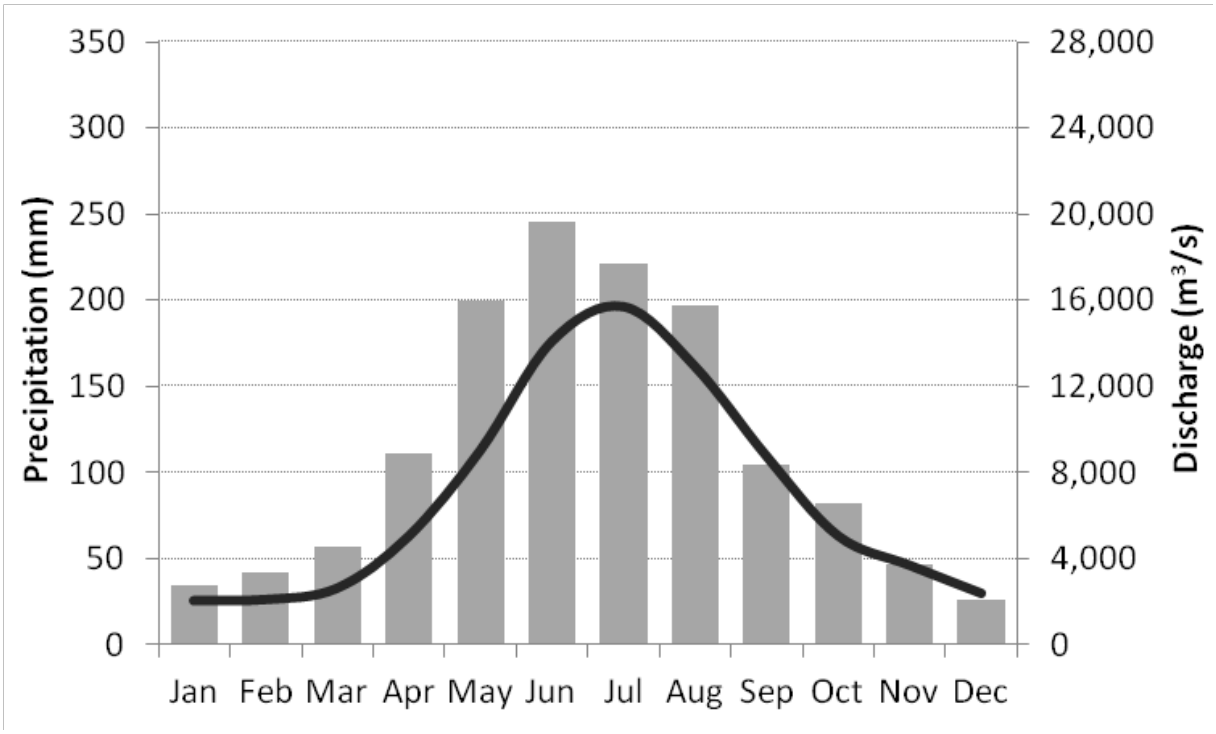

Fig. 3: Average Monthly Precipitation (grey bars) in the Xijiang River Basin and Average Monthly Discharge (black line) at Gaoyao Hydrological Station 1961-2006

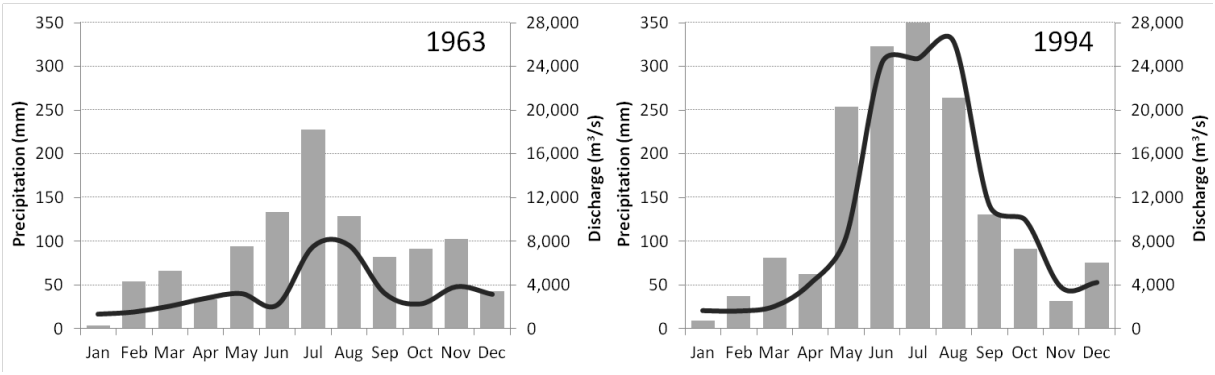

Fig. 4: Average Monthly Precipitation (grey bars) in the Xijiang River Basin and Average Monthly Discharge (black line) at Gaoyao Hydrological Station in 1963 (left) and 1994 (right)

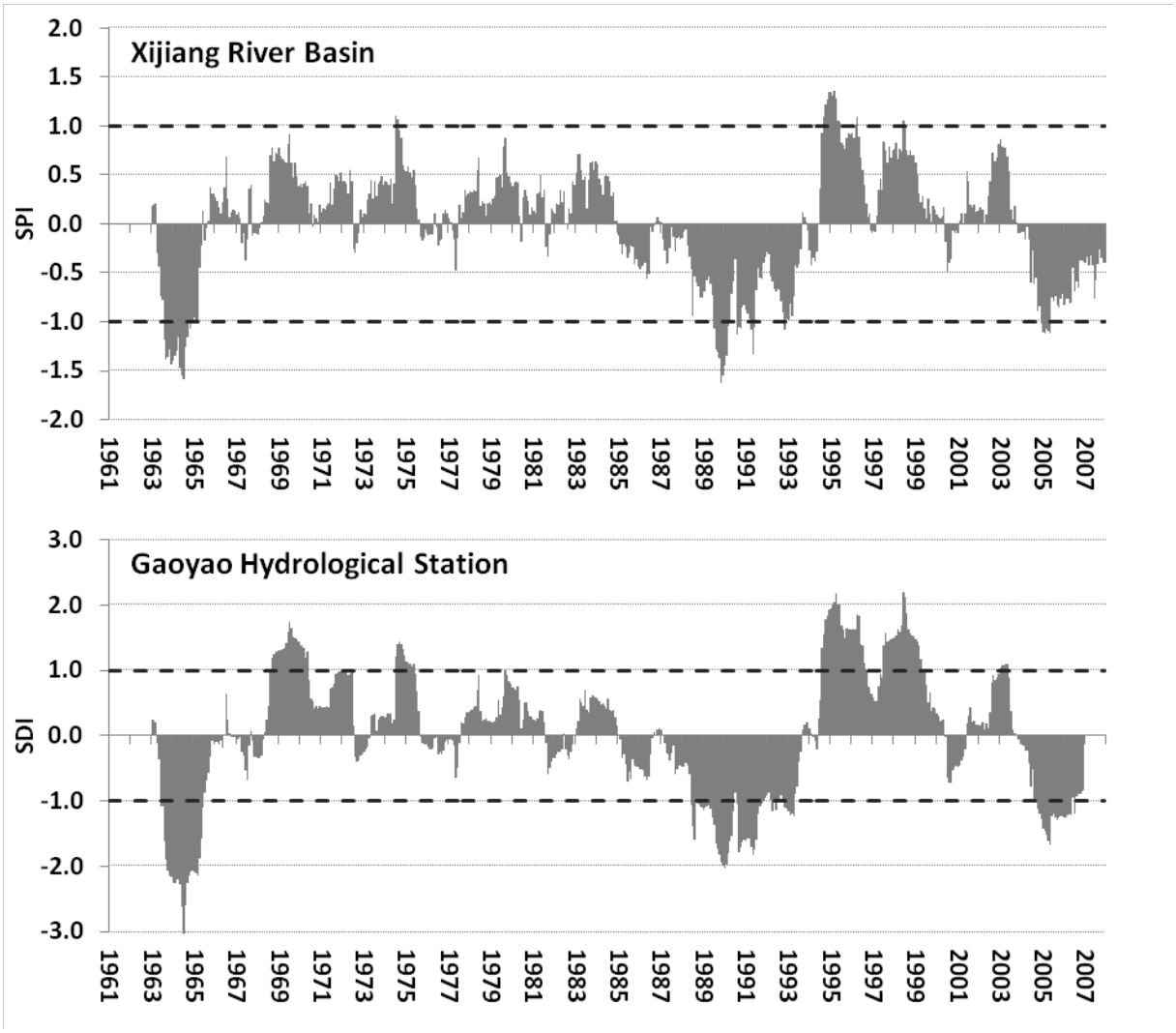

Fig. 5: SPI-24 of the Xijiang River Basin (upper panel) and the SDI-24 of Gaoyao Hydrological Station (lower panel)

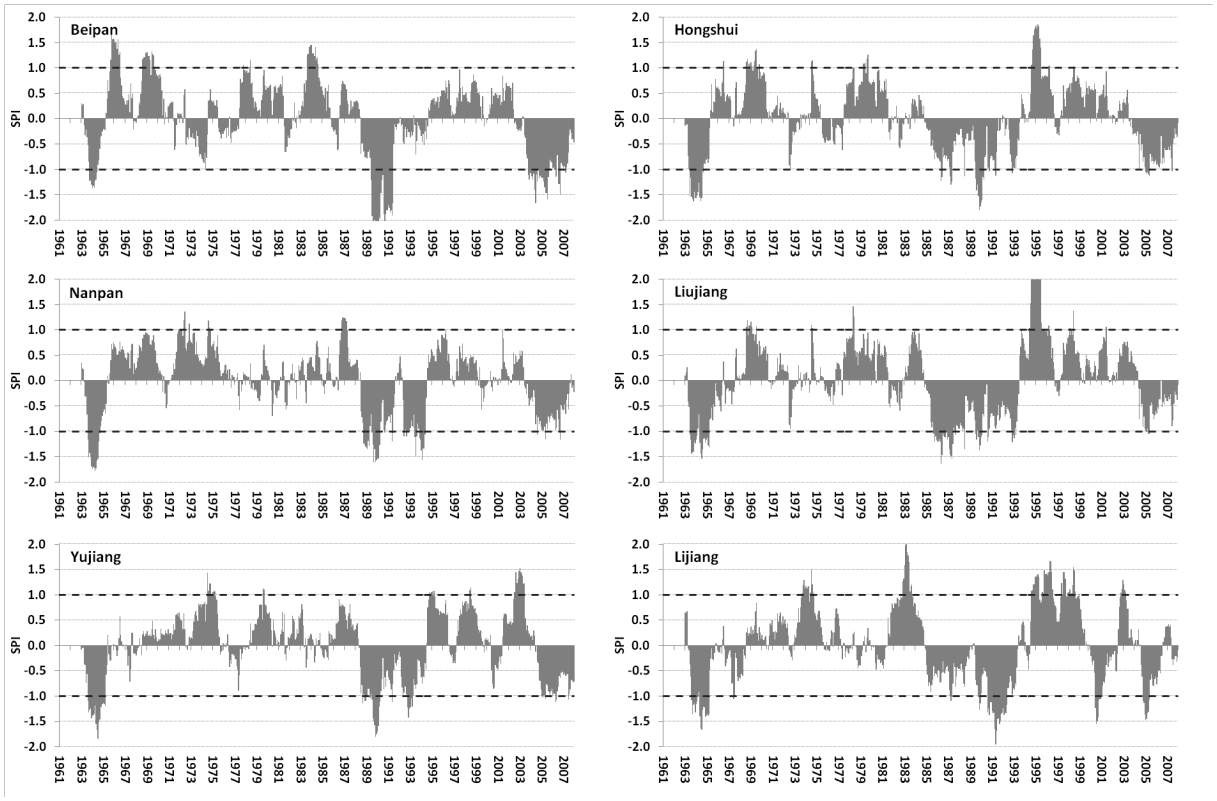

Fig. 6: SPI-24 of the six sub-basins in the Xijiang River Basin

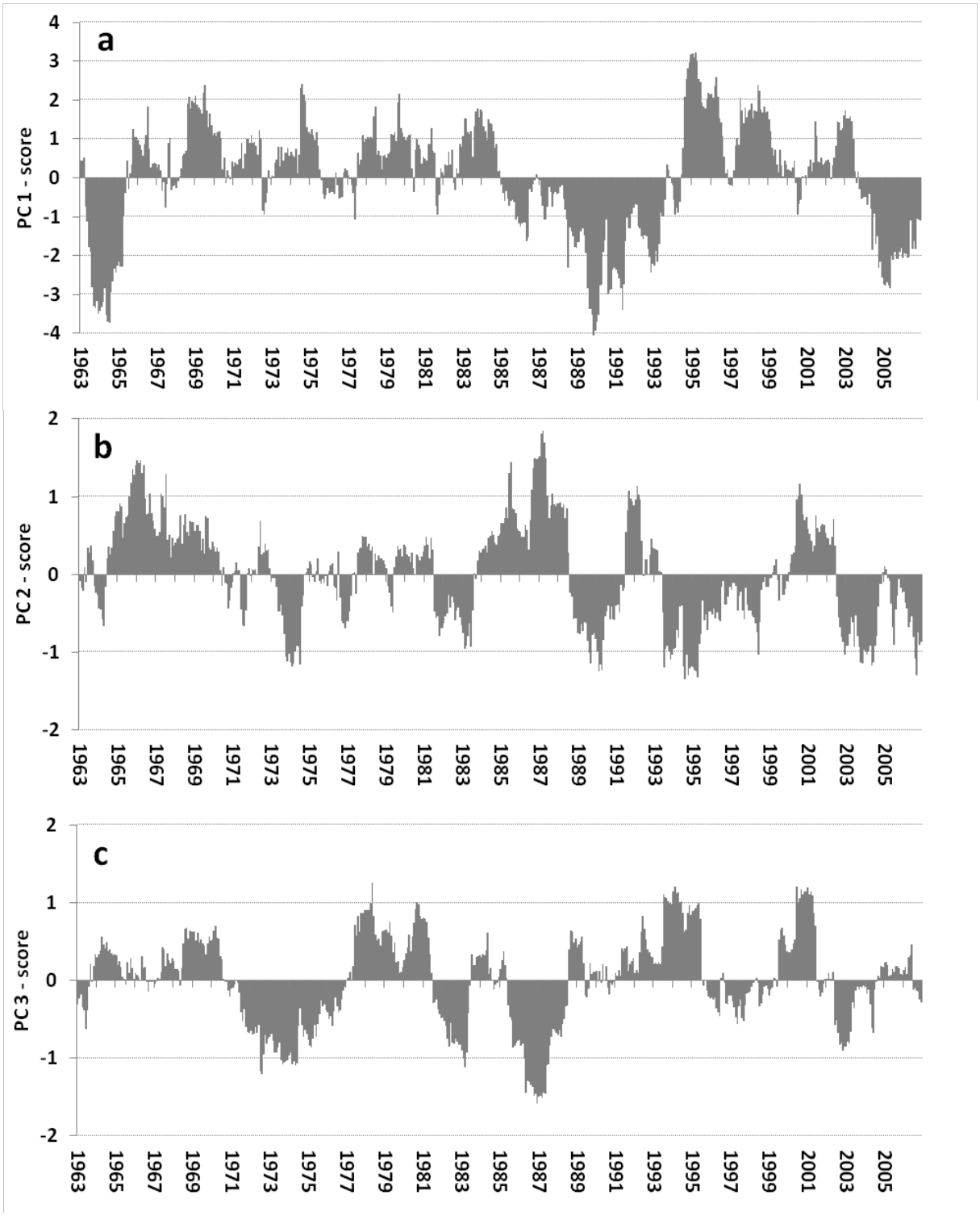

Fig. 7: PC scores of the SPI-24 in the Xijiang River Basin

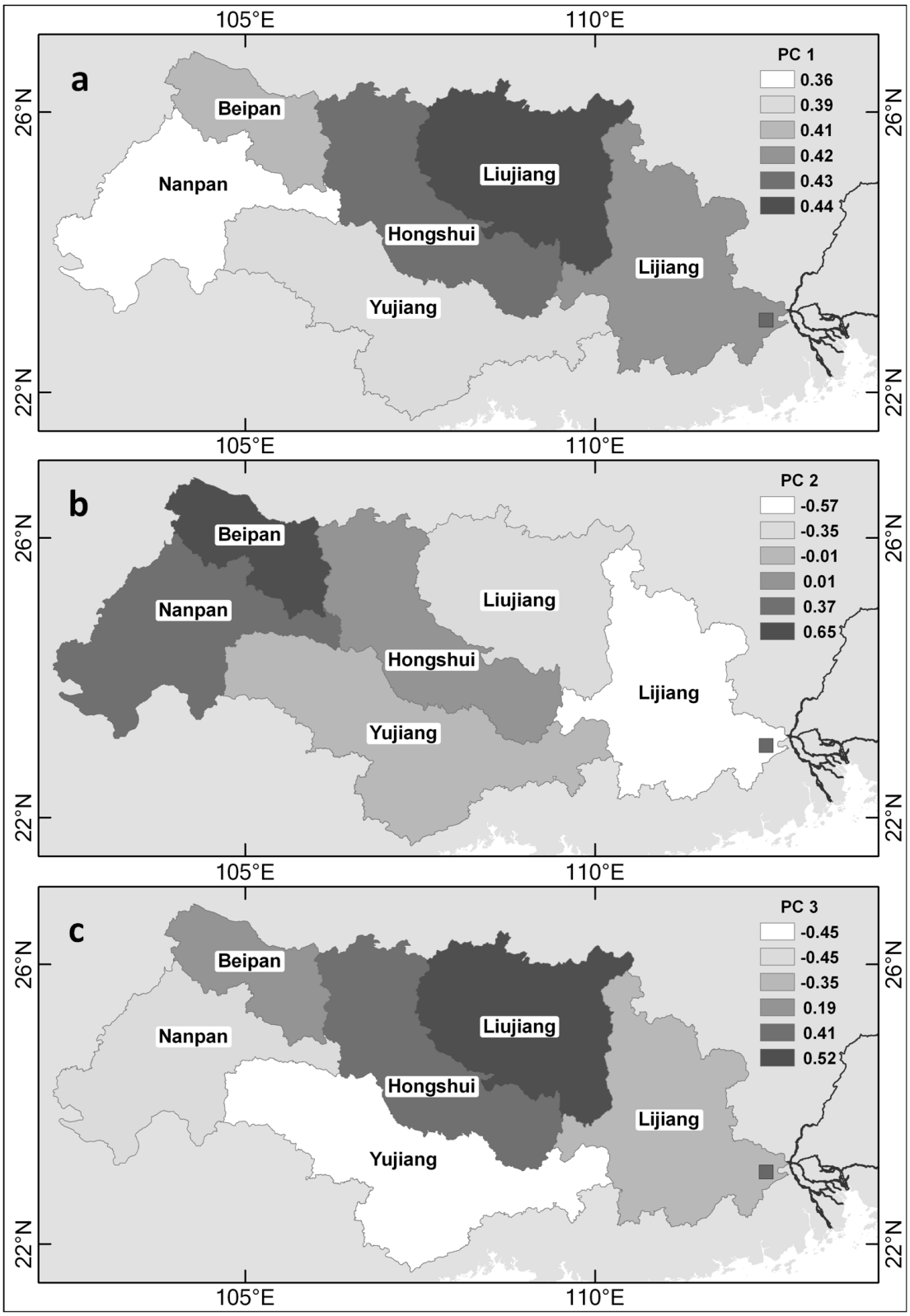

Fig. 8: Loading pattern of PC-1 (a), PC-2 (b), and PC-3 (c) in the six sub-basins of the Xijiang River Basin

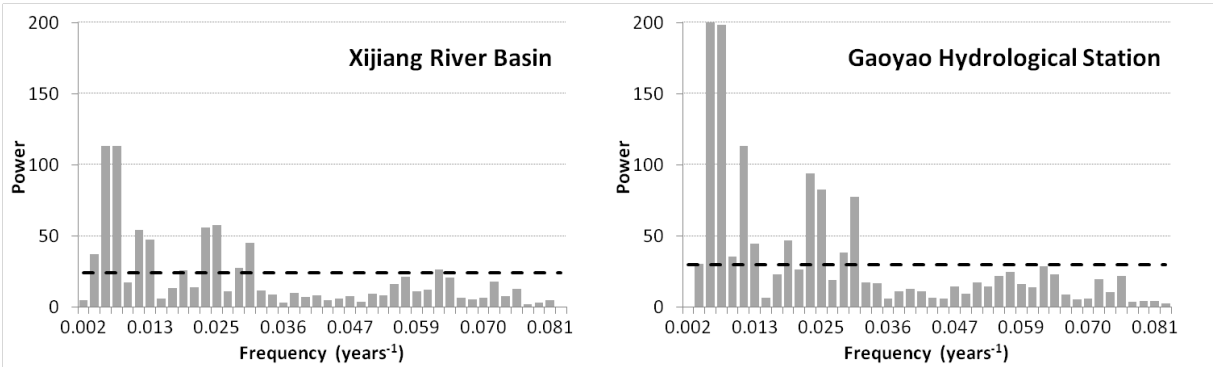

Fig. 9: Spectral analysis of the SPI-24 (left panel) and SDI-24 (right panel)

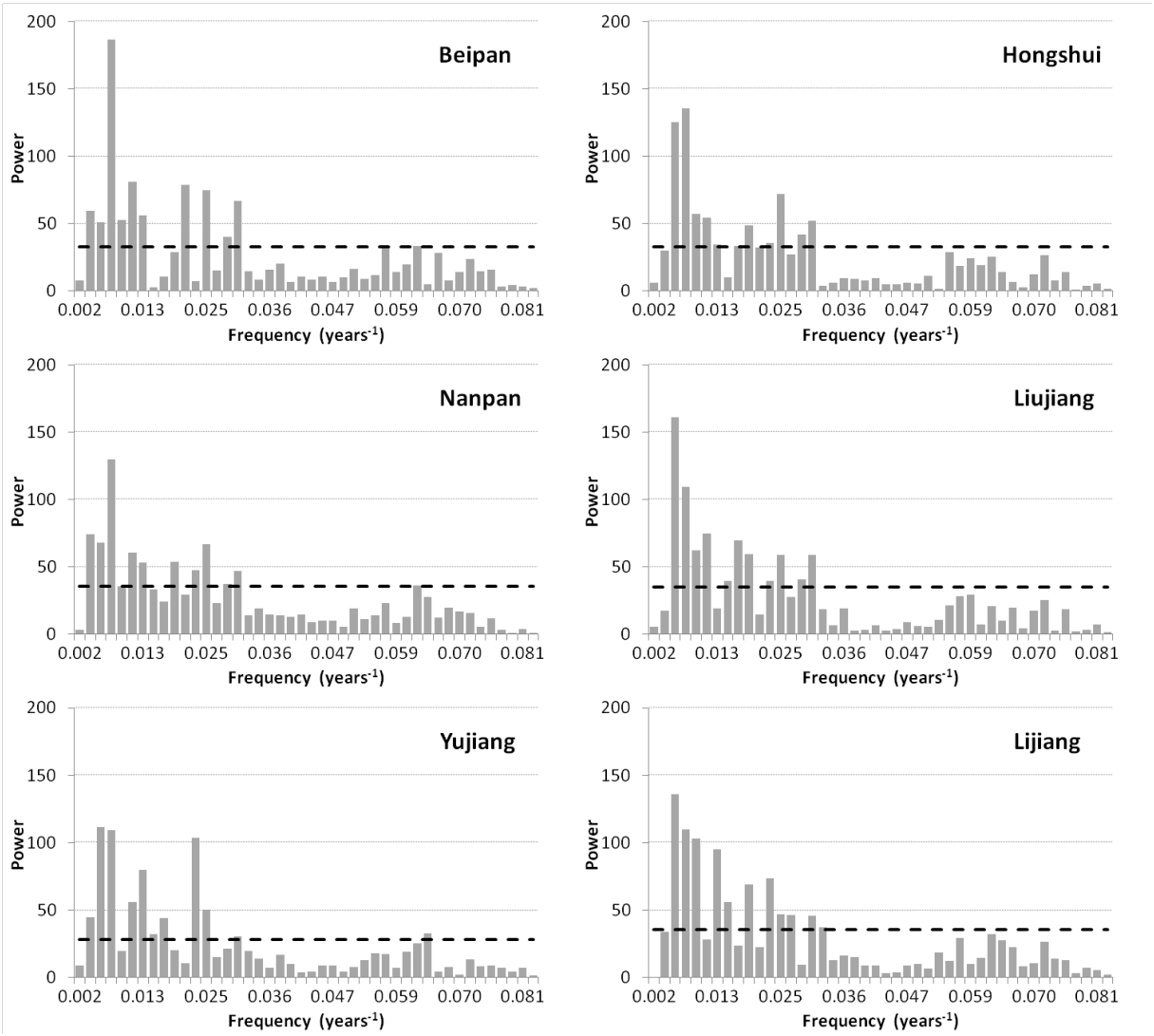

Fig. 10: Spectral analysis of the SPI-24 of the six sub-basins in the Xijiang River Basin

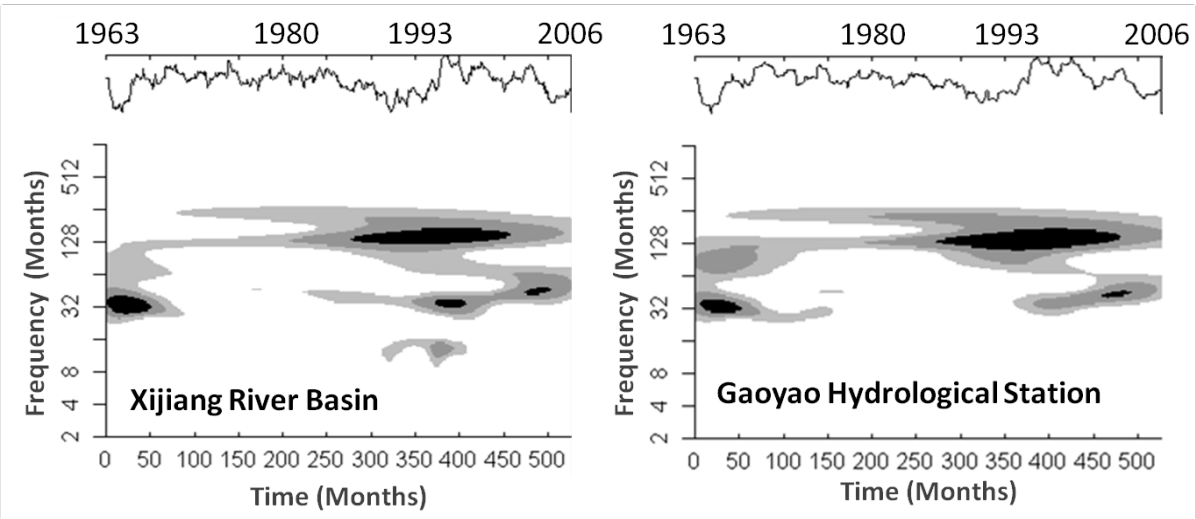

Fig. 11: Wavelet analysis of the SPI-24 (left panel) and the SDI-24 (right panel)

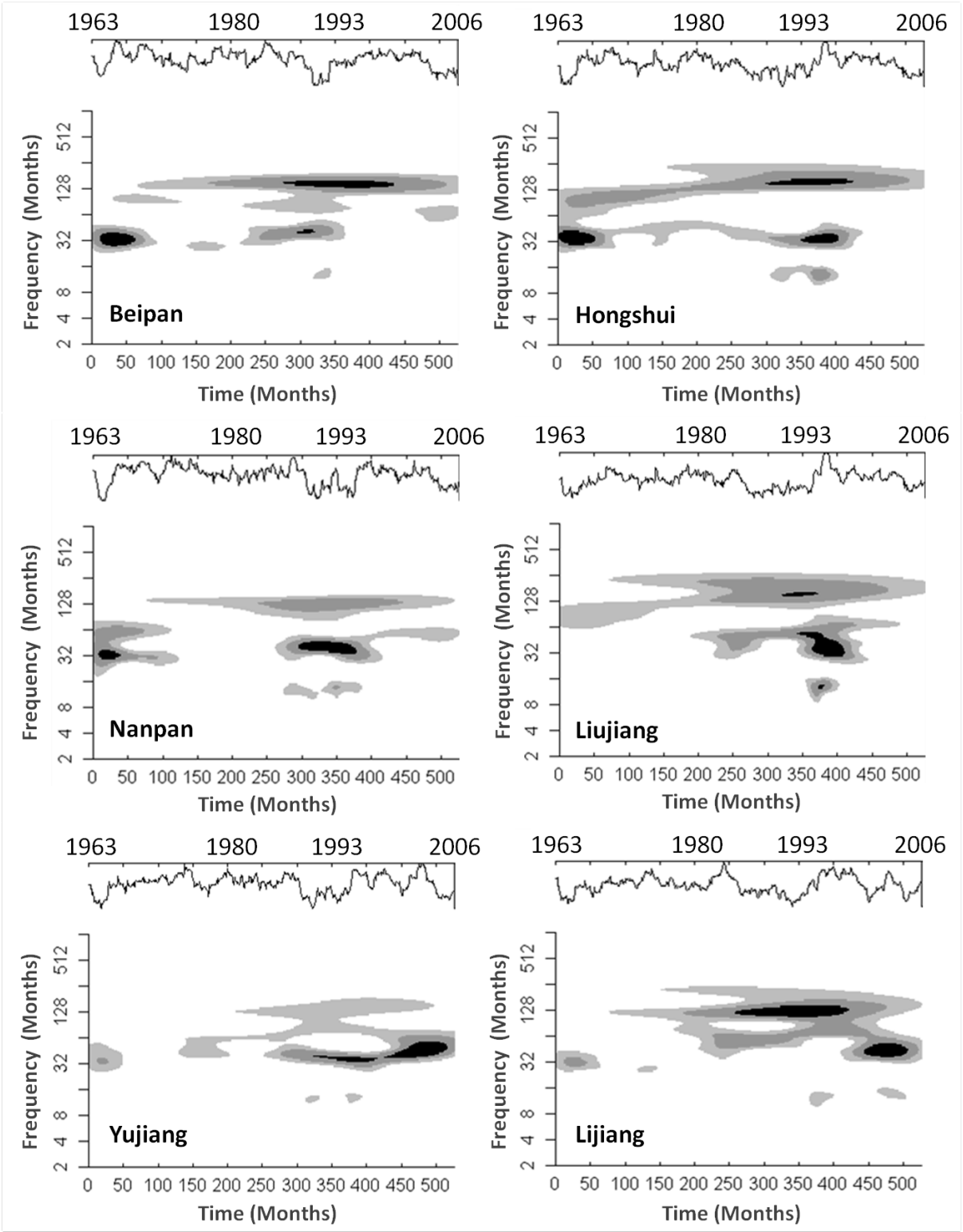

Fig. 12: Wavelet analysis of the SPI-24 of the six sub-basins in the Xijiang River Basin

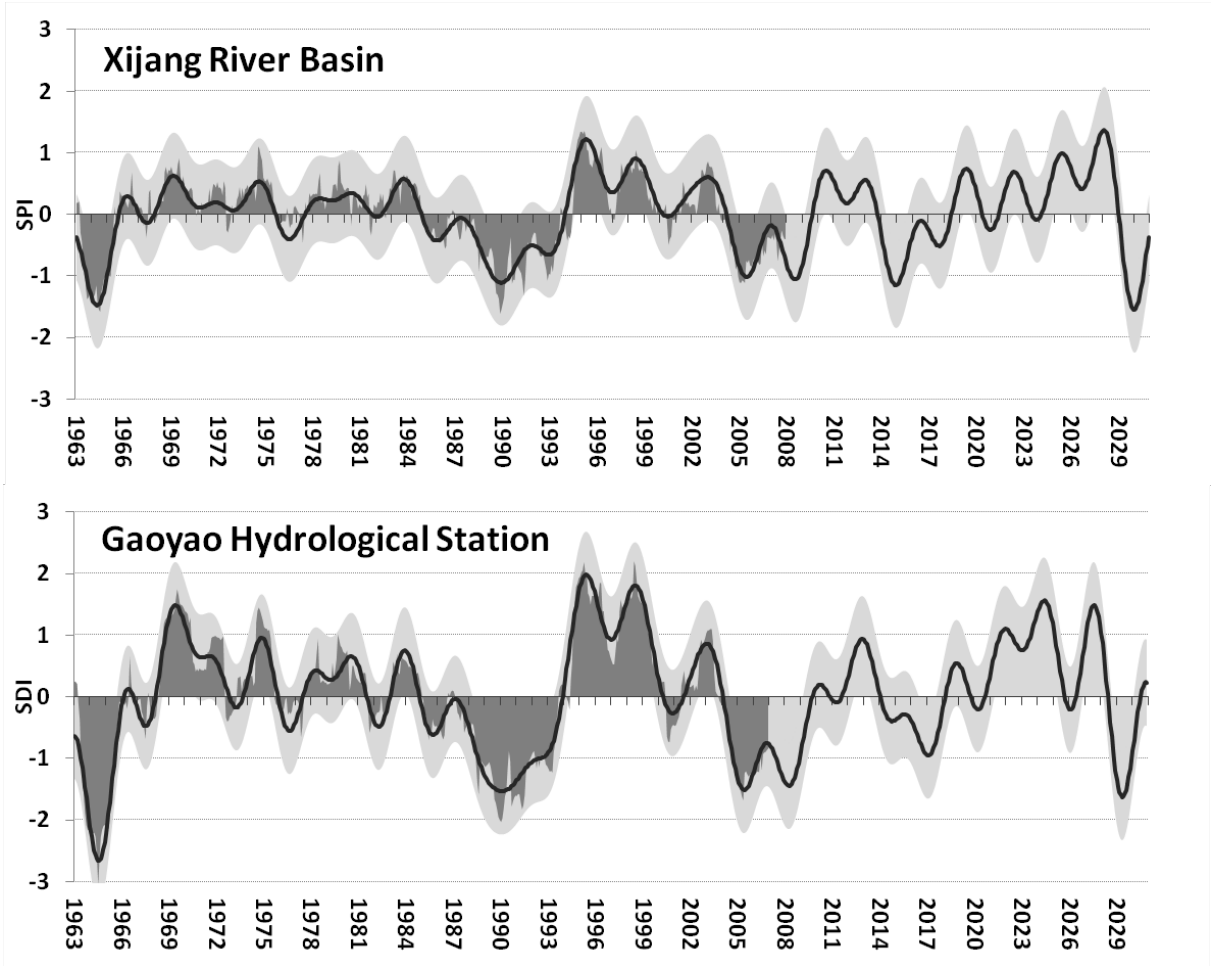

Fig. 13: Observed (dark gray shadings) and reconstructed time series (black line; confidence interval = light gray shading) plus extrapolation (starting in 2007) of the SPI-24 (upper panel) and SDI-24 (lower panel) 1963-2030

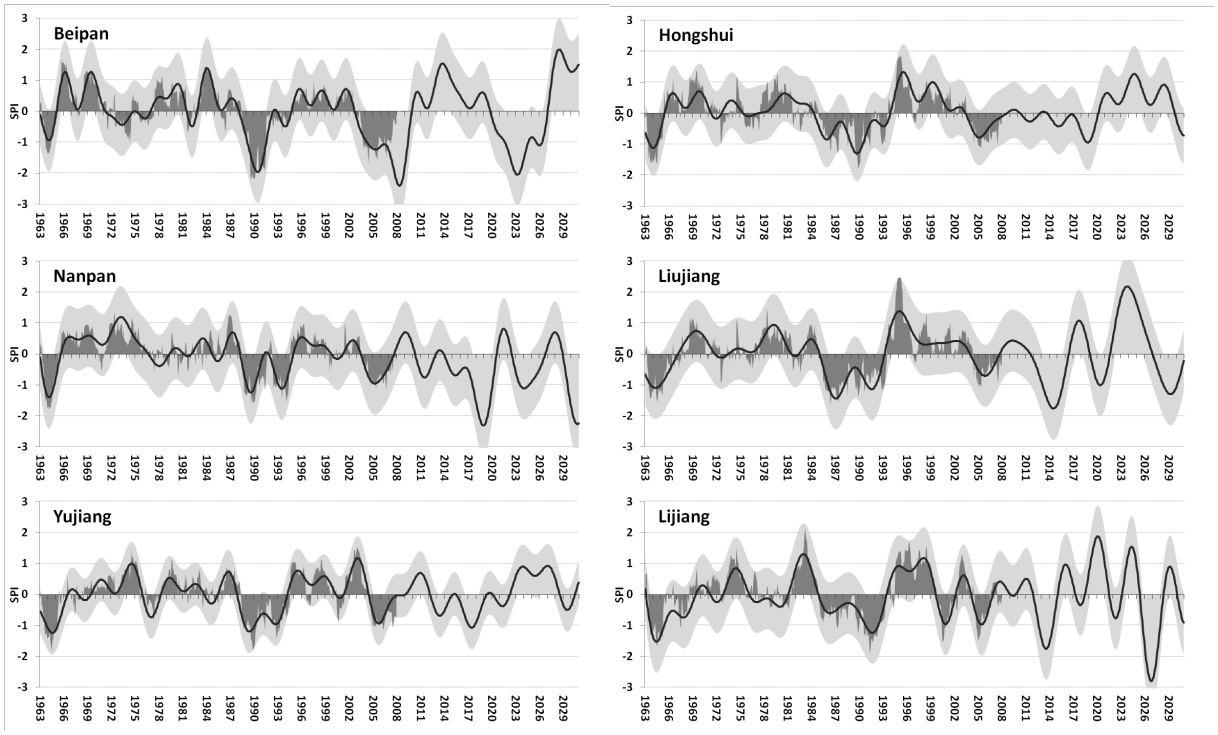

Fig. 14: Observed (dark gray shadings) and reconstructed time series (black line; confidence interval = light gray shading) plus extrapolation (starting in 2007) of the SPI-24 of the six sub-basins in the Xijiang River Basin 1963-2030

Appendix VI

Fischer, T., C. Menz, B. Su, and T. Scholten, (2012): Simulated and projected climate extremes in the Zhujiang River Basin, South China, using the regional climate model COSMO-CLM. Accepted for publication in *International Journal of Climatology*.

Simulated and projected climate extremes in the Zhujiang River Basin, South China, using the regional climate model COSMO-CLM

Thomas FISCHER[1,2], Christoph MENZ[3], Buda SU[1,4], and Thomas SCHOLTEN[2]

[1] National Climate Center of the China Meteorological Administration, Beijing, China

[2] Department of Geosciences, University of Tübingen, Germany

[3] Potsdam Institute for Climate Impact Research, Germany

[4] Nanjing University of Information Science and Technology, China

Corresponding authors:

Thomas Fischer, Buda Su

Email: tom.fischer8@gmx.de, subd@cma.gov.cn

China Meteorological Administration (CMA), National Climate Centre (NCC)

46, Zhongguancun Nandajie, Haidian, Beijing 100 081, PR China

Office: 0086 10 5899 9096, Fax: 0086-10-6217 6804

Abstract

This paper presents a detailed analysis of simulated and projected climate extremes in the Zhujiang River Basin. Daily output from the regional climate model COSMO-CLM (CCLM), driven by ECHAM5, is used. The hindcast simulation covers the period from 1961 to 2000 while the projection concentrates on the near future period from 2011 to 2050. Spatio-temporal statistical characteristics are investigated for three temperature and three precipitation indicators. The six simulated annual and monthly indicators are statistically

compared with synoptic observations. The investigation is based on daily values of 195 grid-points and 192 meteorological stations.

The findings are presented and interpreted in terms of the model's capability. Compared to observations, slightly higher amounts in temperature indicators lower amounts in precipitation indicators are simulated. With the resulting good similarities in the spatial variation and trends we conclude that CCLM is able to satisfyingly reproduce climate extreme for the simulated period. Therefore, our analyses show that CCLM can be used to project climate extremes in the Zhujiang River Basin for the period from 2011 to 2050. The projected changes indicate warmer and wetter conditions in the northern and southern regions, especially in winter and spring. This includes more intense rainfall events, which might potentially increase the risk of flooding in the central parts of the ZRB in these seasons. Warmer and dryer conditions can be expected in the western and eastern regions, especially in summer and fall. These lower precipitation amounts but warmer temperatures will probably increase the evapotranspiration, which potentially leads to a higher risk of drought. Regarding these findings in climate extremes, adverse consequences in various sectors, such as agriculture, water, and energy should be anticipated.

Keywords: climate extremes, simulation, projection, validation, CCLM, Zhujiang, China

1. Introduction

Climatic changes have huge potential impacts on the socio-economic welfare and peoples living conditions. Especially changes in the frequency and magnitude of extreme weather events are an important driver for economic and society changes. Changes in precipitation pattern can lead to both higher drought and higher flood risk, which are potentially linked to high socio economic costs. In recent years, climate change and its implications were investigated in numerous studies (Adger et al., 2007; Huntingford et al., 2003; Klein Tank et al., 2009).

In China, the fast growing population and industrialization has increased the potential for economic damages from severe events due to climate change (Feng et al., 2007). According to the Fourth Assessment Report of the Intergovernmental Panel on Climate Change (IPCC AR4) and China's National Assessment Report on Climate Change increases in annual temperature, total precipitation, and heavy precipitation events have been observed

in China and are very likely to increase in the future (Ding et al., 2007; Fischer et al., 2011a,b; Gemmer et al., 2011; Jiang et al., 2011; Liu et al., 2009; Qian and Lin, 2005; Trenberth et al., 2007; Xu et al., 2011).

Future climate projections give important estimations on potential changes in magnitudes and frequencies of extreme events (from now on defined as climate extremes) and their related hazardous consequences. The analysis of changes in climate conditions (e.g. variability and extremes) at different spatial and temporal scales is of great benefit to national and regional adaptation strategies. Global circulation models (GCM's) are known to be in good agreement with observed magnitudes and tendencies of temperature while it is believed that the coarse resolution results in poor agreement especially with the precipitation patterns (Kharin et al., 2007). High resolution regional climate models (RCM's) represent a huge improvement in modeling of precipitation (Meehl et al., 2000; Pal et al., 2007; Kunkel et al., 2010; Rockel and Geyer, 2008). A number of studies utilize RCM's to investigate climate change impacts at high resolution for European, American, and Asian regions (Alexander and Arblaster, 2009; Trenberth et al., 2007; Sillmann and Roeckner, 2008).

Changes in the intensity and frequency of climate extremes are of major concern for socio-economic welfare. Hence, it is of high importance for regional institutions of various sectors (e.g. water, industry, and agriculture) to be aware of current and future climate extremes related risks within their area. The water sector bears climate change related risks such as floods and droughts and the river basin scale emphasizes the logical spatial extent for a study region. Focusing on climate characteristics and extremes in China, RCM's were mostly applied to analyze future changes in climate conditions on a larger scale (Chen et al. 2011; Ding et al., 2006; Gao et al., 2008; Wang et al., 2003; Xu et al., 2009). To our knowledge there is no study published dealing with the ability of RCM's to simulate climate extremes in the Zhujiang River Basin comprehensively.

The Zhujiang River Basin (ZRB) in South China covers an area of approximately 450,000 km2 with a population of more than 166 million. The region is currently one of the most economically prosperous areas of China, with very high development rates, and one of China's highest GDP per capita of more than 40,000 CNY per year (National Bureau of Statistics of China: www.stats.gov.cn). As large numbers of the population and economic facilities are exposed to certain climate risks (Fischer et al., 2011a,b; Gemmer et al., 2011) and hence highly vulnerable, knowledge on and adaptation to potential climate extremes are

needed to lower the vulnerability. It is presumed that simulations and projections with the COSMO-CLM (CCLM) will potentially alter the knowledge on climate conditions and extremes.

Therefore, the objective of this paper is to evaluate and analyze the simulated and projected climate parameters of the CCLM for the Zhujiang River Basin. We will calculate various error estimations, trends and frequencies of observed and simulated climate indicators and will analyze the projected indicators for the period 2011 to 2050. Based on the results, current climate characteristics can be substantiated and the performance of projections with CCLM can be specified.

In section 2, we describe the applied data and methodologies. Thereafter, we show the results of the validation of CCLM in section 3, and perform an analysis of the projections in section 4. In the final section 5, we discuss and conclude all findings.

2. Data and Methodology

2.1 Observational Data

Daily temperature and precipitation records of 192 meteorological stations in the ZRB (Figure 1) for the period 1961-2007 are provided by the National Meteorological Information Center (NMIC) of the China Meteorological Administration (CMA). Most of the stations are located in hilly low lying areas at an average altitude of under 700m, except in the mountainous western part of the basin. The data sets passed the internal temporal homogeneity check of the China National Meteorological Center (CNMC), which controlled the quality by using the departure accumulating method (Buishand, 1982) and the Pettit's test (Schönwiese, 2006). Gaps in precipitation data account for less than 0.005%, and were reconstructed by the median precipitation from at least three neighboring stations.

2.2 COSMO-CLM

The regional climate model CCLM is based on the weather prediction model LM (Steppeler et al., 2003), and adapted and improved for climate projections (Böhm et al., 2006). It is a dynamical RCM based on thermo-hydro-dynamical equations to describe atmospheric flows with a resolution of 1 to 50 kilometers. Currently CCLM is used in various

studies (Nikulin et al., 2011; Hollweg et al., 2008; Rockel et al., 2008; Rockel and Geyer, 2008; Bachner et al., 2008; Ebell et al., 2008). CCLM uses a nesting technique to downscale a coarse resolution dataset/model (usually a GCM or reanalysis). It uses a rotated geographical grid with a terrain following an altitudinal coordinate system.

The calculation of CCLM is carried out on a 0.44° by 0.44° rotated grid covering the CORDEX-East-Asia domain (http://wcrp.ipsl.jussieu.fr/SF_RCD_CORDEX.html) with 32 atmosphere levels in vertical direction and 9 soil layers. The parameterization of CCLM was optimized with a hindcast simulation of the years 1960 to 2000 driven by ERA40 reanalysis (Uppala et al., 2005). In the following the optimized parameter setup is used for a GCM ECHAM5 driven run covering the same period. Here we used the historical 20th century reconstruction run of the ECHAM5, realization 1, with greenhouse gas concentrations based on observed values. The projection concentrates on the period 2011 to 2050 with the SRES A1B emission scenario which assumes a rapid economic growth and a quick spread of new and efficient technologies with a balanced emphasis on all energy sources (IPCC SRES, 2000). The driving model for the projection was ECHAM5 respectively (ECHAM5_A1B run 1). A full validation of the used CCLM run including future projections for larger regions is in progress and will be published soon. For analytical purposes, CCLM is interpolated to a 0.5° by 0.5° regular geographical grid resulting in 195 grid-points within the Zhujiang River Basin. For comparison purposes, daily data is also used from the ECHAM5_A1B run for 24 grid-points based on the T63 Gaussian grid (approx. 2.8° by 2.8°).

2.3 Indicators

Six indicators are calculated from observed, simulated and projected daily data in order to analyze and describe annual and monthly climate characteristics with particular focus on climate extremes. These are the annual and monthly averaged daily mean temperature (TMEAN), the annual and monthly maximum and minimum daily mean temperature (TMAX and TMIN). The annual and monthly total precipitation sum of wet days (>=1mm/d, PRCPTOT), the maximum annual and monthly total precipitation sum of five consecutive days (RX5DAY) and the annual and monthly sum of dry days, i.e. days with precipitation below 1mm (DRY DAYS).

TMEAN and PRCPTOT were chosen as they represent the two most recognized climate characteristics. TMAX and TMIN are single-day events and are depicted as the most extreme

temperature events (Hottest or Coldest Day) of each year or month. RX5DAY and DRY DAYS represent heavy precipitation or drying events which potentially lead to flood or drought events. The indicators were defined on fixed terms (Table 1) predetermined by the China Meteorological Administration and as recommended by the CCl/CLIVAR Expert Team for Climate Change Detection Monitoring and Indices (ETCCDMI) (Alexander and Arblaster, 2009; Fischer et al., 2011a,b; Klein Tank et al., 2009; Su et al., 2008).

The comparison of the simulated and observed indicators is conducted at two spatial scales. On one hand, we investigate the spatial relation and value for each grid point and meteorological stations within the entire basin. On the other hand, we focus on the region-averaged indicators of four specified regions. Thus, the regionalized indicators are the average of the annual and monthly indicators at all grid points or stations within these regions. The regions are subjectively chosen based on results in past research (Gemmer et al., 2011, Fischer et al., 2011a,b). Each region covers 45-50 stations, i.e. approx. 25% of the available stations. According to their location (Figure 1), the four regions are named Region West (W), North (N), South (S), and East (E).

2.4 Methods

BIAS and RMSE

The difference between observed and simulated indicators for both scales are estimated and analyzed with different methods. To characterize the average difference between the two datasets at a grid point or region, the BIAS or mean error is estimated, which is defined as the positive or negative amount between the observed (o) and simulated (c) mean of the indicators (for 40 years: n = 40). Similar to the BIAS, the root mean squared error (RMSE) is estimated for each point and region to make additional statements about the magnitude of the inter-annual differences as it combines positive and negative discrepancies of the annual amounts. The BIAS is also used to identify the averaged monthly differences of each indicator in the entire basin and partially in the four regions. The equations for BIAS and RMSE are given here:

$$BIAS = \frac{1}{n}\sum_{i=1}^{n}(c_i - o_i) = \bar{c} - \bar{o} \qquad RMSE = \sqrt{\frac{1}{n}\sum_{i=1}^{n}(c_i - o_i)^2}$$

For identifying similarities in the probability distribution of each annual indicator we visualize the sorted simulated annual data points to the observed for the entire ZRB (Alexander and Arblaster, 2009; Schönwiese, 2006).

Spatial correlation and spatial variance

To quantify the differences in the spatial distribution of the observed and simulated indicators for the ZRB, the Pearson product moment correlation coefficient (PCOR) is calculated. This is done by interpolating the unequal distributed station observations as well as the simulation results to a regular geographical grid with 0.5° x 0.5° resolution. The PCOR is here defined as the covariance of observed (o) and simulated (c) means of each grid point divided by the product of their standard deviations (σ) (Sheskin, 2004; Wilks, 2006). The equation for PCOR is as follows:

$$PCOR = \frac{cov\ (\bar{o}|\bar{c})}{\sigma_o\ \sigma_c}$$

The closer the results are to 1.0 the stronger is the spatial correlation of the observed and simulated indicator means. A PCOR above 0.5 is commonly referred to as strong correlation. Here we point out, that the dissimilarities in resolution of the three studied data may cause systematic differences in the spatial correlation coefficients (Corder and Foreman, 2009).

To describe the basin-wide spatial variance in the simulated and observed indicators, the principal component analysis (PCA) is applied to the annual indicators. The spatial variance gives deeper insight in the similarities or dissimilarities of the respective time-series' (Bordi et al., 2004; Leung and Wu, 2005). A set of linearly independent spatial patterns (loadings) are generated, which describe the correlations with the specific principal components (PC). We concentrate here on the first four principle components (PC1 to PC4), as it is assumed that these explain most of the variation from the mean, i.e. the spatial variance (Bordi et al., 2004; Leung and Wu, 2005; Schönwiese, 2006; Wilks, 2006). The assumption is subject to be proven by the results in the validation section. The higher the percentage of explained variance the stronger the station-/grid-based time-series are correlated to the mean. The differences in spatial variance of simulated and observed indicators are estimated according to the findings in the PCA and the visual pattern of PC1.

Trend estimation

The linear regression, based on ordinary least squares, was calculated to determine the absolute decadal trend (unit/10a) of increase/decrease at each point and region. The Mann-Kendall trend test is further applied to each point and region average for the time period 1961-2000 and 2011-2050, respectively, to determine the significance of estimated trends. A comprehensive description on the application and definition of the Mann-Kendall trend test can be found in e.g. Gemmer et al. (2004), Liu et al. (2008), and Yang et al. (2010). The threshold for positive or negative trends (Kendall's Tau) is based on the 0.05 significance level.

3. Validation of CCLM

In the following section we will calculate and analyze the above described statistical values for observed and simulated time-series. The comparison considers the time period from 1961 to 2000. This is done to evaluate the capability of CCLM to simulate the climate indicators for the Zhujiang River Basin representatively. CCLM was driven by the 20th century historical reconstruction run of ECHAM5 based on observed carbon dioxide emissions. After evaluating the hindcast simulation, we will subsequently analyze the projected climate indicators for the time period 2011-2050.

Annual area-averaged BIAS and RMSE

In Figure 2, the spatial distribution of the average TMEAN, TMAX and TMIN (1961-2000) of the observations and the simulations with CCLM and ECHAM5 are presented. In all maps an even distribution with a Northwest-Southeast disparity in the temperature indicators can be distinguished. The distribution patterns of the CCLM simulations are visually more similar with the observations than the ECHAM5 simulations. This is most likely associated with the higher resolution of CCLM resulting in a more accurate representation of the orography, as there is also a Northwest-Southeast gradient in the elevation. The simulated temperatures of CCLM tend to be higher than the observed ones, especially in the south-eastern parts of the basin, where the BIAS is up to 2.7°C.

In Figure 3 the spatial distribution of the averaged means (1961-2000) of PRCPTOT, RX5DAY and DRY DAYS of the observations and the simulations with CCLM and ECHAM5 are presented. The precipitation indicators exhibit more unevenly regionalized differences. Comparing the CCLM simulations with the observations, PRCPTOT shows relatively high positive biases for the central-northern area and the delta region of the Zhujiang River, while an underestimation is found for the central-south area. Especially high positive biases are simulated for RX5DAY in the delta region, while strong negative biases are apparent in the western and central areas. For DRY DAYS very high positive differences are simulated in Region South, but moderate to high negative biases in the other three regions. The simulated spatial distribution of RX5DAY and PRCPTOT of CCLM, especially the difference between the mountainous western and the low lying south-eastern parts, is similar to the observations. However the spatial distribution patterns of DRY DAYS differ significantly. This implies that on one hand CCLM is able to capture the spatial structure, the magnitude of maximum 5-day rainfall events, and also the regional distribution of the total annual distribution, but on the other hand is not able to reproduce the correct number of dry days significantly. Nevertheless, the distribution patterns of the CCLM simulations are visually much more similar with the observations than the ECHAM5 simulations. ECHAM5 simulates PRCPTOT and RX5DAY with much lower and more evenly distributed amounts than CCLM, and also with less DRY DAYS than the observations, which is probably due to the much lower resolution of ECHAM5. Hence, CCLM produces more reliable regional distribution pattern and probabilities in precipitation indicators.

The average annual BIAS and RMSE of the CCLM and ECHAM5 simulations of the three temperature and three precipitation indicators are listed in Table 2 and Table 3. For CCLM, we find a warm BIAS for TMEAN and TMAX in each region, while for TMIN only in Region South a warm BIAS is found, while a cold BIAS is found in Region West and North. The resulting basin-wide BIAS shows a general over-/underestimation of temperature extremes (TMAX too high, TMIN too low), potentially resulting from an overestimation of the diurnal temperature range in CCLM. Looking at the RMSE in the temperature indicators of CCLM the differences in the BIAS can be supported, as the values in RMSE are relatively close to the absolute values in BIAS. The largest RMSE in the temperature indicators are generally found in Region North and East. Compared to the BIAS and RMSE of CCLM, ECHAM5 simulates TMAX closer to the observations at basin and regional scale, except for Region West (Table 3).

The BIAS in PRCPTOT and DRY DAYS of CCLM are negative in all Regions and the ZRB, with the exception of small positive amounts for Region North and Region South, respectively. This means that less total precipitation and fewer dry days are generally simulated by CCLM. In contrary, the basin-averaged BIAS of RX5DAY is positive, with only Region West exhibiting lower maximum 5-day rainfall amounts. The RMSE of the precipitation indicators are very high in Region South and Region East. Most obviously for CCLM are the strong BIAS and RMSE in all three precipitation indicators for Region South (Table 2) which is in accordance to Figure 3. At basin scale, PRCPTOT and DRY DAYS simulated with CCLM are mainly underestimated, while RX5DAY is overestimated. This implies that CCLM generates fewer rain days which are more intense, especially in Region South. The precipitation related indicators show high absolute values for ECHAM5 (Table 3). Large amounts in BIAS and RMSE indicate strong differences between the probability distribution of observed and simulated time-series. This is underlined with the visualization of basin-averaged and sorted observed and simulated annual indicators in scatter plots (Figure 4). Here, we can see very similar distributions of the simulated temperature indicators, except for TMAX, where ECHAM5 is closer to the observed distribution. The distributions of the CCLM-simulated precipitation indicators are even more similar to the observation, whereas the distributions of ECHAM5 are lower. This means that the distribution of annual values simulated with CCLM are closer to the observations than simulated with ECHAM5, except for TMAX. An interesting visualized feature is the sharper angle of the simulated distributions (compared to the diagonal), which indicates a higher variability in annual values.

Monthly distribution

The monthly distributions of observed and simulated area-averaged PRCPTOT and TMEAN for the ZRB are shown in Figure 5. Additionally, the differences between CCLM simulations and observations, i.e. monthly mean differences, for the four regions are displayed in Figure 6. For the entire basin, the simulated PRCPTOT and TMEAN follow relatively well the course of the year. Monthly PRCPTOT is mostly underestimated, which can be found for all regions, except Region West from February to May and Region South from October to December. TMEAN shows a slight underestimation from April to July but a strong overestimation (by more than two degrees) from September to November. CCLM can

simulate monthly PRCPTOT and TMEAN more realistic than ECHAM5, which shows strong deficiencies in spring.

The basin-averaged observed and simulated monthly extreme indicators (RX5DAY and TMAX, DRY DAYS and TMIN) show a similar course of the year and monthly differences as in PRCPTOT and TMEAN for the ZRB (Figure 7). Higher amounts in RX5DAY and DRY DAYS are simulated with CCLM for February to April but lower maximum 5-day rainfall amounts and fewer dry days are simulated for the summer months. Simulated with CCLM, TMAX exhibits stronger differences as TMEAN year-round, with a high overestimation of the summer and fall months, while TMIN shows a distinct underestimation during summer. These differences imply that CCLM generates a larger diurnal temperature range, especially in summer. Compared to ECHAM5, CCLM is closer to the observations considering the inner-annual variability of the precipitation extremes. Here it is remarkable, that CCLM underestimates RX5DAY most of the year, while it simulates a positive BIAS for the whole year. This might be explained by the incorrect simulation of a higher variability in monthly RX5DAY and the averaging of annual RX5DAY for the entire ZRB. Nevertheless, both models seem to be able to capture the monthly precipitation variability of the East Asian Monsoon. Conclusively, CCLM shows a more realistic annual course than ECHAM5, with an underestimation of the precipitation indicators and TMIN and an overestimation of TMAX all during summer. The performance of CCLM can be explained by the higher resolution capturing the regional precipitation pattern better than ECHAM5.

Spatial correlation and spatial variance

Based on the average annual means of observed and simulated grid-points, PCOR of each indicator is estimated for the entire basin. The spatial correlation coefficients for the CCLM-simulated PRCPTOT, RX5DAY, and DRY DAYS are moderately high at 0.45, 0.63, and 0.59, respectively. All CCLM-simulated temperature indicators show high positive spatial correlation coefficients with TMEAN at 0.87, TMAX at 0.65, and TMIN at 0.88. Compared with the CCLM results, ECHAM5-simulated indicators show similar spatial correlation coefficients with the observed indicators, except for DRY DAYS (Figure 3) even though the region-wide BIAS differs broadly. This similarity might be related to the fact that CCLM is dynamically downscaled from ECHAM5. However, the CCLM-simulated indicators correspond temporally and spatially well with the observations.

The first principal component (PC1) of the observed TMEAN describes 70.3% of the spatial variation in the station data (Figure 8a), while the PC1 of the CCLM-simulated TMEAN describes 85.2% of the spatial variation in the gridded data (Figure 8b). For PRCPTOT, the observed PC1 describes 33.2% and the CCLM-simulated PC1 describes 45.1% of the spatial variation (Figure 8c,d). It can be seen that the loading patterns of PC1 for observed and CCLM-simulated TMEAN and PRCPTOT show similar spatial patterns (Figure 8a-d), while more uniform patterns are apparent for the CCLM-simulated loadings. The first four components (PC1-4) describe 87.3% and 97.5% of the spatial variation of the observed and CCLM-simulated TMEAN, respectively. The spatial variation of the observed and CCLM-simulated PRCPTOT can be described by 57.1% and 75.7% with the PC1-4 , respectively. The higher percentages in spatial variation of CCLM imply a lower variability within the simulated time-series. Based on this, the CCLM-simulated spatial variation of PRCPTOT and TMEAN of all 195 grid-points are less diverse than the observed spatial variation of all 192 stations within the ZRB. Taking the similar spatial distribution into account, we conclude that the spatial variation in TMEAN and PRCPTOT are relatively well represented by CCLM.

Trend estimation

According to the Mann-Kendall test, only a small number of time-series show significant trends. The station observations show only a significant increase in TMEAN by 0.14 K per decade in Region East and by 0.12 K per decade in Region South (Table 4). In CCLM-simulated TMAX, a significant decrease is found for Region East, while in ECHAM5-simulated time-series an increase in TMEAN and a decrease in PRCPTOT, RX5DAY, and DRY DAYS, are calculated for Region West. Based on linear regression, the decadal trends and tendencies are presented in Table 4. Both simulations could not simulate the observed significant increases in regional TMEAN. CCLM and ECHAM5 simulate similar trends in TMEAN, but different values in the trends of temperature extremes (TMIN and TMAX). Nevertheless, in regard to the insignificant regression slopes and compared to the observation, CCLM produces more reliable trends than ECHAM5.

Compared to the global circulation model ECHAM5, the regional climate model CCLM seems to capture the annual and monthly means, the annual course of the year, the spatial

distribution patterns and variation, and the trends closer to the observations of all indicators. Both models' capabilities for the temperature indicators are generally higher than that for the precipitation indicators. CCLM is able to satisfyingly reproduce the temperature and precipitation indicators in regional and monthly means, spatial distribution and variation, and temporal trends. Hence, we conclude that CCLM can be used to project spatial distribution patterns, annual and monthly means, and temporal trends of temperature and precipitation indicators in the Zhujiang River Basin, for the future period of 2011 to 2050.

4. Projection of Climate Extremes with CCLM (2011-2050)

In this section, we use CCLM to project the climate for the period 2011-2050 with specific focus on the climate extreme indices based on the emission scenario SRES A1B. We will analyze the differences between the climate reconstruction (1961-2000) and the future projection (2011-2050) to assess possible future changes resulting from a higher atmospheric CO2 concentration modeled by CCLM. According to our projections, conclusions to future changes in climate extremes will be elaborated.

Spatial and temporal differences

In Figure 9, the spatial distributions of the projected differences (2011-2050 relative to 1961-2000) in means of the temperature and precipitation indicators are presented. All projected temperature indicators show an increase in the entire basin, with moderate differences in the South and East and larger differences in Regions West and North (Figure 9a-c). Following this Southeast-Northwest disparity TMEAN exhibits even region-averaged differences from 1.0°C to 1.2°C. TMAX has the strongest increases by 1.2°C to 1.8°C, while TMIN shows a similar distribution but with lower positive differences by 0.8°C to 1.4°C leading to a higher diurnal temperature range.

The projected PRCPTOT and RX5DAY show mostly strong positive differences in Region North and South (Figure 9d-e). Here, the differences are 95mm to 97mm in PRCPTOT and 14mm to 40mm in RX5DAY. Slightly negative differences can be seen in the West and coastal East. Nevertheless, differences range from 16mm to 80mm in PRCPTOT, and from -

1mm to 10mm in RX5DAY from West to East, respectively. Regionally opposing to PRCPTOT and RX5DAY, the projected DRY DAYS show also mostly positive differences (Figure 9f). Here, positive differences to more dry days in the West and East range from 0.6days to 1.1days, while it ranges from 0.2days to 0.7days in the North and South. Hence the projection shows an increase in total rainfall and intensity but a decrease in number of wet days, i.e. an increase in dry days.

Accordingly we can conclude that an average increase is projected for the 50-year interval of the period 2011-2050 relative to 1961-2000 for all indicators: TMEAN (by 1.1°C), TMAX (by 1.6°C), TMIN (by 1.1°C), PRCPTOT (by 73mm), RX5DAY (by 15mm), and DRY DAYS (by 0.7days).

Changes in monthly distribution

In Figure 10, the projected monthly differences (2011-2050 relative to 1961-2000) in means of the temperature and precipitation indicators are presented. All projected temperature indicators show an increase in all months, with higher values in summer, fall and winter (Figure 10a). CCLM projects the highest change in TMIN for winter and in TMAX for summer, leading to much warmer winter and summer. PRCPTOT and RX5DAY show the main positive differences from January to May, while DRY DAYS show negative differences in this time-frame (Figure 10b). The increases in precipitation in the first half of the year are followed by a sudden change in June. No significant changes are observable for the second half of the year.

Relative to 1961-2000, the projection shows warmer and wetter conditions for the first half of the year, but with stronger warming in summer and fall. The lower temperature trends in spring might be associated with the changes in precipitation.

Trend estimation

For the period 2011-2050, significant increasing trends are detected in CCLM-projected TMEAN, TMAX and TMIN for all four regions, while none are apparent for the precipitation indicators (Table 5). The significant trends range from 0.35K to 0.48K per decade in regional TMEAN, from 0.62K to 0.78K per decade in TMAX, and from 0.23K to 0.52K per decade in TMIN. Compared to almost no significant trends in the hindcast

simulation, this is a remarkable feature in all temperature indicators implying a strong projected warming (Figure 11). Such significant trends are not projected for precipitation indicators, i.e. no clear statements on projected trends to more wet or dry conditions can be given (Figure 11).

5. Conclusions and Discussion

In the present study, we validate the regional climate model CCLM on its performance to simulate observed climate characteristics and extremes in the Zhujiang River Basin. This is done to substantiate the provided analysis of future changes in climate extremes projected with CCLM.

Validation of CCLM

In the first part of this study, various error estimations and differences in distributions, variability and trends in indicators of climate extremes from observations and simulations for a 40-year period (1961-2000) were presented. The results show that CCLM has certain abilities to simulate the basic characteristics of climate extremes, in both the spatial and temporal distribution, compared to the observations. The distribution patterns of the CCLM simulations are visually much more similar with the observations than the ECHAM5 simulations. CCLM seems to reduce the even distributed climate patterns of the coarse driving model to more detailed regional patterns, due to the higher resolution. However, the simulated temperatures of CCLM tend to be higher than the observed temperatures. Most obviously for CCLM are the strong BIAS and RMSE in all three precipitation indicators for Region South. Nevertheless, CCLM can simulate monthly PRCPTOT and TMEAN more realistic than ECHAM5, which shows high deficiencies in spring. CCLM shows also a better simulation of the seasonal cycle, especially in regard to the precipitation extremes. The CCLM-simulated annual indicators correspond temporally and spatially well with the observations. CCLM simulates PRCPTOT and TMEAN with lower temporal variability but a similar spatial variation. In its spatial distribution patterns the observed variability in TMEAN and PRCPTOT is well represented by CCLM.

The large BIAS of ECHAM5 in various indices might be partly responsible for the BIAS of CCLM, since the simulations were driven by ECHAM5, which implies that CCLM is not able to correct the anomalous input sufficiently (Wang et al., 2003; Roeckner et al., 2003; Hagemann et al., 2005; Ebell et al., 2008). Further reasons for the overestimation in the means of temperature indicators and underestimation of the precipitation indicators might be the averaging into four regions, as much more local disparities and high variability are found. The fact that all observations are point-based but the simulated grid-points encompass a 0.5° x 0.5° regular grid, which was interpolated from a 0.44 x 0.44 rotated grid, might also play an important role in the differences to the observations (Rockel and Geyer, 2008; Bachner et al., 2008). The differences in their variability and trends can also be explained by the fact that CCLM is driven by a GCM (ECHAM5) rather than reanalysis (e.g. ERA40) or station-based observations. As the Zhujiang River Basin is strongly influenced by the East Asian Monsoon (Wang and Ding, 1997; Yu et al., 2009; Gemmer et al., 2011; Fischer et al., 2011), additionally to the above mentioned reasons, the more distinct underestimation of precipitation indicators in summer and fall might be also related to an underrepresentation of the East Asian Summer Monsoon in the parameterization of the CCLM (and ECHAM5).

But considering these differences, we conclude that CCLM can be used to project spatial distribution patterns, monthly means, and temporal trends of temperature and precipitation indicators in the Zhujiang River Basin, for the period from 2011 to 2050.

Projection of Climate Extremes with CCLM

The projected temperature and precipitation indicators in the Zhujiang River Basin are analyzed for the period from 2011 to 2050 relative to the period from 1961 to 2000. Higher values of all temperature indicators are projected for the entire ZRB, with stronger increases in the west and moderate increases in the eastern part of the basin. Especially the Region North and South will experience higher total precipitation, higher RX5DAY amounts, and slightly less DRY DAYS. The western part and the far eastern corner of the basin are expected to become dryer. Concerning the seasonal cycle, there is a moderate increase of temperature in spring followed by an enhanced increase in summer and fall. Additionally, a tendency to increasing and more intense precipitation is projected. In accordance with the projected changes in means, spatial distribution, and monthly distribution relative to 1961-

2000, we can expect warmer and wetter conditions in Region North and South, especially in winter and spring. This includes more intense rainfall events, which might potentially increase the risk of flooding in the central parts of the ZRB during winter and spring. Warmer and dryer conditions can be expected in Region West and East, especially in summer and fall. The lower precipitation amounts but warmer temperatures will probably increase the evapotranspiration, which potentially leads to a higher risk of drought in these regions.

Our results are barely supported by other articles. Based on downscaled ECHAM5 outputs for the Pearl River basin, the findings of Liu et al. (2009) are similar to our findings in TMEAN and PRCPTOT, but at less detailed regional and temporal resolution. The findings in projected precipitation extremes by Xu et al. (2011) show opposed trends, i.e. increasing trends in annual consecutive dry days and decreasing trends in annual RX5, for the south china basin (comprising the Zhujiang and the Yangtze River basins). These trends have been calculated from three different GCM outputs (CSIRO_MK3_5, MPI_ECHAM5 and NCAR_CCSM3). However, this study covers a larger area with lower resolution, while in our study various more reliable significant trends are found for much smaller regions. According to our evaluation our model seems to simulate the climate extremes reasonably compared to the observations. It should be noted that we use only one RCM driven by one GCM under one emission scenario (SRES A1B), which does not allow exploring uncertainties in future projections of climate extremes satisfyingly (Chen et al., 2011). To assess the uncertainties of future projections of climate extremes in the Zhujiang River Basin, different types of dynamical and statistical downscaling models and driving GCM's under multiple emission scenarios need to be investigated.

Regarding the findings in climate extremes, adverse consequences in various sectors, such as agriculture, water, and energy, should be anticipated. The projected more intense maximum 5-day rainfall events can lead to e.g. higher surface runoff (and eventually flooding), increased soil erosion, and diminished water quality. In contrary the projected increase in dry days might lead to e.g. water scarcity (i.e. drought), soil degradation (i.e. desertification), and lowering of the groundwater table. An increase in dry days can also lead to soil desiccation and soil sealing, which in turn increases the potential of flooding. Hence, an increase in dry days and in maximum 5-day rainfall might be regarded as a positive feedback towards more and stronger drought and flood events. All such impacts might e.g. directly or indirectly affect the plant growth of the agricultural production with high losses

in yield, which will have adverse consequences on the food security of the entire region. The strong increases in temperature extremes in the entire basin might affect most sectors, as e.g. the energy demand or plant growth pattern will change the current economic and agricultural systems. High temperatures in summer will quite severely affect the population and economic sectors, as heat-induced health issues and higher cooling demand of public, private, and industrial sectors will appear. Nevertheless, higher temperatures in winter might e.g. effectively extend the plant growth period (i.e. longer annual agricultural production) and lessens the heating demand (i.e. less energy consumption). Hard and soft measures to adapt to these and other consequences have to be identified and implemented based on specifically issued policies and regulations e.g. integrated in water resource management plans and activities.

Acknowledgments

This study was supported by the National Basic Research Program of China (973 Program) (No. 2010CB428401 and 2012CB955903), the Special Fund of Climate Change of the China Meteorological Administration (CCSF 2011-11), the National Natural Science Foundation of China (40910177), and the Sino-German Centre for Research Promotion, NSFC/DFG (GZ601). We are grateful to the ECMWF for providing the ERA-40 data. The position of Thomas Fischer at the National Climate Center is supported by the German Development Cooperation through the Center for international Migration and Development (www.cimonline.de).

References

Adger, W.N., S. Agrawala, M.M.Q. Mirza, C. Conde, K. O'Brien, J. Pulhin, R. Pulwarty, B. Smit and K. Takahashi, 2007: Assessment of adaptation practices, options, constraints and capacity. Climate Change 2007: Impacts, Adaptation and Vulnerability. Contribution of Working Group II to the Fourth Assessment Report of the Intergovernmental Panel on Climate Change, M.L. Parry, O.F. Canziani, J.P. Palutikof, P.J. van der Linden and C.E. Hanson, Eds., Cambridge University Press, Cambridge, UK, 717-743.

Alexander, L.V. and J.M. Arblaster, 2009: Assessing trends in observed and modelled climate extremes over Australia in relation to future projections. Int. J. Climatology, 29, 417–435.

Bachner S., A. Kapala, and C. Simmer, 2008: Evaluation of daily precipitation characteristics in the CLM and their sensitivity to parameterizations. Meteorologische Zeitschrift, Vol. 17, No. 4, 407-419.

Böhm, U., M. Kücken, W. Ahrens, A. Block, D. Hauffe, K. Keuler, B. Rockel, and A. Will, 2006: CLM - the Climate Version of LM: Brief Description and long-term Applications. COSMO Newsletter, 6, 225-235.

Bordi, I., K. Fraedrich, J.M. Jiang, and A. Sutera, 2004: Spatio-temporal variability of dry and wet periods in eastern China. Theoretical Applied Climatology, 79, 81–91.

Buishand, T.A., 1982: Some methods for testing the homogeneity of rainfall records. Journal of Hydrology, 58, 11-27.

Chen, W.L., Z.H. Jiang, L. Li, and P. Yiou, 2011: Simulation of regional climate change under the IPCC A2 scenario in southeast China. Clim Dyn, 36, 491–507.

Chen, Z., H. Wang, G. Ren, H. Xiang, and L. Xue, 2005: Change of urban heat island intensity and its effect on regional temperature series: a case study in Hubei Province. Chinese Journal on Climatic and Environmental Research 10, 771-779 (In Chinese).

Corder, G.W. and D.I. Foreman, 2009: Nonparametric statistics for non-statisticians: a step-by-step approach. John Wiley and Sons, New Jersey, p.264.

Ding Yihui, Xueli Shi, Yiming Liu, Yan Liu, Qingquan Li, Yongfu Qian, Manqian Miao, Guoqing Zhai, Kun Gao, 2006: Multi-year simulations and experimental seasonal predictions for rainy seasons in China by using a nested regional climate model (RegCM_NCC). Part I: Sensitivity study. Advances in Atmospheric Sciences 23:3, 323-341

Ding, Y., G. Ren, G. Shi, P. Gong, X. Zheng, P. Zhai, D. Zhang, Z. Zhao, S. Wang, H. Wang, Y. Luo, D. Chen, X. Gao, and X. Dai, 2007: China's National Assessment Report on Climate Change (I): Climate change in China and the future trend. Advances in Climate Change Research, 3 (Suppl.), 1-5.

Ebell, K., S. Bachner, A. Kapala and C. Simmer, 2008: Sensitivity of summer precipitation simulated by the CLM with respect to initial and boundary conditions. Meteorologische Zeitschrift, Vol. 17, No. 4, 421-431.

Feng, S., S. Nadarajah, and Q. Hu, 2007: Modeling Annual Extreme Precipitation in China Using the Generalized Extreme Value Distribution. Journal of the Meteorological Society of Japan, 85 (5), 599-613.

Fischer, T., M. Gemmer, L. Liu, and B. Su, 2011a: Temperature and Precipitation trends and Dryness/Wetness pattern in the Zhujiang River Basin, South China, 1961-2007. Quaternary International, Volume 244, Issue 2, 138-148.

Fischer, T., M. Gemmer, L. Liu, and T. Jiang, (2011b): Change-points in climate extremes in the Zhujiang River Basin, South China, 1961-2007. Climatic Change, accepted manuscript.

Gao X., Y. Shi, R. Song, F. Giorgi, Y. Wang, and D. Zhang, 2008: Reduction of future monsoon precipitation over China: comparison between a high resolution RCM simulation and the driving GCM. Meteorology and Atmospheric Physics, Volume 100, Numbers 1-4, Seiten 73-86.

Gemmer, M., S. Becker, and T. Jiang, 2004: Observed Monthly Precipitation Trends in China 1951-2002. Theoretical and Applied Climatology, 77, 39-45.

Gemmer, M., T. Fischer, T. Jiang, B. Su, and L. Liu, 2011: Trends of Precipitation Extremes in the Zhujiang River Basin, South China. Journal of Climate, 24 (3), 750-761.

Groisman, P. et al., 1999: Changes in the probability of heavy precipitation: important indicators of climatic change. Climatic Change, 42, 243-283.

Hagemann, S., K. Arpe, and E. Roeckner, 2005: Evaluation of the Hydrological Cycle in the ECHAM5 Model. Journal of Climate - Special Section, Volume 19, 3810-3827.

Hollweg, H.-D. et al., 2008: Ensemble Simulations over Europe with the Regional Climate Model CLM forced with IPCC AR4 Global Scenarios. Gruppe Modelle & Daten, Technical Report No. 3, Support for Climate- and Earth System Research at the Max Planck Institute for Meteorology, Hamburg, ISSN 1619-2257.

IPCC SRES (2000): Special Report on Emissions Scenarios: A special report of Working Group III of the Intergovernmental Panel on Climate Change, Nakićenović, N., and Swart, R., ed., Cambridge University Press,

Jiang, Z.H., J. Song, L. Li, W.L. Chen, Z.F. Wang, and J. Wang, (2011): Extreme climate events in China: IPCC-AR4 model evaluation and projection. Climatic Change, accepted manuscript, DOI 10.1007/s10584-011-0090-0.

Klein Tank, A.M.G., F. Zwiers, and X. Zhang, 2009: Guidelines on - Analysis of extremes in a changing climate in support of informed decisions for adaptation. World

Meteorological Organisation (WMO), Climate Data and Monitoring, WCDMP-No. 72, WMO-TD No. 1500, Geneva, Switzerland.

Leung Y.K. and M.C. Wu, 2005: Regime shift in summer rainfall in Southern China. In: Seventh joint meeting of seasonal prediction on EastAsian summer monsoon, Nanjing, China, 11–13 May 2005. Reprint no. 586, Hong Kong Observatory

Lin, W., L. Zhang, D. Du, L. Yang, H. Lin, Y. Zhang, and J. Li, 2009: Quantification of land use/land cover changes in Pearl River Delta and its impact on regional climate in summer using numerical modeling. Regional Environmental Change 9, 75-82.

Nikulin, G. et al., (2011): Precipitation climatology in an ensemble of CORDEX-Africa regional climate simulations. Journal of Climate, submitted.

Pal, J.S, F. Giorgi, X.Q. Bi, 2007: The ICTP RegCM3 and RegCNET: Regional climate modeling for the developing world. Bulletin of the AMS, 2007(09), DOI:10.1175/BAMS-88-9-1395

Qian, W. and X. Lin, 2005: Regional trends in recent temperature indices in China. Meteorol. Atmos. Phys., 90, 193–207.

Rockel B. and B. Geyer, 2008: The performance of the regional climate model CLM. Meteorologische Zeitschrift, Vol. 17, No. 4, 487-498.

Rockel B., A. Will and A. Hense, 2008: The Regional Climate Model COSMO-CLM (CCLM). Meteorologische Zeitschrift, Vol. 17, No. 4, 347-348.

Roeckner, E. and Coauthors, 2003: The atmospheric general circulation model ECHAM5. Part I: Model description. Rep. 349, Max Planck Institute for Meteorology, 127 pp.

Schönwiese, C.-D., 2006: Praktische Statistik für Meteorologen und Geowissenschaftler. 4. Auflage, Gebrüder Bornträger Verlagsbuchhandlung, Berlin, Stuttgart, S.302.

Sheskin, D.J., 2004: Handbook of parametric and nonparametric statistical procedures. 3rd Edition, Chapman & Hall, CRC Press, Boca Raton, p.1193.

Sillmann, J. and E. Roeckner, 2008: Indices for extreme events in projections of anthropogenic climate change. Climatic Change, 86, 83–104.

Steppeler, J., Doms, G., Schättler, U., Bitzer, H.W., Gassmann, A., Damrath, U., and Gregoric, 2003: Meso-gamma scale forecasts using the nonhydrostatic model LM. Meteorol. Atmos.Phys., 82, 75–96.

Su, B., Z. Kundzewicz, and T. Jiang, 2008: Simulation of extreme precipitation over the Yangtze River Basin using Wakeby distribution. Theor. Appl. Climatol., 96 (2009), 209-219.

Trenberth, K.E., P.D. Jones, P. Ambenje, R. Bojariu, D. Easterling, A. Klein Tank, D. Parker, F. Rahimzadeh, J.A. Renwick, M. Rusticucci, B. Soden, and P. Zhai, 2007: Observations: Surface and Atmospheric Climate Change. In: Climate Change 2007: The Physical Science Basis. Contribution of Working Group I to the Fourth Assessment Report of the Intergovernmental Panel on Climate Change [Solomon, S., D. Qin, M. Manning, Z. Chen, M. Marquis, K.B. Averyt, M. Tignor and H.L. Miller (eds.)]. Cambridge University Press, Cambridge, United Kingdom and New York, NY, USA.

Uppala, S. M. et al., 2005: The ERA-40 re-analysis. Quarterly Journal of the Royal Meteorological Society, 131, 2961–3012.

Wang, Q. and Y. Ding, 1997: Climatological characteristics of evolution of East Asian winter monsoon. Quarterly Journal of Applied Meteorology 8 (2), 186-196.

Wang, Yuqing, Omer L. Sen, Bin Wang, 2003: A Highly Resolved Regional Climate Model (IPRC-RegCM) and Its Simulation of the 1998 Severe Precipitation Event over China. Part I: Model Description and Verification of Simulation*. J. Climate, 16, 1721–1738.

Wilks, D.S., 2006: Statistical Methods in the Atmospheric Sciences. Second Edition, Elsevier Inc., USA, p.649.

Xu, C., Y. Luo, and Y. Xu, 2011: Projected changes of precipitation extremes in river basins over China. Quaternary International, 244, 149–158.

Xu, Ying, C.H. Xu, X.J. Gao, and Y. Luo, 2009: Projected changes in temperature and precipitation extremes over the Yangtze River Basin of China in the 21st century. Quaternary International, 208, 44–52.

Yu, S., Shi, X., and Lin, X., 2009: Interannual variation of East Asian summer monsoon and its impacts on general circulation and precipitation. Journal of Geographical Science, 19, 67-80.

Zhou, Y., and G. Ren, 2005: Identifying and correcting urban bias for regional surface air temperature series of north china over period of 1961-2000. Chinese Journal on Climatic and Environmental Research, 10 (4), 743-753 (In Chinese).

List of Tables

Table 1 List of climate indicators

Table 2 Average annual BIAS and RMSE of CCLM-simulated indicators in four regions of the Zhujiang River Basin (ZRB), South China, 1961-2000.

Table 3 Average annual BIAS and RMSE of ECHAM5-simulated indicators in four regions of the Zhujiang River Basin (ZRB), South China, 1961-2000.

Table 4 Decadal trend statistics (unit per decade) for six observed, CCLM-simulated, and ECHAM5-simulated indicators in four regions of the Zhujiang River Basin, 1961-2000.

Table 5 CCLM-projected decadal trends (unit per decade) for six annual indicators for the period 2011-2050 in four regions of the Zhujiang River Basin.

List of Figures

Figure 1 Overview map of the Zhujiang River Basin (elevation and main rivers), with the outline of the four regions (W=West-, N=North-, S=South-, and E=East-Region), the meteorological observation stations, and the 0.5° grid-points.

Figure 2 Observed, CCLM-simulated and ECHAM5-simulated averaged annual temperature indicators: (a) TMEAN, (b) TMAX, and (c) TMIN for the Zhujiang River Basin, 1961-2000.

Figure 3 Observed, CCLM-simulated and ECHAM5-simulated averaged annual precipitation indicators: (a) PRCPTOT, (b) RX5DAY, and (c) DRY DAYS for the Zhujiang River Basin, 1961-2000.

Figure 4 Scatter plots of six basin-averaged and sorted annual observed and simulated indicators (CCLM = blue; ECHAM5 = red), (a) TMEAN (°C), (b) TMAX (°C), (c) TMIN (°C), (d) PRCPTOT (mm), (e) RX5DAY (mm), and (f) DRY DAYS (days) for the Zhujiang River Basin, 1961-2000.

Figure 5 Basin-averaged observed (yellow bar and solid line), CCLM-simulated (blue bar and dashed line), and ECHAM5-simulated (red bar and dotted line) monthly PRCPTOT (bars) and TMEAN (lines) for the Zhujiang River Basin, 1961-2000.

Figure 6 Area-averaged monthly differences in (a) PRCPTOT and (b) TMEAN, i.e. the BIAS of monthly averaged observation and CCLM-simulation for Region West (W), North (N), South (S), and East (E) for the Zhujiang River Basin 1961-2000.

Figure 7 same as in Figure 5, but for basin-averaged monthly observed, CCLM-simulated and ECHAM5-simulated (a) RX5DAY precipitation (bars) and TMAX (lines); (b) number of DRY DAYS (bars) and TMIN (lines) for the Zhujiang River Basin, 1961-2000.

Figure 8 Loading patterns of the first principal component (PC1) of (a) observed TMEAN, (b) CCLM-simulated TMEAN, (c) observed PRCPTOT, and (d) CCLM-simulated PRCPTOT, for the Zhujiang River Basin, 1961-2000.

Figure 9 Difference of CCLM-simulated (1961-2000) and CCLM-projected (2011-2050) averaged annual means of (a) TMEAN, (b) TMAX, (c) TMIN, (d) PRCPTOT, (e) RX5DAY, and (f) DRY DAYS in the Zhujiang River Basin.

Figure 10 Difference of CCLM-simulated (1961-2000) and CCLM-projected (2011-2050) basin-averaged monthly means of (a) temperature indicators and (b) precipitation indicators in the Zhujiang River Basin.

Figure 11 CCLM-simulated (1961-2000) and CCLM-projected (2010-2050) averaged annual TMEAN (red line) and PRCPTOT (green bars), including the means of 1961-2000 and 2011-2050 (dark red / dark blue lines) and the linear trend in TMEAN for 2011-2050 (black dashed line) in the Zhujiang River Basin.

Table 1 List of climate indicators

ID	Indicator name	Definitions	Unit
TMEAN	Average Temperature	Annual and monthly mean value of daily mean temperature	°C
TMAX	Maximum Temperature	Annual and monthly maximum value of daily mean temperature	°C
TMIN	Minimum Temperature	Annual and monthly minimum value of daily mean temperature	°C
PRCPTOT	Total wet-day precipitation	Annual and monthly total precipitation in wet days (rainfall >=1mm/d)	mm
RX5DAY	Max 5-day precipitation	Annual and monthly maximum consecutive 5-day precipitation	mm
DRY DAYS	Dry Days	Annual and monthly number of dry days (rainfall < 1mm/d)	d

Table 2 Average annual BIAS and RMSE of CCLM-simulated indicators in four regions of the Zhujiang River Basin (ZRB), South China, 1961-2000.

Indicator	BIAS					RMSE				
Region:	**ZRB**	**W**	**N**	**S**	**E**	**ZRB**	**W**	**N**	**S**	**E**
TMEAN (°C)	1.1	0.4	1.2	1.8	1.1	1.3	0.9	1.5	1.9	1.2
TMAX (°C)	2.6	1.8	3.2	2.7	2.3	2.8	2.2	3.5	3.0	2.6
TMIN (°C)	-0.5	-1.2	-0.9	0.7	0.0	2.0	2.0	2.2	2.5	2.6
PRCPTOT (mm)	-138	-136	44	-509	-60	323	226	353	689	440
RX5DAY (mm)	17.7	-18.3	1.0	83.9	21.7	49.4	29.3	39.2	149.3	81.9
DRY DAYS (d)	-0.6	-7.0	-16.3	54.5	-19.0	16.5	17.6	27.0	56.6	28.5

Table 3 Average annual BIAS and RMSE of ECHAM5-simulated indicators in four regions of the Zhujiang River Basin (ZRB), South China, 1961-2000.

Indicator	BIAS					RMSE				
Region:	ZRB	W	N	S	E	ZRB	W	N	S	E
TMEAN (°C)	1.3	1.4	-0.3	2.3	0.7	1.5	1.6	0.9	2.5	1.0
TMAX (°C)	1.0	2.2	-0.3	1.8	-0.5	1.3	2.6	0.9	2.1	1.1
TMIN (°C)	-0.1	-0.2	-2.9	2.0	0.1	2.2	2.1	3.7	3.4	2.5
PRCPTOT (mm)	-415	-255	-447	-408	-563	471	317	515	490	650
RX5DAY (mm)	-84.8	-52.2	-89.7	-92.2	-110	87.1	58.9	97.5	100.5	113.4
DRY DAYS (d)	-23.2	-17.9	-22.2	-21.6	-27.9	28.2	22.8	27.4	28.0	35.4

Table 4 Decadal trend statistics (unit per decade) for six observed, CCLM-simulated, and ECHAM5-simulated indicators in four regions of the Zhujiang River Basin, 1961-2000.

Region		TMEAN	TMAX	TMIN	PRCPTOT	RX5DAY	DRY DAYS
		(°C/10a)	(°C/10a)	(°C/10a)	(mm/10a)	(mm/10a)	(days/10a)
West	*OBS*	0.06	0.08	0.17	-4.5	2.0	1.3
	CCLM	0.17	-0.02	-0.28	-17.6	-1.2	2.7
	ECHAM	**0.22**	0.17	-0.17	**-41.8**	**-6.0**	**-2.8**
North	*OBS*	0.06	-0.03	0.21	10.4	1.4	1.0
	CCLM	0.00	-0.26	-0.11	-29.8	2.8	2.9
	ECHAM	-0.01	0.03	-0.23	-7.5	-5.6	1.6
South	*OBS*	**0.12**	0.06	0.21	3.5	-0.6	0.7
	CCLM	0.01	-0.21	-0.26	-2.8	8.5	1.5
	ECHAM	0.10	0.09	-0.41	0.4	1.2	1.2
East	*OBS*	**0.14**	0.09	0.20	35.6	-1.8	-1.5
	CCLM	-0.03	**-0.37**	-0.02	-18.4	14.8	3.1
	ECHAM	0.01	0.00	-0.34	8.9	2.7	1.8

*numbers in **bold** show a significant trend above the 0.05 significance level

Table 5 CCLM-projected decadal trends (unit per decade) for six annual indicators in four regions of the Zhujiang River Basin for the period 2011-2050.

Region	TMEAN	TMAX	TMIN	PRCPTOT	RX5DAY	DRY DAYS
	(°C/10a)	(°C/10a)	(°C/10a)	(mm/10a)	(mm/10a)	(days/10a)
West	**0.48**	**0.62**	**0.52**	7.5	1.3	0.2
North	**0.45**	**0.78**	**0.36**	37.5	5.5	0.0
South	**0.35**	**0.65**	**0.36**	-17.6	-3.9	-0.5
East	**0.41**	**0.73**	**0.23**	54.2	10.4	-1.4

*numbers in **bold** show a significant trend above the 0.05 significance level

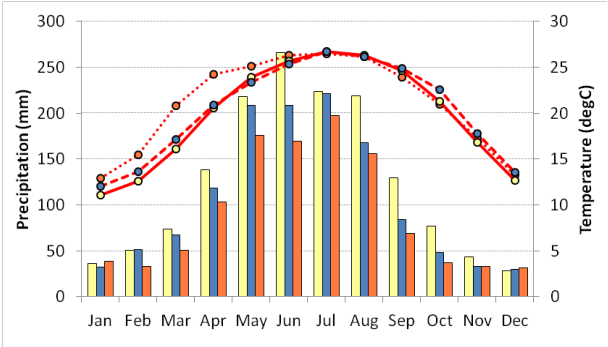

Figure 5 - Basin-averaged observed (yellow bar and solid line), CCLM-simulated (blue bar and dashed line), and ECHAM5-simulated (red column and dotted line) monthly PRCPTOT (bars) and TMEAN (lines) for the Zhujiang River Basin, 1961-2000.

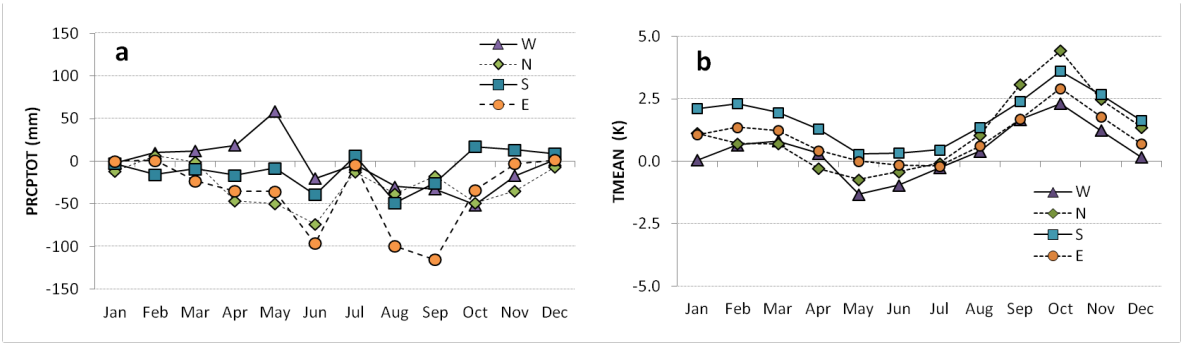

Figure 6 - Area-averaged monthly differences in (a) PRCPTOT and (b) TMEAN, i.e. the BIAS of monthly averaged observation and CCLM-simulation for Region West (W), North (N), South (S), and East (E) for the Zhujiang River Basin 1961-2000.

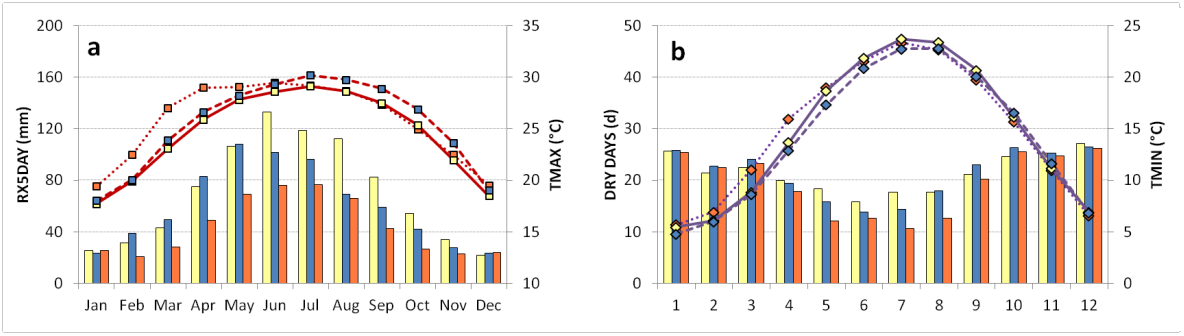

Figure 7 - same as in Figure 5, but for basin-averaged monthly observed, CCLM-simulated and ECHAM5-simulated (a) RX5DAY precipitation (bars) and TMAX

(lines); (b) number of DRY DAYS (bars) and TMIN (lines) for the Zhujiang River Basin, 1961-2000.

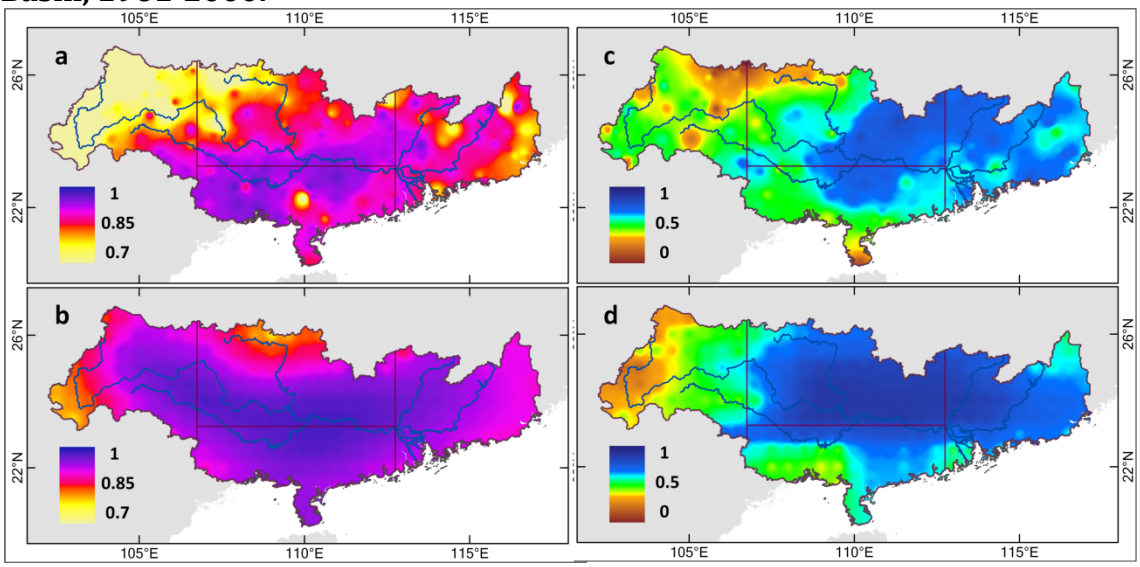

Figure 8 - Loading patterns of the first principal component (PC1) of (a) observed TMEAN, (b) CCLM-simulated TMEAN, (c) observed PRCPTOT, and (d) CCLM-simulated PRCPTOT, for the Zhujiang River Basin, 1961-2000.

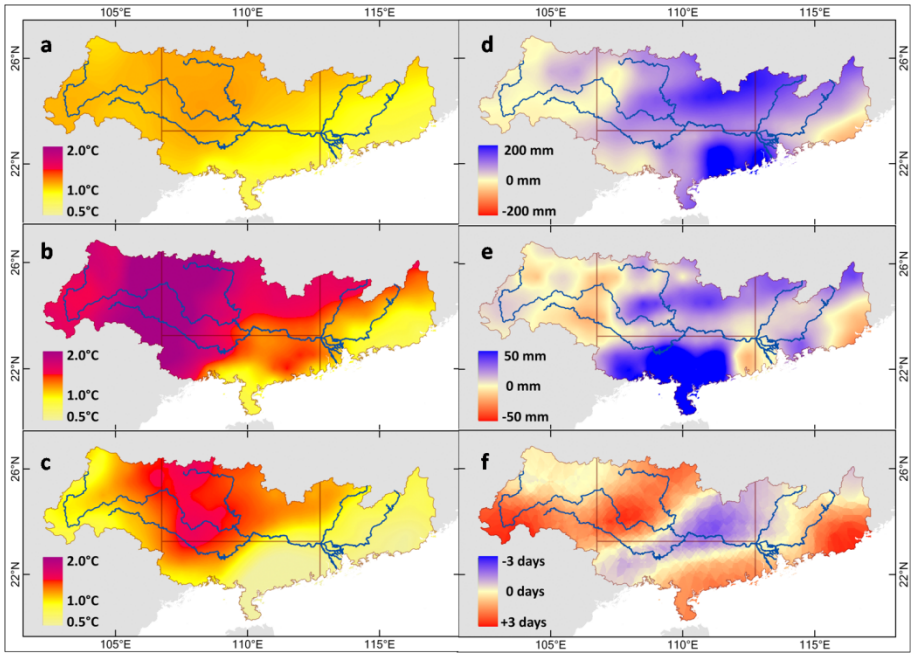

Figure 9 - Difference of CCLM-simulated (1961-2000) and CCLM-projected (2011-2050) averaged annual means of (a) TMEAN, (b) TMAX, (c) TMIN, (d) PRCPTOT, (e) RX5DAY, and (f) DRY DAYS in the Zhujiang River Basin.

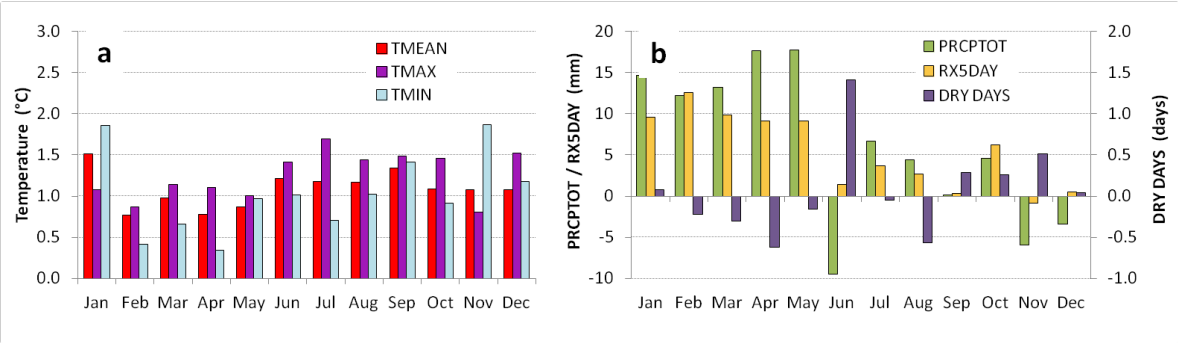

Figure 10 - Difference of CCLM-simulated (1961-2000) and CCLM-projected (2011-2050) basin-averaged monthly means of (a) temperature indicators and (b) precipitation indicators in the Zhujiang River Basin.

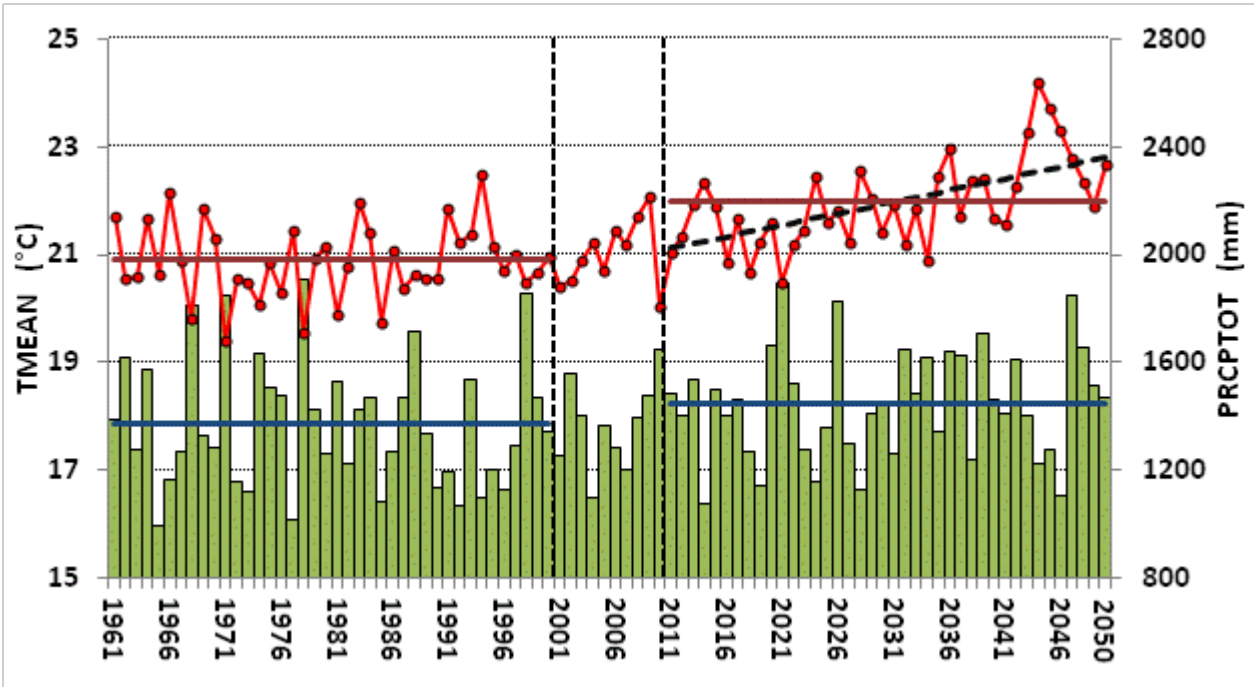

Figure 11 - CCLM-simulated (1961-2000) and CCLM-projected (2010-2050) averaged annual TMEAN (red line) and PRCPTOT (green columns), including the means of 1961-2000 and 2011-2050 (dark red / dark blue lines) and the linear trend in TMEAN for 2011-2050 (black dashed line) in the Zhujiang River Basin.

Appendix VII

Liu, L., T. Fischer, T. Jiang and Y. Luo, (2012): Comparison of uncertainties in projected flood frequency of the Zhujiang River, South China. Accepted for publication in *Quaternary International*.

Comparison of uncertainties in projected flood frequency of the Zhujiang River, South China

Lüliu Liu[a], Thomas Fischer[a,b], Tong Jiang[a], Yong Luo[a]

[a] National Climate Center, China Meteorological Administration, Beijing 100081, China

[b] Department of Geosciences, University of Tübingen, Tübingen 72070, Germany

Abstract

In this study, we investigate uncertainties in the modeling of hydrological impacts of climate change on projected flood frequencies of the Zhujiang River, South China. We applied the hydrological model HBV-D to simulate and project future stream flow based on a multi-model ensemble. A monthly re-sampling technique is used to estimate the natural variability. The magnitude of three uncertainty sources, i.e. emission scenarios, GCM structure, and downscaling techniques, are related to the observed and projected natural variability. The relative change in each uncertainty source and the overall dominance among the three sources are analyzed. The changes in flood frequency are presented for five return periods (2, 5, 10, 20, and 50years) and three future time periods (2020s, 2050s, and 2080s).

The results suggest that in comparison to the natural variability of the multi-model ensemble, the uncertainty sources show much stronger variations. The range of their relative change and their dominance vary with the lead time and return period. In most of the cases, the dominant uncertainty can primarily be attributed to emission scenarios for all three future time periods. The GCM structure is the second dominant source, especially for the projected flood frequency in the 2050s. Downscaling techniques represent the lowest uncertainty ranges of the three sources. The uncertainty and projected impact of climate change differs also between the four applied GCMs, as compared to the natural variability CCSM3 and HIRES show higher ranges than MK3.5 and ECHAM5.

The upper bounds (95% percentile) in uncertainty mostly show an increasing tendency with increasing return period, and partially with increasing lead time. Hence, the more extreme the return period (higher flood frequency) the higher is the uncertainty of the model projections. It is therefore essential that climate change impact assessments consider a wide range of climate scenarios derived from different GCMs under multiple emission scenarios and including several downscaling techniques. The uncertainty due to natural variability should also be considered more intensely. The projection of flood frequency and the identification and quantification of the uncertainties in the modeling is important for the implementation of adaptation policies into water resource planning in the Zhujiang River basin, South China.

Keywords: Uncertainty; Flood Frequency; Natural Variability; Emission; Downscaling; Zhujiang River

1. Introduction

Water is the most severely affected resource by climate change. Any changes in the hydrologic cycle will affect energy production and flood risks. Extreme climatic and hydrological events have become more frequent in recent years, which may be due to anthropogenic global warming (Prudhomme et al., 2003). Water management and climate adaptation measures will very likely become more necessary (Minville et al., 2008). It is important to quantify climate change impacts on water resources to develop and implement mitigation and adaptation policies in the water sector.

In the Zhujiang River basin, increasing annual temperatures and increasing total precipitation in terms of areal mean were detected using datasets of 64 meteorological stations (Liu et al., 2009). The multi-annual mean precipitation (1961-2007) in the basin shows increasing amounts from west to south, from less than 1000 mm in the western mountains to more than 2000 mm at the eastern coastline. Decreasing (increasing) tendencies in total and 5-day maximum precipitation (dry days) were detected in the western and central regions by Fischer et al. (2011), and increasing tendencies to dryer conditions and stronger precipitation intensities were detected by Gemmer et al. (2011).Both studies used 192 quality-controlled precipitation datasets for the period 1961-

2007 and applied the Mann-Kendall test and linear regression to identify trends in climate indicators.

Climate studies suggest that more frequent flood disasters occurred due to heavy rainfall since 1990s (He et al, 2006). A slight upward trend in runoff during the dry season was observed from 1951 to 2000 (Yin, 2010). As for the future, upward trends are projected in seasonal temperature and annual precipitation from 2011 to 2060 using the global circulation model (GCM) ECHAM5/MPI-OM (Liu et al., 2009). Using three GCMs and three greenhouse gas emission scenarios, similar trends are projected in seasonal precipitation and runoff from May to October for the period from 2011 to 2099 in the Xijiang River basin (the largest tributary of the Zhujiang River), while downward trends are projected from December to February. In addition, floods could be more severe and more frequent after 2050 (Liu et al., 2012a,b). In these studies, a large uncertainty in projected values is apparent.

The uncertainty can be partially linked to various conditions and assumptions in greenhouse gas emission scenarios (GHGES) and atmosphere-ocean general circulation models (AOGCM). In order to provide detailed projections of local climate change, the use of regional climate models (RCM) or the application of downscaling methods also add uncertainty to the projected climate data due to the limitations that are inherent in each technique (Déqué et al., 2007). Finally, the fourth source of uncertainty is introduced by the sampling method, as time series of climate data exhibit inter-annual and inner-annual variability. These sources of uncertainties are introduced and put into context with hydrologic impact by Minville et al. (2008). Further, Kay et al, (2009) emphasize that the hydrological model structure and its parameters are two more sources of uncertainty.

Climate uncertainty at both global and regional scale was identified as the dominant driving force in hydrological risk assessments (Preston and Jones, 2008). As stated by Preston and Jones (2008), the largest source of uncertainty can be attributed to the type of GCM used in studies on climate change impacts on the flood regimes of five catchments in Great Britain. This conclusion is based on the application of 16 GCMs with four different emission scenarios (SRES-98). This is underlined, as Prudhomme et al. (2003) indicate that adaptation policies do not rely on results from only very few models and scenarios. The study using PRUDENCE data by Graham et al. (2007) also demonstrates that the uncertainties in the projections of river flow are larger due to the choice of GCMs than due to the applied RCM or emissions scenario. Comparing the results of three GCMs and two RCMs,

Booij (2005) found that the uncertainty due to the hydrological model structure or parameterization is smaller than the uncertainty of each GCM/RCM. This conclusion is also supported by Gosling et al. (2011) and Todd et al. (2011), who compared the uncertainty of hydrological model structure and climate model structure using seven GCMs. The elimination of uncertainty is probably impossible (Koutsoyiannis and Efstratiadis, 2007), but for the design of long-term planning strategies for flood management schemes, the quantification of uncertainty must be accounted for.

So far, few investigations on impacts of climate change in terms of projected flood frequency and hardly any comparisons of sources of uncertainties have been done for the Zhujiang River basin in China. Based on the multi-model ensemble projection of flood frequencies of the Zhujiang River, the objectives of this study are (1) to compare the influence of three sources of uncertainty, with the uncertainty sources being emission scenarios, GCM structure, and downscaling techniques, as relative changes to the natural variability; (2) to detect trends in the magnitude of uncertainty regarding return periods and different future time periods; and (3) how both findings relate to the natural variability and climate change impacts on the projected flood frequency of the Zhujiang River in South China.

In section 2, we give a description of the study area and the used datasets. The basic methodology is outlined in section 3, including a brief description of the calibration and validation of the applied hydrological model, the frequency analysis and the quantification of uncertainty. In section 4, the different sources of uncertainty are described. In section 5, we analyze the results, including the comparison of the magnitude and range in the relative change of the different sources of uncertainty, and how these relate to the natural variability. Finally, we conclude and discuss the results in section 6.

2. Study area and datasets

2.1 Description of the Zhujiang River basin

The Zhujiang River (or Pearl River) basin is one of China's largest river basins. It is located in South China and covers approximately 453,700 km2 (excluding the Leizhou Peninsula region) in the provinces of Guangdong, Guangxi, Guizhou, Yunnan, Hunan, Jangxi, and Fujian in China and partly Northeastern Vietnam (Dai et al., 2007). The basin is

characterized by mountainous areas in the western part but mainly low lands in the central and south-eastern parts, with subtropical and tropical climate. The annual mean temperature varies from 14ºC in the west to 22ºC in the east, and the annual average precipitation is 800 mm in the west and more than 2000 mm at the coastline (Gemmer et al., 2011). Due to the East Asian summer monsoon, precipitation during the flood season (April to September) accounts for 80% of the annual precipitation.

The basin consists of three main tributaries, i.e. the Xijiang River, Beijiang River, and Dongjiang River, and additionally many small rivers within Zhujiang River Delta. The Xijiang River is the largest tributary with a total length of 2,214km and draining an area of 353,100km2 (Liu et al., 2012a). It drains the entire western and central parts of the Zhujiang River basin, while the other two tributaries are found in the east (Fischer et al., 2012a). The watershed area of the Xijiang River outlet at Gaoyao hydrological station accounts for 99.4% of the Xijiang basin area. Due to available data, the Xijiang River basin is chosen as the study region. The location of the basin and the course of the main river system are provided in Figure 1.

2.2 Data

A digital elevation model (DEM) with a scale of 1: 250 000 is used to extract the river network and to define the sub-basins of the Xijiang River basin for hydrological modeling. The DEM was provided by the China Fundamental Geographic Information Center.

Daily climate data of 129 meteorological stations within the Xijiang River Basin for the period of 1960-2006 are provided by the National Meteorological Information Center, CMA. The daily stream flow records from Gaoyao hydrological station are obtained from the annual Water Year Books of the Zhujiang Conservancy Commission of the Ministry of Water Resources, and are also available for the period 1960–2006. All data are used to calibrate and validate the hydrological model. An elevation map including the location of the 129 meteorological stations is provided in Figure 1.

Daily data of precipitation and temperature from four GCMs (Table 1) are available for the simulation period (1961-1990) and for the 21st century and have been retrieved from the IPCC Data Distribution Centre (http://ipcc-ddc.cru.uea.ac.uk). The RCM data (here CCLM) covering the same periods is provided by the Potsdam Institute for Climate Impact Research (PIK). All simulated and projected data are used as input to the hydrological model (here

HBV-D) to simulate the runoff of the Xijiang basin. Based on the provided data, past and potential future changes in flood frequency are analyzed in this study.

3. Methodologies

3.1 Description of the hydrological model (HBV-D)

In comparison with physically-based distributed hydrological models, relatively simple semi-distributed hydrological models are more useful for exploring climate risks over long time-scales and large geographic areas (Preston and Jones, 2008). Based on research using the semi-distributed hydrological model HBV-D, Krysanova and Bronstert (1999) conclude that semi-distributed conceptual hydrological models avoid an increase in the number of parameters with the area, while preserving the underlying conceptual information about the spatially-distributed parameters used for the hydrological response categories defined.

The Hydrologiska Byråns Vattenbalansavdelning (HBV) model is a semi-distributed conceptual hydrological model (Bergström, 1992), with sub-basins as primary hydrological units (HU). Here, we apply the HBV-D model (Krysanova and Bronstert, 1999), which is a derivative of the 'Nordic' HBV model (Saelthun, 1996) including an improved rainfall-runoff coupling. The model divides the basin into a certain number of HU's depending on different parameters. Every HU is categorized into certain elevation and land cover zones, including their climate parameters in order to better comprise the regional characteristics and increase the performance of the model.

Daily potential evapotranspiration (EP) is computed using the formula by Blaney and Criddle (1950) rather than method for monthly EP as suggested by Menzel et al. (2006). Compared to the original HBV, HBV-D results in an improved description of land cover characteristics and more physically sound evapotranspiration schemes, which are more appropriate for investigations of regional hydrological impacts of global change in large basins (Krysanova and Bronstert, 1999).

3.2 Calibration and validation of hydrological model (HBV-D)

Preliminarily, the Xijiang River basin is subdivided into 17 HU's with areas ranging from 754km2 to 54,400km2. The calibration and the validation of the HBV-D model performance are based on the daily stream flow at Gaoyao hydrological station from 1960 to 2006. The stream flow time series is firstly divided into three time-periods: 1960-1975, 1976-1990 and 1991-2006. Daily data of the period 1976-1990 are used to calibrate the model, while data of the other two periods are used to validate the model. A model run was considered to be successful when certain measures of efficiency are in specific efficiency levels. The applied measures of efficiency are the widely used Nash-Sutcliffe coefficient (E_{ns}), the correlation coefficient (Cor), and the relative error (Bias). The definitions and calculation of these measures are provided by Menzel et al. (2006), Liu et al. (2011) and Fischer et al. (2012b).

For all three periods, the thresholds are determined for E_{ns} above 0.8, for Cor above 0.9, and for the Bias below 4%. The results of the calibration and validation periods are shown in (Liu et al., 2012b). It can be seen that all three measures fall in the specific efficiency levels for both the calibration and the validation periods.

Moreover, by comparing the empirical frequency curve of the observed stream flow with the frequency curves of the simulated stream flow for each period, we can see that the model can well simulate the daily stream flow at Gaoyao hydrological station. Although the simulated high frequencies show slightly lower amounts than the empirical high frequencies, i.e. extreme stream flow amounts, the frequency curves of simulated daily stream flow matches well those of the observed (Fig. 2). As can be seen in Figure 2, the simulated stream flow shows more often slightly higher frequencies in stream flow amounts of 4-6 mm/d than the observed. A strong correlation and similar seasonal annual course is further determined for the observed and simulated runoff depth with the precipitation. This is in line with the studies by Liu et al. (2012a,b) and Fischer et al. (2012c), who have concluded that hydrological responses depend strongly on the precipitation patterns; hence, changes in precipitation will impact the stream flow correspondingly.

3.3 Frequency analysis

For many rivers, the stream flow varies significantly from season to season and especially from wet years to drought years and vice versa. Using the method of annual block maxima to estimate flood frequencies, it is possible that the annual maximum peak stream flow does not reach flood potential in drought years, nor does it imply high floods in wet years. Hence, for estimating frequencies in flood occurrence and magnitude, the use of the peaks over threshold (POT) method is preferred over the annual block maxima method. The POT considers all peaks in stream flow above a certain threshold (Begueria, 2005); hence, most flood events will be taken into account. Here, the highest peaks are sampled at an average rate of three events per year, applying the standard independence criteria (Bayliss and Jones, 1992; Kay et al., 2009).

Because of its flexibility and robustness, the Generalized Pareto Distribution (GPD) has been chosen for estimating return periods of flood events (Davison, 1984). In 1975, Pickands (1975) introduced the GPD into the hydro-meteorological field, which was then widely used in the following decades (Smith, 1984; van Montfort and Witter, 1985; Kay et al., 2009; Fang et al., 2007). Kay et al. (2009) indicate that the GPD can be successfully fitted to the magnitudes of the POT with the peak arrival times assumed to correspond to a Poisson distribution (Naden, 1992).

For the estimation of changes in flood frequencies of the Xijiang River, the GPD is applied to simulated peak stream flow events. Based on the fitted GPD, return levels of five return periods (2 years, 5 years, 10 years, 20 years, and 50 years) are estimated for the baseline period (1961-1990) and three future 30-year periods, i.e. the 2020s (2011–2040), the 2050s (2041–2070), and the 2080s (2071–2100; or 2071-2099 for NCAR/CCSM3). The estimated return levels (Fischer et al., 2012a) describe a range of flood events, from annual (2-year return period) to rare events (50-year return period).

3.4 Quantitative estimation of changes in flood frequencies

Magnitude and frequency of flood events are usually used to discuss changes in flood events. The comparison of return periods of flood events will give an indication of how the flood regime may evolve in the future (Prudhomme et al., 2003). In this study, we intend to identify changes in flood magnitude of future periods compared to the current climate. The

flood magnitudes are estimated as return levels of five return periods for observed and future 30-year-periods (by four different GCMs) using the GPD. Based on this, the impact of climate change on flood frequencies will be defined as the relative difference (i.e. Bias) of projected flood flow to the current flood flow at a certain return level. Therefore, the Bias is calculated using the following equation:

$$(Qp - Qc) / Qc * 100\ \%$$

Where, Qp is the flood flow of a certain return period in future, and Qc is the flood flow of the same return period of the baseline period.

The uncertainty of climate change impact is described as the range of the 90% interval in natural variability of the climate system, while described as the relative range of all ensemble members. For example, the uncertainty from GCMs structure is the interval between minimum (5% percentile) and maximum (95% percentile) change of each GCM under the same emission scenarios.

4. Sources of uncertainty

The uncertainties of projected impacts of climate change are usually expressed by changes in pre-defined sources of uncertainty relative to a baseline scenario or baseline period (Kay et al., 2009; Jenkins and Lowe, 2003). On one hand, the relative change to a baseline makes it easy to compare impacts between different regions and different time horizons. On the other hand, e.g. the use of relative changes can avoid the influence of a bias in GCM simulations etc. In our study, the mean of the re-sampled natural variability, based on 100 iterations, is chosen as the baseline scenario. Hence, uncertainty is expressed as the change in an uncertainty source relative to the mean of the re-sampled natural variability in order to remove the bias of absolute values.

4.1 Natural variability of the climate system

Natural variability of the climate system is mainly caused by internal "chaos" of the system or external factors such as solar energy, natural CO2 emissions from volcanic

eruptions etc. The influence of natural variability on the current climate variability can either be added to, or subtracted from any anthropogenic changes identified in the current climate system (Jenkins and Lowe, 2003).We cannot yet predict the effect of this natural variability in a given future period, but we can quantify its range of uncertainty by different approaches.

Kay et al. (2009) specified two methods to assess the effects of climate variability. In the first approach, a large number of climate simulations are generated by a dynamic model, whereas each simulation is based on a different initial condition compared to the control run of the model (Jenkins and Lowe, 2003). However, it is indicated that such model-based climate variability ensemble may or may not be representative of the actual climate variability (Hulme et al., 2002). The other method is based on a stochastic rainfall model with which a large number of rainfall time-series are generated for the current and future climate periods (Cameron, 2006; Kilsby et al., 2007). This approach requires the checking of its ability to simulate extremes as well as its replication of the seasonal cycle. Moreover, it is based on the assumption of a stationary climate system, i.e. the features of the model under current climate are still valid under future climate (Kay et al., 2009). Another method by Menzel et al. (2006) suggests driving certain GCM at a constant greenhouse gas concentration to roughly represent the status of the climate system at a certain time interval. This model is then run for multiple years by using unmodified boundary conditions. The generated time series are considered to represent the whole range of possible natural variability, and serve to identify effects of a changing climate derived by other model scenarios assuming natural conditions (Menzel et al., 2006).

In general, model-based approaches are computationally too large to run GCM or RCM ensembles which integrate multiple hundred years. Therefore, we apply a stochastic rainfall model to explore the effects of climate variability. A set of hundred rainfall time series are generated through monthly re-sampling. This is based on simulated daily rainfall series from a certain GCM for both the baseline (1961-1990) and future climate periods. For example, taking the monthly data from January 1961 to December 1990, a new series is created by first selecting a data of January from any of those 30 years to represent January 1961, then selecting data of any February to represent February 1961, and so on until a time series of the same length as the original is generated. The rainfall data for the baseline and future climate periods are the simulated/projected results of the GCMs (Table 1). Each of the hundred new rainfall time series of every GCM is used to drive HBV-D. Then, the flood

frequencies at five return periods (2, 5, 10, 20, 50 years) are estimated for the baseline and the three future climate periods.

4.2 Uncertainty from emission scenarios

The SRES scenarios (IPCC SRES, 2000), were designed to improve some aspects of the IS92 scenarios and have been used in the second, third and fourth IPCC Assessment Reports. The scenarios have been widely used for projections of future climate conditions. Forty different scenarios are organized into six families containing individual scenarios with common themes. The six families of scenarios are A1FI, A1B, A1T, A2, B1, and B2. They are discussed on their uncertainty in the IPCC Fourth Assessment Report (IPCC AR4, 2007). Only the projections of the GCMs under SRES A2, A1B, and B1 are widely available. Whereas complete series of daily precipitation and average temperature from1961 to 2100 (or to 2099 for CCSM3) for all three scenarios are available only for MK3.5 and CCSM3. Hence, the uncertainty from these emission scenarios is discussed on the basis of the two GCMs (MK3_5 and CCSM3).

4.3 Uncertainty from GCM structure

Each GCM generally project different changes in climatic parameters when forced by a given emissions scenario. The use of different climate sensitivities to a doubling of CO2 leads to different variations and trends in temperature and precipitation (Hulme et al. 2002; Kay et al., 2009). In this study, the uncertainty from these GCM structures is assessed on the basis of runoff simulations by HBV-D focusing on climate change impacts on flood frequency at five return periods. These simulations are based on the precipitation and temperature parameters from the four GCMs (Table 1) under the SRES A1B scenario. The results of the uncertainty from GCM structure are compared with the natural variability (Kay et al., 2009). Here, the natural variability is the average of the GCMs as described in section 4.1.

4.4 Uncertainty from downscaling techniques

The simulations by a hydrological model may produce relative large bias when data from Global Circulation Models (GCMs) is directly used to drive the hydrological model, because the spatial resolution of GCMs is too coarse and does not capture smaller scale climate effects (Cubasch, 2001; Menzel et al., 2006). In order to bridge this gap so-called "downscaling techniques" are usually used. In many studies, dynamical and statistical downscaling models have been developed and implemented (e.g. Wilby and Dawson, 2007; Liu et al., 2011; Xu, 1999; Fowler et al., 2007). In this study, we use the statistical method of daily percentile scaling by Chiew (2006) and the dynamical method of the regional climate model CCLM (Rockel et al., 2008) to estimate the uncertainty from downscaling techniques. CCLM is a regional climate model partially developed by PIK. In this study, CCLM uses a nesting technique to downscale the coarse resolution GCM ECHAM5 under the SRES A1B scenario. The daily percentile scaling method has been used to correct daily precipitation from ECHAM5, CCSM3 and MK3.5 to reduce the simulation bias (Liu and Ren, 2012). This method relates each percentile of GCM simulated daily rainfall to the observed "natural" rainfall of the same percentile. Using this relationship, the GCM projected daily rainfall of future climate periods is converted to the "natural" rainfall in future periods (Chiew, 2006). The difference of the results of both downscaling techniques is compared with the natural variability.

5. Results

5.1 Projected changes in flood frequencies

A multi-model ensemble is used to generate the projected stream flow of Xijiang River and to identify future changes in flood frequency (cf. Liu et al., 2012b). In Figure 3, the frequency curves of changes in projected annual maximum 1-day flood peak flows, i.e. the flood frequency, are shown for three future periods relative to the baseline period (1961-1990). The shift in future periods towards the right side of the baseline scenario implies a projected shift to more intense peak stream flows (Fig. 3). The projected stream flow was generated by HBV-D using the multi-model ensemble which incorporates four GCMs, one RCM (CCLM) and one downscaled ECHAM5 dataset based on daily percentile scaling. In

Figure 4, the change of flood intensity for the 2020s, 2050s, and 2080s are illustrated relative to the mean of the baseline period (1961-1990). The figure shows that there are different bias in the projected flood frequencies depending on the GCM, the emission scenario, and the downscaling method. This large scattering in the projections is due to internal climate variability. The differences can be described by estimating uncertainties of the different sources, i.e. the emission scenario, the GCM structure, and the downscaling technique.

5.2 Validation of simulated and projected natural variability

The observed and simulated natural variability of the climate system is calculated using 100 rainfall time series generated with the monthly re-sampling method based on the original daily rainfall series of the observed and each GCM (Table 1) for both the baseline (1961-1990, Fig. 5) and the three future climate periods (Fig. 6). Differences in the frequencies for the five return periods are shown as percentage anomaly relative to the observed baseline period. As can be seen in Figure 5, the GCMs show similar natural variability as observed, whereas MK3_5 shows a larger range, while CCSM3 and HIRES show slightly smaller ranges, for most of the return periods.

Taking the temporal tendencies of the future periods into account, we observe that the projected natural variability in flood frequency of CCSM3 shows - compared to the baseline period - much higher frequencies than the other three GCMs. This might represent a more significant representation or overestimation of the effects of climate change in CCSM3. The projected bounds for MK3_5 and ECHAM5 are almost completely within the simulated baseline bounds (except for MK3_5 for the 2-year return period), this implies that according to the two GCMs no strong shifts in magnitude and range will occur in the future (Fig. 6).

It is also shown that the uncertainty ranges from natural variability for longer return periods are larger than that for shorter return periods. In addition, the natural variability differs between the GCMs to a high extent, but taking the multi-model-ensemble a relatively good representation of the natural variability is given, which e.g. is in line with the findings for world regions by Ruosteenoja et al. (2003).

5.3 Uncertainty from emission scenarios

The uncertainty from emission scenarios is shown in Figure 7. Here, we compare the natural variability with the re-sampled natural variability under the SRES A2, A1B and B1 scenarios of two combined GCMs (MK3.5 and CCSM3). The uncertainty from scenarios for both GCMs is larger than from natural variability, because the 'future' scenario bounds shift upwards than the 'future' variability bounds, especially in the 2050s and 2080s. For emission scenarios, the differences in the range at the same return periods are largest for the 2080s, while smallest for the 2020s. Moreover, the range becomes wider with larger return periods in the same time period. GPD function chosen to fit the flood frequencies probably results in higher range of the flood intensity with longer recurrence time.

5.4 Uncertainty from GCM structure

In Figure 8, the ranges in uncertainty from GCM structure of four GCMs under SRES A1B are shown. It is projected that the 2050s and 2080s have larger ranges than the 2020s. The uncertainty from GCM structure is larger than the natural variability for the 2050s and 2080s for all five return periods, as the projected frequencies are consistently shifted upwards. In the 2020s, the uncertainty from GCM structure shows disparate pattern in the five return periods. This behavior might be partly correlated with the use of the GPD function, which might not reflect the larger return periods (20- and 50-years) in a verifiable manner. In addition, the 'future' natural variability of the multi-model ensemble of four GCMs is larger than the baseline variability (cf. Fig. 5). This finding explains that the GCM structure is one of the sources of uncertainty.

5.5 Uncertainty from downscaling techniques

The changes in flood frequencies due to different downscaling techniques are shown in Figure 9. Here, ECHAM5 output is downscaled using CCLM and daily percentile scaling. The results are expressed as the relative change to the re-sampled baseline natural variability. It is shown that the change in flood frequency is higher for GCM ECHAM5 than for both the dynamical (CCLM) and statistical (daily percentile scaling) downscaling techniques for almost all return periods and future periods (Fig. 9). This shows that downscaling

techniques have relatively little impact as an uncertainty source in this study. The flood frequency for the downscaling techniques shows an increasing trend with time and return period. Hence, the uncertainties from downscaling are larger than from natural variability for the 2050s and 2080s, because the bounds are shifted upwards in each return period, but are similar or shifted downwards for the 2020s.

5.6 Comparison of uncertainty sources

In Figure 10, bar charts of the relative impact range of the uncertainty sources are shown at five return periods for three future time periods. The order of importance varies with the lead time and return period. The emission scenarios are the dominant source of uncertainty at high return periods, while the GCM structure is dominant at the lower return periods. The emission scenarios are dominant in the 2020s and 2080s, while in the 2050s the emission scenarios and the GCM structure are both similarly dominant. For the 2080s, the importance of downscaling techniques is comparative to the GCM structure, which may be explained by the fact that uncertainty from downscaling is relatively stable with lead time, but uncertainty from GCM structure becomes smaller with lead time.

6. Conclusions and discussion

In this paper, the impact ranges of three uncertainty sources in projected flood frequencies in Zhujiang River, South China have been discussed. The projection is based on a multi-model ensemble, which incorporates results from four GCMs, one RCM, and one daily percentile scaling. To identify relative changes in flood frequencies for each uncertainty source, we applied the single-propagation rather than the multi-propagation approach to the available data.

The results reveal that the order of importance varies with the lead time and return period. The emission scenarios are the dominant source of uncertainty especially at higher return periods, while the GCM structure is the dominant source at the lowest return period in the three future periods. The importance of downscaling techniques is comparative to the GCM structure at most return periods for the 2080s, but relatively less important in the

2020s and 2050s. Kay et al. (2009) discussed the importance of various uncertainty sources in flood frequency over two basins in the UK for the 2080s, they found that the dominance of uncertainty sources vary with the region. They conclude that uncertainty from GCM structure and emission scenarios are more dominant than from downscaling techniques. This is also consistent with the findings of Jenkins and Lowe (2003), who indicate that the largest uncertainty probably lies with the global prediction rather than the RCM downscaling. The magnitude of uncertainty sources is different among the various case studies, but more similar in the dominance of one source. The low ranges in uncertainty based on the two applied downscaling techniques suggest that both methods can be used to analyze regional impacts of climate change (with higher resolution) because only little increases in the uncertainty of projected flood frequencies are expected.

As for the natural variability, the impacts of climate change are stronger represented with CCSM3 and HIRES, as the bounds of future periods are shifted higher upwards than the bounds of the baseline period (1961-1990). Accordingly, climate change impacts are less strong represented with MK3.5 and ECHAM5, as their 'future' bounds are almost completely of similar size and magnitude as the baseline bounds. Hence, we conclude that projected natural variability differs among GCMs, which is also indicated on similar terms by Ruosteenoja et al. (2003). Moreover, larger ranges in natural variability are projected for longer return periods than for shorter periods.

The ranges in uncertainty from GCM structure are higher in the 2050s and 2080s than in the 2020s for the same return period. The uncertainty from emissions is largest in the 2020s, while smallest in the 2050s for the same return periods. The ranges increase with rising return period for the same time period especially in the 2020s and 2080s. This behavior might be correlated to the use of the GPD function, which might not reflect the higher return periods (20- and 50-years) in a verifiable manner. As we investigate changes in 30-year time intervals, the estimations for the 20-year and 50-year return periods should be interpreted carefully as longer return periods are less accurate than shorter periods considering the relatively short time interval (Fischer et al., 2012a).

The results are not fully representative, as some sources of uncertainty are not investigated in this study. For example, the GCM initial conditions, the RCM structure, the hydrological model structure, and the hydrological parameterization are not discussed here. We have neglected the uncertainties from the applied hydrological model (HBV-D), as

several investigations show that uncertainty from hydrological modeling is less important (Kay et al., 2009; Menzel et al., 2006; Liu et al., 2011).

Ideally, more emission scenarios, GCMs, RCMs and statistical downscaling methods should be incorporated into multi-model ensembles, to lower the uncertainty of future climate projections. Finally, further investigations into different climate and hydrological parameters and their uncertainties might give more conclusive suggestions to the tendencies in climate change impacts. According to Wilby and Dawson (2007) and Kay et al. (2009), various sources of uncertainties are involved in the detection of climate change impacts amongst natural variability. In estimating and quantifying the influence of such uncertainty sources, policy-makers can be better convinced of integrating climate change into their long-term plans (Kay et al., 2009), which can strengthen e.g. water resources management in the Zhujiang River basin.

Acknowledgements

Data from four GCMs were obtained from the IPCC data distribution centre (http://ipcc-ddc.cru.uea.ac.uk). Data from CCLM were provided by Potsdam Institute for Climate Impact Research. This study was supported by the National Basic Research Program of China (973 Program; No. 2010CB428401). We also appreciate the help of Dr. Liu B. from the National Climate Center for plotting the graphs of the variation in the impact of climate change on flood frequency.

References

Bayliss, A. and Jones, R., 1992. The peaks-over-threshold database at the Institute of Hydrology. Report to UK Ministry of Agriculture in partial duration series modeling of extremes related to the choice of the threshold values. Journal of Hydrology, 303: 215-230

Bergström, S., 1992. The HBV model - its structure and applications. SMHI Reports RH, No. 4, Norrköping

Begueria, S., 2005. Uncertainties in partial duration series modeling of extremes related to the choice of the threshold value. Journal of Hydrology, 303: 215-230

Blaney, H.F. and Criddle, W.D. 1950. Determining water requirements in irrigated areas from climatologicla and irrigation data. U.S. Soil Conservation Service Technical Paper 96, PP44, Washington D.C.

Booij, M.J., 2005. Impact of climate change on flooding assessed with different spatial model resolutions. Journal of Hydrology, 303: 176-198

Chiew, F.H.S., 2006. An overview of methods for estimation climate change impact on runoff. Hydrology and Water Resources Symposium, Launceston, TAS

Cubasch, U., 2001. Simulations of regional climate change. In: J.L. Lozán et al. (eds), Climate of the 21st century: Changes and Risks, Wissenschaftliche Auswertungen, Hamburg, PP. 173-179

Dai S, Yang S, Cai A, 2007. Variation of Sediment Discharge of the Pearl River Basin from 1955 to 2005. Acta Geographic Sinica, 62(5): 545-554 (in Chinese)

Davison, A.C., 1984. Modeling excesses over high thresholds, with an application. In: Statistical Extremes and Applications, Editor J. Tiago de Oliveira, Reidel, Dordrecht. 461–482

Déqué, M., Rowell, D., Lü Thi D., Giorgi, F., Christensen, J., Rockel, B., Jacob, D., Kjellstrŏm, C.M, Van den Hurk, B., 2007. An intercomparison of regional climate simulation for Europe: assessing uncertainties in model projections. Climate Change, 81: 53-70

Fang B., Guo SL., Wang SW., et al., 2007. Non-identical models for seasonal flood frequency analysis. Hydrological Sciences Journal, 52(5): 974-991

Fischer, T., M. Gemmer, L. Liu and B. Su, 2011. Precipitation Trends and dryness/wetness pattern in the Zhujiang River Basin, South China, 1961-2007. Quaternary International, Volume 244, Issue 2, 138-148

Fischer, T., Su B, Luo Y, and Scholten, T., 2012a. Probability distribution of precipitation extremes for weather-index based insurance in the Zhujiang River Basin, South China. Journal of Hydrometeorology, in print, DOI: 10.1175/JHM-D-11-041.1

Fischer, T., Menz, C., Su B, and Scholten, T., 2012b. Simulated and projected climate extremes in the Zhujiang River Basin, South China, using the regional climate model COSMO-CLM. (manuscript submitted to International Journal of Climatology)

Fischer, T., Gemmer, M., Su B, and Scholten, T., 2012c. Long-term meteorological and hydrological dryness and wetness conditions in the Zhujiang River Basin, South China. (manuscript submitted to Global and Planetary Change)

Fowler, H.J., Blenkinsop, S., Tebaldi, C., 2007. Linking climate change modeling to impacts studies: recent advances in downscaling techniques for hydrological modelling. International Journal of Climatology, 27: 1547-1578

Cameron, D., 2006. An application of the UKCIP02 climate change scenarios to flood estimation by continuous simulation for a gauged catchment in the northeast of Scotland, UK (with uncertainty). Journal of Hydrology, 328: 212-226

Gemmer, M., Fischer, T., Jiang T, Su B, Liu L, 2011. Trends of precipitation extremes in the Zhujiang River basin, South China. Journal o f Climate, 24(3): 750–761

Jenkins, G. and J, Lowe, 2003. Handling uncertainties in the UKCIP02 scenarios of climate change. Hadley Centre technical note 44

Gosling, S. N., Taylor, R. G., Arnell, N. W., and Todd, M. C., 2011. A comparative analysis of projected impacts of climate change on river runoff from global and catchment-scale hydrological models, Hydrology and Earth System Sciences, 15: 279–294

Graham, L.P., Andréasson, J., Carlsson, B., 2007. Assessing climate change impacts on hydrology from an ensemble of regional climate models, models scales and linking methods – a case study on Lule River basin. Climatic Change, 81(supplement): 293-307

He H, Wang P, Jin L, 2006. ANN model to predict annual highest water level in Xijiang River. Journal of Natural Disasters, 15(5): 32-27 (in Chinese)

Hulme M., Jenkins GJ., Lu X., Turnpenny JR., Mitchell TD., Jones RG., Lowe J., Murphy JM., Hassell D., Boorman P., McDonald R., Hill S., 2002. Climate change scenarios for the United Kingdom: the UKCIP02 scientific report. Tyndall Centre for Climate Change Research, School of Environmental Sciences, University of East Anglia, Norwich, UK

IPCC SRES, 2000, Special Report on Emissions Scenarios: A special report of Working Group III of the Intergovernmental Panel on Climate Change, Nakićenović, N., and Swart, R., ed., Cambridge University Press

IPCC AR4, 2007. Fourth Assessment Report of the Intergovernmental Panel on Climate Change, Eds.: M.L. Parry, O.F. Canziani, J.P. Palutikof, P.J. van der Linden and C.E. Hanson, Cambridge University Press, Cambridge, UK

Kay, A., Davies, H., Bell, V., Jones, R., 2009. Comparison of uncertainty sources for climate change impacts: flood frequency in England. Climatic Change, 92:41–63

Kilsby CG., Jones PD., Burton A., Ford AC., Folwer HJ., Harpham C., James P., Smith A., and Wilby R.L., 2007. A daily weather generator for use in climate change studies. Environmental Modelling and Software, 22(12): 1705-1719

Koutsoyiannis, D. and A. Efstratiadis, 2007. Uncertainty assessment of future hydroclimatic predictions: a comparison of probabilistic and scenario-based approaches. Journal of Hydrometeorology, 8: 261-281

Krysanova, V., Bronstert, A., Müller-Wohlferl, D.I., 1999. Modelling river discharge for large drainage basins: from lumped to distributed approach. Hydrological science Journal, 44: 313-333

Liu L, Jiang T, Yuan F, 2009. Observed (1961–2007) and Projected (2011–2060) Climate Change in the Pearl River Basin. Advances in Climate Change Research 5(4): 209–214 (in Chinese)

Liu L.L., Liu Z.F., Ren X.Y., Fischer, T., Xu Y. 2011. Hydrological impacts of climate change in the Yellow River Basin for the 21st century using hydrological model and statistical downscaling model. Quaternary International 244: 211-220

Liu L, Jiang T, Xu J, Zhai J, Luo Y, 2012a. Responses of Hydrological Processes to the Climate Change in the Zhujiang River Basin in the 21st Century. Advances in Climate Change Research, 8(1): 28-34 (in Chinese)

Liu L, Jiang T, Xu J, Luo Y. 2012b. Research on the hydrological processes using multi-GCMs and multi-scenarios. Journal of Hydraulic Engineering, (accepted, in Chinese)

Liu L, and Ren G, (2012). Percentile delta statistical downscaling method and its application in the correction of GCMs daily rainfall in China. Plateau Meteorology, (accepted, in Chinese)

Menzel, L., Thieken, A.H., Schwandt, D., Bürger, G., 2006. Impact of climate change on the regional hydrology – scenario-based modeling studies in the German Rhine catchment. Natual Hazards, 38: 45-61

Minville, M., Brissette, F., Leconte, R., 2008. Uncertainty of the impact of climate change on the hydrology of a Nordic watershed. Journal of hydrology, 358, 70-83

Naden, P.S., 1992. Analysis and use of peaks-over-threshold data in flood estimation. In: Saul AJ(ed) floods and flood management. Kluwer Academic, Dordrecht, 131-143

Pickands, J., 1975. Statistical inference using extreme order statistics. Annuals of Statistics, 3(1): 119-131

Preston, B. and R. Jones, 2008. Evaluating sources of uncertainty in Australian runoff projections. Advances in Water Resources, 31: 758-775

Prudhomme, C., Jakob, D., Svensson, C. 2003. Uncertainty and climate change impact on the flood regime of small UK catchments. Journal of Hydrology, 277: 1–23

Rockel, B., Will, A., and Hense, A., 2008. The regional climate model COSMO-CLM (CCLM). Meteorogoische Zeitschrift, 17 (4): 347-348

Ruosteenoja, K., Carter, T.R., Jylhä, K., Tuomenvirta, H., 2003. Future climate in world regions: an intercomparison of model-based projections for the new IPCC emissions scenarios. The Finnish Environment 644, Finnish Environment Institute, Helsinki

Saelthun, N.R., 1996. The Nordic HBV model. Description and documentation of the model version developed for the project climate change and energy production, NVE Publication 7, Norwegian Resources and Energy Administration, Oslo

Smith, R.L., 1984. Threshold methods for sample extremes. In: Statistical Extremes and Applications, ed. J. Trago de Oliveira, 621–638. Reidel, Dordrecht , the Netherlands

Todd, M., Taylor, R., Osborn, T., et al., 2011. Uncertainty in climate change impacts on basin-scale freshwater resources – preface to the special issue: the QUEST-GSI methodology and synthesis of results. Hydrology and Earth System Sciences, 15: 1035–1046

Van Montfort, M. A. J., and Witter, J. V., 1985. Testing exponentiality against generalized Pareto distribution. Journal of Hydrology. 78: 305-315.

Wilby, R.L. and Dawson, C.W., 2007. SDSM 4.2 - A decision support tool for the assessment of regional climate change impacts: user manual, UK

Xu C.Y., 1999. From GCMs to river flow: a review of downscaling methods and hydrologic modelling approaches. Progress in physical geography 23(2): 229-249

Yin X, 2010. Research on change of discharge at WuZhou station in the Xijiang River during dry season. Pear River, 4:1 , 2, 47 (in Chinese)

Table captions:

Table 1 Components of the four GCMs used in this study

Figure captions:

Fig. 1 Overview map of the Zhujiang River basin in South China (upper panel), and map (lower panel) of Xijiang River basin (red line) indicating elevation (shading), administrative boundaries (grey lines) incl. names, the meteorological stations (red dots) and the outlet (red triangle) at Gaoyao.

Fig. 2 Frequency curves of observed (solid line) and simulated (dashed line) stream flow at Gaoyao hydrological station for the calibration period (a) and the validation periods (b, c).

Fig. 3 Frequency curves of changes in projected annual maximum 1-day flood peak flows (i.e. flood frequency) for three future periods relative to the baseline period (1961-1990) based on a multi-model ensemble (adapted from Fig. 6 in Liu et al., 2012b)

Fig. 4 Box plots of changes in projected annual maximum 1-day flood frequency for three future periods relative to the baseline period (1961-1990). Box plots: the central mark is the median; the box-edges are the 25th and 75th percentiles

Fig. 5 Change in natural variability of monthly re-sampled simulated flood frequencies relative to the mean of each resampling series at five return periods (2, 5, 10, 20 and 50 years) for the baseline period 1961-1990. Observations (black), CCSM3 (red), MK3.5 (blue), ECHAM5 (cyan), and HIRES (green)

Fig. 6 Change in flood frequency of four monthly re-sampled GCMs for the future periods of 2020s (red), 2050s (blue), and 2080s (green) relative to the baseline period of 1961-1990 (black) for five return periods (2, 5, 10, 20 and 50 years). The box plots represent the median (central mark), the 25th and 75th percentiles (edges of the boxes), and the inter-quartile range (length of the whiskers)

Fig. 7 Change in flood frequency of the SRES A2 (square), A1B (diamond) and B1 (circle) scenarios of two combined GCMs (MK3_5 and CCSM3) relative to the re-sampled observed (black +) and simulated (colored +) natural variability for five return periods (2, 5, 10, 20, and 50 years) for the 2020s (red), 2050s (blue), and 2080s

(green). For the variability, the bars show the median and the 90% upper and lower bounds.

Fig. 8 Change in flood frequency of four GCMs under SRES A1B relative to the re-sampled observed (black +) and simulated (colored +) natural variability for five return periods (2, 5, 10, 20, and 50 years) for the 2020s (red), 2050s (blue), and 2080s (green). For the variability, the bars show the median and the 90% upper and lower bounds.

Fig. 9 Change in flood frequency from downscaling techniques (CCLM and daily percentile scaling), using ECHAM5, relative to the re-sampled observed (black +) and simulated (colored +) natural variability for five return periods (2, 5, 10, 20, and 50 years) for the 2020s (red), 2050s (blue), and 2080s (green). Changes for ECHAM5 (squares) and for downscaled ECHAM5 (triangles)

Fig. 10 Bar charts of the relative impact range of three uncertainty sources, i.e. emission scenarios (blue), GCM structure (red) and downscaling techniques (green) for five return periods (2, 5, 10, 20 and 50 years) for the future periods of the 2020s (left panel), 2050s (middle panel), and 2080s (right panel)

Table 1 Components of the four GCMs used in this study

ID	GCM	Country	Atmosphere component	Ocean component	Sea ice component	Land component
1	CSIRO/ MK3_5	Australia	T63 L18 1.875º × 1.875º	MOM2.2 L31 1.875º × 0.925º	n/a	n/a
2	MPI-OM5/ ECHAM5	Germany	ECHAM5 T63 L32 2º × 2º	OM L41 1.0º × 1.0º	OM	n/a
3	NCAR/ CCSM3	USA	CAM3 T85 L26 1.4º×1.4º	POP1.4.3 L40 1.0º × 1.0º	CSIM5.0 T85	CLM3.0
4	MIROC3.2/ HIRES	Japan	T106 L56 1.125 º × 1º	L47 0.2812º × 0.1875º	0.2812º × 0.1875º	0.5625º × 0.5625º

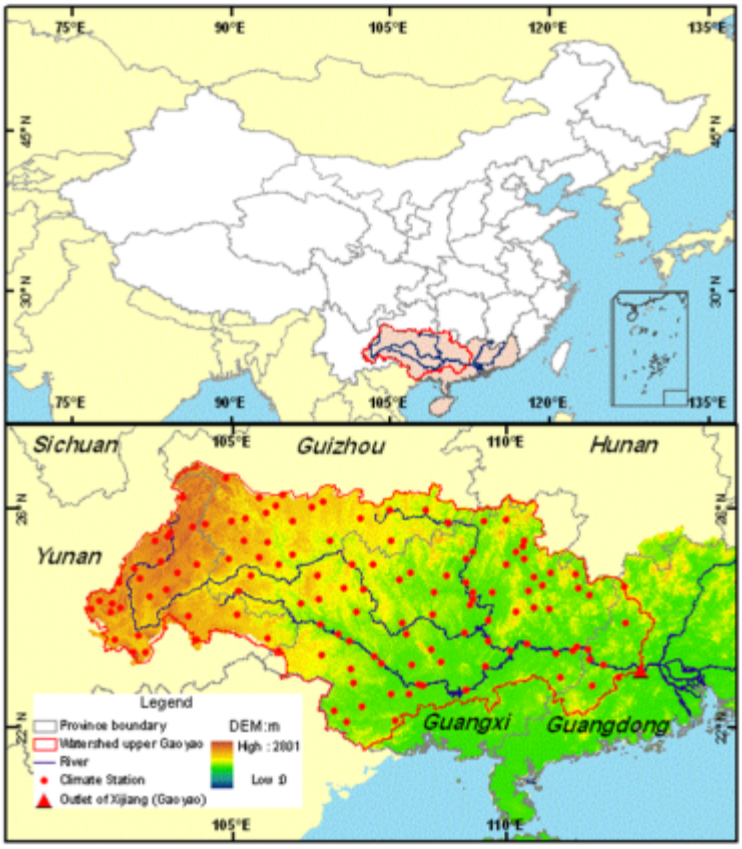

Fig. 1 Overview map of the Zhujiang River basin in South China (upper panel), and map (lower panel) of Xijiang River basin (red line) indicating elevation (shading), administrative boundaries (grey lines) incl. names, the meteorological stations (red dots) and the outlet (red triangle) at Gaoyao.

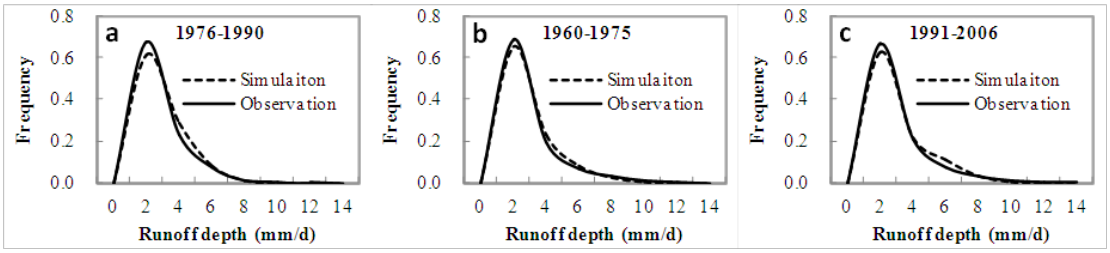

Fig. 2 Frequency curves of observed (solid line) and simulated (dashed line) stream flow at Gaoyao hydrological station for the calibration period (a) and the validation periods (b, c).

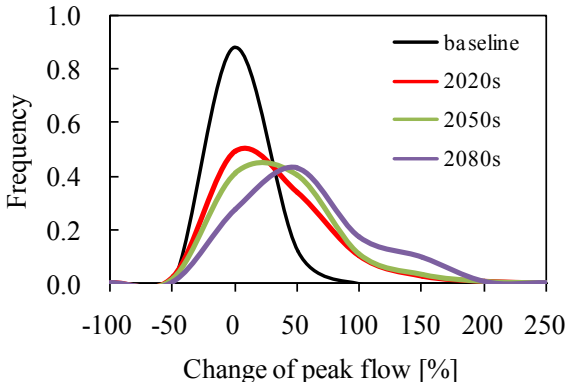

Fig. 3 Frequency curves of changes in projected annual maximum 1-day flood peak flows (i.e. flood frequency) for three future periods relative to the baseline period (1961-1990) based on a multi-model ensemble (adapted from Liu et al., 2012b)

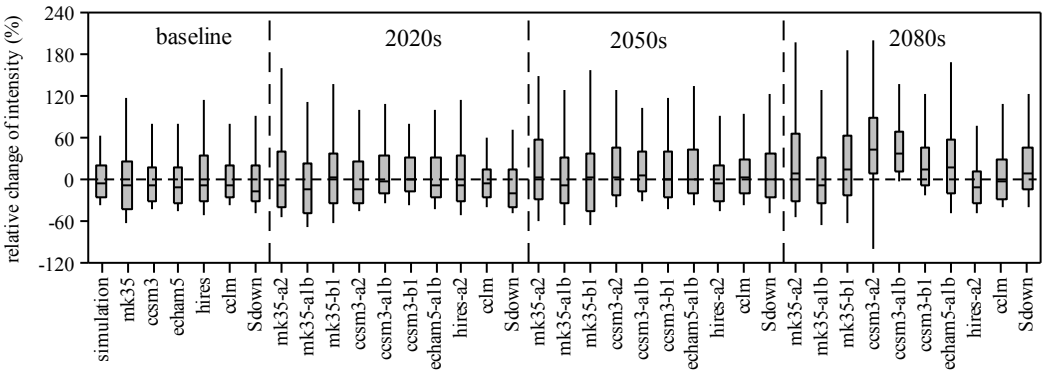

Fig. 4 Box plots of changes in projected annual maximum 1-day flood frequency for three future periods relative to the baseline period (1961-1990). Box plots: the central mark is the median; the box-edges are the 25th and 75th percentiles

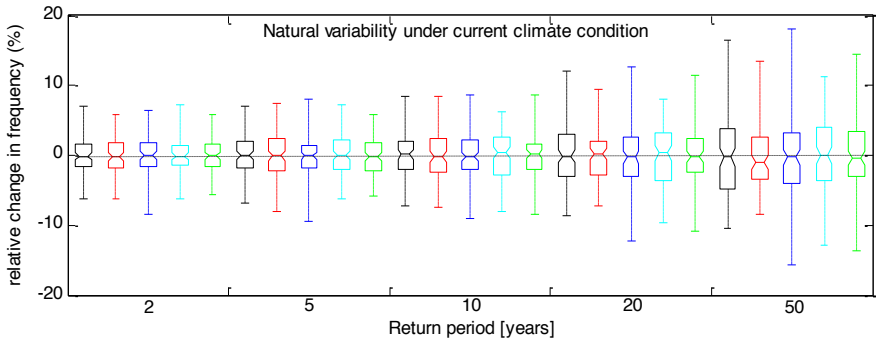

Fig. 5 Change in natural variability of monthly re-sampled simulated flood frequencies relative to the mean of each resampling series at five return periods (2, 5, 10, 20 and 50 years) for the baseline period 1961-1990. Observations (black), CCSM3 (red), MK3.5 (blue), ECHAM5 (cyan), and HIRES (green)

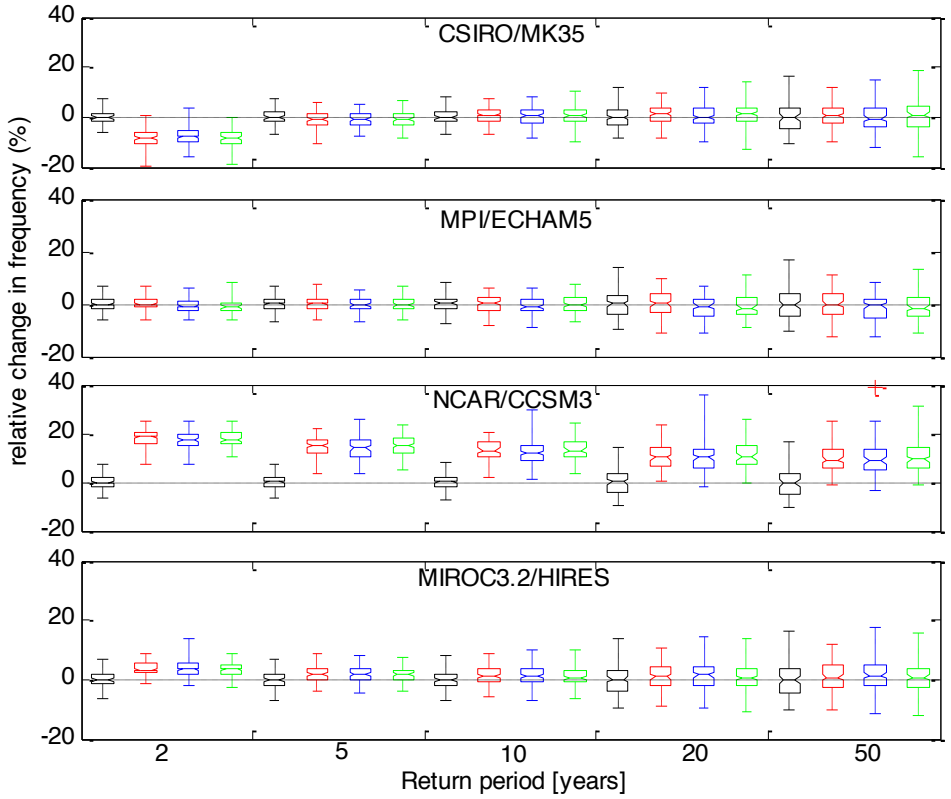

Fig. 6 Change in flood frequency of four monthly re-sampled GCMs for the future periods of 2020s (red), 2050s (blue), and 2080s (green) relative to the baseline period of 1961-1990 (black) for five return periods (2, 5, 10, 20 and 50 years). The box plots represent the median (central mark), the 25th and 75th percentiles (edges of the boxes), and the inter-quartile range (length of the whiskers)

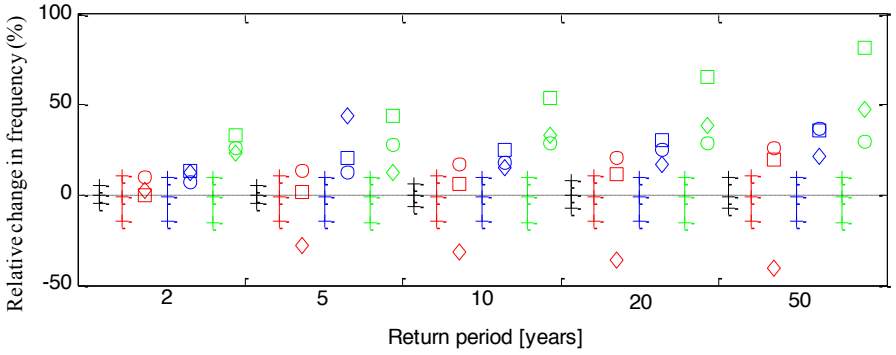

Fig. 7 Change in flood frequency of the SRES A2 (square), A1B (diamond) and B1 (circle) scenarios of two combined GCMs (MK3_5 and CCSM3) relative to the re-sampled observed (black +) and simulated (colored +) natural variability for five return periods (2, 5, 10, 20, and 50 years) for the 2020s (red), 2050s (blue), and 2080s (green). For the variability, the bars show the median and the 90% upper and lower bounds.

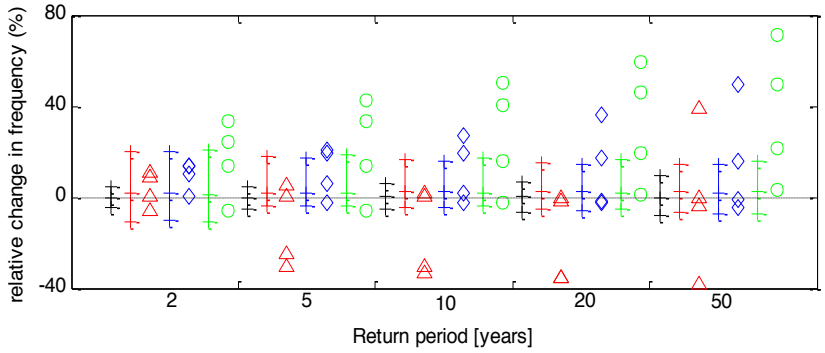

Fig. 8 Change in flood frequency of four GCMs under SRES A1B relative to the re-sampled observed (black +) and simulated (colored +) natural variability for five return periods (2, 5, 10, 20, and 50 years) for the 2020s (red), 2050s (blue), and 2080s (green). For the variability, the bars show the median and the 90% upper and lower bounds.

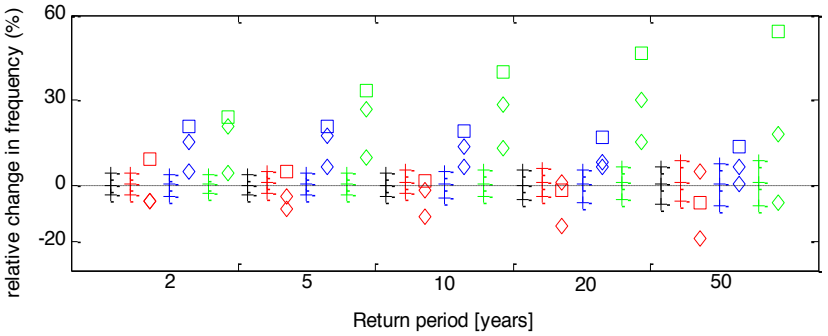

Fig 9 Change in flood frequency from downscaling techniques (CCLM and daily percentile scaling), using ECHAM5, relative to the re-sampled observed (black +) and simulated (colored +) natural variability for five return periods (2, 5, 10, 20, and 50 years) for the 2020s (red), 2050s (blue), and 2080s (green). Changes for ECHAM5 (squares) and for downscaled ECHAM5 (triangles)

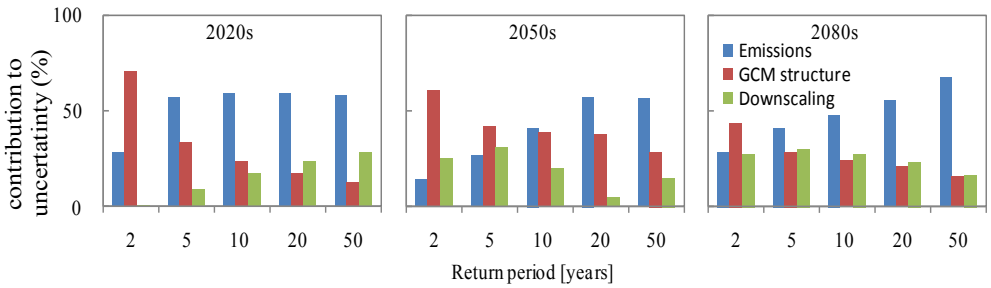

Fig. 10 Bar charts of the relative impact range of three uncertainty sources, i.e. emission scenarios (blue), GCM structure (red) and downscaling techniques (green) for five return periods (2, 5, 10, 20 and 50 years) for the future periods of the 2020s (left panel), 2050s (middle panel), and 2080s (right panel)